SPECIATION, TRANSPORT AND MOBILITY OF METALS IN PRISTINE WATERSHEDS AND CONTAMINATED SOIL SYSTEMS IN ALASKA

By

Amanda J. Barker, B.A.

A Dissertation Submitted in Partial Fulfillment of the Requirements

for the Degree of

Doctor of Philosophy

in

Environmental Chemistry

University of Alaska Fairbanks

December 2016

APPROVED:

Dr. Tom Trainor, Committee Chair
Dr. Thomas Douglas, Committee Member
Dr. Sarah Hayes, Committee Member
Dr. William Simpson, Committee Member
Dr. Tom Green, Chair
Department of Chemistry and Biochemistry
Dr. Paul Layer, Dean
College of Natural Sciences and Mathematics
Dr. Michael Castellini, Dean
Graduate School

Abstract

The fate of metal(loid)s in the environment depends on a variety of physical and geochemical factors. Assessing metal(loid) transport in soil solution and surface water requires detailed knowledge of the speciation, which can often control mobility, toxicity and bioavailability of a given element. The present study details the geochemical analyses of two end member types of systems: a 'pristine' Arctic watershed and a military shooting range with an overall focus on understanding lead (Pb) and antimony (Sb) mobility in shooting range soils. The project uses bulk speciation analyses coupled with micro-scale methods to quantify variations in metal(loid) concentration as a function of environmental conditions and characterize metal(loid) speciation and distribution in relation to parent source material in order to understand the impact that metal(loid) retention versus mobilization has on a given system.

In the Arctic, stream water concentrations of Al, Ba, Fe, and Mn in Imnavait Creek were highest in the late fall (September and October). This pattern appears to correlate with the depth of the active layer throughout the watershed. Increased water infiltration at the permafrost-active layer boundary could significantly impact stream water trace metal(loid) signatures due to mineral weathering of unfrozen soil. In the central Alaskan shooting range, there were significant contributions of Pb and Sb to both the soil and soil solution as a result of the weathering of fragmented bullets. Aqueous concentrations of Sb were higher than Pb in all soil types, indicating Sb is more mobile, despite the fact that bullets introduce approximately two orders of magnitude more Pb than Sb. We observed an association of both Pb and Sb with Fe in soils, which impacts remediation scenarios for ranges as Fe treatments have potential to be effective for system-wide immobilization of major contaminants. Overall, the results from this study

highlight the complexity of metal(loid) speciation, transport and mobility as a function of seasonality, soil type and environmental conditions.

Table of Contents

List of Figures

Page

List of Tables

Page

List of Appendices

Acknowledgments

I would like to extend my sincere gratitude to the many people that contributed their time and energy to this endeavor. This project would not have been possible without the unwavering patience and support of my academic committee, Dr. Tom Trainor, Dr. Thomas Douglas, Dr. Sarah Hayes and Dr. William Simpson. I am also grateful to Dr. Anastasia Ilgen, for assisting in instrument training, data collection and method development. In addition, I would like to thank the beamline scientists and staff at GSE-CARS and SSRL for their support. Finally, I would like to thank Karen Spaleta, Dr. Lisa Mayhew, Dr. Franta Majs, Tiffany Gatesman, Emily Reiter, Jacy Pietsch and the chemistry department at UAF for supporting this project. My time with all of you was special and I am greatly appreciative.

Introduction

The soil environment is physically and chemically dynamic. The fate and transport of metal(loid)s are affected by the overall dynamic nature of the environment (Brusseau, 1989; Dunnivant and Anders, 2006; Hemond and Fechner, 2014). Physically, metal(loid) transport in environmental systems has been shown to be impacted by temperature (Majedi et al., 2013), wind (Dinis and Fiúza, 2006), water infiltration (Knechtenhofer et al., 2003), hydraulic conductivity (Loretta and Li, 2001), grain size and surface area of soil (Horowitz and Elrick, 1987). Chemically, the soil environment tends to be highly heterogeneous (Seuntjens et al., 2002) and consists of a wide range of chemical species that are constantly undergoing transformation (Lyman, 1995). Metal(loid)s can partition between phases (air, soil, water, biota) (Lyman, 1995; Walker et al., 2006; Pachana et al., 2010) and transport is facilitated by key environmental mediums like water (Knechtenhofer et al., 2003; Pachana et al., 2010), colloids (Kaplan et al., 1995) and sediment (Horowitz, 1985). Understanding metal(loid) transport in the environment requires detailed investigation into various environmental compartments (soil, interstitial waters, dissolved, bound, etc.) and knowledge of physicochemical processes that control overall transport.

Identifying potential sources and sinks of metal(loid)s in the environment are necessary to quantifying environmental impact and planning remediation strategies (Horowitz, 1985). Sources of metal(loid)s can vary in the environment, but with the absence of mining or industrial activities, mineral weathering is a major source of metal(loid)s (Filella et al., 2009; Jin et al., 2010). Non-geogenic sources of metal(loid)s in the environment are often a result of mining activities (Rodriguez et al., 2008; Kossoff et al., 2012), industrial processes (Bradl, 2002; Wuana

and Okieimen, 2011), agriculture practices (Zhang and Shan, 2008), bullet deposition (Scheinost et al., 2006) and environmental disasters (Bird and Grossman, 2011). Regardless of the source, released metal(loid)s can migrate in the environment through dissolution, colloidal transport and complexation (Bradl, 2002; He et al., 2005) and have been shown to accumulate in environmental sinks, such as interstitial waters (Cantwell and Burgess, 2001), organic matter (Sklodowski et al., 2006; Clemens and Ma, 2016), clay minerals (Ilgen and Trainor, 2012; Cai et al., 2014), Fe oxides (Yin et al., 2016) and Mn oxides (Gunawardana et al., 2015). The mechanisms by which metal(loid)s can accumulate in various sinks are controlled primarily by adsorption, precipitation, co-precipitation, complexation and incorporation into crystal lattices (Horowitz, 1985). Once accumulated, metal(loid)s can potentially be remobilized, thus providing a secondary source of metal(loid)s into the environment (Pachana et al., 2010). Key factors affecting metal(loid) mobilization are pH (Kaplan et al., 1995; Cao et al., 2003; Houben et al., 2013), ionic strength (Ilgen et al., 2014), temperature (Majedi et al., 2013), redox conditions (Wilson et al., 2010) and speciation (Johnson et al., 2005).

Speciation, as defined by the International Union of Pure and Applied Chemistry (IUPAC), is 'the process yielding evidence of the atomic or molecular form of an analyte or the oxidation state and local structure of the element of interest' (Hill, 1997). For example, antimony (Sb) is typically found in the environment in one of two oxidation states: Sb(III) and Sb(V). The numerical distinction signifies different electron configurations and therefore different number of valence electrons. The respective Sb species behave differently in environmental systems in that Sb(V) is more mobile than Sb(III), but Sb(III) is considered to have greater toxicity and bioavailability (Johnson et al., 2005; Filella et al., 2009; Wilson et al., 2010). Key factors that

can affect metal(loid) speciation in the environment are redox conditions (Barker et al., 2014), time (Ilgen et al., 2014), pH (Hill, 1997) and sunlight (Shiller et al., 2006).

Characterizing the speciation of metal(loid)s in various environmental compartments can be challenging and requires prior knowledge of each metal(loid) of interest in order to ensure appropriate sample collection and methodology. For example, hydrochloric acid (HCl) has been shown to be an effective preservation agent for iron (Fe) and arsenic (As) speciation in surface waters (Ritchie et al., 2013), but can accelerate the oxidation of Sb species, which have been shown to be effectively stabilized instead by organic complexing agents (Ilgen and Trainor, 2012). Understanding the exact speciation of metal(loid)s in the environment is imperative for assessing the overall toxicity of a given system because toxicity is often controlled by speciation. Once metal(loid)s enter the environment they are long-term persistent contaminants, meaning they cannot be biologically destroyed, only transformed from one species to another (Knox et al., 2000; Singh and Gräfe, 2010).

Overall monitoring of metal(loid) transport, mobility and speciation in the environment typically focuses on quantifying concentrations in bulk phases, characterizing mineral phase assemblage, capturing metal(loid) distribution, investigating elemental associations and determining speciation. Quantifying metal(loid) concentrations can be achieved by inductively coupled plasma-mass spectrometry (ICP-MS) for bulk aqueous phases and x-ray fluorescence (XRF) for bulk solid phases. Mineralogy and long range crystalline order of solid species can be investigated using x-ray diffraction (XRD) techniques. Metal(loid) distribution and elemental associations are often examined using electron-probe micro-analysis (EPMA) or synchrotron-based x-ray absorption spectroscopy (XAS) for solid phases and field-flow fractionation (FFF) for aqueous phases. Metal(loid) speciation can be investigated using a variety of techniques,

particularly liquid-chromatography (LC) coupled to ICP-MS (LC-ICP-MS) for aqueous phase speciation and synchrotron-based techniques for solid phase speciation: extended x-ray absorption fine structure (EXAFS) or x-ray absorption near edge structure (XANES). Proper sample collection, element specific sample preservation and methodical sample analysis is required for any detailed monitoring of metal(loid) transport, mobility and speciation in addition to making any future predictions of metal(loid) accumulation versus mobilization in the environment.

As metal(loid)s comprise a major fraction of the earth, it is necessary to understand their interactions with the environment and their behavior with respect to changes or disturbances in their setting. Metal(loid)s are both useful and valuable and have been shown to be fundamental to scientific and industrial advances for humans, in addition to providing essential nutrients for sustained existence on Earth (Kabata-Pendias, 2010). Metal(loid)s have also been shown to be effective tracers for landscape-scale processes, including stable isotope geochemistry (Wiederhold, 2015), permafrost active layer dynamics (Barker et al., 2014) and processes involving oxidation and reduction (Bullen, 2012). Long term monitoring of metal(loid)s requires prior knowledge of element-specific environmental sampling collection and storage methods and necessitates the use of a variety of instrumentation for sample analysis (Horowitz, 1985; Hill, 1997). Any future predictions of the transport, mobility and speciation of metal(loid)s should (1) include information on the sources and sinks of metal(loid)s particular to an environmental compartment, (2) discuss overall transport mechanisms controlling the mobilization versus immobilization of metal(loid)s and (3) address metal(loid) behavior with respect to fluctuating environmental parameters like pH, redox conditions, salinity and organics/colloid fraction, in order to fully capture the complex relationship between metal(loid)s and their environment.

Chapter 1 Late Season Mobilization of Trace Metals in Two Small Alaskan Arctic Watersheds as a Proxy for Landscape Scale Permafrost Active Layer Dynamics[1]

1.1 Abstract

Increasing air temperatures in the Arctic have the potential to degrade permafrost and promote the downward migration of the seasonally thawed active layer into previously frozen material. This may expose frozen soils to mineral weathering that could affect the geochemical composition of surface waters. Determining watershed system responses to drivers such as a changing climate relies heavily on understanding seasonal controls on freshwater processes. The majority of studies on elemental concentrations in Arctic river systems have focused on sampling only from spring snowmelt to the summer season. Consequently, there remains a limited understanding of surface water geochemistry, particularly with respect to trace metals, during late fall and early winter. To examine the variability of metal concentrations as a function of seasonality, we measured trace metal concentrations from spring melt to fall freeze-up in 2010 in two high Arctic watersheds: Imnavait Creek, North Slope, Alaska and Roche Mountanee Creek, Brooks Range, Alaska. We focused on aluminum (Al), barium (Ba), iron (Fe), manganese (Mn), nickel (Ni) and zinc (Zn). Concentrations of 'dissolved' (<0.45μm) Al, Ba, Fe, and Mn in Imnavait Creek waters and Ba in Roche Mountanee waters were highest in late fall/early winter. To link observed surface water concentrations at Imnavait Creek to parent soil material we analyzed the elemental composition of a soil core from the watershed and tracked the soil temperatures as a function of time and depth. The results from this study show a distinct seasonal

[1]Barker, A.J., Douglas, T.A., Jacobson, A.D., McClelland, J.W., Ilgen, A.G., Khosh, M.S., Lehn, G.O., Trainor, T.P. 2014. Late Season Mobilization of Trace Metals in Two Small Alaskan Arctic Watersheds as a Proxy for Landscape Scale Permafrost Active Layer Dynamics. Chemical Geology. 381, 180-193.

signature of trace metal concentrations in late fall that correlates with the depth of the thawed active layer.

1.2 Introduction

Climate warming in the Arctic has led to increasing air temperatures (Peterson et al., 2002, Arndt et al., 2010), resulting in thawing of permafrost and the downward migration of the seasonally thawed active layer into previously frozen material (Hinzman and Kane, 1992; Osterkamp and Romanovsky, 1997; 1999; Jorgenson et al., 2006; Christiansen et al., 2010; Romanovsky et al., 2010; Smith et al., 2010). This active layer response to climate warming may influence the geochemical composition of rivers in the Arctic via increasing trace element transport, increasing organic carbon mobilization, and evolving biogeochemical cycles, among other factors (Vuceta and Morgan, 1978; Kane et al., 1989; McNamara et al., 1997; Rember and Trefry, 2004; White et al., 2007; Pokrovsky et al., 2011; Muskett and Romanovsky, 2011). This partly reflects the fact that the majority of subsurface flow in permafrost systems occurs in the active layer (McNamara et al., 1997). Consequently, the downward expansion of the active layer may increase the exposure of labile mineral phases to weathering processes and provide an enhanced weathering signal in the soil-pore and surface waters.

With the absence of mining or industrial activities, mineral weathering is the major source of trace metals to surface waters in pristine Arctic rivers. Therefore, developing a mechanistic understanding of trace metal behavior and transport in the subsystem of soils and surface waters can provide insight into active layer chemical weathering processes. In addition,

the redox environment of a given watershed controls trace metal mobility. As a consequence, observations of changes in fluxes of redox sensitive elements can be used to evaluate redox conditions. Many studies have used biogeochemical tracers such as dissolved organic carbon, radiogenic isotopes, nutrient fluxes and major ion concentrations to investigate watershed dynamics, permafrost degradation, carbon sources, the timing of spring melt, and seasonal controls on elemental export (Cooper et al., 2005; 2008; Petrone et al., 2006; McClelland et al., 2007; Keller et al., 2007; 2010; Townsend-Small et al., 2010; Bagard et al., 2011). However, only a few studies have employed trace metals as a proxy for permafrost dynamics at the watershed scale (Martin et al., 1993; Dai and Martin, 1995; Rember and Trefry, 2004; Bagard et al., 2011). Furthermore, most of these studies only measured concentrations of trace metals in surface water samples without considering the composition of soil and soil pore water, and none have examined dissolved trace metal data in the context of the soil thermal regime (i.e., the timing of thawing and freezing of the active layer). As a result, there is a lack of information linking the trace metal composition of subsurface and surface flow within Arctic watersheds to the geochemistry of underlying soils and seasonal permafrost active layer dynamics.

Trace metal concentrations in surface waters fluctuate on a yearly basis partly due to variations in precipitation, temperature, the extent of active layer thaw, the composition of the underlying soils and the degree to which the watershed responds to climate warming (Hinzman et al., 1991; Bagard et al., 2011). Due to the strong seasonality of Arctic freshwater processes (Chapin et al., 2005; Bagard et al., 2011), the response of riverine trace metal signatures to increasing active layer depth should be most evident during late fall, when the active layer is at its deepest yearly extent and the base flow component is increasing toward the yearly maximum winter values (McNamara et al., 1998; Peterson et al., 2002; Yang et al., 2002; Hinzman et al.,

2005). Any increase in the flux of major and trace elements to subsurface flow in late fall could potentially be evident as a pulse, different than the pulse for groundwater dominated streams. Many studies reporting trace and major element concentrations in Arctic river systems have only focused on spring and/or summer flow regimes (Martin et al., 1993; Dai and Martin,1995; Guieu et al., 1996; Rember and Trefry, 2004). As such, there remains a limited understanding of trace metal transport and behavior in Arctic rivers during late fall and early winter (Bagard et al., 2011) when mineral weathering processes continue to occur.

It is also possible that major and trace ions mobilized in late fall are stored in the shallow subsurface during freeze up and contribute to the following year's spring thaw signal. Mobilization of major and trace elements to surface waters during early spring is typically attributed to the dominant Arctic runoff event of spring snowmelt when precipitation that has accumulated all winter is released (McNamara et al., 1997; Rember and Trefry, 2004; Petrone et al., 2006). However, elemental transport to surface waters during spring snowmelt potentially encompasses contributions from previously mobilized species stored in the subsurface/surface as well as input from the snowpack (Bagard et al., 2011). With increasing depth of permafrost thaw and the potential increase in late fall mineral weathering fluxes to watersheds there are potential ramifications for a change in biogeochemical fluxes from watersheds during the spring and fall seasons. Our goal was to examine whether trace metal concentrations in surface waters draining areas of continuous permafrost can provide a signal of permafrost active layer dynamics distinguishable over normal variability at the watershed-scale. Since our data is not part of a multi-year set, we primarily hope to establish a baseline of measurements for longer-term monitoring in the future.

We collected surface water samples for trace metal analysis from spring melt in mid-May through the initiation of fall freeze-up in mid-October. We mainly focused on Imnavait Creek, a small headwater stream underlain by continuous permafrost and dominated by tussock sedge tundra with organic rich soils (Osterkamp and Payne, 1981; Walker et al., 1989). In the Imnavait watershed, we excavated a 1 meter deep soil pit to identify and define soil horizons and collected a 61 cm soil core to quantify the vertical distribution of trace metals. To continuously measure soil temperature as a function of depth through time, we installed thermistors into the active layer and the top of the permafrost table within the watershed.

We attempted to correlate our findings to a broader area in the Arctic by collecting and analyzing surface waters from a larger watershed, Roche Mountanee Creek. As a relatively small, low gradient stream dominated by organic-rich soils, Imnavait Creek typifies many small watersheds throughout the high Arctic. In contrast, we employ Roche Mountanee Creek as an analog for permafrost active layer processes occurring in higher gradient, larger watersheds containing primarily exposed bedrock. The overall design of this study offers potential for extrapolating our findings to broader areas in the Arctic.

In this study we aimed to: (1) quantify variations in metal concentrations as a function of seasonality in two high Arctic streams, (2) characterize metal concentrations in soil layers within the Imnavait Creek watershed and relate them to freezing and thawing processes, (3) track the influence of water sourcing from the snowmelt signal, precipitation and groundwater signal on trace metal fluctuations in surface waters, (4) develop a conceptual model relating trace metal chemical composition in surface waters to permafrost active layer dynamics at Imnavait Creek, and (5) compare the model to the seasonal variability in metal concentrations at a

physiographically different watershed to determine if relationships identified in Imnavait Creek are broadly applicable to other Arctic watersheds.

1.3 Materials and Methods

1.3.1 Field Study

Two watersheds located in the northern foothills of the Brooks Range in the Alaskan Arctic were examined in this study: Imnavait Creek (2.2 km^2) and Roche Mountanee Creek (89 km^2) (Figure 1.1). Imnavait Creek is a small headwater stream located in a valley formed on Sagavanirktok glaciation till (Hamilton, 1986). A network of water tracks drain the hillslopes of the watershed and the creek is comprised of a chain of small ponds intermittently connected by water tracks that flow into the Kuparuk River (McNamara et al., 1997). The area is dominated by erosional topography (Black, 1976) underlain by continuous permafrost 250 to 300 meters deep (Osterkamp and Payne, 1981). Vegetation predominantly consists of tussock sedge tundra (Walker et al., 1989) with organic rich soils and sphagnum moss/ericaceous plants (Kane et al., 1989). This accumulated acidic vegetation, as well as the saturated soil conditions, are primary contributors to the overall low pH values of stream water (approximately 4.5-6.5) throughout the summer (Everett et al., 1989; Walker et al., 2002).

The soils at Imnavait Creek are organic-rich, poorly drained silty loams covered by a peaty layer. They consist of highly weathered clays and silicates under acidic and often water-logged conditions during the spring and summer (Walker et al., 1989; Kane et al., 2000). There are also embedded mineral layers consisting of silt overlying glacial till (Kane et al., 1989; McNamara et al., 1997; 1998). The soil is weathered to a greater extent than areas south of the

North Slope within the Brooks Range (Figure 1.1) and the parent material may less effectively neutralize organic and carbonic acids (Ping et al., 1998). Portions of the soil profile have been described as having a high chroma color, indicating the oxidation of iron minerals, whereas adjacent zones are gleyed, pointing to more reducing conditions (Ping et al., 1998).

Roche Mountanee Creek is located approximately 30 km south of Imnavait Creek along the Dalton Highway. The drainage basin has extensive bedrock exposure and is underlain by continuous permafrost. In addition to some tussock sedge tundra along the lower section of the watershed the predominant vegetation is low-lying alder bush. The area has shrub-covered lowlands and tundra-covered and rocky uplands. Ridgelines reach about 1.5 km above sea level. The pH of this river ranges from circumneutral to slightly basic due to the carbonate-rich terrain and the minimal presence of organic vegetation and soils (Till et al., 2008).

A total of 60 surface water samples were collected from Imnavait Creek and Roche Mountanee Creek between early May and mid-October 2010. We extracted a soil core from the Imnavait drainage and in the Imnavait watershed we installed a thermistor string (Onset Computer Corporation, Bourne, MA) to continuously monitor soil temperatures at four depths spanning the surface to approximately 60 cm downward.

1.3.2 Soil Core Collection and Analysis and Soil Pit Excavation

A soil core representing the upper 60 cm of the soil column in the Imnavait watershed was extracted using a 10 cm diameter Snow, Ice, and Permafrost Research Establishment (SIPRE) corer. The core was collected from the same location into which the vertical thermistor string was installed (Figure 1.1). The core was collected during the winter of 2009, wrapped frozen in freezer paper (Reynolds, Lake Forest, IL), transported frozen and stored frozen in a

cold room until analysis. The soil core was collected the winter before collecting surface water measurements and based on yearly thaw depth probing conducted every fall along a grid of 121 points in the Imnavait Creek watershed (Circumpolar Active Layer Monitoring Network-CALM II, 2004-2008) we believe the core represents approximately 40 cm of material that thaws each year (active layer) and approximately 20 cm of the permafrost. The collected core was within 20 meters of the main drainage and relatively level with the main drainage. A soil pit was excavated near the coring location that is nearest the main drainage in Figure 1.1 in July, 2011.

Initially, a soil pit profile was not considered within the scope of this project, but was decided upon only after analysis of all the 2010 samples. Excavating a soil pit gave insight to the relative depth of the permafrost-active layer boundary within the watershed. The 1x1 meter soil pit was excavated to a depth of 90 cm with shovels and a jackhammer and soil horizons were identified following established soil classification methods (Soil Survey Division Staff, 1993; Ping et al., 2013). In addition, we tested for reducing conditions of a hydric soil system using alpha-alpha-dipyridyl, as outlined in Ping et al., (1998), and established by the U.S. Department of Agriculture (USDA, 1999). The soil horizon profiles and alpha-alpha-dipyridyl solution were provided as part of a field workshop on Arctic Soils offered by the University of Alaska Fairbanks taught by Dr. Chien-Lu Ping and Dr. Gary Michaelson of the Palmer Research Center, School of Natural Resources and Agriculture Sciences, University of Alaska Fairbanks.

The frozen soil core was sectioned into 5 cm long sub-samples using a band saw and carbon steel band saw blade (93.5 in x 3/8 inch with 6 tpi) in a cold room at the Cold Regions Research and Engineering Laboratory, Ft. Wainwright, AK. The frozen core sections were thawed for 24 hours at approximately 22°C in plastic bags. Pore water was separated from the soil solids by centrifugation (7,000 rpm for 20 minutes). Water samples were decanted, passed

through 0.20 μm nylon filters (Whatman, Kent, United Kingdom) fitted to a sterile plastic syringes and acidified with 6N ultrapure HNO_3. Soil pore water samples were analyzed following the ICP-MS procedures outlined above for surface water samples.

Each 5 cm subsection of the core was dried at 50°C for approximately 12 hours overnight and sieved to <75 μm (< #200 sieve). Approximately 5-7 gram subsamples were mixed with 5-7 drops of a binder (polyvinyl alcohol) and pressed into a powder pellet using a hydraulic bottle jack at 20,000 psi. Each pellet was analyzed using a PANalytical (Almelo, The Netherlands) Axios four kW wavelength dispersive x-ray fluorescence spectrometer (XRF). The calibration standards for major elements were made using the geologic reference materials BIR-1, PCC-1, JA-2, JB-2, JP-1, JR-1, GXR-3, GXR-1, MRG-1, and SGR-1, as described in Ilgen et al., 2011. Samples and standards were analyzed in triplicate with corresponding errors reported and detection limits calculated based on analysis of the reference standards.

1.3.3 Surface Water Collection and Analysis

All water sample collection sites were located upstream of the Dalton Highway. Nitrile gloves were worn while sampling and water was collected from the main channel of flow using a peristaltic pump outfitted with Masterflex Tygon E-LFL pump tubing (Cole-Parmer, Vernon Hills, Illinois) and precleaned 0.45 μm polycarbonate medium-capacity filter capsules (Geotech Environmental Equipment, Denver, CO). The tubing and filter capsules were flushed for a minimum of 10 seconds before collecting samples into trace metal grade precleaned acid washed 125 mL HDPE bottles. Samples were acidified within six hours of collection with 6 N ultrapure HNO_3 (Baseline Nitric Acid, Seastar Chemicals, Sidney, BC) in a clean hood at the Toolik Field Station.

Chloride concentrations were quantified on a Dionex ICS-3000 ion chromatograph with an AS-19 anion column (Dionex Corporation Sunnyvale, California) at the Cold Regions Research and Engineering Laboratory Alaska Geochemistry Laboratory. Each sample had a 10 mL injection volume. A gradient method using potassium hydroxide eluent ranged from 20 mM to 35mM for anion analyses. The system flow rate was 1 mL/min and the operating temperature was 30°C. The ion chromatograph was calibrated through repeat analysis of five calibration standards with concentrations ranging from 0.1 to 120 mg/L. Laboratory analytical anion standards with values from 0.1 to 120 mg/L were analyzed repeatedly to verify system calibration and assess analytical precision. Based on these analyses the calculated precision for the analyses is ±5 %. Peaks were identified using Chromeleon (Dionex, Sunnyvale, California) and were verified visually.

Surface water trace metal concentrations were measured using an Agilent 7500ce (Agilent Technologies, Santa Clara, CA) inductively coupled plasma-mass spectrometer (ICP-MS) following the general procedure outlined in Creed et al. (1994). To minimize polyatomic interferences from ions having identical mass-to-charge ratios as the analytes the ICP-MS was operated in collision/reaction cell (CRC) mode using either He or H_2 gases following established protocols (Wilbur and Soffey, 2004). Al, Ba, Be, B, Cd, Co, Pb, Au, Mn, Mo, P, Sc, Ag, Te, Tl, Sn, Ti, Zn and the rare earth elements were analyzed in normal mode (no CRC). As, Cr, Cu, Ni and V were analyzed using CRC pressurized with He gas and Fe and Se were analyzed using CRC pressurized with H_2 gas. Of the above elements, Al, Ba, Fe, Mn, Ni, and Zn were above the limit of detection of the ICP-MS.

Six calibration standards were prepared by diluting $1x10^6$ µg/L single element standard solutions and a combined rare earth element standard provided by ULTRA Scientific

(Kingstown, RI). All glassware was washed, and dilutions were made using 2% ultrapure HNO_3 (BDH Aristar Plus, Poole Dorset, UK). A single stock solution of 1,000 µg/L was prepared by diluting 0.1 mL of the $1x10^6$ µg/L single element standard solutions to 100 mL in an acid-washed 100 mL volumetric flask. The 2% ultrapure HNO_3 was also used as a blank. Calibration was performed at the beginning of each analytical run. The resulting calibration curves had R^2 values of 0.998 or better. A check standard and blank were run after every 10 samples and all samples were analyzed in triplicates to quantify analytical uncertainty for each sample.

To correct for temporal variations in signal intensity, an internal standard containing 50 µg/L of Ge, In and Tl was added to all blanks, standards and samples. All detected values fell within the 1-100 µg/L calibration range or were subsequently diluted with ultrapure water (Barnstead Nanopure, Thermo Scientific, Waltham, MA) with a resistivity of 18.1 MΩ and reanalyzed. To confirm the accuracy of the pipettes, the mass of the volume delivered was monitored with an analytical balance. Percent relative standard deviation (% RSD) values were first screened for any significant errors. Values were then corrected for background from repeated analyses of blanks. Measurement error was assigned to each sample analyzed based on the triplicate measurements and shown in each data table.

The surface waters of Imnavait Creek and Roche Mountanee were monitored for in-situ pH measurements during the collection of each sample using a YSI-probe-600xL (YSI, Inc., Yellow Springs, Ohio). The pH probe was calibrated twice per day with 4.0 and 7.0 buffer solutions provided by YSI, Inc. The pH probe was situated 10 meters downstream of where the samples were collected and allowed to equilibrate until the pH measurement was stable.

1.3.4 Thermistor Installation

A thermistor array was installed in the Imnavait watershed study area in 2009 into a hole drilled using a 10 cm diameter, 1 meter long SIPRE augur bit (Figure 1.1). The core material (described above) was removed and an array of four thermistors, attached to a wooden stake, was lowered into the hole. Temperature probes were set approximately 1, 29 , 42 and 53 cm apart. The depth of each thermistor was measured from the ground surface, and a slurry of water mixed with local soil was poured into the hole. The thermistors were connected to a battery powered ONSET-HOBO U12 datalogger (Onset Computer Corporation, Bourne, MA) that logged temperatures hourly in degrees Celsius.

1.4 Results

1.4.1 Soil Pit Profile and Chemical Composition of Soil Column

The soil pit profile excavated for this study and detailed horizons are shown in Figure 1.2. The top portions of the horizons have a high chroma color, whereas the lower portions appear more gleyed, potentially signifying a redox boundary. With further testing of the lower portion of the soil (~ 5 g excavated at roughly 50cm depth) with 3-5 drops of alpha-alpha-dipyridyl yielded a positive pink color within 30 sec, signifying the presence of ferrous iron and reducing conditions. In addition, there was a clear difference in color along the soil horizons and the different redox zones were observed visually upon excavation of the soil pit in Imnavait Creek. The upper 0-20 cm portion exhibited the typical orange-rust color characteristic of Fe(III) during excavation and after. Upon excavation of the lower 25-90 cm, the soil horizons initially displayed a dark, lustrous gray-black color, but within minutes of being exposed to the

atmosphere, orange-rich bands began to appear from 25-90 cm. The optical image in Figure 1.2 was taken approximately 5 minutes after excavation of the full soil pit and after the testing with alpha-alpha-dipyridyl. This change in soil chroma as a function of excavation time is likely due to in-situ oxidation of Fe(II) to Fe(III).

Within the watershed and adjacent to the soil pit, we collected a 61 cm soil core. Vertical metal concentrations in mg/kg (ppm) determined by XRF are provided in Table 1.1 and plotted as a function of soil core depth in Figure 1.3. Fe, Mn and Zn are enriched in the organic layer, likely due to their association with natural organic matter (NOM) present (Figure 1.2). By comparison, Al, Ba, Cr, Ti, and Zr, as well as Rb, and V (not shown in Figure 1.3, but data provided in Table 1.1) are enhanced in the lower soil horizons. Ni concentrations stay relatively constant throughout the soil core (Table 1.1). Because Cr and V typically accumulate in reducing zones, their enriched concentrations relative to the upper portions of the soil column can reveal their environmental setting (Kimbrough et al., 1999). This clear separation between metals either accumulating in the upper portions of the soil column or enhanced lower in the soil column qualitatively correlates with the variation in redox conditions within the soil.

The soil pore water concentrations are provided in Table 1.2 and are plotted as a function of depth along the core in Figure 1.4. These data represent the soluble fraction likely available for transport to the surrounding surface water. Al, Ba, Fe, and Mn and to some extent Zn, all are present as soluble species in both the upper (~10-20 cm) and deeper (~35-50 cm) parts of the soil column.

1.4.2 Soil Thermal Regime

Temperature data from the logger installed at Imnavait Creek is shown in Figure 1.5. The soil temperature at the surface correlates with fluctuations in the local ambient air temperature. When the soil begins to thaw in the Arctic spring, it thaws predominantly from the top-down. Soil at 1, 29, 42 and 53 cm depth was fully frozen as of April 28, 2010 when we initiated measurements. Thawing (temperatures rising above 0° Celsius) began on May 13 at the surface, on May 23 at 29 cm depth, on June 12 at 42 cm depth and on July 29 at 53 cm depth.

1.4.3 Surface Water Metal Concentrations at Imnavait Creek

Surface water concentrations of Al, Ba, Fe, Mn, Ni, and Zn (in µg/L) are provided in Table 1.3 and are plotted as a function of sampling date in Figure 1.6. The remaining measured metals outlined in the methods section were at or below the detection limit of the analytical method. Late fall and early winter yielded the highest influx of Al, Ba, Fe, and Mn to Imnavait Creek. Ni concentrations were relatively constant throughout the summer. Zn behaved similarly to Al, Ba, Fe, and Mn except that concentrations do not rise towards the end of fall consistent with the observation that Zn does not have an enhanced solubility signature deeper in the soil column (Figure 1.4). Mn and Zn concentrations peaked during spring snowmelt and late fall. All other metals exhibited a gradual increase in concentrations until the end of September, with peak values in early October. We expected to see high, relative metal influxes to surface water as a result of spring snowmelt, but for Fe, Al, Ba and Ni that was not the case, likely a result three possible attributions: (1) low, relative solubility of the species present at the top layers of the surface (2) the Fe, Al and Ba concentrations seem low in comparison to the high, relative influx of these metals late in the season and/or (3) our sampling season missed peak snowmelt values

for these specific metals. Highest measured concentrations of 175.6 µg/L (Al), 15.4 µg/L (Ba), 3383.0 µg/L (Fe), and 165.2 µg/L (Mn), occurred on October 8, 2010. Maximum Zn concentrations of 4.3 and 4.4 µg/L occurred on May 19 (spring freshet) and August 7. Ni concentrations stayed relatively constant between 1.1 and 2.0 µg/L throughout the melt season.

Imnavait Creek exhibits acidic surface water conditions for the entirety of summer. The pH values for Imnavait Creek as a function of sampling date is presented in Figure 1.7. In the spring, pH values are at their lowest for the entire season, dipping below 5 to a value of 4.79 on May 17, 2010. For the majority of late May-June, pH values average to 5.80 with a range from 5.54 to 6.02. Throughout the end of July until mid-August, daily pH variability increases with an average value of 5.71, ranging from 5.06 to 6.62. During late fall, pH fluctuates to a greater extent in September than October. Imnavait Creek surface water in September has an average pH of 5.99, ranging from 5.32 to 6.64. For October, the average is 5.65, ranging from 5.24 to 6.00. Overall, Imnavait Creek in late fall/early winter, including both September and October months, exhibits an average pH of 5.84, ranging from 5.24 to 6.64. The lowest pH for the time period occurs in October and the highest pH occurs in September.

1.4.4 Surface Water Metal Concentrations at Roche Mountanee Creek

Metal concentrations observed in the surface waters of Roche Mountanee Creek in 2010 are provided in Table 1.4 and plotted as a function of sampling date in Figure 1.8. Al, Fe and Mn concentrations increased during the first spring melt flows in mid-May, when flow is predominately derived from surface soils and the organic layer. Al and Fe also exhibited increased concentrations during rain events in late July and early August. In the fall, Al, Fe, and Mn concentrations decreased to the lowest values measured, mostly hovering at or below their

respective detection limits. The pattern for Ba in Roche Mountanee Creek mimics the patterns for Al, Ba, Fe, and Mn in Imnavait Creek with the highest concentrations occurring in late fall. The highest measured Ba concentration of 70.0 µg/L occurred on October 13. On May 18, Al, Fe and Mn concentrations peaked at 107.0, 194.8, and 4.2 µg/L, respectively.

For the most part, Roche Mountanee surface water is slightly basic. pH values range from 6.98 to 8.06. The pH values for Roche Mountanee as a function of sampling date is presented in Figure 1.7. pH values in the spring for Roche Mountanee range from 6.98 to 8.06, with an average value of 7.73. During late July and early August, pH values range from 7.32 to 8.03, with an average pH value of 7.75. During late September and the first half of October, pH values range from 7.17 to 8.06, with an average pH value of 7.52. The lowest observed pH value occurs on May 17, 2010 and the highest recorded pH value occurs on both May 23 and September 13, 2010.

1.5 Discussion

1.5.1 Seasonal Controls on Metal Fluctuations in Imnavait Creek Surface Water

As shown in Figure 1.4, pore waters in the oxidizing zone (~10-20 cm depth) of the organic layer have relatively high metal concentrations. In comparison, pore waters deeper in the soil column (~30-55 cm) also exhibit an enhanced relative mobility of metals. This depth corresponds to the typical maximum vertical extent of seasonal thaw (the active layer) each fall. In the case of Fe, the soluble-rich bands in both the oxidizing and reducing zones are comparable in terms of their bulk aqueous metal concentrations (Figure 1.4). However, when compared to

the source concentration originally present in the core in solid form (Figure 1.3), the difference is substantial. There is approximately 140,000 mg/kg Fe present in the 15-20 cm portion of the organic layer with approximately 5.5 mg/L of that being soluble. In comparison, there is approximately 25,000 mg/kg Fe present in the reduced zone lower in the soil column (~35-55 cm) and approximately 4 mg/L becomes mobilized upon thawing. Based on the solubility signatures depicted in Figure 1.4, the Fe species at the surface is fully oxidized Fe(III), likely in the form of amorphous ferric (hydr)oxides and/or Fe(III)-organo-complexes. Similar Fe redox species were detected in boreal catchments by Sundman et al., (2014) and characterized using x-ray absorption spectroscopy (XAS). Therefore, based on several observations, including field tests for reducing, hydric soils, observations of the soil pit profile during sampling, and the solubility signature of dissolved Fe in Figure 1.4, Fe in the active layer predominantly occurs as Fe(II), which is much more soluble than Fe(III) (Schwertmann, 1991).

The metal solubility profiles elucidated from the data in Figures 1.3 and 1.4 is summarized in Figure 1.9 by plotting the metal partition coefficients (Kd) as a function of depth of the soil core. K_d values were calculated using the ratio of metal concentrations in the solid fraction of the soil core to the metal concentrations in the pore water extracted from the soil fraction (values shown in Table 5). Therefore, a small, relative partition coefficient is indicative of high, relative partitioning from the solid to the aqueous phase.

Fe, Al and to some extent Mn, Ba and Zn exhibit a band of high, relative solubility from 10-15 cm. We expected to see evidence of this solubility band by a mass Fe mobilization and to some extent Al to Imnavait Creek during spring snowmelt (Figure 1.6), but as stated previously there is potential that these species present above 10 cm soil depth are not as soluble or Fe and Al mobilized before our sampling began May 19, 2010. We do not have bulk metal

concentrations for the soil column above 10 cm due to the prevalence of moss and plants instead of actual soil. However, Mn and Zn concentrations have a relative peak in mid-May, unlike Fe, Al or Ba, therefore signal dilution from snowmelt as the sole factor seems unlikely. We would expect all metals to behave similarly if that were the case.

In the summer months, the soil column continues to thaw and the active layer deepens, this is evident by slightly increasing surface water metal concentrations over the course of June, July and August for Fe, Al, Mn, Ni, Zn and Ba (Figure 1.6), correlating with low partition coefficients for Fe and Mn and to some extent Al, Ba and Zn at soil depths 20-45 cm (Figure 1.9). According to the soil thermal regime (Figure 1.5), the soil is thawed for depths 0, 29 and 42 cms at this time, but remains frozen at depth 53 cm.

The soil at depth 53 cm initiated thawing on July 29th, 2010. All metals exhibit bands of small, relative partition coefficients (high, relative solubility) at depths 45-61 cm. Aluminum mostly obeys this except at lower depths (50-61 cm) the solubility decreases, again. The low partition coefficient of these metals in the lower portions of the soil column correlated to the subsequent thawing of these layers and likely produces the high, relative surface water concentrations in Imnavait Creek in late September, early October. This is evident for Fe, Al, Mn, and Ba, but not Zn or Ni. Nickel concentrations stay relatively constant throughout the sampling season, except for in mid-May when they are at the detection limit for the analytical method. Zinc concentrations decrease during late fall, which suggests that any increase in the concentration of metals in surface waters during this time of year as an effect of discharge is likely not a factor, as all metals would be expected to continue to increase like Fe, Al, Mn and Ba. Furthermore, Zn geochemistry in late Arctic fall is potentially more complex than our interpretations can predict.

1.5.2 Permafrost Active Layer Dynamics Inferred at Roche Mountanee Creek

The majority of this project focused on characterizing soil and surface water samples from Imnavait Creek, a small, organic-rich, low gradient tundra stream. In an attempt to correlate our findings at Imnavait Creek to a broader area in the Arctic, including to a large watershed with higher gradient and exposed bedrock, we analyzed surface water collected from Roche Mountanee Creek (Table 1.4 and Figure 1.8). We did not collect a core, excavate a soil pit, or install thermistors at Roche Mountanee Creek, and no CALM site is present there. Thus, we mainly use data from Roche Mountanee Creek to investigate whether the seasonal dynamics present in Imnavait Creek also occur for a larger, higher gradient stream with different soil, active layer and permafrost composition.

The soils at Roche Mountanee are sourced predominantly from carbonate bedrock with minimal organics present in the surface and shallow subsurface (Till et al., 2008). The Al, Fe and Mn concentrations measured during the spring are derived from the weathering of the thin, upper portions of the subsurface. Once the source of those metals weather and subsequently freezes (assuming temperature fluctuations behave similarly as recorded at Imnavait, Figure 1.5), Al, Fe and Mn concentrations substantially drop during the summer and are at the detection limit of our analytical method during the fall and early winter.

We interpret the late season increase in Roche Mountanee surface water Ba concentrations to the late fall mobilization of Ba from the weathering of carbonate rocks in the active layer. The fluid characteristic of the late season flow path in comparison to the spring and summer primarily embodies water-rock interactions. Because bedrock has a low permeability, the thaw front has to move fairly deep into the active layer. Therefore, Ba concentrations in

Roche Mountanee increase in the late fall when the pore water flow paths are forced deeper into the soil column due to freezing of the surface and shallow subsurface.

1.5.3 Surface Water Trace Metal Signatures as a Function of Snowmelt, Precipitation and Groundwater Influence

Discharge and primary source of water play a role in the overall transport of metals to surface waters. However, discharge measurements can be convoluted, particularly when there are multiple main channels and if ice is present. In addition, identifying the primary source of water contributing to the overall discharge of a river at any given time of the year is necessary to understanding seasonal element fluctuations, as a whole. For this study, we employed surface water chloride concentrations as a tracer for estimating the primary source of water flow to Imnavait Creek and Roche Mountanee. We utilized chloride because it occurs in the environment primarily as a free ion, rarely complexes or forms ion pairs and moves through soil without being significantly transformed (Lockwood et al., 1995; Albek, 1999).

Trace metal-chloride relationships for Roche Mountanee and Imnavait Creek surface waters are shown in Figure 1.10 (a) and (b). Only Ba values are presented for Roche Mountanee surface water because concentrations of Fe, Al and Mn were primarily present at or below the detection limit for our method. Roche Mountanee Ba-chloride relationship represents a simple, ideal model for estimating the dominant water source in our Arctic systems. The snowmelt signature is characterized by having high chloride concentrations, derived from the snowpack and low relative metal contributions, considering pristine snowpack should contain trace amounts of metals. The melting process of the snowpack mobilizes metals into the local surface water and with the changing season from spring to summer the dominant source of water in the

Arctic is from precipitation. It is important to note that during the spring and summer, there are potentially additional sources of precipitation, i.e., melting of adjacent glaciers and base flow influence, but these are considered minor in comparison to summer precipitation events.

In the fall, pore waters are forced deeper in the soil column as a result of the top-down freezing processes in the Arctic and the water source is dominated by groundwater influence. This is highlighted in Figure 1.10 and evident by a signature of older, deeper water. Ba concentrations in late fall increased as a result of weathering the lower portions of the soil column and mobilizing Ba in the soil pore water. There is an increase in chloride concentrations above the normal variability of summer rain events, but not to the extent that the melting of the snowpack in May provides. However, there is still variability in chloride concentrations late in the season, even in October (Table 1.4), indicating Ba signal concentration due solely to lack of precipitation late in the season (Figure 1.6) is likely not a factor.

For Imnavait Creek, metal-chloride relationships are more muddled than at Roche Mountanee. The snowmelt signature is apparent, but the transition from being dominated by precipitation to a groundwater-dominated creek is less clear, than in Roche Mountanee. For Fe, Mn and to some extent Al and Ba, the transition is visible. This transition occurs while the soil surface and shallow subsurface is frozen and the soil column at lower depths is thawed (Figure 1.9). For Zn and Ni, the chloride relationship is unclear, likely attributed to the low overall concentrations of Zn and Ni creating a lack of sensitivity in this kind of relationship.

One goal of this project was to determine if we could detect other dominant sources of water in addition to snowmelt, precipitation and groundwater that would influence trace metal transport to local surface waters. In particular, the thawing of the top centimeters of the

permafrost may provide another source of metals to surrounding surface waters, but our metal-chloride results likely indicate (1) if there is a metal signature from permafrost thaw it is not discernable over the metal signature from groundwater for our dataset and (2) longer monitoring strategies are necessary to determine if and to what extent metal fluctuations to surface waters are influenced by permafrost thaw.

1.5.4 A Conceptual Model of Permafrost Active Layer Dynamics

A conceptual model for the soil thawing and freezing process and the deepening of the active layer throughout the course of 2010 is schematically illustrated in Figure 1.11. As our model suggests, the organic layers and upper portion of the soil column begin to thaw following the snow melt in mid-May and are fully thawed by the end of May. This exposes the surface soil to oxidation and weathering processes, releasing soluble metals from the soil and vegetation surface and flushing them into nearby surface waters. Once the soil below the surface and organic layer begins to thaw and the active layer extends downward, acidic pore water from the surface reaches the reducing front of the subsurface and mobilizes metals.

When the soil begins to freeze in the fall, it freezes predominantly from the top-down (Figure 1.11). Top-down freezing forces pore water flow paths deeper into the reducing zone of the soil column, where Fe, Al, Ba and Mn are mobile (Figure 1.4), and exhibit low, relative partition coefficients.. Acidic conditions, deepening flow paths and greater source concentrations with respect to depth during this time of the year contribute to the overall high, relative metal concentrations shown in Figure 1.6. Zn concentrations decrease because the source of Zn decreases (Figure 1.3) and Ni concentrations stay relatively constant because the partition coefficient is assumed to be constant with respect to depth. During the time of the season when

the active layer is at its deepest yearly extent, the surface of the soil column is frozen (late September/October in Figure 1.11), and the surface water geochemical composition roughly correlates to the solubility of the metal species in the exposed soil layers.

An anticipated increase in active layer thaw depths (Hinzman and Kane, 1992; Osterkamp and Romanovsky 1997; 1999; Jorgenson et al., 2006, Christiansen et al., 2010; Romanovsky et al., 2010; Smith et al., 2010), or, due to subsidence, a downward movement in the thaw front over time (Belshe et al., 2012; LeBlanc et al., 2012) would liberate previously frozen soils and expose them to mineral weathering processes. This is presented as the downward movement of the top of the stippled "permafrost" layer in Figure 1.11 in September and November. The baseline results from this study demonstrate there is likely a key relationship between the extent of the active layer thaw, redox environment of the soil as a function of depth and trace metal fluctuations to local surface waters and that relationship is complex and warrants the attention of multi-year monitoring. However, any future effects of this anticipated downward progression as a whole are unknown.

1.6 Conclusions

Future climate scenarios predict a warmer Arctic, which is expected to cause permafrost degradation and the downward movement of the seasonally thawed active layer, exposing fresh soil to mineral weathering processes. This expected result of a warmer Arctic affects trace metal signatures in surface waters due to mineral weathering providing a significant source of metals in pristine systems. One goal of this study was to discern whether geochemical signatures of trace metals in surface waters could provide a landscape or watershed scale proxy for thawing

processes in permafrost soils. Our results show a distinct seasonal signature of trace metal concentrations in Imnavait and to a lesser extent Roche Mountanee Creeks. Stream water concentrations of Al, Ba, Fe, and Mn in Imnavait Creek were highest in the late fall (September and October). This pattern appears to correlate with the depth of the active layer throughout the watershed. The signal for Ba was detectable in both a low gradient tundra stream and a larger high gradient bedrock dominated stream. Other metals (Al, Fe, and Mn) experienced enhanced concentrations in late fall flows in the smaller low gradient stream, but these metals did not exhibit a late fall increase in the higher gradient bedrock dominated stream, likely due to the difference in the soil composition, pH, organic ligand content and soil water flow rates for the two compared streams.

Our findings show that the transport, mobility and ultimate fate of metals to local surface waters as a result of pristine mineral weathering is complex and likely controlled by a variety of factors, particularly speciation. The transport and behavior of trace metals strongly depends on local soil conditions, especially the redox environment. Increased water infiltration at the permafrost-active layer boundary as a result of increasing air temperatures could significantly impact stream water trace metal signatures due to mineral weathering of unfrozen soil being a major contributor of metals to local surface waters. Therefore, deepening of the active layer may cause detectable changes in surface water geochemical signatures. Over time, as permafrost degrades and exposes previously frozen, metal-rich layers, we hypothesize that the late season trace metal signal could be differentiated from the groundwater-dominated signal. However, there are many noteworthy limitations to this hypothesis, particularly differentiating between fluctuating active layer thicknesses due to normal variability, as opposed to longer-term trends. In order to establish a noteworthy trend relating surface water metal concentrations with

increasing active layer depth/degrading permafrost, a watershed likely warrants continuous monitoring of active layer dynamics, in addition to soil and surface water geochemical measurements.

Presently, this study offers many improvements on previous efforts and provides a baseline of data for future monitoring in Arctic Alaska. Our results capture the seasonality of trace metals in two Arctic watersheds from spring snowmelt until early winter, a measurement that is widely overlooked. Our findings highlight a correlation between the top-down freezing processes that occurs in Arctic soils to metal fluctuations in local surface waters. In addition, our results highlight the complexity of metal transport as a function of seasonality in the presence of permafrost, necessitating the need for longer summer sampling seasons in the Arctic.

1.7 Acknowledgments

Funding for this project was from the U.S. National Science Foundation, Office of Polar Programs to Douglas (#0806714), Jacobson (#0806643) and McClelland (#0806827). Toolik Field Station of the University of Alaska Fairbanks-Institute of Arctic Biology and CH2MHILL Polar Field Services provided logistical support. Numerous students and collaborators are acknowledged on this project for field and laboratory assistance. Soil horizon profiles were provided as part of a field workshop on Arctic Soils offered by the University of Alaska Fairbanks taught by Dr. Chien-Lu Ping and Dr. Gary Michaelson of the Palmer Research Center, School of Natural Resources and Agriculture Sciences, University of Alaska Fairbanks. Air temperature data are courtesy of the National Science Foundation funded (award #1023052) SnowNET Project through a collaboration with Matthew Sturm (CRREL-Alaska, now at the

University of Alaska Fairbanks). Toolik area precipitation data were provided by Jessie Cherry of the University of Alaska Fairbanks. Soil characterization and metal analysis (XRD, XRF and ICP-MS instrumentation) was accomplished at the University of Alaska Fairbanks-Advanced Instrumentation Laboratory with the assistance of Karen Spaleta, Maciej Sliwinski and Ken Severin.

1.8 References

Albek, E. 1999. Identification of the different sources of chlorides in streams by regression analysis using chloride-discharge relationships. Water Environ. Res., 71, 1310.

Arndt, D.S., Baringer, M.O. Johnson, M.R. eds. 2010: State of the climate in 2009. Bulletin of the American Meteorology Society 91:6, S1-S224.

Bagard, M.L., Chabaux, F., Pokrovsky, O.S., Viers, J., Prokushkin, A.S., Stille, P., Rihs, S., Rihs, S., Schmitt, A.D., Dupré, B. 2011. Seasonal variability of element fluxes in two Central Siberian rivers draining high latitude permafrost dominated areas. Geochimica et Cosmochimica Acta. 75, 3335-3357.

Belshe, E.F., Schuur, E.A.G., Bolker, B.M., Bracho, R. 2012. Incorporating spatial heterogeneity created by permafrost thaw into a landscape carbon estimate. Journal of Geophysical Research. 117:G01026.

Black, R.F. 1976. Periglacial features indicative of permafrost: ice and soil wedges. Quaternary Research. 6, 3-26.

Chapin, F.S., III, Sturm, M., Serreze, M.C., McFadden, J.P., Key, J.R., Lloyd, A.H., McGuire, A.D., Rupp, T.S., Lynch, A.H., Schimel, J.P., Beringer, J., Chapman, W.L., Epstein, H.E., Euskirchen, E.S., Hinzman, L.D., Jia, G., Ping, C.L., Tape, K.D., Thompson, C.D.C., Walker, D.A., Welker, J.M. 2005. Role of land-surface changes in Arctic summer warming. Science. 310, 657-660.

Christiansen, H.H., Etzelmüller, B., Isaksen, K., Juliussen, H., Farbrot, H., Humlum, O., Johansson, M., Ingeman-Nielsen, T., Kristensen, L., Hjort, J., Holmlund, P., Sannel, A.B.K., Sigsgaard, C., Åkerman, H.J., Foged, M., Blikra, L.H., Pernosky, M.A., Ɵdegård, R. 2010. The thermal state of permafrost in the Nordic area during IPY 2007-2009. Permafrost Periglacial Pro. 21, 158-181.

Cooper, L., Benner, R., McClelland, J., Peterson, B., Holmes, R., Raymond, R., Hansell, D., Grebmeier, J., Codispoti, L. 2005. Linkages among runoff, dissolved organic carbon, and the stable oxygen isotope composition of seawater and other water mass indicators in the Arctic Ocean. Journal of Geophysical Research 110:G02013.

Cooper, L., McClelland, J.W., Holmes, R.M., Raymond, P.A., Gibson, J.J., Guay, C.K., Peterson, G.J. 2008. Flow-weighted values of runoff tracers (δ18O, DOC, Ba, alkalinity) from the six largest arctic rivers. Geophysical Research Letters, L18606.

Creed, J., Brockhoff, C., Martin, T. 1994. EPA method 200.8, Revision 5.4 Determination of trace elements in waters and wastes by inductively coupled plasma - mass spectrometry. United States Environmental Protection Agency.

Dai, M.H., Martin, J.M. 1995. First data on trace metal level and behavior in two major Arctic river-estuarine systems (Ob and Yenisey) and in the adjacent Kara Sea, Russia. Earth and Planetary Science Letters. 131, 127-141.

Everett, K.R., Marion, G.M., Kane, D.L. 1989. Seasonal geochemistry of an Arctic tundra drainage basin. Holarctic Ecology. 12, 279-289.

Guieu, C., Huang, W.W., Martin, J.M., Yong, Y.Y. 1996. Outflow of trace metals into the Laptev Sea by the Lena River. Mar. Chem. 53, 255-267.

Hamilton, T.D. 1986. Late Cenezoic glaciation of the Central Brooks Range. In: Hamilton, T.D., Reed, K.M., Thorson, R.M. (eds), Glaciation in Alaska: the Geologic Record. Alaska Geological Society. 9-49.

Hinzman, L.D., Kane, D.L., Gieck, R.E., Everett, K.R. 1991. Hydrologic and thermal properties of the active layer in the Alaskan Arctic. Cold Reg. Sci. Techno. 19, 95-110.

Hinzman, L.D., Kane D.L. 1992. Potential response of an Arctic watershed during a period of global warming. Journal of Geophysical Research-Atmospheres. 97, 2811-2820.

Hinzman, L.D., Bettez, N.D., Bolton, W.R., Chapin, F.S., Dyurgerov, M.B., Fastie, C.L., Griffith, B., Hollister, R.D., Hope, A., Huntington, H.P., Jensen, A.M., Jia, G.J., Jorgenson, T., Kane, D.L., Klein, D.R., Kofinas, G., Lynch, A.H., Lloyd, A.H., McGuire, A.D., Nelson, F.E., Oechel, W.C., Osterkamp, T.E., Racine, C.H., Romanovsky, V.E., Stone, R.S., Stow, D.A., Sturm, M., Tweedie, C.E., Vourlitis, G.L., Walker, M.D., Walker, D.A., Webber, P.J., Welter, J.M., Winker, K.S., Yoshikawa, K. 2005. Evidence and implications of recent climate change in northern Alaska and other arctic regions. Climatic Change. 72, 251-298.

Ilgen, A.G., Rychagov, S.N., Trainor, T.P. 2011. Arsenic speciation and transport associated with the release of spent geothermal fluids in Mutnovsky Field (Kamchatka, Russia). Chemical Geology, 288, 115-132.

Jorgenson, M.T., Shur, Y.L., Pullman, E.R. 2006. Abrupt increase in permafrost degradation in Arctic Alaska. Geophysical Research Letters. 33:L02503.

Kane, D.L., Hinzman, L.D., Benson, C.S., Everett, K.R. 1989. Hydrology of Imnavait Creek, an Arctic watershed. Holarctic Ecology. 12, 262-269.

Kane, D.L., Hinzman, L.D., McNamara, J.P., Zhang, Z., Benson, C.S. 2000. An Overview of a Nested Watershed Study in Arctic Alaska, Nordic Hydrology. 31:4/5, 245-266.

Keller, K., Blum, J.D., Kling, G.W. 2007. Geochemistry of soils and streams on surfaces of varying ages in Arctic Alaska. Arctic, Antarctic, and Alpine Research. 39, 84-98.

Keller, K., Blum, J.D., Kling, G.W. 2010. Stream geochemistry as an indicator of increasing permafrost thaw depth in an arctic watershed. Chemical Geology. 273, 76-81.

Kimbrough, D.E., Cohen, Y., Winer, A.M., Creelman, L., Mabuni, C. 1999. A critical assessment of chromium in the environment. Critical Reviews in Environmental Science and Technology. 29:1.

LeBlanc, A., Short, N., Oldenborger, G., Mathon-Dufour, V., Allard, M. 2012. Geophysical investigation and InSAR mapping of permafrost and ground movement at the Iqaluit Airport. Cold Regions Engineering. 644-654.

Lockwood, P.V., McGarity, J.W., Charley, J.L. 1995. Measurement of chemical weathering rates using natural chloride as a tracer. Geoderma. 64:3-4, 215-232.

Martin, J.M., Guan, D.M., Elbaz-Poulichet, F., Thomas, A.J., Gordeev, V.V. 1993. Preliminary assessment of the distribution of some trace elemtns (As, Cd, Cu, Fe, Ni, Pb and Zn) in a pristine aquatic environment: the Lena River estuary (Russia). Mar. Chem. 43, 185-199.

McClelland, J.W., Stieglitz, M., Pan, F., Holmes, R.M., Peterson, B.J. 2007. Recent changes in nitrate and dissolved organic carbon export from the upper Kuparuk River, North Slope, Alaska. J. Geophys. Res. 112:G04S60.

McNamara, J.P., Kane, D.L., Hinzman, L.D. 1997. Hydrograph separations in an Arctic watershed using mixing model and graphical techniques. Water Resources Research. 33:7, 1707-1719.

McNamara, J.P., Kane, D.L., Hinzman, L.D. 1998. An analysis of stream flow hydrology in an Arctic drainage basin: a nested watershed approach. Journal of Hydrology. 206, 39-57.

Muskett, R.R., Romanovsky, V.E. 2011. Alaskan permafrost groundwater storage changes derived from GRACE and ground measurements. Remote Sensing. 3, 378-397.

Osterkamp, T.E., Payne, M.W. 1981. Estimates of permafrost thickness from well logs in northern Alaska. Cold Reg. Sci. and Technol. 5, 13-27.

Osterkamp, T.E., Romanovsky, V.E. 1997. Thawing of the active layer on the coastal plain of Alaskan Arctic. Permafrost and Periglacial Processes. 10:1, 17-37.

Osterkamp, T.E., Romanovsky, V.E. 1999. Evidence for warming and thawing of discontinuous permafrost in Alaska. Permafrost and Periglacial Processes. 8, 1-22.

Peterson, B.J., Holmes, R.M., McClelland, J.W., Vorosmarty, C.J., Lammers, R.B., Shiklomanov, I.A., Shiklomanov, A.I., Rahmstorf, S. 2002. Increasing river discharge to the Arctic Ocean, Science. 298, 2171-2173.

Petrone, K.C., Jones, J.B., Hinzman, L.D., Boone, R.D. 2006. Seasonal export of carbon, nitrogen, and major solutes from Alaskan catchments with discontinuous permafrost, Journal of Geophysical Research. 111. G02020.

Ping, C.L., Bockheim, J.G., Kimble, J.M., Michaelson, G.J., Walker, D.A. 1998. Characteristics of cryogenic soils along a latitudinal transect in arctic Alaska. Journal of Geophysical Research, 103, 917-28.

Ping, C.L., Clark, M.H., Kimble, J.M., Michaelson, G.J., Shur, Y., Stiles, C.A. 2013. Sampling Protocols for permafrost-Affected Soils. Soil Horizons. 54:1.

Pokrovsky, O.S., Shirokova, L.S., Kirpotin, S.N., Audry, S., Viers, J., Dupré, B. 2011. Effect of permafrost thawing on organic carbon and trace element colloidal speciation in the thermokarst lakes of western Siberia. Biogeosciences. 8, 565-583.

Rember, R., Trefry, J. 2004. Increased concentrations of dissolved trace metals and organic carbon during snowmelt in rivers of the Alaskan Arctic. Geochimica et Cosmochimica Acta. 68:3, 477-489.

Romanovsky, V.E., Drozdov, D.S., Overman, N.G., Malkova, G.V., Kholodov, A.L., Marchenko, S.S., Moskalenko, N.G., Sergeev, D.O., Ukraintseva, N.G., Abramov, A.A., Gilichinsky, D.A., Vasiliev, A.A. 2010. Thermal State of Permafrost in Russia, Permafrost Periglacial Pro. 21, 136-155.

Schwertmann, U. 1991. Solubility and dissolution of iron oxides. Plant and Soil. 130, 1-25.

Smith, S.L., Romanovsky, V.E., Lewkowicz, A.G., Burn, C.R., Allard, M., Clow, G.D., Yoshikawa, K., Throop, J. 2010. Thermal state of permafrost in North America-A contribution to the international polar year. Permafrost Periglacial Pro. 21, 117-135.

Soil Survey Division Staff. 1993. Soil survey manual. Soil Conservation Service. U.S. Department of Agriculture Handbook 18.

Sundman, A., Karlsson, T., Laudon, H., Persson, P. 2014. XAS study of iron speciation in soils and waters from a boreal catchment. Chemical Geology. 364, 93-102.

Till, A.B., Dumoulin, J.A., Harris, A.G., Moore, T.E., Bleick, H.A., Siwiec, B.R. 2008. Bedrock geologic map of the southern Brooks Range, Alaska, and accompanying conodont data: U.S. Geological Survey Open-File Report 2008-1149, 88 p.

Townsend-Small, A., McClelland, J.W., Holmes, R.M., Peterson, B.J. 2010. Seasonal and hydrologic drivers of dissolved organic matter and nutrients in the upper Kuparuk River, Alaskan Arctic. Biogeochemistry. 103, 109-124.

(USDA) U.S. Department of Agriculture, Soil Survey Staff, 1999. Soil Taxonomy: A Basic System of Soil Classification for Making and Interpreting Soil Surveys. Agriculture Handbook. Number 436.

Vuceta, J., Morgan, J.J. 1978. Chemical modeling of trace metals in fresh waters: role of complexation and adsorption, Environ. Sci. Tech. 12:12, 1302-1309.

Walker, D.A., Gould, W.A., Maier, H.A., Raynolds, M.K. 2002. The Circumpolar Arctic Vegetation Map: AVHRR-derived base maps, environmental controls, and integrated mapping procedures. International Journal of Remote Sensing. 23:21, 4551-4570.

Walker, M.D., Walker, D.A., Everett, K.R. 1989. Wetland Soils and Vegetation, Arctic Foothills, Alaska. US Department of the Interior Biological Report. 89:7.

White, D., Hinzman, L., Alessa, L., Cassano, J., Chambers, M., Falkner, K., Francis, J., Gutowski, W.J., Jr., Holland, M., Holmes, R.M., Huntington, H., Kane, D., Kliskey, A., Lee, C., McClelland, J., Peterson, B., Rupp, T.S., Straneo, F., Steele, M., Woodgate, R., Yang, D., Yoshikawa, K., Zhang, T. 2007. The Arctic freshwater system: changes and impacts. Journal of Geophysical Research. 112:G04S54, 21 p.

Wilbur, S., Soffey, W. 2004. Performance Characteristics of the Agilent 7500ce - The ORS Advantage for High Matrix Analysis, Agilent.

Yang, D., Kane, D.L., Hinzman, L.D., Zhang, X., Zhang, T., Ye, H. 2002. Siberian Lena River hydrologic regime and recent change. J. Geophys. Res. 107:D23.

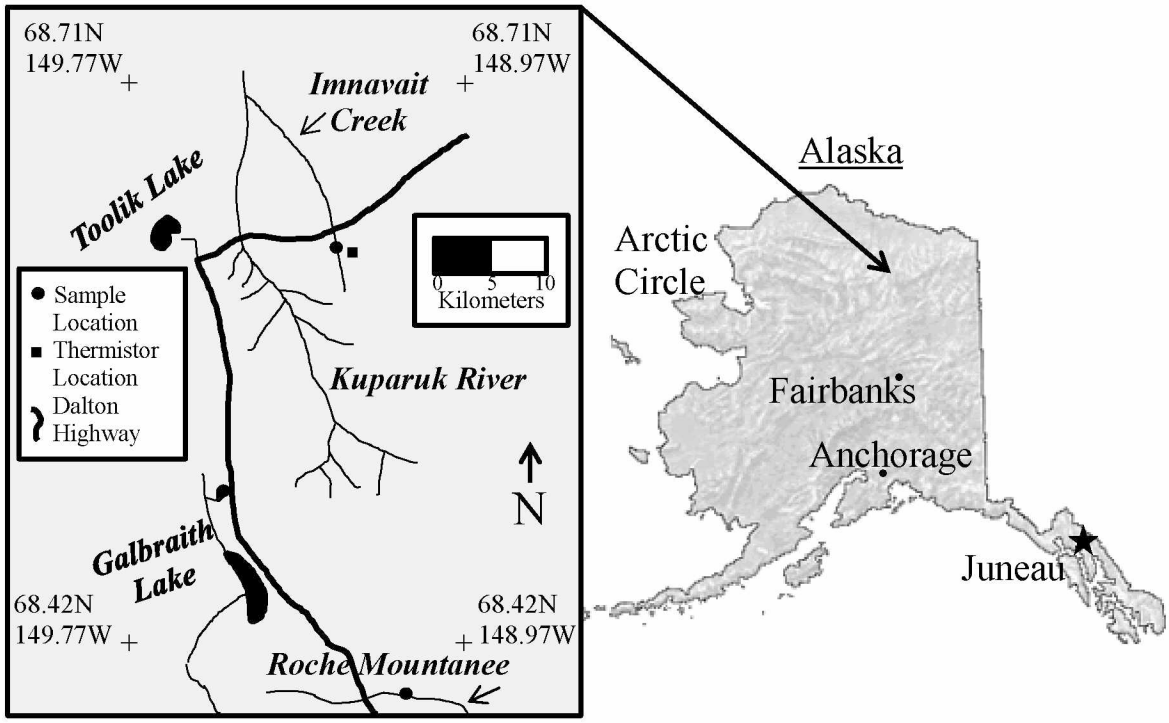

Figure 1.1 Map of study area.

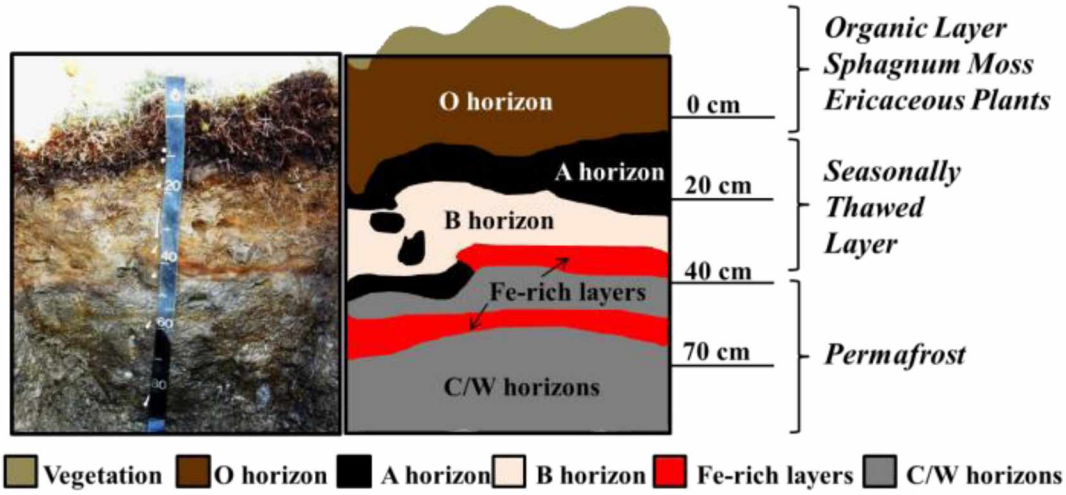

Figure 1.2 Soil pit profile

Soil pit profile and detailed soil horizons at Imnavait Creek watershed basin. Profile shows an oxidation/reduction front at approximately 40 cm depth, substantial organic layer on the surface and cryoturbation.

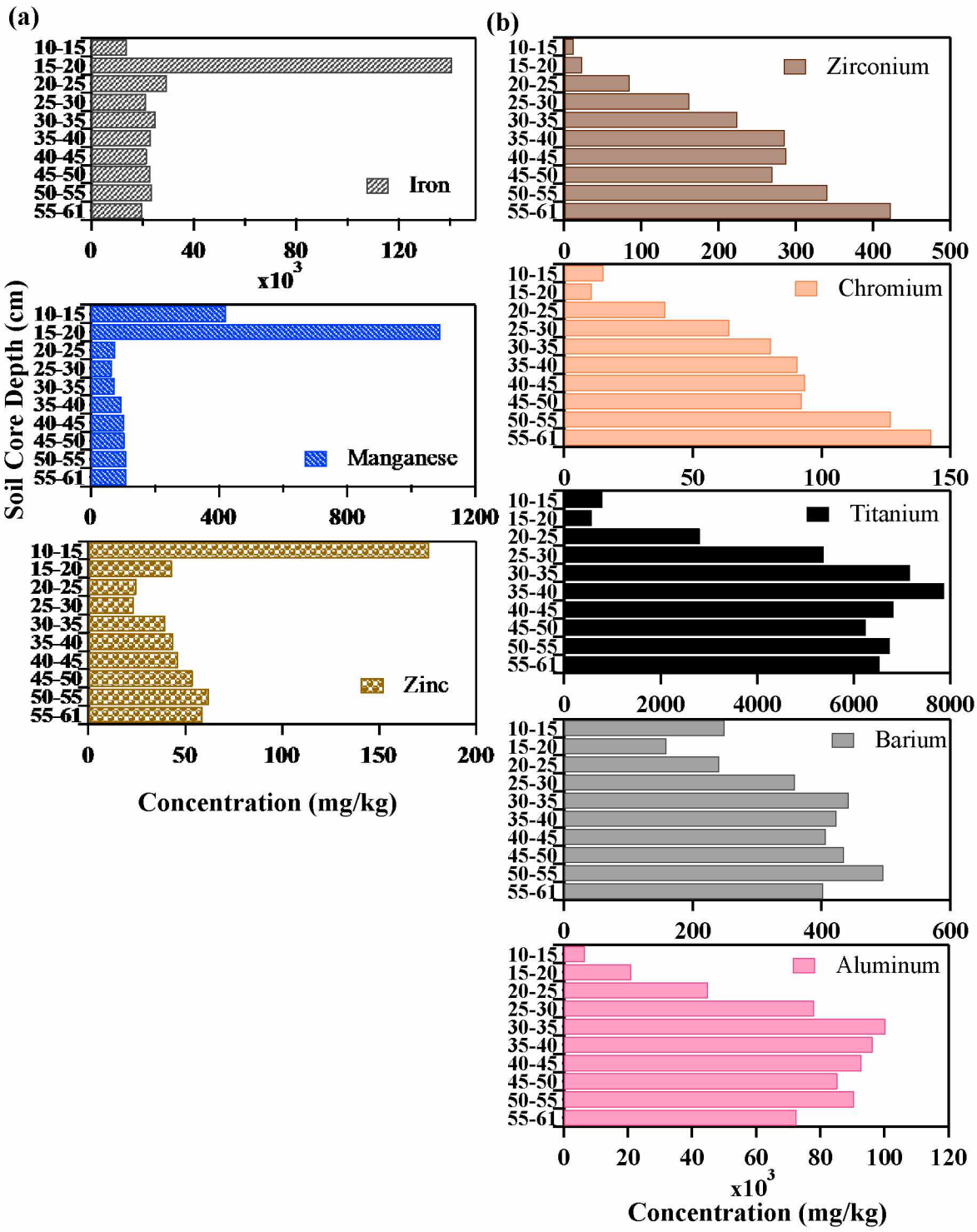

Figure 1.3 Vertical metal distributions

Metal distributions in soil core show element enhancement associated with (a) the organic layer in an oxidizing zone or (b) in the lower portion of the soil column in a reducing zone.

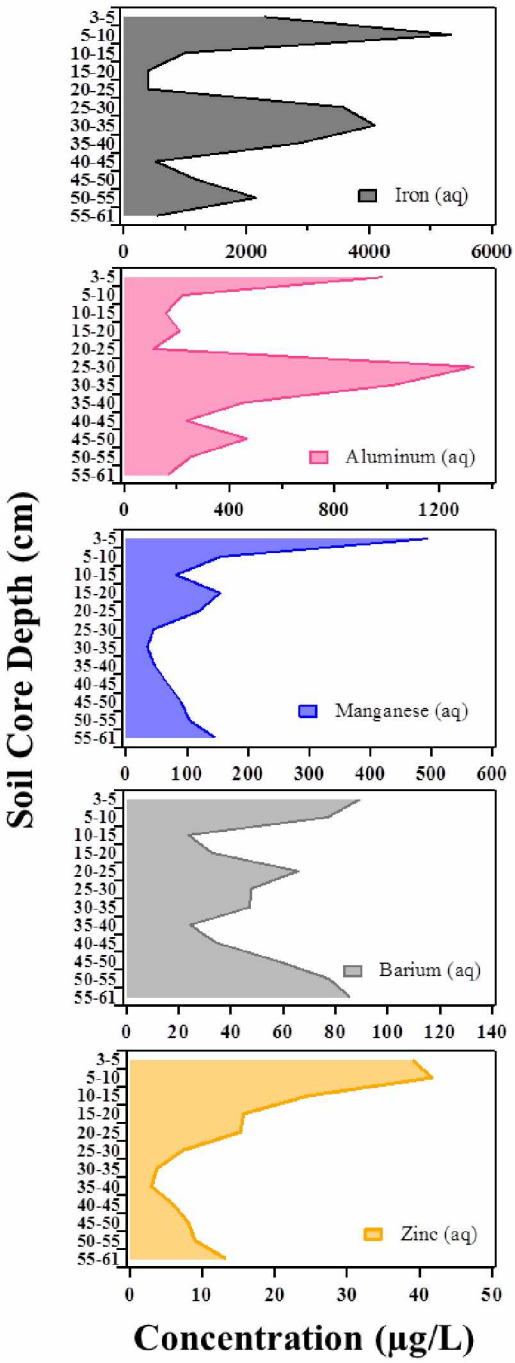

Figure 1.4 Vertical soluble metal distributions

Vertical soluble metal distributions measured in the soil water extracted from a soil core collected from Imnavait Creek watershed in late March/early April 2009.

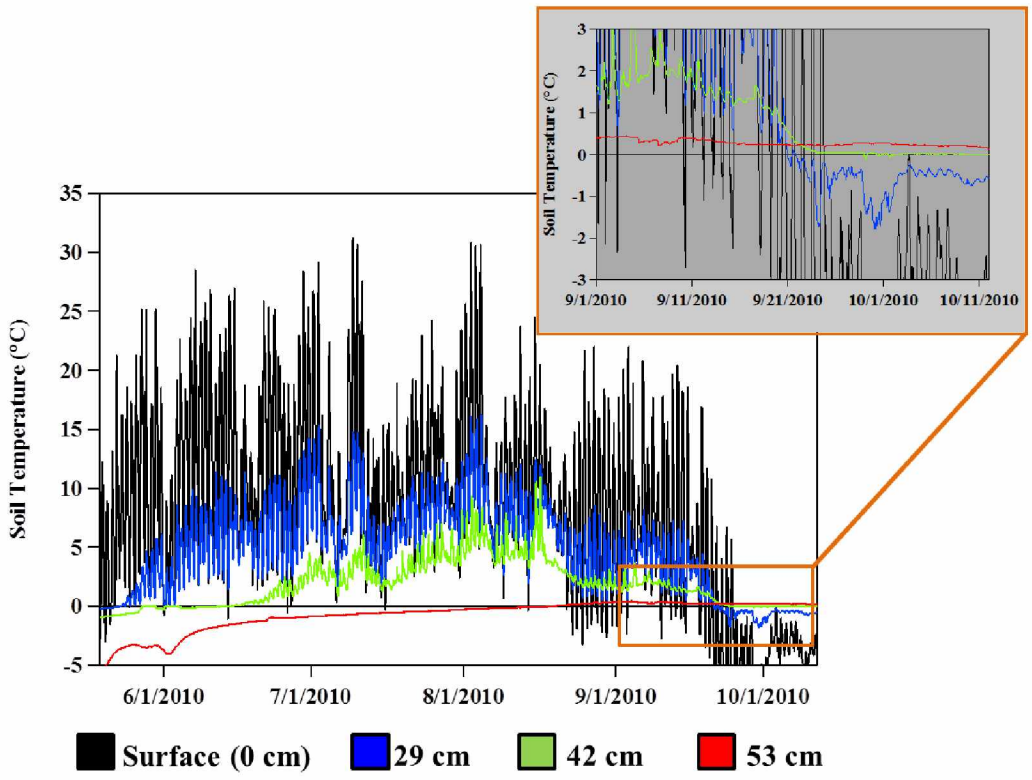

Figure 1.5 Soil temperature

Imnavait Creek watershed soil temperature (°C) at multiple soil depths as a function of date in 2010. Soil in the Arctic freezes from the top-down forcing pore water flow paths deeper in the soil column.

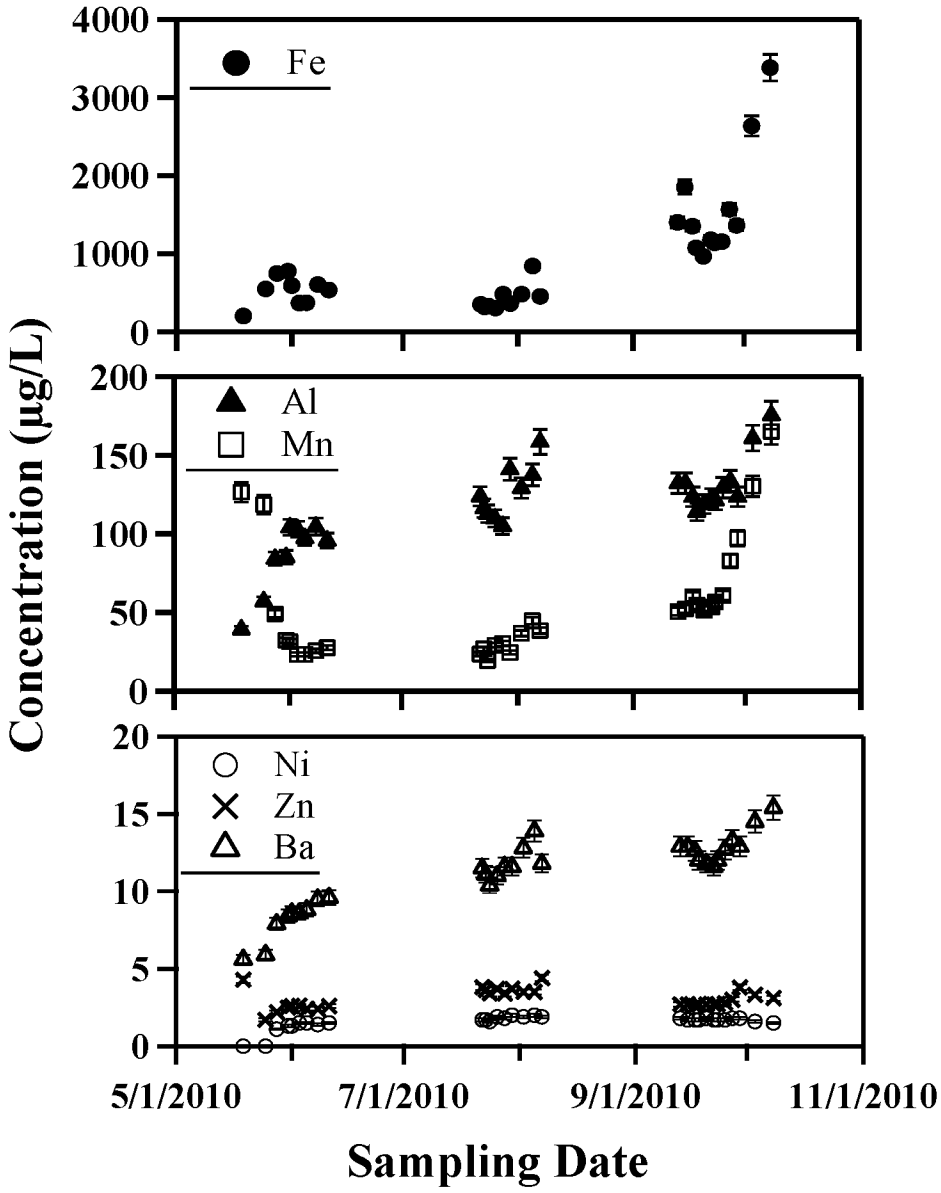

Figure 1.6 Surface water metal concentrations at Imnavait Creek

Imnavait Creek surface water soluble metal concentrations (µg/L) as a function of date in 2010.

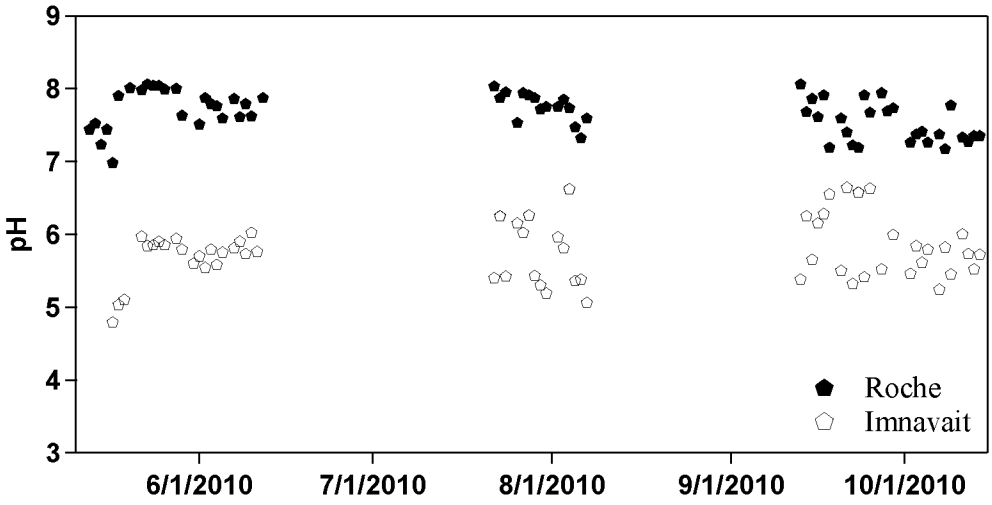

Figure 1.7 Surface water pH

Imnavait Creek and Roche Mountanee surface water pH values over the course of spring-fall 2010

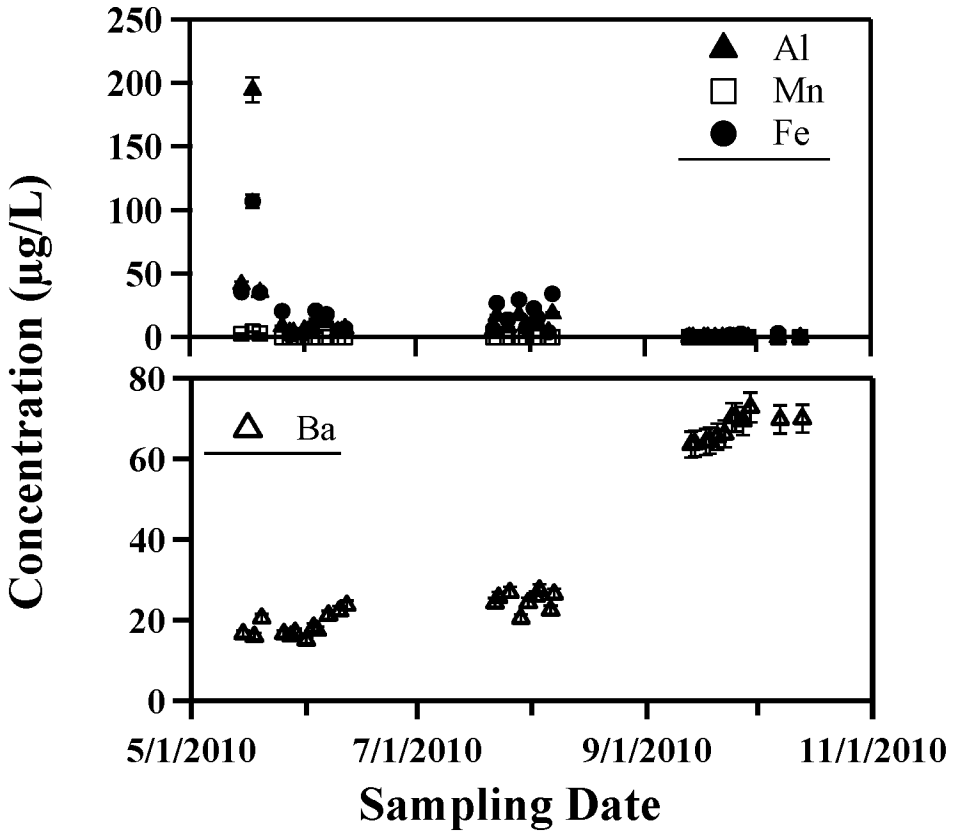

Figure 1.8 Surface water metal concentrations at Roche Mountanee Creek

Roche Mountanee Creek surface water soluble metal concentrations (µg/L) as a function of date in 2010.

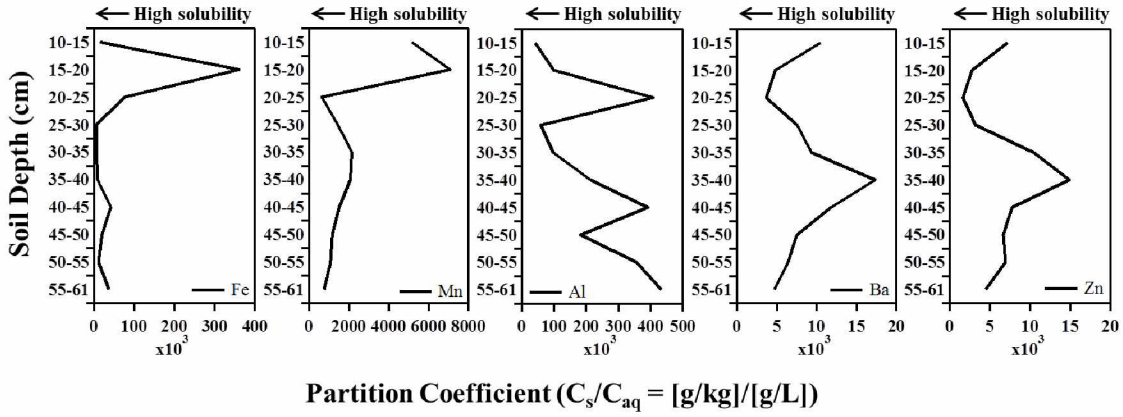

Figure 1.9 Partition coefficients

Plot of the partition coefficients (K_d) for the Imnavait Creek soil core collected in late March/early April. Values were calculated using the ratio of metal concentrations (g/kg) in the solid fraction of the soil to the metal concentrations (g/L) in the pore water fraction.

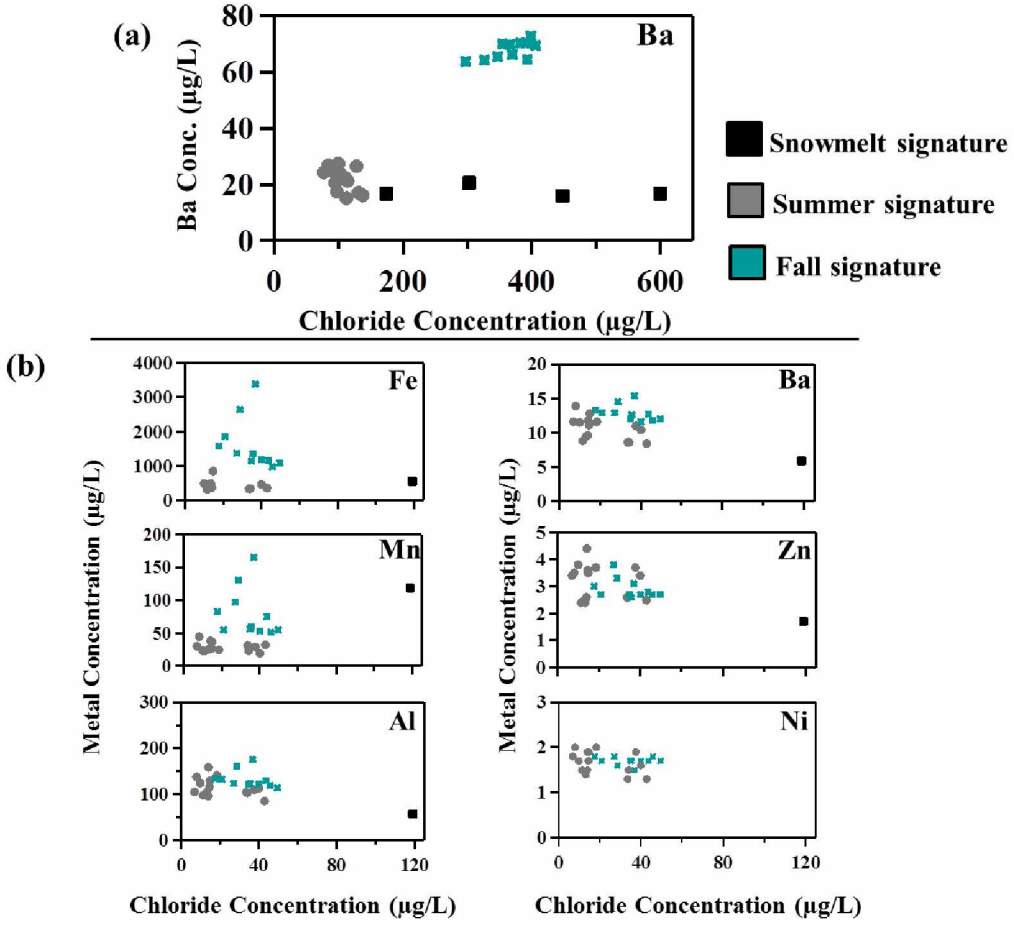

Figure 1.10 Metal-chloride relationships

Metal-chloride relationships for (a) Roche Mountanee and (b) Imnavait Creek surface waters over the course of Spring-Fall 2010.

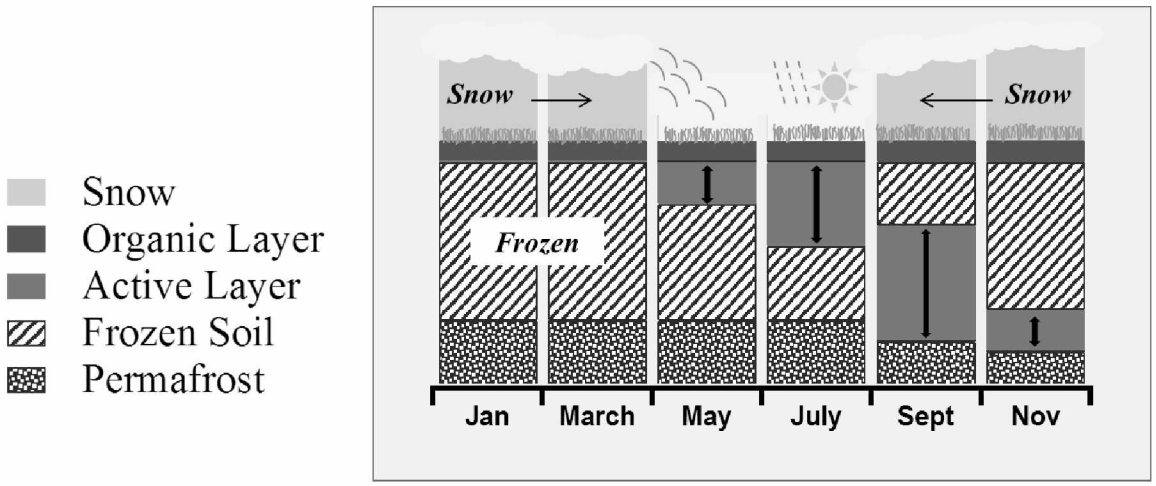

Figure 1.11 Schematic of freeze-thaw process

Schematic depicting the freezing and thawing process in Arctic soils and the observed deepening of the active layer during late fall of 2010.

Table 1.1 XRF soil core results

XRF results for the soil core collected from Imnavait Creek watershed, location shown in Figure 1. (-) indicates below detection limit or limit of detection not calculated if present in the lowest row in each section

Core 1 sections (cm)	Sc (ppm)	+/-	Ti (ppm)	+/-	V (ppm)	+/-	Cr (ppm)	+/-	Mn (ppm)	+/-	Ba (ppm)	+/-
10-15	6.4	0.2	796.3	8.0	12.2	0.2	15.4	2.8	420.6	4.2	249.0	2.5
15-20	3.2	0.1	572.1	5.7	14.6	0.3	10.7	1.9	1088.4	10.9	158.7	1.6
20-25	7.5	0.2	2809.3	28.1	45.2	0.9	39.4	7.1	76.7	0.8	240.7	2.4
25-30	10.5	0.3	5374.9	53.7	65.5	1.3	64.2	11.6	65.4	0.7	358.5	3.6
30-35	11.2	0.3	7165.0	71.7	85.6	1.7	80.2	14.4	74.3	0.7	442.0	4.4
35-40	11.2	0.3	7871.1	78.7	82.1	1.6	90.6	16.3	97.3	1.0	422.8	4.2
40-45	9.9	0.3	6825.5	68.3	83.5	1.7	93.5	16.8	102.8	1.0	406.4	4.1
45-50	10.7	0.3	6248.3	62.5	80.5	1.6	92.4	16.6	105.2	1.1	434.8	4.3
50-55	10.7	0.3	6749.9	67.5	80.3	1.6	126.9	22.8	111.1	1.1	495.8	5.0
55-61	9.6	0.3	6541.8	65.4	68.4	1.4	142.7	25.7	110.5	1.1	402.4	4.0
Detection Limit	1.5	0.0	2.8	0.0	1.9	0.0	1.3	0.2	2.4	0.0	-	-

Core 1 sections (cm)	Fe (ppm)	+/-	Ni (ppm)	+/-	Cu (ppm)	+/-	Zn (ppm)	+/-	Al (ppm)	+/-	Pb (ppm)	+/-
10-15	14054.8	4216.4	20.2	2.0	42.3	0.8	175.9	1.8	6530	65.3	6.4	0.5
15-20	140713.9	42214.2	18.3	1.8	24.7	0.5	43.1	0.4	20950	209.5	4.8	0.4
20-25	29548.2	8864.5	13.9	1.4	48.1	1.0	24.5	0.2	45020	450.2	6.3	0.5
25-30	21505.3	6451.6	16.7	1.7	44.9	0.9	23.5	0.2	77990	779.9	7.6	0.6
30-35	25282.0	7584.6	18.7	1.9	42.0	0.8	39.3	0.4	100360	1003.6	13.1	1.1
35-40	23261.2	6978.4	18.7	1.9	36.1	0.7	43.8	0.4	96330	963.3	12.1	1.0
40-45	21533.8	6460.1	19.5	1.9	33.8	0.7	46.2	0.5	92870	928.7	12.7	1.0
45-50	23019.5	6905.9	19.8	2.0	36.8	0.7	53.8	0.5	85320	853.2	11.1	0.9
50-55	23550.5	7065.1	23.7	2.4	34.0	0.7	62.2	0.6	90480	904.8	10.0	0.8
55-61	19772.0	5931.6	20.9	2.1	22.5	0.4	58.9	0.6	72540	725.4	7.6	0.6
Detection Limit	3.3	1.0	1.0	0.1	1.0	0.0	1.0	0.0	1.0	0.0	1.0	0.1

Core 1 sections (cm)	Br (ppm)	+/-	Rb (ppm)	+/-	Sr (ppm)	+/-	Y (ppm)	+/-	Zr (ppm)	+/-	Tl (ppm)	+/-
10-15	14.1	1.8	7.1	0.4	22.8	0.2	2.2	0.0	12.7	2.0	2.5	0.2
15-20	19.6	2.5	6.6	0.3	13.5	0.1	15.0	0.1	23.2	3.7	1.9	0.2
20-25	13.7	1.8	22.4	1.1	27.4	0.3	15.2	0.2	84.8	13.6	3.9	0.3
25-30	13.5	1.7	38.2	1.9	43.2	0.4	22.3	0.2	162.0	25.9	6.1	0.5
30-35	8.6	1.1	50.5	2.5	54.2	0.5	27.1	0.3	224.5	35.9	7.9	0.7
35-40	6.6	0.9	47.4	2.4	60.0	0.6	28.3	0.3	285.4	45.7	7.0	0.6
40-45	9.0	1.2	46.7	2.3	54.8	0.5	25.4	0.3	287.6	46.0	7.3	0.6
45-50	10.0	1.3	41.9	2.1	50.5	0.5	22.0	0.2	269.7	43.2	5.4	0.5
50-55	8.0	1.0	43.9	2.2	55.3	0.6	21.7	0.2	341.1	54.6	6.8	0.6
55-61	6.5	0.8	34.2	1.7	52.2	0.5	19.9	0.2	423.4	67.7	5.5	0.5
Detection Limit	1.0	0.1	1.0	0.1	1.0	0.0	1.0	0.0	1.0	0.2	1.0	0.1

Table 1.2 Metal concentrations for soil pore water

Metal concentrations for soil pore water samples extracted from the soil core collected from Imnavait Creek watershed. (-) indicates below detection limit, (*) indicates qualitative values outside the calibration

Core 1 (cm)	B (µg/L)	+/-	Al (µg/L)	+/-	P (µg/L)	+/-	Sc (µg/L)	+/-	Ti (µg/L)	+/-
3-5	90.1	0.3	984*	3	771*	3.6	1.4	0.1	4.3	0.1
5-10	24.1	0.3	223.9	1.8	1397*	6.6	-	-	3.0	0.1
10-15	-	-	158.3	0.6	405*	5.6	-	-	-	-
15-20	-	-	210.4	4.4	124*	10.0	-	-	-	-
20-25	-	-	110.4	2.3	208*	1.6	-	-	1.5	0.1
25-30	-	-	1330.0	256.4	572*	11.9	1.2	0.1	1.8	0.1
30-35	-	-	1029.0	8.6	136*	1.3	1.9	0.1	16.5	0.1
35-40	11.8	0.4	451.5	9.9	89.4	0.7	1.2	0.1	8.3	0.2
40-45	22.1	0.3	237.4	3.3	100.2	1.8	1.4	0.1	8.1	0.1
45-50	-	-	467.7	1.5	99.4	0.9	1.4	0.1	8.0	0.1
50-55	2.4	0.1	253.8	3.3	105.4	0.1	1.4	0.1	6.4	0.1
55-61	15.4	0.5	167.6	1.9	97.0	1.4	-	-	2.1	0.1

Core 1 (cm)	Mn (µg/L)	+/-	Fe (µg/L)	+/-	Co (µg/L)	+/-	Ni (µg/L)	+/-	Cu (µg/L)	+/-
3-5	495*	3	2292*	29	1.8	0.1	-	-	1.3	0.1
5-10	155*	1	5324	47.9	1.5	0.1	-	-	-	-
10-15	81.6	0.8	1000	13.4	1.3	0.1	-	-	-	-
15-20	154*	10	390	1.1	2.3	0.2	1.8	0.2	-	-
20-25	120*	1	390	2.8	-	-	3.9	0.1	6.5	0.4
25-30	45.4	1.0	3580	485.8	-	-	-	-	-	-
30-35	34.6	0.2	4090	89.6	-	-	-	-	12.5	0.1
35-40	47.0	0.6	2840	18.7	-	-	-	-	-	-
40-45	67.8	1.0	520	4.5	-	-	-	-	1.5	0.1
45-50	90.3	0.5	1190	21.1	-	-	-	-	1.4	0.1
50-55	103.1	0.7	2160	18.8	1.8	0.1	2.7	0.1	-	-
55-61	146*	1	540	7.0	1.8	0.1	1.1	0.1	-	-

Core 1 (cm)	Zn (µg/L)	+/-	Sr (µg/L)	+/-	Y (µg/L)	+/-	Ba (µg/L)	+/-	Tl* (µg/L)	+/-
3-5	39.0	0.1	7.7	0.1	-	-	89.4	1.1	1890*	59
5-10	41.7	0.1	7.0	0.1	-	-	77.2	0.4	1098*	86
10-15	24.5	0.2	6.6	0.1	-	-	23.8	0.1	1064*	23
15-20	15.7	1.2	4.4	0.4	-	-	32.9	3.1	1759*	228
20-25	15.3	0.1	6.0	0.1	-	-	65.8	0.5	2547*	59
25-30	7.4	0.1	2.3	0.1	-	-	47.5	1.6	342*	53
30-35	3.8	0.1	1.9	0.1	2.5	0.1	47.3	0.7	258*	39
35-40	3.0	0.1	1.5	0.1	1.1	0.1	24.4	0.2	-	-
40-45	6.0	0.1	1.9	0.1	1.5	0.1	34.4	0.5	-	-
45-50	8.1	0.1	2.3	0.1	1.9	0.1	57.8	0.6	-	-
50-55	9.0	0.1	2.7	0.1	1.4	0.1	77.6	0.6	-	-
55-61	13.3	0.1	4.4	0.1	-	-	85.5	1.3	-	-

Table 1.3 Trace concentrations in Imnavait Creek

Trace concentrations (µg/L) of species found in Imnavait Creek surface waters over the course of spring through fall 2010. (-) indicates below detection limit (/) indicates samples not analyzed for chloride

	Al	+/-	Mn	+/-	Fe	+/-	Ni	+/-	Zn	+/-	Ba	+/-	Cl	+/-
19-May	39.2	0.7	126.7	1.3	187.8	1.6	-	-	4.3	0.1	5.6	0.1	/	/
25-May	57.2	1.1	118.7	1.1	551.0	3.9	-	-	1.7	0.1	5.9	0.1	118.9	5.9
28-May	84.1	0.6	49.1	0.9	750.4	5.1	1.1	0.1	2.2	0.1	7.9	0.1	/	/
31-May	85.2	0.6	32.3	0.3	776.7	6.8	1.3	0.1	2.5	0.1	8.4	0.1	42.9	2.1
1-Jun	104.2	1.0	31.5	0.3	593.3	1.2	1.3	0.1	2.6	0.1	8.6	0.1	33.6	1.7
3-Jun	102.9	0.3	23.3	0.1	369.6	4.8	1.5	0.1	2.6	0.1	8.6	0.1	34.1	1.7
5-Jun	97.5	0.9	23.4	0.2	374.5	3.1	1.5	0.1	2.4	0.1	8.8	0.1	11.4	0.6
8-Jun	104.6	2.0	25.7	0.3	607.5	4.6	1.4	0.1	2.4	0.1	9.5	0.1	13.3	0.7
11-Jun	95.8	2.3	27.6	0.4	538.8	3.7	1.5	0.1	2.6	0.1	9.6	0.1	13.9	0.7
22-Jul	123.9	1.0	23.6	0.2	352.7	2.2	1.7	0.1	3.8	0.1	11.5	0.1	9.9	0.5
23-Jul	116.3	1.4	26.8	0.3	323.4	1.1	1.7	0.1	3.6	0.1	11.1	0.3	14.6	0.7
24-Jul	112.8	1.7	19.4	0.2	333.6	4.0	1.6	0.1	3.4	0.1	10.4	0.1	40	2.0
26-Jul	109.9	0.8	29.1	0.2	307.0	3.6	1.9	0.1	3.7	0.1	11.0	0.1	37.6	1.9
28-Jul	105.0	0.3	30.2	0.2	485.1	9.6	1.8	0.1	3.4	0.1	11.6	0.1	6.9	0.3
30-Jul	141.1	1.1	24.5	0.1	362.8	3.7	2.0	0.1	3.7	0.1	11.6	0.1	18.4	0.9
2-Aug	129.2	2.5	36.7	0.6	484.3	5.9	1.9	0.1	3.5	0.1	12.8	0.2	14.8	0.7
5-Aug	137.6	1.9	44.8	0.6	844.2	7.0	2.0	0.1	3.5	0.1	13.9	0.1	8	0.4
7-Aug	158.7	2.0	38.6	0.4	456.2	4.7	1.9	0.1	4.4	0.1	11.8	0.1	14.1	0.7
13-Sep	132.2	1.9	50.6	0.7	1403.7	12.5	1.8	0.1	2.7	0.1	12.9	0.1	/	/
15-Sep	132.3	1.6	54.9	0.2	1855.0	8.3	1.7	0.1	2.7	0.1	12.9	0.1	20.9	1.0
17-Sep	123.6	1.1	60.0	0.2	1354.7	13.3	1.7	0.1	2.6	0.1	12.6	0.1	35.5	1.8
18-Sep	114.1	0.4	54.9	0.2	1077.7	16.4	1.7	0.1	2.7	0.1	12.0	0.2	49.6	2.5
20-Sep	119.0	1.4	51.4	0.8	969.8	10.0	1.8	0.1	2.7	0.1	11.8	0.1	45.7	2.3
22-Sep	122.6	4.3	53.4	0.2	1179.7	11.9	1.7	0.1	2.7	0.1	11.6	0.1	40	2.0
23-Sep	121.4	1.9	56.5	0.4	1143.7	7.5	1.7	0.1	2.7	0.1	12.0	0.2	34.8	1.7
25-Sep	129.5	1.8	75.2	0.9	1156.0	10.5	1.7	0.1	2.8	0.1	12.7	0.2	43.7	2.2
27-Sep	133.7	0.4	82.9	0.4	1570.7	23.7	1.8	0.1	3.0	0.1	13.3	0.3	17.6	0.9
29-Sep	123.6	2.0	97.3	0.6	1366.7	12.4	1.8	0.1	3.8	0.1	12.9	0.1	27.1	1.4
3-Oct	161.0	4.0	130.4	0.2	2640.0	28.8	1.6	0.1	3.3	0.1	14.5	0.2	28.7	1.4
8-Oct	175.6	2.9	165.2	2.3	3383.0	9.5	1.5	0.1	3.1	0.1	15.4	0.2	36.8	1.8

Table 1.4 Trace concentrations in Roche Mountanee

Trace concentrations (μg/L) of species found in Roche Mountanee surface waters over the course of spring through fall 2010. (-) indicates below detection limit, (/) indicates samples not analyzed for chloride, (*) indicates outside the calibration range for the analytical method, therefore value is qualitative

	Al	+/-	Mn	+/-	Fe	+/-	Ba	+/-	Cl	+/-
15-May	41.5	1.1	2.7	0.1	35.4	2.5	16.7	0.2	599.7	30.0
18-May	194.8*	5.5	4.2	0.1	107.0	0.8	16.0	0.1	447.6	22.4
20-May	35.4	7.6	2.9	0.1	35.2	1.5	20.6	0.3	302.5	15.1
26-May	8.4	0.7	-	-	20.3	0.6	16.7	0.4	174.1	8.7
28-May	3.9	0.1	-	-	1.8	0.1	16.1	0.2	137.1	6.9
29-May	4.0	0.1	-	-	2.1	0.1	17	0.3	130.2	6.5
1-Jun	5.7	0.1	-	-	3.1	0.1	15.1	0.1	111.7	5.6
3-Jun	7.0	0.2	-	-	7.3	0.1	18.3	0.2	/	/
4-Jun	13.8	0.3	-	-	20.8	0.2	17.5	0.3	96.8	4.8
7-Jun	11.5	0.5	-	-	17.8	0.1	21.3	0.1	113.4	5.7
10-Jun	4.7	0.2	-	-	5.1	0.1	22.4	0.1	109.4	5.5
12-Jun	6.8	0.5	-	-	6.9	0.1	23.7	0.2	94.9	4.7
22-Jul	5.7	0.1	-	-	6.2	0.1	24.3	0.3	76.8	3.8
23-Jul	16.9	1.5	-	-	26.8	0.1	25.7	0.1	/	/
26-Jul	7.8	0.1	-	-	13.8	0.2	26.9	0.2	84	4.2
29-Jul	17.3	0.3	-	-	29.3	0.1	20.5	0.2	94.3	4.7
31-Jul	9.7	2.3	-	-	7.5	0.1	24.4	0.2	100.7	5.0
2-Aug	13.0	0.5	-	-	22.6	0.1	25.9	0.5	94.9	4.7
3-Aug	9.6	0.1	-	-	15.1	0.3	27.5	0.3	99.1	5.0
6-Aug	4.4	0.1	-	-	3.8	0.1	22.5	0.3	/	/
7-Aug	18.5	0.8	-	-	34.1	0.3	26.5	0.1	127.3	6.4
13-Sep	-	-	-	-	1.1	0.1	63.6	0.4	/	/
14-Sep	-	-	-	-	-	-	63.8	0.5	297.1	14.9
17-Sep	-	-	-	-	-	-	64.2	0.3	326.1	16.3
18-Sep	-	-	-	-	-	-	64.5	1.0	392.5	19.6
20-Sep	-	-	-	-	-	-	65.5	0.3	346.7	17.3
22-Sep	-	-	-	-	-	-	66.2	1.0	369.4	18.5
24-Sep	-	-	-	-	1.8	0.1	70.3	0.8	390	19.5
25-Sep	-	-	-	-	-	-	70.3	0.6	382.2	19.1
27-Sep	-	-	-	-	2.6	0.1	69.4	0.2	405.4	20.3
29-Sep	-	-	-	-	-	-	72.8	0.5	398.3	19.9
7-Oct	-	-	-	-	3.2	0.1	69.8	0.4	365.7	18.3
13-Oct	-	-	-	-	-	-	70	0.6	354.4	17.7

Table 1.5 Partition coefficients for soil core

Partition coefficients (K_d) for the Imnavait Creek soil core. K_d values were calculated using the radio of metal concentrations (g/kg) in the solid fraction of the soil to the metal concentrations (g/L) in the pore water fraction.

	Iron Partitioning Coefficient		
Core 1 (cm)	C_s (g/kg)	C_{aq} (g/L)	K_d (Cs/Caq)
10-15	14.0548	0.001000	14050
15-20	140.7139	0.000390	36100
20-25	29.5482	0.000390	75800
25-30	21.5053	0.003580	6007
30-35	25.282	0.004090	6181
35-40	23.2612	0.002840	8191
40-45	21.5338	0.000520	41400
45-50	23.0195	0.001190	19340
50-55	23.5505	0.002160	10900
55-61	19.7720	0.000540	36600

	Barium Partitioning Coefficient		
Core 1 (cm)	C_s (g/kg)	C_{aq} (g/L)	K_d (Cs/Caq)
10-15	0.2490	0.0000238	10500
15-20	0.1587	0.0000329	4830
20-25	0.2407	0.0000658	3660
25-30	0.3585	0.0000475	7550
30-35	0.4420	0.0000473	9350
35-40	0.4228	0.0000244	17300
40-45	0.4064	0.0000344	11800
45-50	0.4348	0.0000578	7520
50-55	0.4958	0.0000776	6390
55-61	0.4024	0.0000855	4700

	Manganese Partitioning Coefficient		
Core 1 (cm)	C_s (g/kg)	C_{aq} (g/L)	K_d (Cs/Caq)
10-15	0.4206	0.0000816	5150
15-20	1.0884	0.000154	7070
20-25	0.0767	0.000120	639
25-30	0.0654	0.0000454	1440
30-35	0.0743	0.0000346	2150
35-40	0.0973	0.0000470	2070
40-45	0.1028	0.0000678	1520
45-50	0.1052	0.0000903	1170
50-55	0.1111	0.0001031	1077
55-61	0.1105	0.000146	757

	Zinc Partitioning Coefficient		
Core 1 (cm)	C_s (g/kg)	C_{aq} (g/L)	K_d (Cs/Caq)
10-15	0.1759	0.0000245	7170
15-20	0.0431	0.0000157	2750
20-25	0.0245	0.0000153	1600
25-30	0.0235	0.0000074	3200
30-35	0.0393	0.0000038	10000
35-40	0.0438	0.0000030	15000
40-45	0.0462	0.0000060	7700
45-50	0.0538	0.0000081	6600
50-55	0.0622	0.0000090	6900
55-61	0.0589	0.0000133	4440

	Aluminum Partitioning Coefficient		
Core 1 (cm)	C_s (g/kg)	C_{aq} (g/L)	K_d (Cs/Caq)
10-15	6.530	0.0001583	41250
15-20	20.950	0.0002104	99570
20-25	45.020	0.0001104	407800
25-30	77.990	0.0013300	58639
30-35	100.360	0.0010290	97532
35-40	96.330	0.0004515	213400
40-45	92.870	0.0002374	391200
45-50	85.320	0.0004677	182400
50-55	90.480	0.0002538	356500
55-61	72.540	0.0001676	432800

Chapter 2 Lead and Antimony Speciation Associated with Weathering Bullets in Newly Constructed Target Berms[1]

2.1 Abstract

Understanding Pb and Sb speciation associated with the weathering of bullets is essential for identifying the potential for mobile species to migrate, as well as assess the overall toxicity of a shooting range. In the present study, we fired 5.56 mm bullets into newly constructed berms composed of well-characterized test soils (sand, sandy loam, loamy sand and silt loam) during a controlled event in order to observe the progression of Pb and Sb oxidation as a function of time and soil properties. After four years reaction time, an iron amendment was added to a subset of the test berms of each soil type to study remediation strategies. Bulk speciation analysis coupled with micro-scale spectroscopic methods show that both Sb(III) and (V) species are present in soil solution depending on the type of soil matrix, but Sb(III) is no longer observed after 9 months. In addition, Sb is mobilized to a greater extent than Pb in all test soil types, attributable to the overall low solubility of the dominant Pb species present in the crust and soil fraction; a mixture of lead oxide, lead carbonate and lead sorbed onto iron (III) oxides. Based on the results, this study suggests constructing target berms out of 100% silt loam soil, which is shown to be naturally effective at immobilizing both Pb and Sb, and adding $Fe(OH)_3$ coated sand/$CaCO_3$ buffer to the berm runoff. Results stemming from this study are essential for understanding the potential for off-site migration, as well as determining the ultimate bioavailability and toxicity of lead and antimony in shooting soils.

[1]Barker, A.J., Douglas, T.A., Ilgen, A.L., Trainor, T.P. Lead and antimony speciation associated with weathering bullets in newly constructed test berms. Prepared for submission in Geochimica et Cosmochimica Acta.

2.2 Introduction

Shooting range training facilities contain high loadings of metal(loid)s within soil and soil porewater, particularly lead (Pb), antimony (Sb), copper (Cu), nickel (Ni) and zinc (Zn) (Murray et al., 1997; Basunia and Landsberger, 2001; Strømseng et al., 2009; Sanderson et al., 2013; Martin et al., 2013; Guemiza et al., 2014). In the U.S., it is estimated that over 3,000 small arms ranges (SARs) are managed by the Department of Defense (DoD) and another 9,000 non-military outdoor ranges exist (ITRC, 2003; US EPA, 2005). In the late 1990's, EPA estimated that four percent of all the Pb produced in the U.S., about 2 million tons per year, was consumed in the production of bullets (US EPA, 2005). Once bullets are deposited into a berm they fragment, increasing the surface area and exposing fresh metallic surfaces to the soil environment. The bullet fragments weather causing zero-valent metals to oxidize, which form a crust rich in secondary mineral phases often encapsulating surfaces and acting as a control on metal(loid) release to solution (Vantelon et al., 2005). In addition, metal(loid)s can be released directly into soil solution and the extent to which mobilized metal(loid)s fractionate between soil surfaces (clay minerals, Al, Mn and Fe oxides, organic matter) and soil porewater depends on a variety of factors including time, soil conditions and saturation levels (Jorgensen and Willems, 1987; Cao et al., 2003; Sanderson et al., 2013).

The core of a bullet is composed of a Pb-alloyed core with Sb added as a hardening agent, with average concentrations ranging from 0.7 wt. % Sb (Randich et al., 2002) for a 0.22 caliber (5.56 mm) to 1.8 wt. % Sb for a 0.357 caliber (9 mm) round (Keto, 1999). Concentrations of Sb in shooting range soils have been reported from 1-517 mg/kg in a Texas firing range (Basunia and Landsberger, 2001) to upwards of 10,000 mg/kg at a Swiss shooting range reported by Johnson et al., 2005 of the <0.5 mm sieved bank material including bullets. Lead

concentrations have been found in the range of 11 to 4675 mg/kg (Basunia and Landsberger, 2001), 1142 mg/kg (Hardison et al., 2004) and 68,000 mg/kg (Vantelon et al., 2005). In addition to Pb and Sb, elevated (above background) concentrations of Cu have been reported in shooting range soils, approximately 13 to 359 mg/kg (Basunia and Landsberger, 2001).

Firing and subsequent deposition of bullet slugs to soil represents a pathway of metal release to soil pore waters. Concentrations of Pb have been reported in shooting range surface waters ranging from 60-2900 µg/L (US EPA, 1994) with maximum Pb values reported of 838 µg/L by Stansley et al. (1992); 2256 µg/L by Murray et al. (1997); and 1495 µg/L by Okkenhaug et al. (2016). Antimony concentrations in soil-waters have been reported to range from 19-349 µg/L in untreated shooting range soil over 4 years (Okkenhaug et al., 2016). In addition, Pb and Sb have also been shown to accumulate in plant roots and soil organism communities (Rooney et al., 1999; Labare et al., 2004; Migliorini et al., 2004; Robinson et al., 2008; Feng et al., 2009; Pourrut et al., 2011; Okkenhaug et al., 2011) demonstrating characteristics of bioavailability in soil. Given that both Pb and Sb are toxic and Sb(III) is a suspected carcinogen (US EPA, 1979; IARC, 1989; WHO, 2003; 2011), there is a growing concern that metal(loid) accumulation in shooting range systems may pose a serious contamination risk to groundwater, surface water, plants and site reclamation (US EPA, 1994; Mellor and McCartney, 1994; Cao et al., 2003; Robinson et al., 2008; Martin et al., 2013).

Understanding the overall processes controlling mobilization versus retention of metal(loid) species requires understanding speciation. Antimony is primarily found in the environment in two oxidation states, Sb(III) and Sb(V), which unless in highly acidic systems, readily hydrolyze in aqueous solution to $Sb(OH)_3$ and $Sb(OH)_6^-$, respectively (Johnson et al., 2005). Lead is predominantly found in the environment in only one oxidation state: Pb(II)

(Hardison et al., 2004; Vantelon et al., 2005). Both Pb and Sb have been shown to complex with colloidal sized particles, such as clay minerals, Fe-, Al-, and Mn- oxy/hydroxides, and humic/fulvic acids, which has implications affecting the overall transport and mobility of contaminants in shooting range soils (Denaix et al., 2001; Klitzke et al., 2012). In particular, Pb forms a variety of stable mineral phases with oxides and carbonates in addition to forming stable sorption complexes on the surfaces of humus and Si-, Fe-, Mn- and Al- oxides (Rooney et al., 2007; Clausen et al., 2011). Lead partitioning between soil and soil solution is largely controlled by pH (Reddy et al., 1995; Clausen et al., 2011) and has been shown to become more mobilized at lower pHs while the capacity of soil to adsorb Pb increases at higher pHs (USGS, 1976; Reddy et al., 1995; Cao et al., 2003). This is different than Sb in solution, which has been shown to be more mobile at higher pHs for Sb(V) species, while Sb(III) is independent of pH (Johnson et al., 2005).

Numerous studies have focused on shooting range soil and water monitoring for metal fate, transport and speciation (Murray et al., 1997; Cao et al., 2003; Johnson et al., 2005; Vantelon et al., 2005; Scheinost et al., 2006; Rooney et al., 2007; Ackermann et al., 2009; Clausen et al., 2011; Guemiza et al., 2014). However, the majority of studies focus on older shooting range facilities (20-90 years old) that have been heavily used, resulting in a gap in knowledge concerning Pb and Sb transport and speciation in initial stages (Hardison et al., 2004). In this study, we constructed shooting range test berms comprised of four different, well-characterized soils and fired approximately 2,000 - 5.56 mm bullets into each of the berms in the summer of 2010 at the Cold Regions Test Center (CRTC) outside of Delta Junction, Alaska. Sampling occurred during the summer seasons for a total of 5 years. Samples were collected to determine Pb and Sb aqueous concentrations and speciation using the berm liquid runoff as well

as solid-phase speciation. After 4 years of reaction time, slurries of $FeCl_2$ and $CaCO_3$ were added to a set of duplicate test berms to evaluate the potential of this treatment as a low-cost, easy to apply remediation strategy for range managers. Given the natural attenuation of both Pb and Sb by Fe present in soil via surface complexation reactions, it has been postulated that Fe additions have the potential to work as an effective sorbent in shooting range soil systems (Dzombak and Morel, 1990; Belzile et al., 2001; Leuz et al., 2006). Remediation strategies designed for small arms ranges should ideally immobilize both Pb and Sb, which can be challenging due to differences in mobility with pH among their respective mobile species (Jardine et al., 2007; Mitsunobu et al., 2010; Griggs et al., 2011; Okkenhaug et al., 2011; Sanderson et al., 2013; Ogawa et al., 2015; Okkenhaug et al., 2016).

The main goals of this project were to establish a baseline of initial oxidation products in both the solid and aqueous phase as a result of bullet weathering from deposition to 5 years reaction time. Select Pb and Sb species may occur initially, but are most likely overlooked by previous studies due to long term instability. We also tracked Pb and Sb distribution, transport from parent source, correlations with other elements and metal speciation as a function of time amid varying soil properties. The results from this study provide a unique dataset to understanding the overall fate, transport and speciation of Pb and Sb in shooting range soils. Finally, this study outlines suggestions for the construction of future shooting ranges in addition to defining remediation strategies.

2.3 Methods

2.3.1 Field Site Construction

Twelve test berms were constructed in central Alaska on the Donnelly Training Area (DTA), located approximately 10 miles southeast of Delta Junction, Alaska. The test berms are comprised of four different types of soil: silt loam, loamy sand, sandy loam and sand and each cover an area approximately 2 square meters. The layout for the site is depicted in Figure 2.1. The silt loam end member was sourced locally from DTA and the sand end member was purchased from Delta Sand and Gravel. The soil end members were mixed by Delta Sand and Gravel in a large soil mixer and construction began in August 2010 in conjunction with Cold Regions Test Center (CRTC) on the Texas Range of DTA. The different types of soil were loaded into a dump truck, transferred to a front-loader and unloaded in mounds onto water-proof plastic geoliner sheets (Alaska Tent and Tarp, Fairbanks, Alaska). The open sides of the geoliner sheets were then rolled and set with wooden stakes in order to direct runoff to one location (Figure 2.1). Plastic 5 gallon buckets covered with 1mm nylon screen mesh were installed at the mouth of each berm to collect the berm runoff. Each bucket was covered with a sheet of plywood for protection. Soil moisture and temperature probes were installed into a subset of berms of each soil type and were installed 180 degrees away from bullet pocket and 1 m up from the ground at a depth of 0.5 m into the berm. Data loggers for soil/air temperature and soil moisture (Onset HOBO Data Loggers, Bourne, MA) were logged every hour for 5 years and downloaded twice per year. There were periodic breaks in data collection primarily due to equipment failure or to animals chewing/destroying the logger cords. Of the twelve separate berms and four soil types, four berms remained untouched and are classified as 'pristine' berms. The other 8 berms (duplicates of each soil type) were fired into in a controlled firing event in September 2010 and

are classified as the 'contaminated' berms. The firing event was facilitated by CRTC and Alaska Army National Guard Ft. Greely MP Company, 49th Missile Defense Battalion. We fired 2,000 military-issued 5.56 mm bullets into each of the 8 contaminated berms. Shortly after the berms were loaded the winter season began and the berms remained untouched until May 2011.

In August 2014, an Fe amendment was added to a subset of the contaminated berms, 5, 7, 9 and 11 (one of each of the soil types) in order the investigate the cost, ease of application and overall effectiveness of Fe as a treatment for limiting Pb and Sb mobility. The Fe amendment was added as a solution made up by adding 40 g of Fe(II) in the form of $FeCl_2$ (Alfa Aesar, 99.5% metals basis powder, Haverhill, MA) to 15 liters of drinking water (Water Wagon, Fairbanks, AK) in a pre-washed 15 L capacity fertilizer sprayer pump (Echo, MS-401) and manually mixed. In another 15 L sprayer, we added 75 g of $CaCO_3$ (Powder, J.T. Baker, Center Valley, PA) to 15 liters of drinking water and manually mixed. We sprayed the two mixtures independently, but in tandem, to each of the selected berms. Timing of the application was chosen to ensure the berm soils were dry at the time of application. The overall Fe addition process took approximately 30 minutes per berm.

2.3.2 Sampling

The number of samples varied each summer as a result of fluctuating precipitation, but each berm was sampled 1-16 times for aqueous metal concentrations and 1-2 times for solid phase metal distribution and speciation, on average per year. The pristine berms were routinely monitored for background concentrations of metals, approximately 1-4 sample collections per summer.

2.3.2.1 Berm Runoff

Sampling the berm runoff consisted of collecting the liquid from the plastic buckets situated at the base of the bullet pockets draining from the geoliner. We also sampled the small pan lysimeters when they contained runoff. During the winter, we collected snow samples and during spring snowmelt we collected samples from the drainage. All liquid samples were collected in HDPE trace metal grade Nalgene bottles (Nalgene, Waltham, MA) or sterilized 15 and 50 mL plastic centrifuge tubes (VWR International, Radnor, PA). Samples for trace metal analysis were filtered to either 0.45 or 0.2 µm and acidified with 6 N ultrapure HNO_3 (BDH Aristar Plus, Poole Dorset, UK). Samples for Sb speciation were filtered to 0.45 µm and stabilized with 0.1M EDTA (BDH, VWR International, Radnor, PA) solution (1 mL for every 10 mL), further outlined in Ilgen et al., 2014. All liquid samples were stored at 4°C in a refrigerator until analysis.

2.3.2.2 Bulk Soil Samples

Soil samples were collected from the pristine berms during construction in August 2010 for soil characterization. Samples for Pb/Sb solid phase analysis were collected 1-2 times per summer. At the end of the sampling summer in 2015, triplicate soil samples were collected from each of the 12 berms for bulk metal analysis. Soil was collected using plastic scoopulas (30 increments picked at random for each of the triplicate measurements) and Whirl-Pak sampling bags (Nasco, Salida, California) or plastic bags (Ziploc, Racine, WI). Samples were stored in a sample freezer (-18 °C) until analysis.

2.3.2.3 Collection of Micro-focused Samples

Heterogeneous soil samples containing contaminated soil and bullet fragments were collected using plastic scoopulas and Buehler SamplKups (Buehler Company, Lake Bluff, Illinois). The cups were inserted into the surface of the soil until they were two-thirds full and a plastic scoopula was then inserted in order to retain the soil in the cup. This method was carried out for all samples in order to preserve bullet distribution within the soil and minimize disturbance. The samples were then transported back to a research lab at the University of Alaska Fairbanks and impregnated with 301-2FL low stress optical epoxy (Epoxy Technology EPO-TEK (Billerica, Massachusetts). Samples were allowed to cure for 3 days under vacuum and then removed from the SamplKups; the result was a circular soil plug approximately 3 cm tall and 2.5 cm wide. Soil plugs were sliced into 0.5-1 mm sections using a rotating diamond saw (Buehler Company, Lake Bluff, Illinois) and then ground to approximately 250-500 microns thick using a rotating diamond plate (Buehler Company, Lake Bluff, Illinois). Slices were mounted to 25 x 25 x 1 mm quartz microscope slides (Quartz Scientific, Fairport Harbor, OH) using Loctite gel epoxy (Loctite, Düsseldorf, Germany) and polished to approximately 50-250 microns thick using aluminum oxide powder (grit sizes 400, 570 and 1000) (Buehler Company, Lake Bluff, Illinois) or cerium oxide polishing compound (Ed Rouleau, Taylor Jewelry Company, Fairbanks, AK). After polishing, the thin sections were rinsed with 'DI water' (ultrapure water with a resistivity of 18.1 MΩ, Barnstead Nanopure, Thermo Scientific, Waltham, MA) and wrapped in plastic wrap until analysis.

2.3.3 Analysis

2.3.3.1 Berm Water Runoff

The pH of select field samples was analyzed using a Thermo Scientific Orion Refillable Ag/AgCl pH electrode (Thermo Scientific, Waltham, MA). The probe was calibrated with 4.01, 7.00 and 10.01 buffer solutions (Hach Company, Loveland, Colorado) at 25°C with a calibration curve $R^2 \geq 0.97$.

Samples were analyzed for trace metal concentrations further, procedure outlined in section 1.3.3. Al, Ba, Ca, Cd, Co, K, Mg, Mn, Na, P, Pb, Sb, Sn, Te, Ti and Zn were analyzed in normal mode (no CRC). As, Cr, Cu and Ni were analyzed using CRC pressurized with He gas and Fe was analyzed using CRC pressurized with H_2 gas.

Samples for Sb speciation analysis were analyzed using liquid chromatography coupled to an ICP-MS (LC-ICP-MS). Five standards of 1-100 µg/L $Sb(III)_{(aq)}$ and $Sb(V)_{(aq)}$ were prepared by dissolving $SbCl_3$ (J.T. Baker, Center Valley, PA) and $KSb(OH)_6$ (Electron Microscopy Sciences, Hatfield, PA) with DI water. The concentration of Sb in the standards was verified by ICP-MS analysis prior to LC analysis, analytical method of ICP-MS described previously. Antimony species (III/V) were separated in the samples using an IonPac AS12A 4x200 mm Carbonate Eluent Anion-Exchange Column (Dionex, Sunnyvale, CA). The eluent solution consisted of ammonium bicarbonate and tartaric acid. Description of the analytical method for preparing EDTA preservation solution and eluent solution is outlined by the Centre of Expertise in Environmental Analysis of Quebec (2013). The injection volume was 100 µL, flow rate was set at 1.5 mL/min and the radio frequency (RF) power was set to 1500 W. An ICP-MS standard of 50 µg/L ^{115}Indium was added as an internal standard to the mobile phase. The

retention time for Sb(III) and Sb(V) was approximately 2.3 and 1.4 minutes, respectively. Antimony (^{121}Sb) counts were divided by the internal standard (^{115}In). The background was subtracted and the area under the resulting peaks was integrated using the Microcal Origin 6.0 software package (Northhampton, MA).

2.3.3.2 Soils

Each bulk soil sample collected from the pristine and contaminated berms was dried at 50°C for approximately 12 hours and sieved to <75 μm (< #200 sieve). Approximately 5-7 gram subsamples were mixed with 5-7 drops of a binder (polyvinyl alcohol) and pressed into a powder pellet using a hydraulic bottle jack at 20,000 psi. Each pellet was analyzed using a PANalytical (Almelo, The Netherlands) Axios four kW wavelength dispersive x-ray fluorescence spectrometer (XRF). The calibration standards for major elements were made using the geologic reference materials BIR-1, PCC-1, JA-2, JB-2, JP-1, JR-1, GXR-3, GXR-1, MRG-1, and SGR-1, as described in Ilgen et al., 2011. Samples and standards were analyzed in triplicate with corresponding errors reported and detection limits calculated based on analysis of the reference standards.

To identify crystalline phases present in the four types of pristine soil, randomly orientated dried (60°C for 2 hours) soil was analyzed by X-ray powder diffraction (XRD) using an X'Pert PRO Material Research Diffractometer (PANalytical) equipped with a Cu (Kα λ = 1.54277 Å) X-ray tube with a generator set at 45 kV and 40 mA. Scans were collected from 5 to 65° 2Θ and a counting time of 180 s per point at 0.0125° step size. Diffraction patterns were processed using PANalytical's X'Pert HighScore Plus 2.2 software package and Bragg peaks

were matched by hand using the Indiana Geological Survey's Table of Key Lines (Indiana University, Bloomington, Indiana).

Samples were analyzed for elemental distribution and speciation using x-ray fluorescence (XRF) mapping and x-ray absorption near edge spectroscopy (XANES) techniques, which were collected at beamline station 10-2 (bulk analysis), 2-3 (micro-focused analysis for Pb) and 14-3 (micro-focused analysis for Sb) at the Stanford Synchrotron Radiation Lightsource (SSRL) in Menlo Park, California. Samples were mapped on BL10-2 for bulk elemental distribution and BL2-3 for micro-speciation with a 2.5 x 2.5 μm beam generated by Pt-coated Kirkpatrick-Baez mirrors (Xradia Inc.) with the SPEAR accelerator ring operating ~350-500 mA at 3.0 GeV. The incident energy was tuned to 13,055 eV, just above the Pb L_{III} absorption edge, using a Si (111) double crystal monochromator. Samples were rastered at a 45° incident angle to the incoming x-ray beam. A Si drift Vortex detector (SII Nano Technology, Northridge, CA) positioned perpendicular to the incident beam was used to monitor sample fluorescence. Dwell time and step size differed for each sample depending on the size of the area of interests. In general, the dwell time was set at 100 ms with a 40 μm step size for the bulk line and 5-10 μm step size and 10-25 ms dwell time. Samples were selected to map at multiple energies (13,025 eV, 13,037 eV, 13,041 eV, 13,045 eV and 13,053 eV) to investigate Pb oxidation state variability across an area in the sample. Micro-focused XANES data was collected from select Pb spots within the samples.

The incident energy on BL14-3 was tuned to 4,170 eV, just above the Sb L_{III} absorption edge, using a water-cooled Si (111) double crystal monochromator. The sample chamber was flushed with He gas to purge oxygen levels in the chamber to below 2% O_2. Samples were scanned above (4,150 eV) and below (4,100 eV) the Sb L_{III} absorption edge to investigate the x-

ray overlaps with Ca in the samples. Samples were rastered at a 45° incident angle to the incoming x-ray beam and the fluorescence signal was detected using a Si drift Vortex detector (SII Nano Technology, Northridge, CA). Step size and dwell time was set at 5-10 μm and 10-25 ms, respectively. Select samples were selected to map at multiple energies (4,120 eV, 4,142 eV, 4,148 eV and 4,170 eV) to investigate Sb oxidation state variability across an area in the sample. Micro-focused XANES data was collected from select Sb spots within the samples.

The XRF maps and XANES spectra were analyzed using the Microanalysis Toolkit (Webb, 2005). All spectra and model compounds were calibrated to the first inflection of the absorption edge of a Pb and Sb foil standard at 13,035 eV and 4132 eV, respectively, which were collected at the beginning and end of the beam run and periodically throughout the run as a check for monochromater drift. Spectra were corrected for deadtime (if needed) and the background was subtracted, averaged and normalized to a unit edge step using the SIXPACK software package (Webb, 2005). The XANES spectra were compared to standard and model compounds using linear combination fitting (LCF). Data processing is described in more detail in Kelly et al., (2008). Antimony standards included Sb foil (provided by SSRL standard reference foils), metallic Sb powder (99.999% metallic Sb powder, ~200 mesh size; Alfa Aesar, Ward Hill, MA), Sb_2O_3 (J.T. Baker, Center Valley, PA), Sb_2O_5 (Alfa Aesar, Ward Hill, MA), $NaSb(OH)_6$ (Alfa Aesar, Ward Hill, MA), $KSb(OH)_6$ (Electron Microscopy Sciences, Hatfield, PA) and lewisite. Lead standards included Pb foil (provided by SSRL standard reference foils), zero-valent Pb (analysis of a fresh, unfired bullet alloyed core), PbO (Litharge, Alfa Aesar, Haverhill, MA), $PbCO_3$ (Alfa Aesar, Haverhill, MA), hydrocerrusite (normalized absorption provided by Hayes et al., 2012) and Pb(II) sorption model compound with synthesized Fe oxides. The Pb(II) sorption compound was prepared by mixing 40 mL of a 0.1 M solution of $Pb(NO_3)_2$ (Alfa Aesar,

Haverhill, MA) with 1 g of 2-line ferrihydrite (pH = 8.06) and adjusting the pH to 6.5 using 1 M KOH (~2 drops). The preparation for ferrihydrite is outlined in Schwertmann and Cornell, (2007). The slurry was rotated for 24 hours, centrifuged at 6000 rpm for 30 minutes and the solid and supernatant liquid was separated by gravity filtration. The solid was air dried, stored in a sealed container (Nalgene, Fisher Scientific, Waltham, MA) and analyzed within 6 days from preparation.

2.3.3.3 Statistical Analysis

For data analysis, the statistical package JMP Pro 11 (JMP, Version 11, SAS Institute Inc., Cary, NC) was used to determine differences and variability for Pb and Sb as a function of time and soil type. One-way ANOVA was determined using bivariate analysis with a significance level of $p < 0.05$. To determine which means were different, student's t test was used as a post hoc multiple comparison technique. Levels (A, B, C, D, E, etc.) were reported to indicate statistical significance and levels not connected by the same letter were determined to be not significantly different at $p < 0.05$.

2.4 Results

2.4.1 Pristine Soil and Bullet Characterization

Pristine samples of the four soil types (silt loam, sand, loamy sand and sandy loam) before construction of the berms were analyzed for soil texture, bulk elements, background aqueous and solid phase Pb/Sb concentrations and mineral phases. Tabulated results are shown in Table 2.1 and x-ray diffraction results can be found in Appendix A, Figure 2.13. The soil pHs

(1g to 1mL DI water) range from 5.34 for the silt loam end member to 8.38 for the sand end member. The 'mixed' soil types have soil pH values of 5.66 for the loamy sand and 6.75 for the sandy loam. The silt loam end member can be characterized as having greater surface area, higher organic matter content and a higher cation exchange capacity (CEC) than the sand end member (Table 2.1). The sand end member contains higher concentrations of Ca, Fe, Si, As, Cu, Mn, Ni, Pb, Sb, Sn, Sr, Ti and Zn, while the silt loam end member contains higher concentrations of Al and Ba (Table 2.1). The soil types were below detection limit for $Pb_{(aq)}$, but contain 'background' $Sb_{(aq)}$, ranging from 1.1 to 2.4 µg/L. Major mineral phases in common between the soil types are quartz (SiO_2) and plagioclase $(Na,Ca)(Si,Al)_4O_8$. Chlorite $(Mg,Fe,Li)_6AlSi_3O_{10}(OH)_8$ and mica/illite $(KAl_3Si_3O_{10}(OH)_2$ were found exclusively in silt loam-containing soils.

Information on the lot of bullets used in the test berm experiment is presented in Table 2.2. Data was collected and provided by Defense Ammunition Center (DAC) – Munitions Items Disposition Action System (MIDAS). The bullet jacket is comprised primarily of Cu and Zn, to a lesser extent. Trace amounts of Pb and Fe are present. The bullet core consists of Fe with trace amounts of Mn, C and S. The bullet slug is 99% Pb and 1% Sb, accounting for approximately 31.7 g Pb and 0.3 g Sb per bullet deposited into the test berms.

2.4.2 Total Pb and Sb Concentrations in Berm Soils

XRF analysis of the pristine and 'fired' (contaminated) berms for the different soil types are shown in Table 2.3. These results show that the solid phase concentrations of Pb, Sb, Cu, Sn and Zn are significantly elevated in the contaminated berm soils, which was expected considering the initial composition of the unfired bullets. Concentrations of Ni were found to be

relatively constant between the berm types. Concentrations of Pb are 50 times higher than Sb in the contaminated soils, on average (Table 2.3). Copper concentrations were the second highest to Pb, then Sb, Zn and Sn.

The pristine soil containing sand had higher concentrations of Pb, Sb, Cu, Sn and Zn than the soils containing primarily silt loam. For the contaminated soils, the sand had higher concentrations of Pb, Sb, Cu, Sn and Zn. The degree to which the bullets were fragmented in the sand soil was greater than in the soils containing loam, which could have led to a higher percentage of the bullets to be sampled as part of the soil fraction. Since the sampling procedure for the contaminated berms was careful to not include any large bullet fragments, the higher concentrations of metals in the sand containing soils is likely a consequence of the greater fragmentation capacity of the large particles in sand. The sand containing soils do naturally have higher concentrations of Pb, Sb, Cu, Sn and Zn (Table 2.1), but that alone does not explain the large difference between soil type concentrations seen in the contaminated berms. Comparing the duplicate berms showed higher concentrations of Pb, Sb, Cu, Sn and Zn in the un-amended berms (6, 8, 10, 12) than in the Fe amended berms (5, 7, 9, 11). The only exception is for Sb in the sand duplicate where Sb concentrations are higher in the amended berm (5) than un-amended (6). For the most part the differences are small, particularly for Sb, Sn and Zn, but for Pb and Cu the differences are more substantial.

2.4.3 Total Pb and Sb Concentrations in Berm Runoff

Trace metal analysis of the berm water runoff highlights key differences in solution behavior between Pb and Sb as a function of soil type. Box plots showing the distribution of Pb and Sb concentrations over the course of 4 sampling summers are shown in Figure 2.2. Sampling

summer 2015 was not included for comparison because Fe amendments were added to a subset of the berm soil types. Statistically significant differences ($p < 0.05$) in the distributions are indicated with lettered levels (A, B, C for Pb and A, B, C, D, E for Sb). Levels not connected by the same letter are significantly different at $p < 0.05$. The highest concentrations of Sb are found in the sand runoff, whereas the highest concentrations of Pb are found in the loamy sand runoff. In general, Sb concentrations are higher than Pb for the sand and sandy loam runoff. Concentrations of Pb were not significantly different ($p < 0.05$) in the runoff from the sand and silt loam soils. Pb concentrations did vary significantly in the runoff from the loamy sand duplicate berms, with duplicate 'b' containing the highest concentrations of Pb over four years (Figure 2.2). The other duplicate berm soil types for Pb besides loamy sand did not vary significantly. Concentrations of Sb varied significantly between end member soil types (sand versus silt loam). For both Pb and Sb, the silt loam soil runoff contained the lowest concentrations, exhibiting a greater retention capacity (Figure 2.2).

In relation to weathering time, Pb and Sb concentrations varied from 2011 to 2015. Box plots showing concentrations of Pb as a function of summer sampling season 1 (2011), 2 (2012), 3 (2013), 4 (2014) and Fe versus control (August 22, 2016 to end of sampling 2015) is shown in Figure 2.3 and Figure 2.4 for Sb. For Pb, the presence of sand in the berm soils corresponded to a greater amount of significantly different sampling years, potentially indicating sandy soil creates higher variability in aqueous Pb concentrations leaching from bullets. While there were spikes in concentrations for the silt loam draining berms, overall the majority of the data and the means were not significantly different over the course of 5 years (Figure 2.3). For Sb, sand soil runoff contained the highest concentrations annually, but did not show significant variability between years (Figure 2.4). Only the sandy loam soil showed significantly different data sets comparing

2011 to 2015. Similar to Pb, the silt loam runoff contained generally low concentrations of Sb and showed little variability over the course of 5 years, except for 2012 to 2013 in Berm 12 (Figure 2.4h).

The $FeCl_2/CaCO_3$ amendment was added to a subset of the berms (5, 7, 9, and 11) at the end of summer 2014 in order to study Pb and Sb retention, results are shown for Pb in Figure 2.3 a, c, e and g in comparison to the control berms that were not amended (Figure 2.3 b, d, f, h) and for Sb in Figure 2.4 a, c, e and g in comparison to the control berms that were not amended (Figure 2.4 b, d, f, h). The Fe amendment had little effect on Pb immobilization in berm soil runoff, except in the sand draining soils where Pb distributions were significantly lower in the control sand berm (un-amended) than the Fe amended berm (Figure 2.3). The Fe versus 'ctrl' distributions are marked (*) if distributions are significantly different at $p < 0.05$. For the remainder of the berms, the runoff was not significantly different at $p < 0.05$ comparing the amended and un-amended berms. Antimony, however, behaves much differently than Pb after the Fe addition and is significantly immobilized in all the soil types except the silt loam (Figure 2.4, g and h), where concentrations of Sb were already low (Figure 2.2). In addition, the silt loam draining Berm 11 contained little runoff during 2015 and sampling was limited.

2.4.4 Sb Speciation

The speciation of aqueous Sb was found to be different between the sand and silt loam soil types as a function time. The speciation of mobile Sb species was investigated for the soil types of the test berms for years 1-2, results are shown in Figure 2.5b and c, with the retention times for Sb standards of 100 µg/L Sb(III), Sb(V) and DI water are shown in Figure 2.5a. Analysis of the sand and sandy loam berm runoff in 2011 showed the sole presence of Sb(V).

There is detectable Sb(III) in the loamy sand runoff of one of the duplicate sets of berms (Figure 2.5b) and was quantified to be 35 μg/L Sb(III). This is the only observation of Sb(III) in the runoff during the 5 year monitoring, in the high loam content berms after less than 1 year of weathering. All other Sb samples tested were found to be fully oxidized. The silt loam-draining berms were not quantified for Sb speciation due to the overall low sample volume collected from the berm runoff and the low concentrations of total Sb, however, we expect similar behavior in that Sb(III) is the initial aqueous oxidation product. At the beginning of summer 2 (2012) we analyzed the test berms again, but found only fully oxidized Sb in 2012 for all soil types (Figure 2.5c). Oxidation of Sb was expected to be fast, as determined by Ilgen et al., 2014, and sequential oxidation is rarely observed in shooting range berms due to the lack of Sb(III) stability in oxidizing soil conditions and the usually long reaction time shooting range berms have before analysis.

The speciation of Sb in the soil fraction was investigated for all test berm soil types as a function of time using XRF mapping and Sb L_{III}-edge μ-XANES spot analysis and is presented in Figure 2.6. Corresponding linear combination fitting results are shown in Table 2.4. Zero-valent Sb occurred within the bullet core and Sb(V) occurred in the soil fraction in the silt loam soil type, adjacent to the bullet core (XRF map not shown). The normalized absorption edge energies (Figure 2.6) show differences between the zerovalent Sb absorption (4132.0 eV), trivalent Sb oxide absorption (4133.4 eV) and pentavalent Sb oxide absorption (4143.1 eV). Spectra were compared to a variety of Sb(III) and Sb(V) compounds with metallic Sb and Sb_2O_5 contributing to the best fit. Only the silt loam-containing soil sample is shown due to the higher content sand soils showing little accumulation of Sb in the soil fraction making collection of spectra challenging and with high signal to noise ratio. Instead, Sb was present as a diffuse signal

throughout the soil. Antimony is present in bullets in low percentages and has been shown to partition to soil solution to a greater extent than Pb in all systems (Figure 2.2), leading to low concentrations for XANES analysis, particularly for sand-containing soils. Furthermore, studying Sb L_{III}-edge in soil samples is difficult due to abundance of Ca typically found in natural soil samples. The Sb L_{III}-edge is at 4132.0 eV, whereas the Ca K-edge is at 4038.5 eV. The emission line for Sb-$L\alpha_1$ is 3603.8 eV and Ca-$K\alpha_1$ is 3692.3 eV. This difference in less than 100 eV leads to some overlap in the fluorescence channel data. As a result, we mapped above and below the Sb L_{III}-edge and used filtering and masking techniques within the program MicroToolKit (Webb, 2005) in an effort to separate Sb and Ca fluorescence overlap. Using these methods, differentiating between zero-valent Sb and Sb(V) was achieved for soil samples (Figure 2.6).

2.4.5 Pb Speciation

The Pb speciation was investigated for all test berm soil types as a function of time using XRF and Pb L_{III}-edge μ-XANES spot analysis. Overall, 90 samples were analyzed from the four types of soil as a function of year from 2011 to 2014. The results are shown in Figure 2.7 with LCF parameters presented in Table 2.5. Overall, the Pb speciation in the soil fractions consisted primarily of metallic Pb, litharge, cerussite, hydrocerussite and Pb sorbed to Fe(III) oxides when comparing the berm samples to various standards and model compounds. Pb L_{III}-edge μ-XANES spectra (Figure 2.7) and fitting parameters (Table 2.5) are shown for samples with the best fits with careful attention to ensure the samples presented are representative, as a whole.

Fired bullets are not uniformly fragmented in soil often resulting in highly heterogeneous distributions of metals. Lead and Fe distribution are shown for samples collected after two years of weathering in Figure 2.8. Metallic Pb was detected in each soil type throughout the sampling

years and remained a large fraction of the total Pb in the samples. In addition to metallic Pb, the primary Pb products were litharge, cerussite and hydrocerussite for the first two summer seasons (2011-2012) (Figure 2.8). These species occurred primarily as a crust around the Pb alloy or present as Pb hotspots throughout the soil (Figure 2.8). After two years, the presence of Pb sorbed species was detected and the best fits of many soil samples included contributions of Pb(II) sorbed to Fe(III) oxides (Table 2.5). While the majority of the spots for years 3 and 4 include contributions from sorbed species, there are also spots that are characterized differently. There are distributions that only contain metallic Pb and are either part of the bulk metal alloy or present in small (~1-50 μm) highly concentrated globular areas, similar to the initial weathering samples. This highlights the heterogeneity of bullet samples and emphasizes the fact that metal release from the weathering of bullets is discontinuous. After four years reaction time, there is still a large percentage of metallic Pb present, but major Pb phases consists of litharge, cerussite, hydrocerussite and Pb(II) sorbed.

2.5 Discussion

2.5.1 Evolution of Bullet Corrosion Products as a Function of Time

The weathering of Pb in the bullet alloy exhibits distinct transformation stages as a function of time. The dominant Pb oxidation products within 2 years of weathering appear to be PbO, cerussite and hydrocerrusite, which tend to form as a crust around the surface of the fragmented bullet alloy. These species can also occur with Pb^0 hotspots that are separated from the parent bullet and heterogeneously dispersed within the soil fraction (Figure 2.8). The overall occurrences and average percent contributions of each detected Pb corrosion product is shown in

Table 2.6. For all soil types within the 2 years, Pb^0 and cerrusite yield the highest average percentage of Pb species. After 3 years weathering time, sorbed Pb species were detected as a large percentage of the overall composition of the corrosion products. The appearance of sorption products after 3 years weathering time is likely an indication that oxidation and weathering reactions are kinetically limited and it takes several years for the sorbed species to accumulate to detectable levels for the analytical method. The XANES spectra of sorbed Pb (Figure 2.7) does not have many distinctive features and could potentially be present at low concentrations during the first two years and not detected using Pb L_{III} XANES methods. Based on these findings, a summary of the overall dominant Pb weathering corrosion stages are summarized in Figure 2.9. Upon exposure to air and water, the fragmented bullet alloy initially oxidizes to a combination of PbO, cerussite and hydrocerussite, with cerussite being the dominant weathering product from 0-2 years. Dissolution of PbO, cerussite and hydrocerussite releases Pb^{2+} into soil solution. After 3 years weathering time, sorption corrosion products are detectable by XANES spectroscopy with hydrated Pb^{2+} bound to the surface of Fe(III) oxides via sorption processes. After 4 years weathering time, cerussite and Pb sorbed to the surface of Fe(III) oxides are the dominant solid-phase corrosion products.

The initial detection and quantification of $Sb(III)_{(aq)}$ in the high content loam berm is a novel result, revealing information about the overall oxidation kinetics of Sb^0 – Sb(III) – Sb(V) in shooting range soil runoff during the initial stages. While colder temperatures found near the Arctic have been shown to slow mineral weathering reaction rates (Langman et al., 2014), chemical interactions do not entirely cease to occur during the winter months (Mikan et al., 2002), particularly because the sun is still active and freeze/thaw periods do occur (Barker et al., 2014). Initial oxidation of Sb^0 to $Sb(OH)_{3(aq)}$ occurred within 9 months in the loamy sand soil

(Figure 2.10). While this study did not detect any Sb(III) solid formation, based on the findings in Chapter 3 from an older shooting range berm, we anticipate Sb(III) is formed as a transient product, leading to the release of $Sb(OH)_3$ in solution. Once oxidized, $Sb(OH)_{3(aq)}$ is released into solution and in the higher content sand berms, oxidized within 9 months. In the higher content loam berms, both oxidation states exist initially in runoff and are fully oxidized on the order of 1-2 years.

2.5.2 Transport of Pb and Sb

Elemental correlations in the berm water runoff indicate that both Pb and Sb behave similarly in the higher silt loam content berms, with R-squared values of the linear regression averaging to 0.67 (Figure 2.11). There was no correlation (R^2<0.50) found in their behavior in the higher sand content berms. Element correlations and linear regression R-squared values are shown in Table 2.7 for individual elements and matching pairs. Both Pb and Sb were also shown to behave similarly to Cu in certain soil types, likely sourced from zero valent metal oxidation from bullet weathering. For Sb, the correlations with Cu were found in all the soil types and 5 out of the 8 contaminated berms with an R-squared value average of 0.57, while Pb and Cu correlations were only found in the 100% silt loam (berm 11) with an R-squared value of 0.84 (Table 2.7). This result was anticipated considering the abundance of zero-valent Pb, Sb and Cu deposited in the test berms and the likelihood the metals would mobilize upon fragmentation. In addition, Sb was found to behave similarly to Ca and to a lesser extent Fe and K, potentially indicative of colloidal association and transport (Figure 2.11). Associations with other positively charged cations investigated (Na, K, Mg) were not found, but this could be primarily because concentrations were too low.

Concentrations of Pb and Sb in 200 and 450 nm size fractions were investigated in order to compare this study to other shooting range studies that have determined colloids are a major component in the overall transport of Pb and Sb (Yin et al., 2010; Klitzke et al., 2012). Concentrations of Pb and Sb were unchanged between the two different size fractions. However, concentrations of Al, Mn, Fe, Ba, Zn were consistently lower in the 200 nm filter samples than in the 450 nm filter samples indicating the presence of nano-sized particles (between 200 and 450 nm) in the berm water runoff (data not shown). The majority of the particle fractions (200-450 nm) for all the test berms (1-12) consisted of Al (27%), Fe (33%) and Ba (63%) and to a lesser extent Mn (7%) and Zn (18%). Colloidal transport of Pb and Sb by particles ranging from 200-450 nm was not detected. The weak correlations between Sb and Fe (Table 2.7) may be a product of colloidal transport of Fe particles <200 nm.

2.5.3 Natural Versus Artificial Attenuation of Metals in Soil

Soil type plays a significant role in the overall retention of the deposited metals in our systems. Average concentrations of both Pb and Sb were relatively low in the runoff from the silt berms in comparison to the sand berms. Furthermore, concentrations were also considerably less variable in the silt loam runoff (besides a spike in Pb concentrations in Berm 11 in 2014), representing a relatively low and steady leaching rate. Both soils have similar elemental concentrations (excluding Mn fraction; Table 2.1). However, the silt loam soil also has triple the surface area and 30 times the organic matter (L.O.I.; Table 2.1). The higher surface area, low particle size and high organic content of the soil fraction translate to minimal transport of water from the berm to the runoff lysimeter and a greater retention capacity for moisture. The silt loam soil also requires a greater amount of water (precipitation) to saturate the berms. During sampling after a large rain event, the silt loam berm lysimeters were often completely dry in

comparison to the full sand berm lysimeters. Transport of water out of the loam systems is small in comparison to the sand (Appendix A, Figure 2.15). This likely plays a role in the overall flushing out of metals from the berms. The loam berms retained moisture and retained Pb and Sb to a greater extent than the sand berms (Appendix A, Figure 2.15). The variability in the concentrations of Pb and Sb in the runoff from the sand-containing berms is indicative of the permeability of the sand. While pH likely played a role in precipitating Pb in the 100% sand system, concentrations were still on average higher than the loam berm, highlighting the natural ability for silt loam soil type to immobilize Pb and Sb in shooting range systems.

The Fe amendment ($FeCl_2$ + $CaCO_3$ buffer) added in 2014 represents a cost-effective, easy-to-apply solution to minimize Pb and Sb migration off-site. The addition immobilized Sb by 63% compared to the control (no addition), on average, except in the 100% silt loam berms where the addition made little impact in the overall immobilization of Sb. For Pb, the Fe addition was effective at immobilizing Pb in the mixed soils, but not in the 100% end members, where Pb was more mobilized, initially. The total element concentrations for Pb, Sb, Cu, Ni and Zn are shown in Table 2.8 with the date of the Fe addition highlighted (August 22, 2014). The runoff from the 100% silt loam – Fe amended berm does not have data for August 22, 2014 because there was no runoff to be collected. The runoff from the addition was entirely retained by the soil. In the mixed berms, concentrations of Pb were 44% lower as a result of the Fe amendment, on average. While the Fe amendment proved excellent at retaining Sb, it only moderately retained Pb. Furthermore, the application of the Fe amendment to the actual bullet pocket initially mobilized certain elements (Pb, Ni, Cu, and Zn; Table 2.8) due to an instantaneous drop in pH caused by Fe hydrolysis in solution. The $CaCO_3$ component was added in tandem in order

to buffer the pH, but in a subset of the berms there was still a measurable drop in pH. The pH drop had no effect on Sb mobility.

2.5.4 Landscape-scale Shooting Range Design and Remediation Strategies

Designing a shooting range and implementing remediation strategies for DoD land should be tackled in parallel and consist of 3 major consideration points. The first major consideration is whether the berms will be natural or man-made. If the berms are natural then they consist of a natural hillside or slope, which is fired upon. If the berms are man-made then they primarily consist of disrupted soil that has been manually moved to a target location. This consideration will affect whether or not there can be any separation between pristine ground and the contaminated berm. The second major consideration is what type of soil comprises the berm or hillside. This will affect the overall speciation and mobility of the target contaminant species in bullets (Pb and Sb). The third major consideration is how to apply or implement a remediation strategy that is effective for both Pb and Sb, which are the major contaminants of interest. The remediation strategy must be easily applied, cost-effective and target both Pb and Sb species, which were shown in this study to be variable in oxidation state and variable in the local structure. All of which affect the potential for off-site migration of Pb and Sb.

Based on the findings in this study, Figure 2.12 presents a schematic for the landscape-scale design of shooting range berms and remediation strategies for DoD land managers. This recommendation is based on limiting both Pb and Sb migration in runoff while being cost-effective and easy to implement. The design starts with silt loam soil loaded onto an impenetrable waterproof geoliner and the geoliner is funneled into a trough. If a natural hillside is used instead of a berm then the geoliner cannot be utilized. This is not as ideal considering

there will be no separation between the pristine and contaminated soils, but this study did find that there was minimal downward leaching into the soil fraction and overland runoff produced the majority of the Pb and Sb concentrations. Inside the trough, a mixture of $Fe(OH)_3$ – coated sand. The Fe is already oxidized and precipitated, therefore dramatic fluctuations in pH should not be a concern. The coated sand increases particle size and porosity, creating a higher degree of infiltration and interaction with the runoff. Additional treatments over time will most likely be required and can be added on a monthly or yearly basis. While the Fe addition directly to the soil was very effective for Sb immobilization, it did not produce the same results for Pb immobilization (Table 2.8). The silt loam soil type was naturally effective at immobilizing both Pb and Sb over sand. While the silt loam soil did stabilize Sb(III) initially, which has been shown to be more toxic than Sb(V), it rapidly oxidized to Sb(V) in solution. Given the transitory nature of Sb(III) in shooting range soils, the overall benefits of using silt loam for construction outweigh the concerns.

2.6 Conclusion

The overall setup and design of this study made it possible to observe initial transformation pathways and corrosion products of Pb and Sb in newly constructed target berms. The initial products formed have often been overlooked in previous studies due to a focus on older, heavily used shooting range samples. Liquid speciation analysis confirms the presence of $Sb(III)_{(aq)}$ in the berm runoff of the high content loam mixed soil, indicating Sb(III) is likely the initial oxidation product formed from the weathering of Sb^0 in the alloy. Solid-phase analysis of the shooting range soil show Sb(V) dominates in the soil fraction and zero-valent Sb in the bullet

alloy. Distribution of Pb in the samples and speciation analysis showed metallic Pb and cerussite as the dominant corrosion products after 2 years and revealed a time-dependence unique to sorption processes, overall.

In addition, the aqueous concentrations of Sb were determined to be greater than Pb in all the soil types indicating Sb is more mobile despite the fact that Sb is present ~2 orders of magnitude less in bullets than Pb. The highest concentrations of Sb were found in the sand soil runoff and the highest concentrations of Pb were found in the mixed soil runoff. For both species, the 100% silt loam soil runoff contained the lowest concentrations, highlighting the overall natural effectiveness silt loam soil has on metal(loid) retention. Correlations ($R^2 > 0.6$) existed between Pb and Sb, Pb/Sb with Cu, Sb with Ca, and weak correlations ($R^2 < 0.6$) existed between Sb and Fe and Sb and K in the berm runoff. Information from this study will be useful to understanding the overall mobility and speciation of Pb and Sb with respect to soil properties and reaction time in shooting range soils.

This study establishes an overall procedure for designing shooting ranges and implementing remediation strategies in parallel that is cost effective, easy to implement and effective at immobilizing both Pb and Sb. The design takes into account natural hillsides versus man-made berms that are often used to construct shooting ranges. One key difference in this study and other shooting range remediation studies is the addition of the amendment to only the runoff instead of the bullet pocket/soil in order to minimize mobilization of one element over the other since Pb and Sb behave differently in soil. Instead, the berms are constructed of 100% silt loam type soil, which this study showed was effective at naturally retaining Pb and Sb and minimizing local migration. Overall, this study establishes an initial baseline of Pb and Sb speciation products from deposition to 5 years in the future, which has been often overlooked by

similar studies. In particular, this study offers a baseline of information for shooting ranges in Alaska. In addition, this research offers a suggestion for safely building shooting ranges that have minimal introduction of Pb and Sb into the surrounding environment.

2.7 Acknowledgments

Funding for this project was from the Department of Defense, Strategic Environmental Research and Development Program (ER-1770). Cold Regions Test Center assisted in designing/building the target berms and assisted in the coordination of firing 16,000 5.56 mm bullets at the Donnelly Training Area, Ft. Greely, Alaska. The Stanford Synchrotron Radiation Lightsource of Stanford Linear Accelerator Center in Menlo Park, California provided assistance with collection of x-ray absorption and fluorescence data. The project received continual support from Dr. Sam Webb, Dr. Benjamin Kocar, Dr. Courtney Roach and Cynthia Patty of SSRL throughout the beamtime allocations. Numerous students and collaborators are acknowledged on this project for field and laboratory assistance. Maciej Śliwiński, Karen Spaleta and Ken Severin from the Advanced Instrumentation Laboratory at the University of Alaska Fairbanks assisted in analyzing samples. Fellow graduate students, Tiffany Gatesman and Erik Talvi assisted with data collection at SSRL.

2.8 References

Ackermann S., Gieré R., Newville M. and Majzlan J. (2009) Antimony sinks in the weathering crust of bullets from Swiss shooting ranges. *Sci. Total Environ.* **407**, 1669-1682.

Barker A.J., Douglas T.A., Jacobson A.D., McClelland J.W., Ilgen A.G., Khosh M.S., Lehn G.O. and Trainor T.P. (2014) Late season mobilization of trace metals in two small Alaskan arctic watersheds as a proxy for landscape scale permafrost active layer dynamics. *Chem. Geol.* **381**, 180-193.

Basunia S. and Landsberger S. (2001) Contents and leachability of heavy metals (Pb, Cu, Sb, Zn, As) in soil at the Pantex firing range, Amarillo, Texas. *Air Waste Manage. Assoc.* **51**, 1428-1435.

Belzile N., Chen Y. and Wang Z. (2001) Oxidation of antimony (III) by amorphous iron and manganese oxyhydroxides. *Chem. Geol.* **174**, 379-387.

Cao X.D., Ma L.Q., Chen M., Hardison D.W. and Harris W.G. (2003) Weathering of lead bullets and their environmental effects at outdoor shooting ranges. *J. Environ. Qual.* **32**, 526-534.

Centre of Expertise in Environmental Analysis of Quebec. (2013) Determination of the speciation of antimony, arsenic, chromium and selenium: Method by high pressure liquid chromatograph coupled to a spectrometer mass ionizing source argon plasma, *MA. 200 - Spec. Met. 1.1, REV. 1*, Ministry of Sustainable Development, Environment, Wildlife and Parks Quebec, 21 p.

Clausen J.L., Bostick B. and Korte N. (2011) Migration of Lead in Surface Water, Pore Water, and Groundwater With a Focus on Firing Ranges. *Critical Reviews in Environmental Science and Technology* **41**, 15, 1397-1448.

Defense Ammunition Center (DAC), Munitions Items Disposition Action System (MIDAS). Detailed Structure for CTG 5.56 mm Ball M855.

Denaix L., Semlali R.M. and Douay F. (2001) Dissolved and colloidal transport of Cd, Pb, and Zn in a silt loam soil affected by atmospheric industrial deposition. *Environmental Pollution* **114**, 1, 29-38.

Dzombak D.A. and Morel F. M. M. (1990) Surface Complexation Modeling, Hydrous Ferric Oxide; John Wiley & Sons: New York.

Feng R.W., Wei C.Y., Tu S.X., Wu F.C. and Yang L.S. (2009) Antimony accumulation and antioxidative responses in four fern plants. *Plant and Soil* **317**, 93-101.

Griggs C.S., Martin A.W., Larson S.L., O'Connor G., Fabian G., Zynda G. and Mackie D. (2011) The effect of phosphate application on the mobility of antimony in firing range soils. *Science of the Total Environment* **409**, 12, 2397-2403.

Guemiza K., Mercier G. and Blais J. (2014) Pilot-Scale Decontamination of Small-Arms Shooting Range Soil Polluted with Copper, Lead, Antimony, and Zinc by Acid and Saline Leaching. *J. Environ. Eng.* **141**, 1.

Hardison Jr. D.W., Ma L.Q., Luongo T. and Harris W.G. (2004) Lead contamination in shooting range soils from abrasion of lead bullets and subsequent weathering. *Science of the Total Environment* **328**, 175-183.

Hayes S.M., Webb S.M., Bargar J.R., O'day P.A., Maier R.M. and Chorover J. (2012) Geochemical Weathering Increases Lead Bioaccessibility in Semi-Arid Mine Tailings. *Environ. Sci. Technol.* **46**, 11, 5834-5841.

(IARC) International Agency for Research on Cancer. (1989) IARC Monograph 47. Lyon.

Ilgen A.G., Rychagov S.N. and Trainor T.P. (2011) Arsenic speciation and transport associated with the release of spent geothermal fluids in Mutnovsky Field (Kamchatka, Russia). *Chem. Geol.* **288**, 115-132.

Ilgen A.G., Majs F., Barker A.J., Douglas T.A. and Trainor T.P. (2014) Oxidation and mobilization of metallic antimony in aqueous systems with simulated groundwater. *Geochimica et Cosmochimica Acta*. **132**, 16-30.

(ITRC) Interstate Technology and Regulatory Council Small Arms Firing Range Team. (2003) Characterization and Remediation of Soils at Closed Small Arms Firing Ranges. *Technical/Regulatory Guidelines*.

Jardine P.M., Parker J.C., Stewart M.A., Barnett M.O. and Fendorf S.E. (2007) Decreasing Toxic Metal Bioavailability with Novel Soil Amendment Strategies. SERDP ER-1350 Final Report.

Johnson C., Moench H., Wersin P., Kugler P. and Wenger C. (2005) Solubility of antimony and other elements in samples taken from shooting ranges. *J. Environ. Qual.* **34**, 248.

Jorgensen S.S. and Willems M. (1987) The fate of lead in soils – the transformation of lead pellets in shooting-range soils. *Ambio*. **16**, 11-15.

Kelly S.D., Hesterberg D. and Ravel B. (2008) Analysis of Soils and Minerals Using X-ray Absorption Spectroscopy in *Methods of Soil Analysis. Part 5. Minerological Methods.* (pp. 387-465). SSSA Book Series, no. 5.

Keto R.O. (1999) Analysis and comparison of bullet leads by inductively-coupled plasma mass spectrometry. *J. Forensic. Sci.* **44**, 1020-1026.

Klitzke S., Lang F., Kirby J.K. and Hamon R. (2012) Lead, antimony and arsenic in dissolved and colloidal fractions from an amended shooting-range soil as characterized by multi-stage tangential ultrafiltration and centrifugation. *Environmental Chemistry* **9**, 5, 462-473.

Labare M.P., Butkus M.A., Riegner D., Schommer N. and Atkinson J. (2004) Evaluation of lead movement from the abiotic to biotic at a small-arms firing range. *Environmental Geology* **46**, 6, 750-754.

Langman J.B., Moore M.L., Ptacek C.J., Smith L., Sego D. and Blowes D.W. (2014) Diavik Waste Rock Project: Evolution of Mineral Weathering, Element Release, and Acid Generation and Neutralization during a Five-Year Humidity Cell Experiment. *Minerals* **4**, 257-278.

Martin A.W., Lee L.S. and Schwab P. (2013) Antimony migration trends from a small arms firing range compared to lead, copper, and zinc. *Science of the Total Environment* **463-464**, 222-228.

Migliorini M., Pigino G., Bianchi N., Bernini F. and Leonzio C. (2004) The effects of heavy metal contamination on the soil arthropod community of a shooting range. *Environmental Pollution* **129**, 331-340.

Mikan C.J., Schimel J.P. and Doyle A.P. (2002) Temperature controls of microbial respiration in arctic tundra soils above and below freezing. *Soil Biology and Biochemistry* **34**, 11, 1785-1795.

Mitsunobu S., Takahashi Y., Terada Y. and Sakata M. (2010) Antimony (V) Incorporation into Synthetic Ferrihydrite, Goethite, and Natural Iron Oxyhydroxides. *Environ. Sci. Technol.* **44**, 10, 3712-3718.

Mellor A. and McCartney C. (1994) The effects of lead shot deposition on soils and crops at a clay pigeon shooting site in northern England. *Soil Use Manage.* **10**, 124-129.

Murray K., Bazzi A., Carter C., Ehlert A., Harris A., Kopec M., Richardson J. and Sokol H. (1997) Distribution and mobility of lead in soils at an outdoor shooting range. *Journal of Soil Contamination* **6**, 79-93.

Okkenhaug G., Zhu Y.G., Luo L., Lei M., Li X. and Mulder J. (2011) Distribution, speciation and availability of antimony (Sb) in soils and terrestrial plants from an active Sb mining area. *Environmental Pollution* **159**, 2427-2434.

Okkenhaug G. Gebhardt K.A.G., Amstaetter K., Bue H.L., Herzel H., Mariussen E., Almås A.R., Cornelissen G., Breedveld G.D., Rasmussen G. and Mulder J. (2016) Antimony (Sb) and lead (Pb) in contaminated shooting range soils: Sb and Pb mobility and immobilization by iron based sorbents, a field study. *Journal of Hazardous Materials* **307**, 336-343.

Ogawa S., Katoh M. and Sato T. (2015) Simultaneous lead and antimony immobilization in shooting range soil by a combined approach of hydroxyapatite and ferrihydrite. *Environ. Technol.* **36**, 20, 2647-2656.

Pourrut B., Shahid M., Dumat C., Winterton P. and Pinelli E. (2011) Lead uptake, toxicity, and detoxification in plants. *Rev. Environ. Contam. Toxicol.* **213**, 113-136.

Randich E., Duerfeldt W., McLendon W. and Tobin W. (2002) A metallurgical review of the interpretation of bullet lead compositional analysis. *Forensic Sci. Int.* **127**, 174-191.

Reddy K.J., Wang L. and Gloss S.P. (1995) Solubility and mobility of copper, zinc and lead in acidic environments. *Plant and Soil*, **171**, 53-58.

Robinson B.H., Bischofberger S., Stoll A., Schroer D., Gurrer G., Roulier S., Gruenwald A., Attinger W. and Schulin R. (2008) Plant uptake of trace elements on a Swiss military shooting range: Uptake pathways and land management implications. *Environmental Pollution* **153**, 669-676.

Rooney C.P, McLaren R.G. and Cresswell R.J. (1999) Distribution and phytoavailability of lead in a soil contaminated with lead shot. *Water, Air and Soil Pollution* **116**, 3, 535-548.

Rooney C.P., McLaren R.G. and Condron L.M. (2007) Control of lead solubility in soil contaminated with lead shot: Effect of soil pH. *Environmental Pollution* **149**, 149-157.

Sanderson P., Naidu R. and Bolan N. (2013) Effectiveness of chemical amendments for stabilization of lead and antimony in risk-based land management of soils of shooting ranges. *Environ. Sci. Pollut. Res.* **22**, 8942-8956.

Scheinost A., Rossberg A., Vantelon D., Zifra I., Kretzschmar R., Leuz A., Funke J. and Johnson C. (2006) Quantitative antimony speciation in shooting range soils by EXAFS spectroscopy. *Geochim. Cosmochim. Acta* **70**, 3299-3312.

Stansley W., Widjeskog L. and Roscoe D.E. (1992) Lead contamination and mobility in surface water at trap and skeet ranges. *Bull. Environ. Contam. Toxicol.* **49**, 640-647.

Strømseng A.E., Ljones M., Bakka L. and Mariussen E. (2009) Episodic discharge of lead copper and antimony from a Norwegian small arm shooting range. *J. Environ. Monit.* **11**, 6, 1259-1267.

Schwertmann U. and Cornell R.M. (2007) Iron Oxides in the Laboratory: Preparation and Characterization. Wiley-VCH Verlag GmbH, Weinheim, Germany.

(US EPA) United States Environmental Protection Agency. (1979) Water Related Fate of the 129 Priority Pollutants. USEPA, Washington, DC, Vol.1.

(US EPA) United States Environmental Protection Agency (1994) Proceeding under Section 7003 of the Solid Waste Disposal Act. Westchester County Sportsmen's Center. Administrative Order of Consent. Docket no. II RCRA-94-7003-0204. USEPA, Washington, DC.

(US EPA) United States Environmental Protection Agency. (2005) Best Management Practices for Lead at Outdoor Shooting Ranges. EPA-902-B-01-001.

(USGS) United States Geological Survey. (1976) Lead in the Environment. Geological Survey Professional Paper 957, Editor: T.G. Lovering.

Vantelon D., Lanzirotti A., Scheinost A.C. and Kretzschmar R. (2005) Spatial distribution and speciation of lead around corroding bullets in a shooting range soil studied by micro-x-ray fluorescence and absorption spectroscopy. *Environ. Sci. Technol.* **39**, 4808-4815.

Webb S.M. (2005) SIXPack: a graphical user interface for XAS analysis using IFEFFIT. *Phys. Scr.* **T115**, 1011-1014.

(WHO) World Health Organization. (2003) Antimony in Drinking Water; *Background Document for Development of WHO Guidelines for Drinking Water Quality*, World Health Organization.

(WHO) World Health Organization. (2011) Lead in Drinking Water; *Background Document for Development of WHO Guidelines for Drinking Water Quality*, World Health Organization.

Yin X., Gao B., Ma L.Q., Saha U.K., Sun H. and Wang, G. (2010) Colloid-facilitated Pb transport in two shooting-range soils in Florida. *Journal of Hazardous Materials.* **177**, 1-3, 620-625.

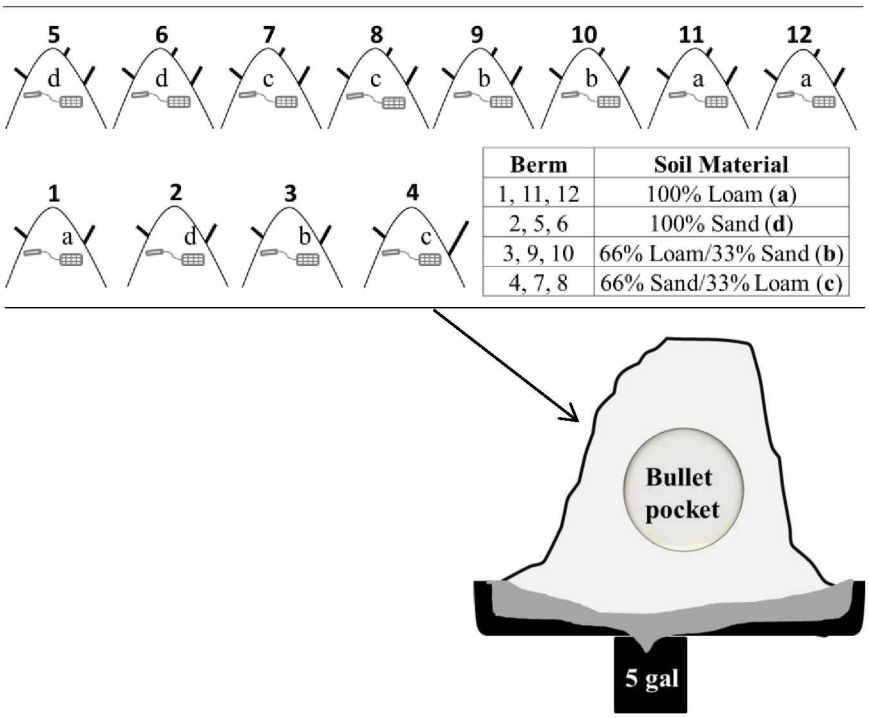

Figure 2.1 Site layout for test berms

Site layout for the test berms on Donnelly Training Area (DTA) outside of Delta Junction, Alaska. Berms are comprised of four types of soil and are designated as contaminated, Berms 5-12 and pristine, Berms 1-4. Expanded view of water runoff funneling is shown on bottom right.

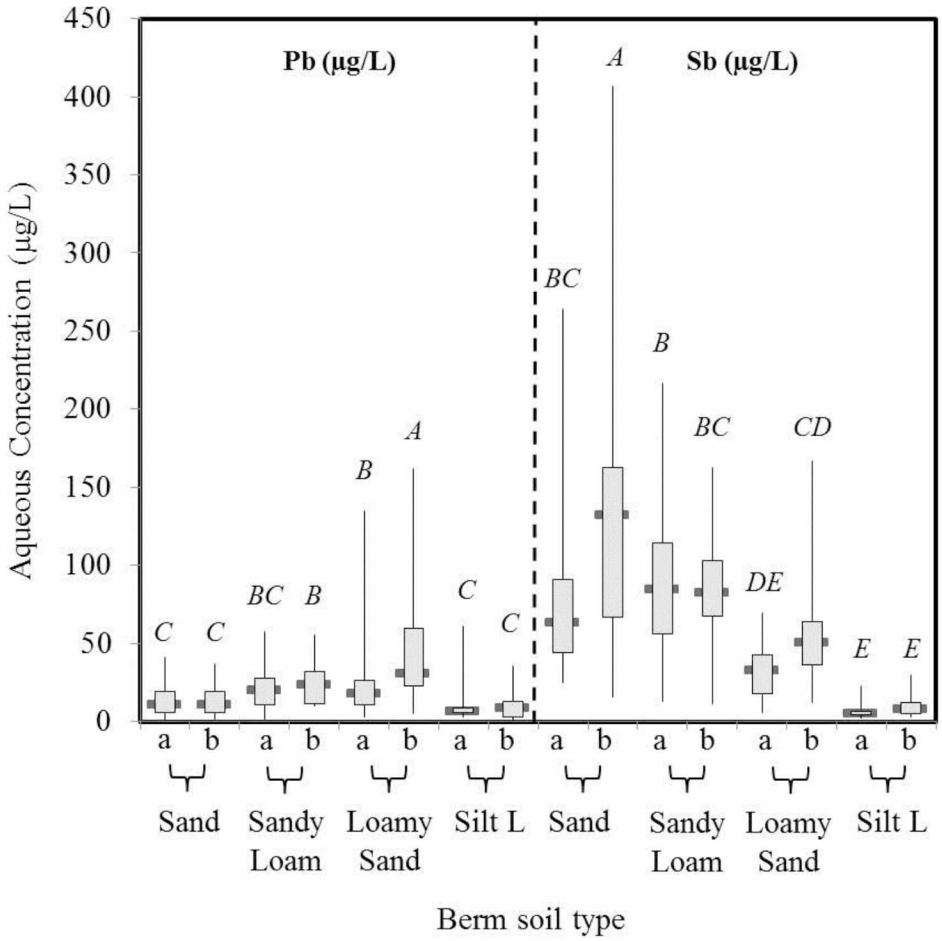

Figure 2.2 Box plot diagram of total Pb and Sb

Box plot diagram of total Pb (left half) and Sb (right half) concentrations from 2011 to 2014 (prior to Fe addition) as a function of soil type (sand, sandy loam, loamy sand and silt loam) for the duplicate contaminated test berms (a) refers to berms 5, 7, 9, 11 and (b) refers to berms 6, 8, 10, 12. Gray lines indicate median values during the 4 years. The gray boxes depict the lower (25^{th} percentile) and upper (75^{th} percentile) quartiles. A, B, C, D, E indicates levels that are statistically different at $p < 0.05$. Levels are not comparable between Pb and Sb.

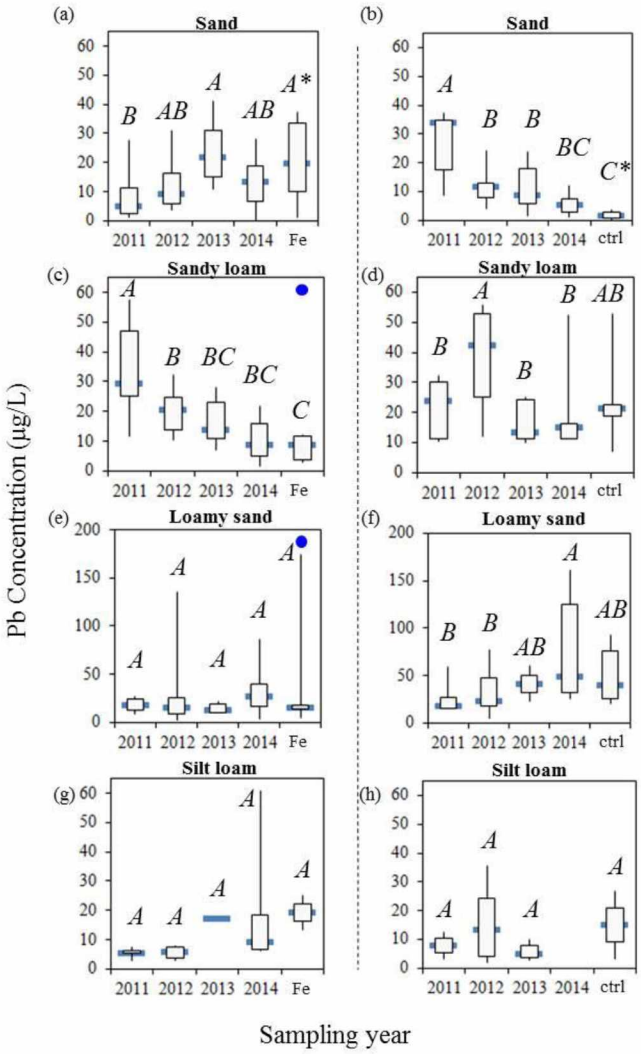

Figure 2.3 Pb concentrations in berm runoff

Pb concentrations in berm runoff as a function of soil type for the duplicate berms (a) 5, (b) 6, (c) 7, (d) 8 (e) 9, (f) 10, (g) 11 and (h) 12. 'Fe' indicates amended berms and 'ctrl' indicates un-amended berms. A, B, C indicate levels that are statistically different at $p < 0.05$, but are not comparable between duplicate soil types. '*' signifies statistical differences between Pb distributions between the Fe versus control berm runoff. Blue circle indicates there was initial spike in Pb concentrations in the immediate runoff from the Fe addition that did not reach the sample collector (4398.0 ± 14.9 and 1177.0 ± 9.1 µg/L for (c) and (d).

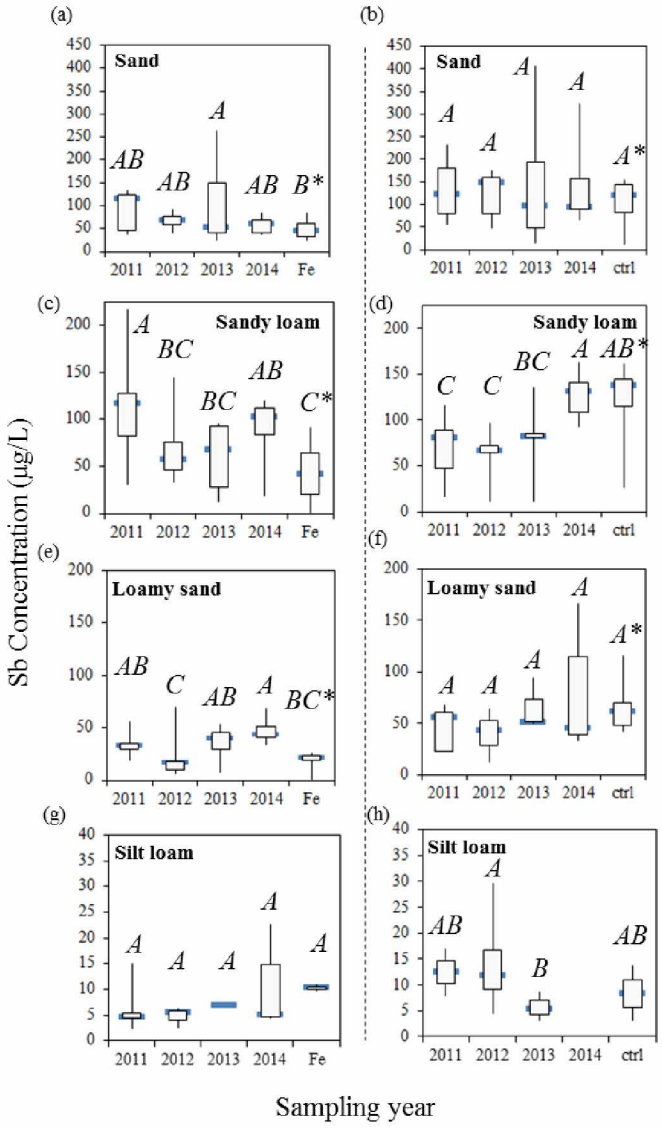

Figure 2.4 Sb concentrations in berm runoff

Sb concentrations in berm runoff as a function of soil type for the duplicate berms (a) 5, (b) 6, (c) 7, (d) 8 (e) 9, (f) 10, (g) 11 and (h) 12. 'Fe' indicates amended berms and 'ctrl' indicates un-amended berms. A, B, C indicate levels that are statistically different at $p < 0.05$, but are not comparable between duplicate soil types. '*' signifies statistical differences between Sb distributions between the Fe versus control berm runoff.

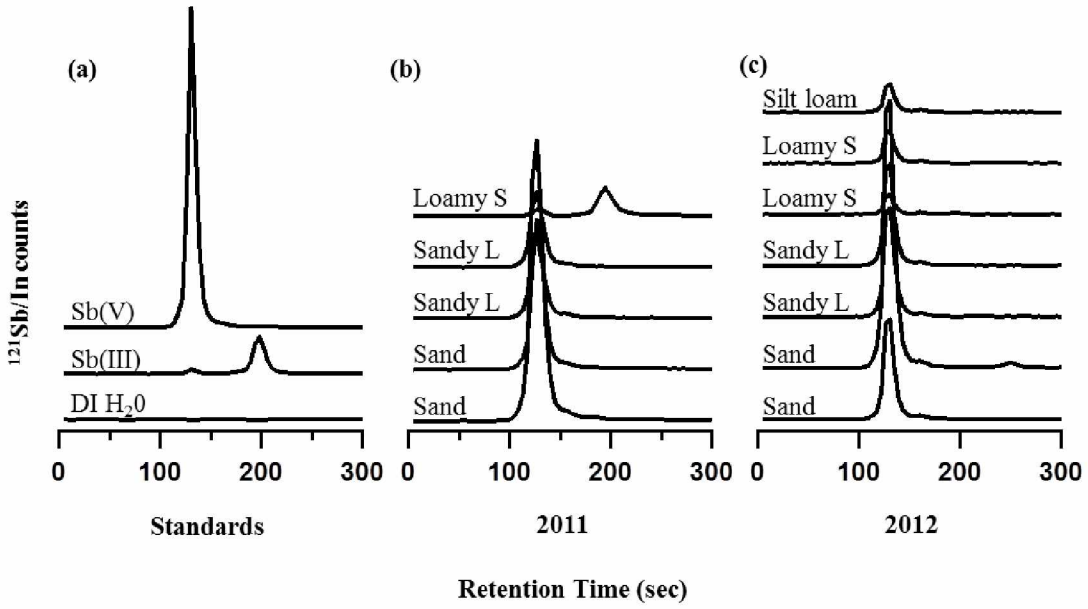

Figure 2.5 Speciation of Sb

Speciation for Sb (III)/(V) in (a) standards and berm water runoff collected (b) summer 2011 and (c) summer 2012 analyzed by LC-ICP-MS.

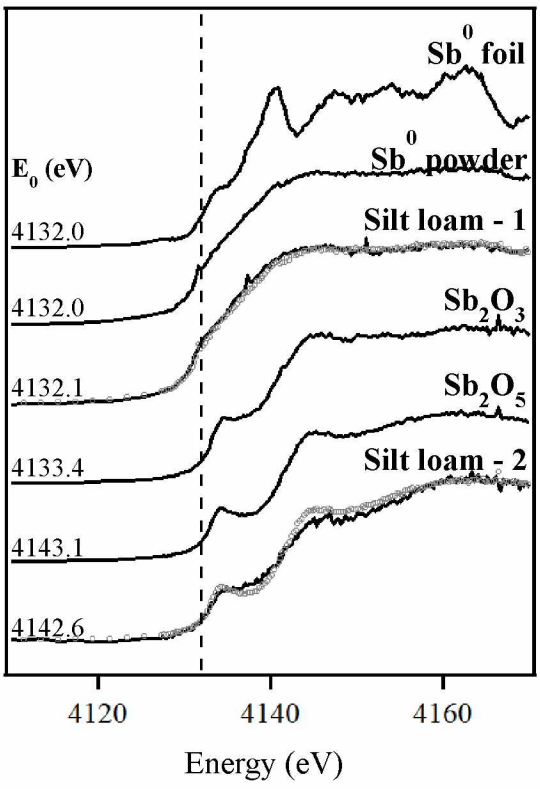

Figure 2.6 Normalized Sb-LIII μ-XANES

Normalized Sb-L_{III} μ-XANES spectra for the silt loam berm 12 soil end member. Sample data is in black lines with corresponding LCF plotted in gray circles. Standards are black lines without any overlying gray circles. Dotted line corresponds to the absorption edge for Sb-L_{III} edge (4132.0 eV).

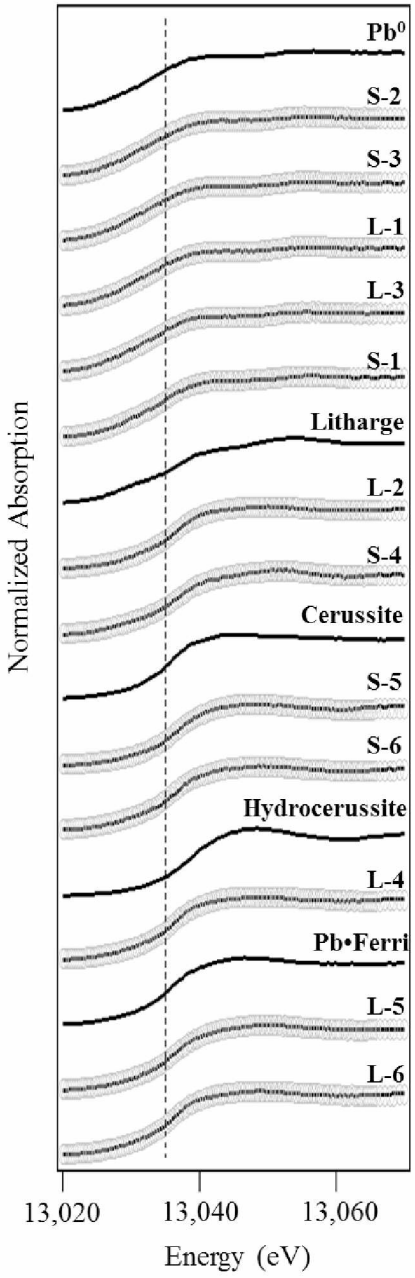

Figure 2.7 Normalized Pb-LIII μ-XANES

Normalized Pb-L_{III} μ-XANES for the end member test berms (5, 12) over 4 years. Sample data is in black lines with corresponding LCF plotted in gray circles. Standards are in black with no fits present. Pb•Ferri corresponds to Pb sorption product with synthesized Fe(III) oxides.

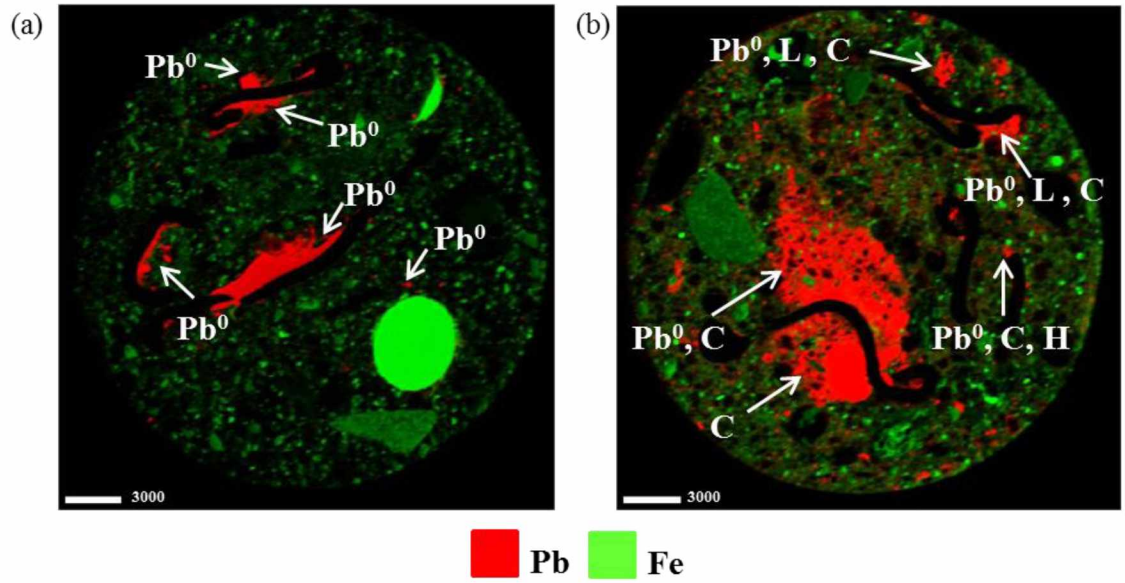

Figure 2.8 XRF maps of bullets after 2 years weathering

XRF maps showing distributions of Pb (red) and Fe (green) in thin sections collected from the (a) sand and (b) sandy loam test berms in the summer of 2012. Thin section area is 25x25 mm and scale bar units are in µm. Pb^0 = metallic Pb, L = litharge, C = cerussite, H = hydrocerussite.

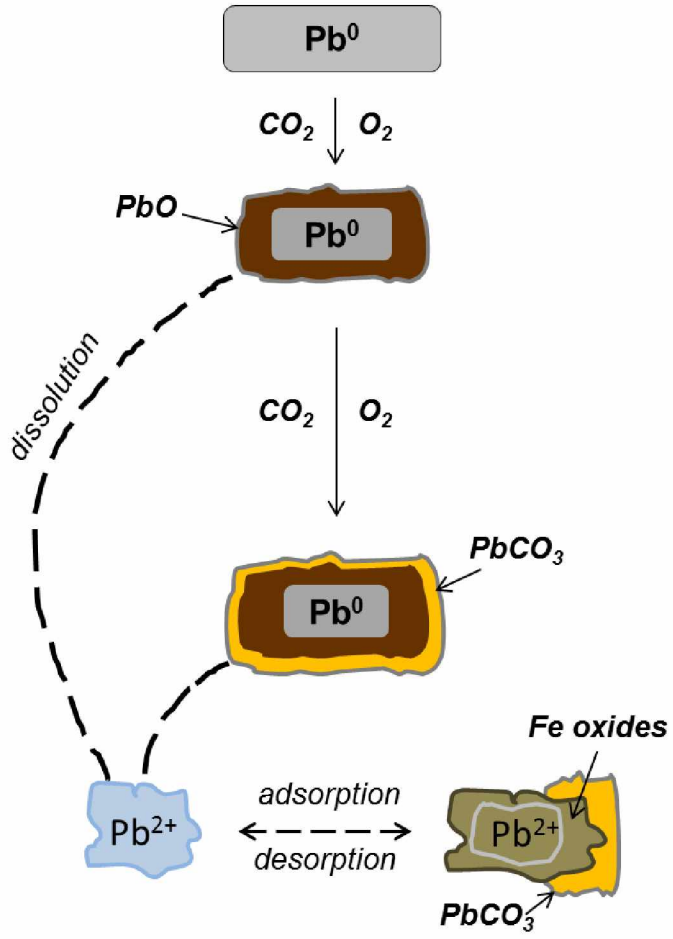

Figure 2.9 Simplified weathering pathways for Pb

Schematic of the overall dominant corrosion stages of Pb weathering from a fragmented 5.56 mm bullet. XANES analysis showed the dominance of Pb adsorption to the surface of Fe(III)oxides as a central corrosion product.

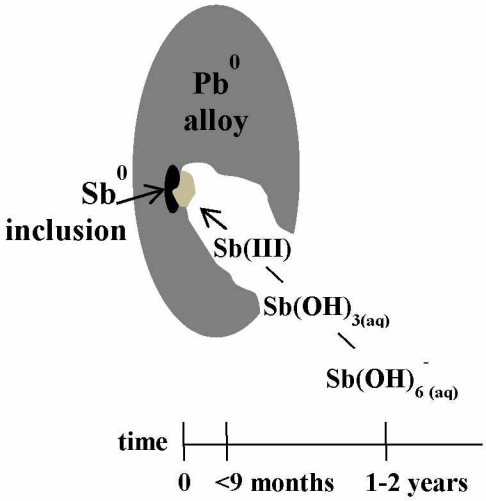

Figure 2.10 Simplified stages of initial Sb oxidation

Schematic of the initial stages of Sb oxidation from a fragmented 5.56 mm bullet as a function of reaction time. Oxidation of Sb^0 to $Sb(III)_{(aq)}$ occurs within 9 months in Alaska loamy sand soil and complete oxidation to $Sb(V)_{(aq)}$ occurs within 1-2 years.

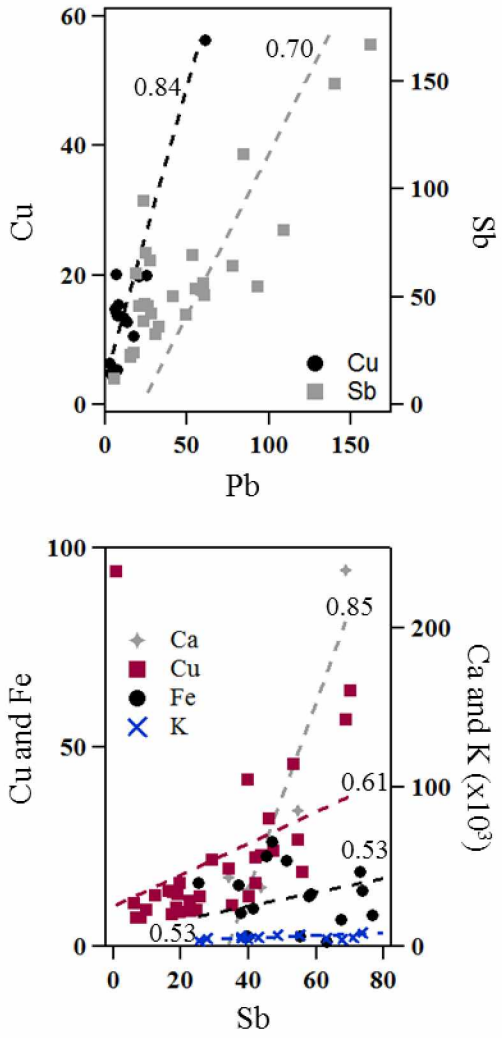

Figure 2.11 Correlation plots of Pb and Sb

Correlation plots of Pb (top) with Cu (Berm 11) and Sb (Berm 10) in the shooting range berm runoff and Sb (bottom) with Cu (Berm 9), Fe (Berm 5), Ca (Berm 9) and K (Berm 5).

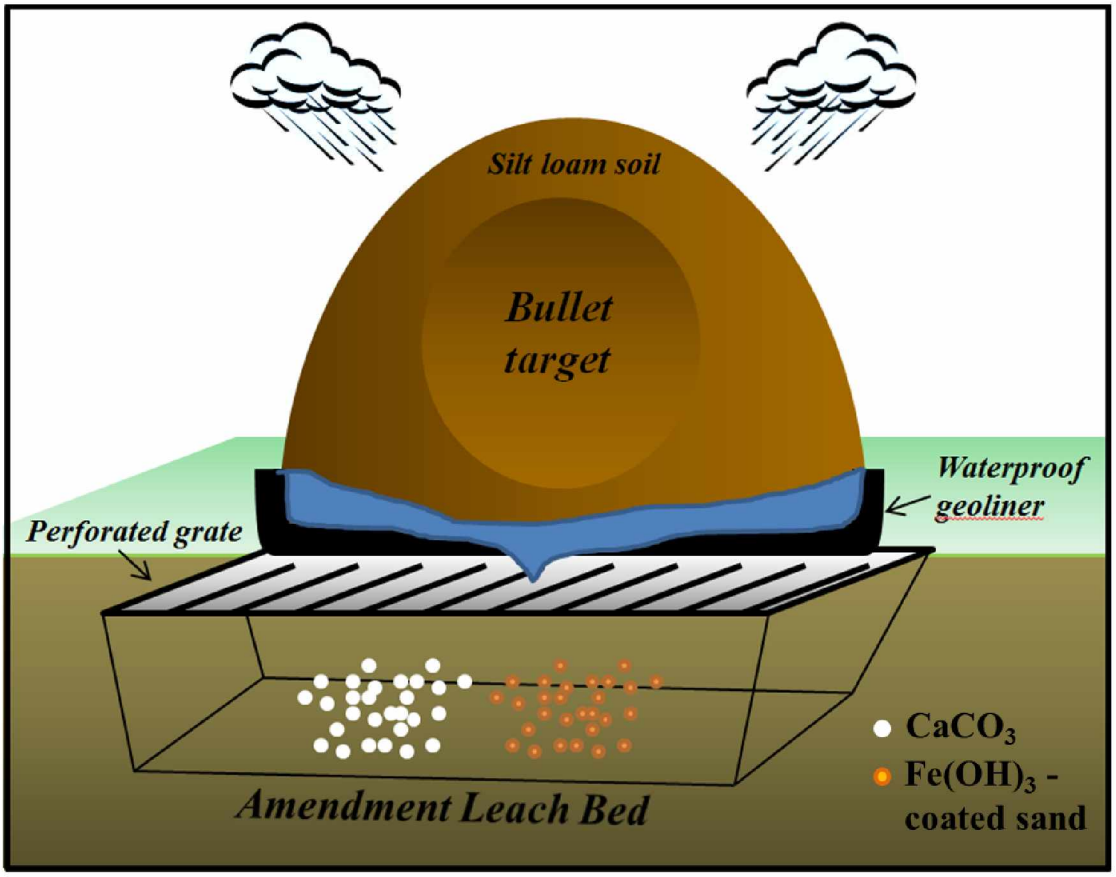

Figure 2.12 Landscape-scale shooting range design

Schematic of landscape-scale shooting range design and remediation strategy to limit the overall mobility of Pb and Sb off-site. Berms are constructed with silt loam soil on top of an impenetrable, waterproof geoliner. Using the geoliner, berm runoff is funneled into a man-made grate on top of a trough. The trough is sprinkled with $Fe(OH)_3/CaCO_3$ buffer once every month (depending on precipitation).

Table 2.1 Pristine soil characterization

Soil characterization for the four types of soil used to construct the test berms.

	Soil type 1	(±)	Soil type 2	(±)	Soil type 3	(±)	Soil type 4	(±)
Soil Classification	*Silt Loam*		*Sand*		*Loamy sand*		*Sandy loam*	
Soil Texture								
% sand	26	0.8	96	2.9	52	1.6	74	2.2
% silt	71	2.1	2.0	1.0	46	1.4	24	0.7
% clay	3.0	1.0	2.0	1.0	2.0	0.1	2.0	0.1
surface area (m^2/g)	5.2	0.10	1.9	0.10	3.8	0.10	3.7	0.10
Chemical Characteristics								
soil pH	5.3	0.27	8.4	0.42	5.7	0.28	6.8	0.34
Organic matter % (L.O.I)	3.8	/	0.1	/	3.2	/	1.3	/
Non-purgeable organic carbon (ppm)	12	/	3.0	/	16	/	12	/
Chemical Quantification								
Al2O3 (%)	15.0	0.0100	13.6	0.0100	14.8	0.0100	14.8	0.0100
CaO (%)	1.73	0.0100	2.41	0.0100	1.99	0.0100	2.11	0.0100
Fe2O3 (%)	5.73	0.0100	5.98	0.0100	5.95	0.0100	5.95	0.0100
SiO2 (%)	58.9	0.0200	62.1	0.0200	56.3	0.0200	56.0	0.0200
As (mg/kg)	15.8	1.83	18.2	1.92	20.1	1.82	21.0	1.84
Ba (mg/kg)	831	3.28	779	3.35	808	3.25	831	3.29
Cu (mg/kg)	26.5	0.527	54.3	0.602	29.6	0.533	32.2	0.541
Mn (mg/kg)	599	3.00	1020	3.84	686	3.14	689	3.16
Ni (mg/kg)	34.2	0.530	38.3	0.573	36.2	0.538	36.9	0.546
Pb (mg/kg)	19.5	0.666	30.0	0.724	25.4	0.678	20.4	0.668
Sb (mg/kg)	bld	/	6.37	1.57	6.29	1.52	6.56	1.52
Sn (mg/kg)	8.30	1.06	13.4	1.11	8.30	1.06	7.87	1.06
Sr (mg/kg)	193	0.296	204	0.313	203	0.301	202	0.302
TiO2 (mg/kg)	9650	7.22	10700	7.87	9630	7.19	9620	7.22
W (mg/kg)	6.30	1.20	6.60	1.28	5.48	1.21	6.74	1.21
Zn (mg/kg)	69.3	0.372	101	0.418	72.7	0.375	74.0	0.377
Background Aqueous Conc.								
Sb (µg/L)	2.0	0.10	2.4	0.10	1.1	0.10	1.4	0.10
Pb (µg/L)	bld	/	bld	/	bld	/	bld	/

'/' = error not quantified

Table 2.2 Pristine bullet characterization

Bullet chemical composition provided by Defense Ammunition Center (DAC) – Munitions Items Disposition Action System (MIDAS).

Jacket		Mass (g)
	Cu	17.82
	Zn	1.96
	Pb	0.01
	Fe	0.01
Core		
	Fe	9.80
	Mn	0.08
	C	0.05
	S	0.01
Slug		
	Pb	31.68
	Sb	0.32

Table 2.3 Total metal concentrations in test berms

Total metal concentrations in the 12 test berms collected at the end of summer 2015, analyzed by XRF. Pristine soil concentrations showed for comparison. LLD = lower limit of detection.

Berm	Soil type	Status	Pb (mg/kg)	+/-	Sb (mg/kg)	+/-	Cu (mg/kg)	+/-	Ni (mg/kg)	+/-	Sn (mg/kg)	+/-	Zn (mg/kg)	+/-
1	Silt loam	Pristine	19.5	0.666	bld	/	26.5	0.527	34.2	0.530	8.30	1.06	69.3	0.372
2	Sand	Pristine	30.0	0.724	6.37	1.57	54.3	0.602	38.3	0.573	13.4	1.11	101	0.418
3	Loamy sand	Pristine	25.4	0.678	6.29	1.52	29.6	0.533	36.2	0.538	8.30	1.06	72.7	0.375
4	Sandy loam	Pristine	20.4	0.668	6.56	1.52	32.2	0.541	36.9	0.546	7.87	1.06	74.0	0.377
5	Sand (a)	Fired	14500	7.83	281	2.21	658	1.35	36.5	0.645	74.8	1.39	172	0.555
6	Sand (b)	Fired	16400	8.36	275	2.21	733	1.42	34.8	0.647	75.1	1.40	172	0.566
7	Sandy loam (a)	Fired	1680	2.46	42.5	1.61	132	0.700	37.5	0.562	17.4	1.10	88.8	0.405
8	Sandy loam (b)	Fired	2810	3.22	61.8	1.66	215	0.809	37.6	0.565	19.1	1.12	99.2	0.421
9	Loamy sand (a)	Fired	1260	2.12	25.7	1.57	129	0.687	36.2	0.552	11.4	1.08	88.0	0.400
10	Loamy sand (b)	Fired	1680	2.49	32.5	1.60	165	0.739	36.8	0.556	14.3	1.10	94.8	0.409
11	Silt loam (a)	Fired	301	1.17	9.56	1.53	50.0	0.568	34.0	0.532	8.24	1.06	69.1	0.375
12	Silt loam (b)	Fired	459	1.39	12.0	1.53	62.8	0.590	34.1	0.533	10.3	1.06	71.7	0.380
		LLD	2.47		5.91		1.28		1.30		3.43		1.07	

Table 2.4 Fitting parameters for LCF of normalized Sb-LIII μ-XANES

Fitting parameters for the LCF of the normalized Sb-L_{III} μ-XANES from the silt loam constructed target berm with Sb^0 standard and Sb_2O_5.

Year	Berm	Soil type	Spot	Sb(0)	Sb_2O_5	Sum (%)	X^2	red. X^2
2	12	Loam	1	100		100	9.3E-02	5.6E-04
2	12	Loam	2		100	100	2.7E-01	1.5E-03

Table 2.5 Fitting parameters for LCF of normalized Pb-LIII μ-XANES

Select linear combination fitting results for the constructed target berms using Pb reference spectra, samples were collected in 2011-2014. Sum (%) refers to the actual sum of the partial contributions for the overall best fit. X^2 and reduced X^2 are derived from the fit refinement process. Pb(0) = Metallic bullet alloy; L = Litharge (PbO); C = Cerussite; H = Hydrocerussite; Ferri = Pb(II) sorbed on synthesized Fe(III)oxies; error associated with fit in parenthesis.

Year	Berm	Soil type	Name	Pb(0)	L	C	H	Ferri	Sum (100%)	X^2	red. X^2
1	5	Sand	S-1	65 (1)	14 (1)	23 (1)			101	9.6E-03	7.0E-05
2	5	Sand	S-2	~99					99	1.1E-02	8.1E-05
2	5	Sand	S-3	~100					100	1.8E-02	1.3E-04
3	5	Sand	S-4		45 (1)	28 (2)	26 (1)		99	1.4E-02	1.1E-04
3	5	Sand	S-5			57 (1)	38 (1)		95	8.9E-03	7.0E-05
4	5	Sand	S-6		20 (2)			74 (1)	93	2.1E-02	1.5E-04
2	12	Silt loam	L-1	~100					101	1.6E-02	1.3E-04
2	12	Silt loam	L-2	15 (3)	10 (3)	50 (2)	25 (2)		100	1.1E-02	7.9E-05
3	12	Silt loam	L-3	100					100	1.8E-02	1.3E-04
3	12	Silt loam	L-4		16 (1)	70 (3)	14 (1)		100	1.8E-02	1.3E-04
4	12	Silt loam	L-5		26 (1)	30 (3)	23 (1)	22 (1)	100	1.1E-02	8.0E-05
4	12	Silt loam	L-6		17 (1)	63 (3)	10 (1)	11 (2)	100	1.3E-02	9.4E-05

*Refers to Pb(II) sorption product with synthesized Fe(III)oxides
(#) Refers to linear combination fitting error

Table 2.6 Occurrence and average contributions of Pb components

Occurrence and average contributions of Pb components over the 4 years of summer sampling. (-) indicates species was not detected, but number of samples was relatively low, (/) denotes species was not detected. Pb(0) = Metallic bullet alloy; L = Litharge (PbO); C = Cerussite; H = Hydrocerussite; Ferri = Pb(II) sorbed on synthesized Fe(III) oxides; Fine = Pb(II) sorbed on the fine fraction of pristine silt loam soil.

		Year			
		1	2	3	4
Sand	Pb(0)	65	100	/	/
	L	14	/	50	16
	C	23	/	43	/
	H	-	/	32	/
	Ferri	-	/	/	64
	Fine	-	/	41	27
Sandy Loam	Pb(0)	-	48	45	36
	L	-	31	50	41
	C	-	61	27	57
	H	-	23	/	25
	Ferri	-	/	58	46
	Fine	-	/	45	/
Loamy sand	Pb(0)	-	68	33	/
	L	-	20	19	22
	C	-	32	30	52
	H	-	21	21	11
	Ferri	-	/	43	30
	Fine	-	/	32	15
Silt loam	Pb(0)	-	48	100	100
	L	-	19	29	20
	C	-	59	50	49
	H	-	25	15	20
	Ferri	-	/	38	19
	Fine	-	/	/	/

Table 2.7 Linear correlations between elements in runoff

Linear correlations between elements in the contaminated test berm runoff (Berms 5-12). Linear regression was performed and R-squared values reported. '-' indicates there was no correlation detected between the element and element pair. R-squared values above 0.50 were reported.

		Element correlations in contaminated berms							
Element	Pair	5	6	7	8	9	10	11	12
Pb	Cu	-	-	-	-	-	-	0.84	-
Pb	Sb	-	-	-	-	-	0.70	0.63	-
Sb	Ca	-	-	-	0.79	0.85	-	-	-
Sb	Cu	-	0.51	0.59	-	0.61	-	0.60	0.52
Sb	Fe	0.53	-	-	-	-	-	-	-
Sb	K	0.53	-	-	-	-	-	-	-
Fe	Ni	-	-	0.91	-	0.50	0.50	-	0.67
Ni	Cu	-	-	-	-	0.84	-	0.62	-
Na	K	0.62	-	0.83	0.66	0.81	-	-	-
Na	Mg	-	0.86	0.83	0.94	0.95	-	0.94	-
Na	Ca	-	-	0.98	0.92	1.00	-	1.00	-
Mg	K	0.83	-	0.94	-	0.91	-	-	-
Mg	Ca	0.72	-	1.00	0.99	1.00	0.96	0.98	-
Ca	K	0.68	-	0.92	-	0.93	-	-	-

'-' indicates no correlation

Table 2.8 Total Aqueous Metal Concentrations after Fe Addition

Metal concentrations before and after the Fe additions in a subset of the test berms of each soils type. Berm 5 (sand), Berm 7 (sandy loam), Berm 9 (loamy sand) and Berm 11 (silt loam).

Berm 5	Pb	+/- (ug/L)	Sb	+/- (ug/L)	Cu	+/- (ug/L)	Ni	+/- (ug/L)	Zn	+/- (ug/L)
5/5/2014	1.2	0.023	63.3	0.272	4.7	0.17	bld	-	4.1	0.088
6/19/2014	18.9	0.566	39.7	0.854	4.8	0.13	bld	-	2.7	0.088
6/25/2014	28	0.29	67.8	1.15	5.8	0.11	bld	-	2.6	0.088
6/28/2014	19	0.030	37.8	0.140	4.9	0.17	bld	-	2.1	0.088
6/30/2014	0.6	0.01	55.3	1.02	6.5	0.08	bld	-	4.3	0.088
7/8/2014	18.2	0.236	37.8	1.50	4.9	0.08	bld	-	7.2	0.066
7/30/2014	8.32	0.125	73.8	0.222	9.1	0.12	0.9	0.1	8.5	0.073
8/6/2014	8.23	0.101	84.9	3.17	11	0.062	1	0.1	9.7	0.084
8/22/2014*	***12.4***	***0.145***	***83.4***	***3.85***	***8.3***	***0.16***	***bld***	***-***	***8.2***	***0.060***
8/29/2014	35.9	0.176	38.0	0.144	6.6	0.15	bld	-	9.5	0.074
9/5/2014	37.2	0.982	27.7	1.33	5.6	0.056	bld	-	8.5	0.27
6/11/2015	1.34	0.101	48.7	0.390	3.1	0.090	bld	-	5.8	0.077
7/3/2015	7.98	0.097	71.1	5.18	5.6	0.076	bld	-	5.9	0.077
7/23/2015	19.9	0.088	43.1	2.97	5.2	0.060	bld	-	7.2	0.083
9/3/2015	31.3	0.153	25.4	0.160	5.6	0.57	bld	-	6.9	0.083

Berm 7	Pb	+/- (ug/L)	Sb	+/- (ug/L)	Cu	+/- (ug/L)	Ni	+/- (ug/L)	Zn	+/- (ug/L)
5/5/2014	1.6	0.093	18.7	0.0637	4.6	0.19	bld	-	1.2	0.077
6/19/2014	15.8	0.197	112	0.257	31.4	0.988	2.6	0.067	1.2	0.077
6/25/2014	12.5	0.0926	113	1.44	25.6	1.48	2.1	0.16	bld	-
6/28/2014	4.9	0.093	119	0.597	27.9	1.53	2.7	0.15	bld	-
6/30/2014	15.8	0.167	111	0.789	36.9	0.307	6.2	0.067	4.5	0.050
7/8/2014	21.7	0.0926	92.1	1.45	24.2	0.261	1.9	0.067	4.7	0.077
7/14/2014	4.4	0.093	80	0.52	17.4	0.0643	2.1	0.067	5.5	0.077
8/6/2014	5.1	0.10	84.3	1.20	17.4	0.0853	2.4	0.067	4	0.08
8/22/2014*	***1177***	***9.063***	***0.3***	***0.1***	***40.6***	***0.146***	***47***	***0.35***	***10.5***	***0.0766***
8/29/2014	3.9	0.10	9.1	0.51	11.4	0.0537	23.3	0.145	13.6	0.0766
9/5/2014	bld	-	41.6	0.295	11.5	0.0866	4.7	0.14	1.7	0.077
6/11/2015	3	0.1	32.2	0.235	11.1	0.0853	1.4	0.067	4.5	0.077
7/3/2015	11.8	0.179	66.7	0.420	18.5	0.556	1.2	0.066	1.3	0.077
7/23/2015	12	0.054	62.7	0.176	15.3	0.178	0.9	0.1	1.3	0.077
9/3/2015	8.8	0.054	90.9	0.873	19.3	0.0559	2	0.1	1.5	0.077

Berm 9	Pb	+/- (ug/L)	Sb	+/- (ug/L)	Cu	+/- (ug/L)	Ni	+/- (ug/L)	Zn	+/- (ug/L)
6/19/2014	31.2	0.134	43.8	0.210	22.8	0.896	5.5	0.35	8.2	0.083
6/25/2014	24.2	0.107	41.9	0.595	22.3	0.738	3.6	0.16	1.1	0.13
6/28/2014	26.5	0.0902	47.2	0.765	24.0	1.39	4.3	0.34	2.3	0.13
6/30/2014	9.1	0.031	34.1	0.235	19.5	0.195	3.7	0.082	5.2	0.13
7/8/2014	48.5	0.378	54.4	0.0980	26.8	0.150	4.0	0.054	7.6	0.13
7/14/2014	3.4	0.045	40.0	0.312	12.6	0.0641	2.5	0.056	5.1	0.13
7/30/2014	85.9	1.11	68.8	1.20	57.1	0.360	9.3	0.11	9.9	0.13
8/22/2014*	***4389***	***14.92***	***0.7***	***0.1***	***94.0***	***1.34***	***55.6***	***0.578***	***49.3***	***0.399***
8/29/2014	14.5	0.299	24.4	1.05	9.1	0.19	3.9	0.18	6.7	0.10
9/5/2014	174	3.79	bld	-	19.0	0.184	39.0	0.425	58.1	0.290
6/11/2015	5.5	0.068	19.6	0.147	8.7	0.11	1.7	0.11	3.1	0.13
7/3/2015	18.3	0.188	22.4	1.31	11.4	0.0503	0.9	0.1	2.4	0.13
7/23/2015	16.1	0.182	18.6	1.36	9.8	0.11	1.2	0.056	1.7	0.13
9/3/2015	13.4	0.0791	25.6	0.138	12.6	0.109	1.5	0.056	7.5	0.13

Berm 11	Pb	+/- (ug/L)	Sb	+/- (ug/L)	Cu	+/- (ug/L)	Ni	+/- (ug/L)	Zn	+/- (ug/L)
5/5/2014	6.6	0.072	5.0	0.071	20.1	1.09	11.1	0.653	8.3	0.065
6/19/2014	11.3	0.100	4.8	0.025	13.4	0.230	3.8	0.11	1.8	0.065
6/25/2014	7.0	0.10	4.6	0.012	13.7	0.471	3.9	0.17	1.8	0.065
6/28/2014	6.4	0.09	4.6	0.066	14.3	0.767	4.6	0.24	1.9	0.065
7/8/2014	20.6	0.235	18.3	0.161	19.7	0.0610	3.1	0.089	8.0	0.12
7/14/2014	60.9	0.366	22.8	0.112	56.3	0.445	10.8	0.0887	24.4	0.303
6/11/2015	13.3	0.0890	10.9	0.695	12.8	0.0610	5.1	0.089	8.6	0.065
9/3/2015	25.1	0.163	9.7	0.10	20.0	0.182	8.8	0.12	16.3	0.151

Units are in µg/L

*Addition of $FeCl_2/CaCO_3$

'bld' = below detection limit of analytical method

'-' = error not calculated

2.9 Appendix A

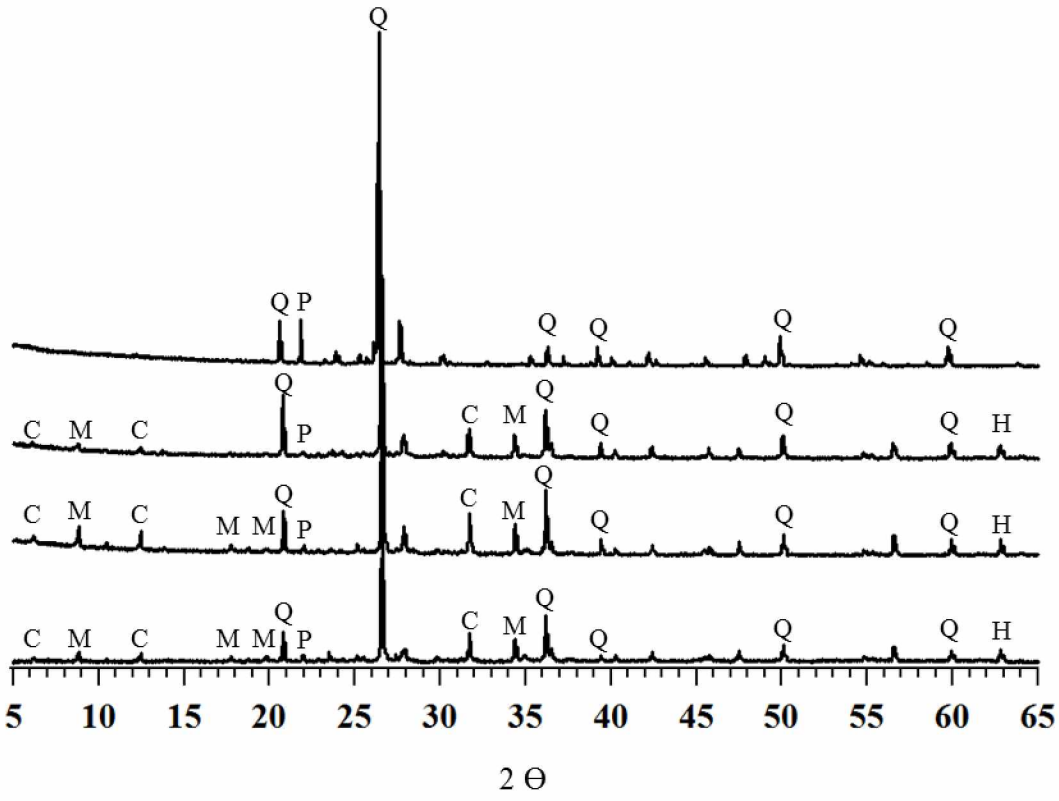

Figure 2.13 X-ray diffraction patterns for pristine soil

X-ray diffraction (Cu Kα) patterns for pristine samples of the four well-characterized soils that comprise the target berms: (a) sand (b) sandy loam (c) loamy sand (d) silt loam. Major peaks identified are Q = quartz, C = Chlorite, M = Mica, P = Plagioclase.

Soil moisture and thermal regime

The soil moisture and soil temperature of the berms were monitored to track water retention and the freezing/thawing cycles. In this study, soil moisture is defined as the volumetric water content, which has units of m^3/m^3. The berm saturation profiles and temperature results are shown in Appendix Figure 2.14, Figure 2.15 and Figure 2.16.

The average soil moisture for the berms ranged from 0.07 to 0.12 m^3/m^3 and was highest for the mixed and silt loam berms. In order of increasing loam content, the average soil moistures were 0.07, 0.12, 0.12 and 0.10 m^3/m^3. The highest soil moisture values were recorded in the silt loam end member in 2011 and the loamy sand in 2013 and 2014. In 2014-2015, we measured saturation as a function of soil surface depth for the 100% silt loam system, results shown in Appendix Figure 2.16. The 'surface' measurement corresponds to a probe inserted 0.2 m into the side of the soil berm, whereas the 'buried' measurement corresponds to 0.5 m. There is greater soil moisture variability closer to the surface of the loam berm. Overall, there is an order of magnitude decrease in soil moisture as a function of berm soil depth for the loam soil, indicating the dominance of surface flow in these types of systems and limited downward percolation. In general, the loam soil is colder and has an average soil temperature of 1.14 °C, whereas the average soil temperature for the sand soil is 2.53 °C. There is more variability in the soil temperatures in 2013-2015, most likely due to the berm soil mounds settling and pushing the probes closer to the surface over time where they have more influence from air temperatures.

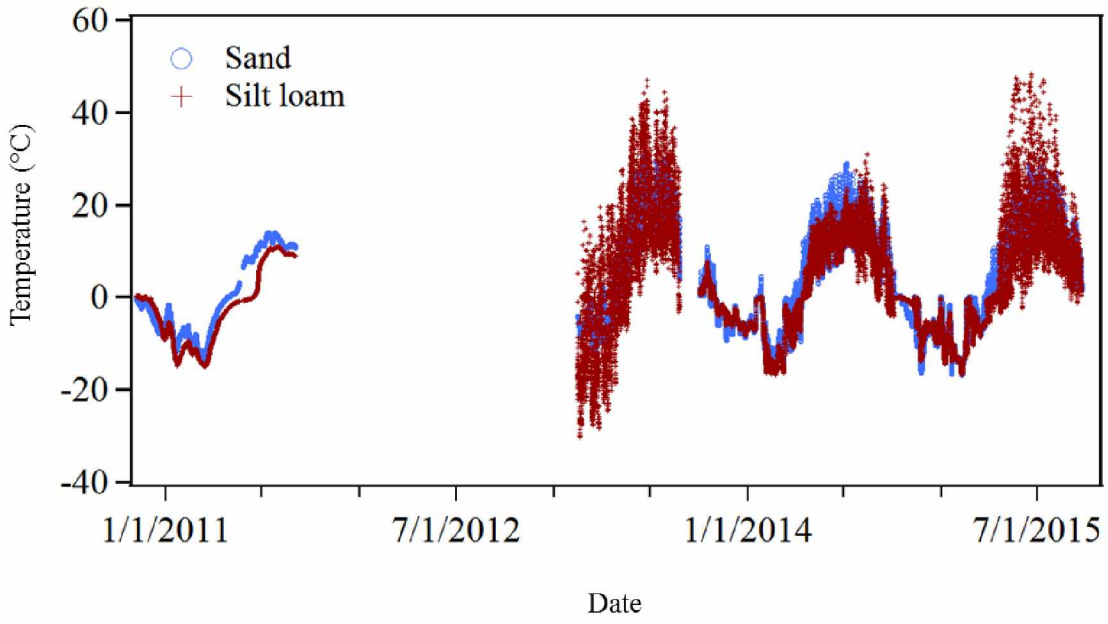

Figure 2.14 Soil temperature

Temperature (°C) as a function of end member berm soil type throughout 4 summers in Alaska. Summer 2012 data is excluded due to small animals repeatedly chewing the wires.

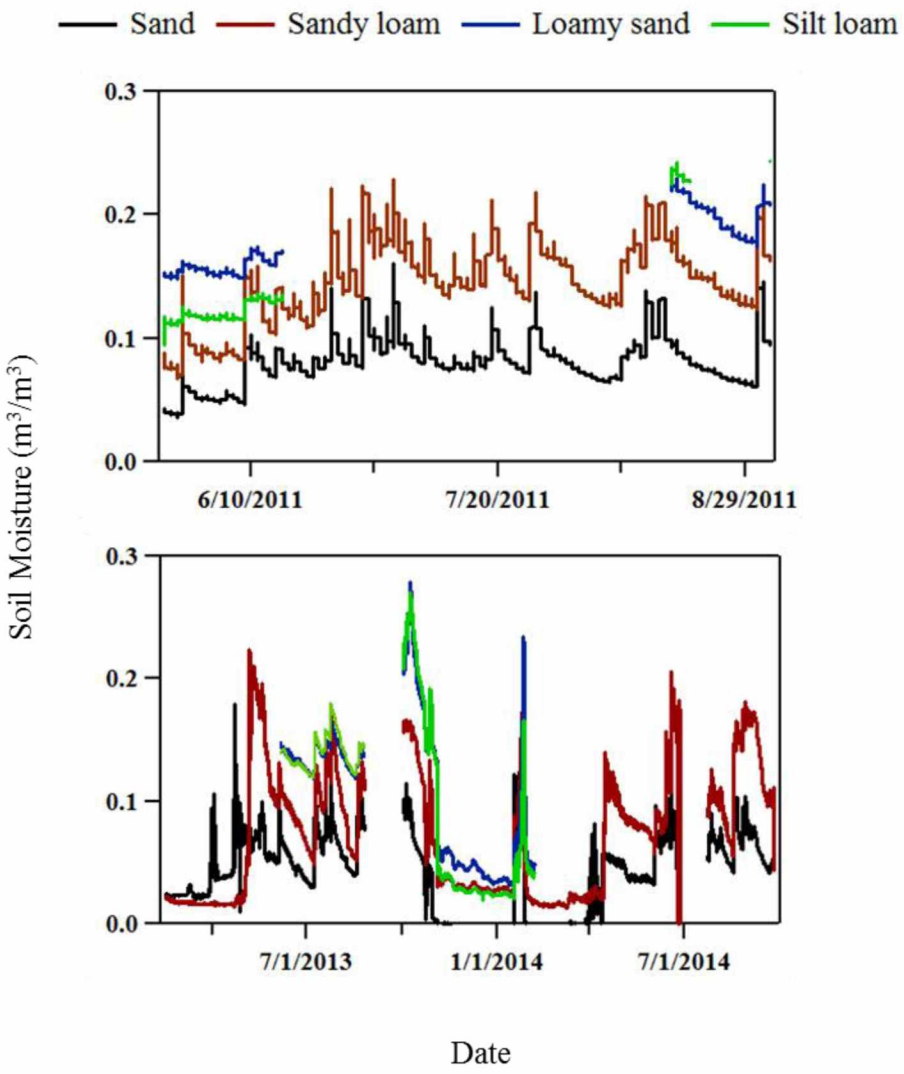

Figure 2.15 Soil moisture

Soil moisture (m^3/m^3) as a function of berm soil end member type throughout 3 summers in Alaska.

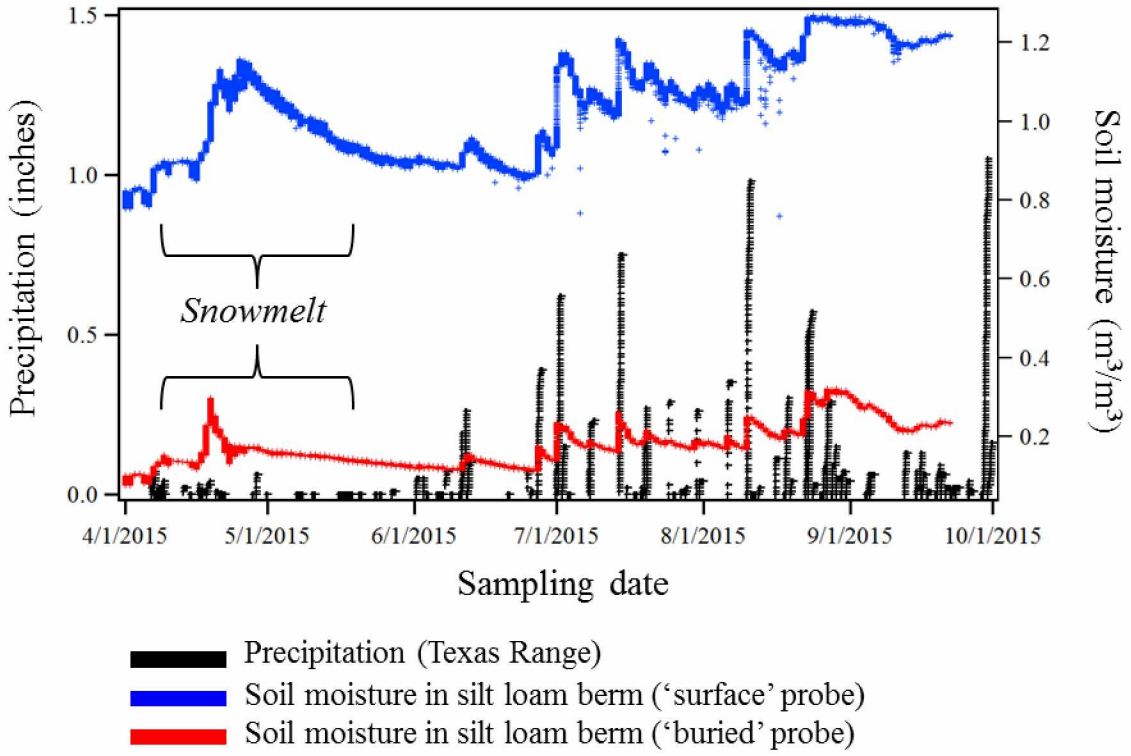

Figure 2.16 Soil moisture and precipitation for 2015 season

Precipitation and soil moisture data for the Texas Range on DTA. Precipitation was downloaded from MesoWest, University of Utah monitoring station. 'Surface' probe was inserted 0.2 m and 'buried' probe was inserted 0.5 m into the silt loam berm soil (Berm 11).

Chapter 3 Lead and Antimony Speciation Associated with the Weathering of Bullets in a Historic Shooting Range in Alaska [1]

3.1 Abstract

Lead and antimony are toxic and found in bullets used in military training exercises. Small arms shooting ranges present a unique opportunity to study the fate of Pb and Sb in various types of soil and soil porewaters, where their fate is largely controlled by microscale morphological and chemical variations exclusive to a particular soil system. In this study, we analyzed bullet and soil samples from a historic military shooting range located in the interior of Alaska. Bulk speciation analysis coupled with micro-scale methods demonstrate that the presence of Sb(V) in octahedral coordination with 5 O and 3 Fe atoms is the primary species present in the weathering crust. However, trivalent Sb bound to 3 O atoms is likely the initial oxidation species as detected in the weathering bullet alloy from this study and a laboratory oxidation sample with metallic Sb. Similar methods show that cerussite, hydrocerussite and litharge comprise the bulk of the Pb concentration in the weathering crust, but Pb(II) sorbed to Fe(III) oxides are present in the soil fraction distal to the source material. These results show differences in speciation between the weathering crust and soil fraction in shooting range samples and highlight the natural association of Pb and Sb with Fe. Understanding metal speciation is a critical first step in developing and implementing remediation strategies in small arms shooting ranges.

[1]Barker, A.J., Mayhew, L.E., Douglas, T.A., Ilgen, A.L., Trainor, T.P. Lead and antimony speciation associated with the weathering of bullets in a historic shooting range in Alaska. Prepared for submission in Science of the Total Environment.

3.2 Introduction

Training ranges in the United States managed by the Department of Defense (DoD) often contain extremely high loadings of toxic metal(loid)s and organics, including but not limited to Pb, Sb, copper (Cu), zinc (Zn), arsenic (As) and polycyclic aromatic hydrocarbons (PAH) (Basunia and Landsberger, 2001; ITRC, 2003; Scheetz and Rimstidt, 2008; Clausen and Korte, 2009; U.S. Army Corps of Engineers, 2014). The primary contaminants are Pb and Sb and to a lesser extent, Cu, which are the major components of bullet fragments (Randich et al., 2002; Johnson et al., 2005; Laporte-Saumure et al., 2011). Small arms ranges typically employ backstops consisting of a natural hillside or artificial soil mound called a berm. Bullets impact the berm and fragment, exposing fresh metallic surfaces to weathering processes, which leads to the release of metal(loid) species into solution. Once Pb and Sb enter into the environment they are long-term persistent contaminants that transform from one species to another (Knox et al., 2000; Grisbert et al., 2003; Singh and Gräfe, 2010). In addition, both Pb and Sb are toxic (US EPA, 1979; Rooney et al., 1999) and Sb is a suspected carcinogen (IARC, 1989; WHO, 2003). Therefore, Pb and Sb contamination from small arms training facilities pose a major public health and environmental concern stemming from the fact that Pb and Sb can migrate in soil solution.

The soil material at shooting range sites can far exceed crustal soil background concentrations for Pb and Sb of 10-30 mg kg^{-1} and 1 mg kg^{-1}, respectively (Agency for Toxic Substances, 1992; Rooney et al., 1999; Adriano, 2001; Filella et al., 2009). In the United States, it was estimated that 80,000 tons of Pb produced was made into bullets in the late 1990s (US EPA, 2005) and the U.S. DoD on average expended more than 2 million pounds of Pb annually (ITRC, 2003). Lead accounts for approximately 93.1 wt.% of the bullet mass (Laporte-Saumure

et al., 2011) and comprises the bulk of the bullet. Antimony is added to Pb as a hardening agent with Sb wt.% on average reported anywhere between 0.7 wt.% (Randich et al., 2002) to 1.9 wt.% (Laporte-Saumure et al., 2011) to 2-5 wt.% (Johnson et al., 2005). A copper alloy is used to jacket bullets (4.5 wt.%) and contains trace amounts of Ni and Zn (0.5 wt.%) (Laporte-Saumure et al., 2011). Previously reported Pb concentrations for shooting range soils can range up to 150,000 mg kg^{-1} (Jorgensen and Willems, 1987; Basunia and Landsberger, 2001; Cao et al., 2003; Knechtenhofer et al., 2003; Johnson et al., 2005), while Sb load is significantly less, ranging from 1-13,800 mg kg^{-1} (Basunia and Landsberger, 2001; Johnson et al., 2005).

The mobility and extent to which Pb and Sb can migrate depends predominantly on their speciation (Cao et al., 2003, Johnson et al., 2005; Singh and Gräfe, 2010). Therefore, it is important to understand the overall mineralogical and morphological composition of Pb species present in both the corroding bullet crust and shooting range soil material due to controls on the overall concentration and mobility of Pb. Lead is typically found in the environment in one oxidation state, Pb(II), which forms upon dissolution and subsequent oxidation of metallic Pb (Cao et al., 2003; Vantelon et al., 2005; Scheinost et al., 2006). The activity of Pb^{2+} in solution has been shown to be primarily limited in shooting range soils by the solubility of secondary minerals that form as a weathering crust around the corroding bullets, which include but are not limited to: $PbCO_3$ (cerussite), $Pb_3(CO_3)_2(OH)_2$ (hydrocerussite), PbO (massicot or litharge), and to a lesser extent $PbSO_4$ (anglesite) (Chen et al., 2002; Cao et al., 2003; Hardison et al., 2004; Vantelon et al., 2005). In addition, amorphous species may form since Pb^{2+} in solution is strongly bound by soil organic matter, clays and manganese or iron oxides via adsorption processes (Manceau et al., 1996; Mozafar et al., 2002).

Antimony is typically found in the environment in two oxidation states, +3 and/or +5. Both species strongly hydrolyze in water as $Sb(OH)_3$ and $Sb(OH)_6^-$ and Sb(III) forms complexes with organic ligands (Johnson et al., 2005). $Sb(OH)_3$ is a neutral species and thus expected to adsorb to Fe oxides over a wide pH range, it is considered relatively immobile in environmental systems. In contrast, $Sb(OH)_6^-$ adsorbs to Fe oxides only at a low pH (<2.5) and remains mobile at neutral and alkaline pHs (Scheinost et al., 2006). The dominant aqueous form of Sb observed in soil solution and shooting range soil porewater is $Sb(OH)_6^-$ (Johnson et al., 2005; Filella et al., 2009). Similar to Pb, the activity of Sb in solution is limited by secondary mineral formation and partitioning to sorbents available in the soil fraction. Among other alteration products, Sb(III) may be limited by the formation of Sb_2O_3, sénarmontite or valentinite (Zotov et al., 2003). Whereas, Sb(V) may be limited by the formation of Sb_2O_5, for example, that has a solubility in the molar range at pH 7 (Johnson et al., 2005). In addition to Fe oxides, Sb has been shown to partition to other natural sorbents that may be present including: Mn and Al hydr(oxides), clay minerals and humic acids (Thanabalasingam and Pickering, 1990; Tighe et al., 2005; Ilgen and Trainor, 2012).

While investigations of berm soil material have been the subject of numerous reports both in the U.S. and abroad (Cao et al., 2003; Vantelon et al., 2005; Scheinost et al., 2006; Ackermann et al., 2009; Conesa et al., 2010; Okkenhaug et al., 2013; Sanderson et al., 2015), there is little known about the speciation of Pb and Sb in shooting ranges in Alaska despite housing three Army bases: Ft. Wainwright (Fairbanks, AK), Ft. Greely (Delta Junction, AK) and Ft. Richardson (Anchorage, AK). More importantly, like other cold regions, Alaska presents a unique opportunity to study metal leaching from bullets and subsequent mineral weathering as a function of the cold climate. For half the calendar year, the Alaskan arctic and subarctic

maintains temperatures below 0°C, which translates to less time the surface and subsurface of the shooting range berms will be exposed to weathering processes. As a result, shooting ranges that are relatively 'old' may still be 'young' in terms of Pb and Sb weathering from bullets and can thus provide a unique dataset addressing the gap in knowledge concerning small arms ranges in cold regions.

The focus of this study was to understand the chemical fate and transformation pathways of Pb and Sb as a result of bullet weathering at a shooting range site outside of Fairbanks, Alaska. Metal speciation tends to be the limiting factor for determining bioavailability of a contaminant, as well as dictating the potential for off-site transport, thus we employed grain-scale characterization methods (electron-microprobe analysis (EMPA), micro-focused x-ray absorption spectroscopy (XAS) and x-ray fluorescence (XRF) measurements) to determine the speciation of Pb and Sb as a function of element spatial distribution relative to the source materials (bullet slugs). Results from this study provide key insights into the geochemical behavior of metals in cold regions that control the overall mobility and bioavailability of toxic metals. This is of particular importance in Alaska, where the soil thermal regime and temperature dynamics play an important role in metal geochemistry and weathering pathways may be altered by unique temperature and soil conditions (Barker et al., 2014).

3.3 Methods

3.3.1 Field Study

Soil samples and bullet fragments were obtained from a hillside used as a natural berm-style backdrop at the Meadows Range Donnelly Training Area, Fort Greely near Delta Junction,

Alaska. While no longer active, the Meadows Range was heavily used for small arms training exercises approximately 15-20 years ago. Multiple types of ammunition rounds were fired into the berm including .50 caliber, 7.62 mm and 5.56 mm caliber bullets. The 5.56 mm ammunition round was the only size round this study examined. The bullet alloy was composed of 99 wt. % Pb and 1 wt. % Sb (DAC, 2010).

3.3.2 Sample Collection and Preparation

Reference in this paper to DI water means ultrapure water with a resistivity of 18.1 MΩ (EMD Millipore, Billerica, Massachusetts) at 25°C.

3.3.2.1 Thin Section Preparation

Samples were collected from Meadows Range in the summer of 2010, 2011 and 2012. Heterogeneous soil samples and incremental bulk soil samples were collected in the same method as reported in section 2.3.2. In order to investigate metal speciation in a controlled environment, a subset of the pristine soil fraction (5g) was sieved to 2 mm and dried at 60°C for 2 hours, then uniformly mixed with 0.5 g of 99.999% metallic Sb powder, ~200 mesh size (Alfa Aesar, Ward Hill, MA) and 0.5 g of 99.999% metallic Pb powder, 200 mesh size (Alfa Aesar, Ward Hill, MA) and loaded into a plastic (HDPE) column connected to Tygon tubing (Saint-Gobain Performance Plastics, Courbevoie, France). The column and tubing were previously acid-washed with 2% HNO_3 (Ultrex Ultrapure Reagent, J.T. Baker, Center Valley, PA). An additional 5 g of the soil fraction was incrementally added on top of the Sb/Pb soil mixture for a total of 9 increments (50 g total including the Sb/Pb soil mixed bottom layer). A 5mM electrolyte solution of KNO_3 (prepared by dissolving 0.5 g of reagent grade KNO_3 into 1 L of DI water and

subsequently filtered to 0.45µm using a nylon filter tip) was reverse-flushed through the column at 0.5 mL/min for 2 hours. Soil was drained and kept frozen at -18 °C until analysis.

3.3.2.2 Weathering Crust Preparation

To investigate the speciation of the weathering crust, approximately 15 bullets were scraped and the powder was consolidated into one sample using plastic spatulas. The crust was spread evenly in a thin layer on a piece of tape (Scotch Brand, 3M, St. Paul, MN) and covered with double-sided tape (Scotch Brand, 3M, St. Paul, MN) for a total of three layers. In addition, a pristine bullet was removed from the firing cartridge, sliced length-wise in half using a Diamond Saw (Buehler Company, Lake Bluff, Illinois) and served as a representation of a 'pristine' bullet similar to the bullets fired into Meadows Range.

3.3.3 Sample Analysis

The pH of pristine, local soil was analyzed within 2 hours of collection and is outlined in section 2.3.3.2. The soil type was determined based on the fractionation of particles and the soil particle triangle classification system (Soil Survey Division Staff, 1993).

For the identification of crystalline phases, total metal concentrations and Pb distribution in the historic shooting range soil, the soil was prepared and analyzed as reported in section 2.3.3.2.

Elemental distribution and semi-quantitative element wt. percentage analysis were conducted on a JEOL JXA-8530F field emission electron microprobe in both wavelength-dispersive (WDS) and energy-dispersive (EDS) mode. Samples were carbon coated (Edwards carbon coating system, AIL, Fairbanks, AK) prior to analysis to reduce the effects of charging.

Analyses were conducted with an accelerating voltage of 15 keV. WDS element maps were collected at a constant probe current of 200nA. Estimated minimum detection limits (MDL) for WDS maps were extrapolated from standards run for WDS point analyses and calculated according to Potts (1992); Pb = 0.34 wt% (0.0017 mol%); Sb = 0.25 wt% (0.0021 mol%); Fe = 0.34 wt% (0.0061 mol%). WDS maps were used to locate areas of interest for collection of quantitative WDS point data. Point analyses were collected at a probe current of 25nA. Lead and Sb were counted for 20 seconds on peak and 20 seconds on background (10 s below and 10 s above the peak). Iron and Cu were counted 25 seconds on peak and 20 seconds on background (10 s below and 10 s above the peak). Standards used were PbS, Sb_2Te_3, hornblende, and chalcopyrite for Pb, Sb, Fe, and Cu respectively. Qualitative EDS data were used to help locate spots of interest for WDS analyses and to identify all elements present to ensure that non-analysis of any major elements was not the cause of WDS data totals < 100. The EDS spectra were also collected simultaneously with WDS spectra. Percent analytical error and 99% confidence detection limits in weight percent were calculated for quantitative EMP-WDS analyses. For all analyses, typical detection limits for Pb and Sb are< 0.1 wt%. Typical analytical errors for (1) high Pb, low Sb areas =Pb< 0.5wt% (0.0024 mol%), Sb 0.5-5wt% (0.0041-0.041mol%), (2) low Pb, high Sb areas =Pb</= 1.5wt% (0.0072 mol%), Sb = 0.1wt% (0.00082 mol%). It was not possible to account for the error due to geometry effects resulting from sample surface topography, which is magnified by the hardness differences at the bullet-soil interface and between the bullet, soil, and epoxy. The presence of oxygen, carbon, and hydrogen can be inferred in calculations but could not be measured with the EMP system used in this study. Thus, while WDS totals of less than 100% may signify the presence of oxide, carbonate, or hydrous

mineral phases, it was not possible to definitively identify the presence of these phases because of our inability to achieve a flat sample surface.

Samples were analyzed for Sb elemental distribution, spatial correlation and speciation using synchrotron-based x-ray spectroscopy. Extended x-ray absorption fine structure (EXAFS) data was collected at beamline sector 13 IDE (GSECARS), Advanced Photon Source (APS), Argonne National Laboratory. The incident energy for the Si(111) water-cooled monochromator was set at the peak derivative mid-point of the antimony K-edge spectra of an Sb(0) reference foil, corresponding to 30,491 eV. The monochromator was detuned by 20% for harmonic rejection using platinum-coated Kirkpatrick-Baez mirrors. The monochromator step size was 5 eV in the pre-edge, 0.5 eV in the near edge region and 0.05 $Å^{-1}$ in the EXAFS region. Samples were placed at 45° to the Vortex silicon drift diode array detector. The EXAFS data were processed using the Athena interface of the Demeter package (Ravel and Newville, 2005) to the IFEFFIT (Newville, 2001) program. Data processing is described in more detail in Kelly et al., (2008), but included background subtraction using AUTOBKG algorithm (Newville et al., 1993), normalization and conversion into k-space. The data was then Fourier transformed over the k-range of approximately 3.0 to 9.0 or 3.0 to 10.5, depending on the sample. The amplitude reduction factor, s_0^2, was set to 0.97 based on fitting of $KSb(OH)_6$ (Electron Microscopy Sciences, Hatfield, PA) standard in the same analysis window and reported by Ilgen et al., (2014). The resulting Fourier transformed antimony K-edge EXAFS spectra was modeled using Artemis (Ravel and Newville, 2005), which fits theoretical paths calculated with Feff 6 (Zabinsky et al., 1995; Newville, 2001) based on the structures of Sb(0) (Wyckoff, 1963), valentinite (Whitten et al., 2004) and Sb_2O_5 (Jansen, 1979).

3.4 Results

3.4.1 Characterization of historic shooting range soil

Pristine soil from the historic shooting range is a silty loam that was previously characterized in section 2.4.1 and Table 2.1 (soil type 1).

Total metal concentrations for the contaminated berm soil are shown in Table 3.1. Bulk concentrations of Pb (77.91 mg/kg) are almost an order of magnitude higher than Sb (8.43 mg/kg). While background concentrations of Sb in Alaskan sediment can be elevated, particularly as a result of mining activities (43 to 6000 mg/kg reported by Eppinger et al. (2000); 6.6 to 7230 mg/kg reported by Ritchie et al. (2013)) compared to average crustal abundances reported as 0.2 mg/kg by Onishi and Sandell (1955) in Filella et al. (2009), background concentrations for the local soil in this study were below the instrumental detection limit of 5.9 mg/kg.

3.4.2 Characterization of an Unfired 5.56 mm Bullet

Electron microprobe analyses were conducted on an intact, unfired, military-issued 0.22 caliber (5.56 mm) bullet in order to understand the initial anatomy and composition prior to weathering and alteration, shown in Figure 3.1. The pristine bullet is 30 mm long, 6 mm wide in the center, 1 mm wide at the tip and consists of four distinct chemical zones of varying thickness (Figure 3.1a). The outermost layer consists mainly of Fe, approximately 500 – 1500 μm thick, and surrounds a Cu-rich interlayer, approximately 50 – 100 μm thick. A discontinuous Pb-rich interlayer (50 – 150 μm thick) exists between the Cu-rich interlayer and the slug (500 – 4000 μm thick), the innermost region of the bullet (Figure 3.1b). Electron microprobe analyses revealed that the distribution of Pb and Sb within the bullet is heterogeneous. Lead is the main component

in the matrix but occurs in different proportions with Sb in the matrix of the slug (87 and 13 mol%, respectively) than in the Pb-rich interlayer (96 and 4 mol%, respectively) (Table 3.2), making these two regions chemically distinct (Figure 3.1c). Lead also occurs as discrete ~2x2 μm, ~100 mol% spheres, which form as a result of melting during analyses conducted at high beam currents (≥ 100nA) and are thus an artifact of the analytical method, shown in Figure 3.1d, Table 3.2).

Antimony is relatively evenly distributed within the matrix of the slug (Figure 3.1e), except that it occurs as diffuse, discrete, roughly circular Sb-rich spherical 'hotspots' (40 mol% Sb). The hotspots are ~2-5 μm in diameter and are embedded within the Pb-matrix and not specifically associated with Pb spheres that are an artifact of melting during analysis. The Sb-rich hotspots are more common within the Pb-rich interlayer, where they have a higher Sb content (88 mol % Sb) and contain the majority of the Sb present (Figure 3.1f). When averaged across the entire area of the Pb-rich interlayer, Sb is present at a level of 4 mol% Sb.

3.4.3 Chemical Characterization and Speciation Analysis of a Weathered Bullet

The fragmentation process that occurs once a bullet impacts soil often exposes the Pb and Sb alloyed core and Fe slug to the environment. X-ray fluorescence maps were collected on a spent bullet that had weathered for approximately 15 years within the shooting berm soil in order to track the elemental distribution after bullet fragmentation upon impact with soil. Tri-color plots showing distributions of Pb (red), Fe (green) and Cu (blue) are shown in Figure 3.2a. The steel and Cu jacket partially separated from one another, leaving the Pb/Sb alloyed core exposed. While Pb comprises the bulk of the alloyed core, there are also particles of Pb present within the soil matrix.

3.4.3.1 Electron Microprobe Analysis

The back-scattered electron image of Region 1 (outlined in white box in Figure 3.2b) depicts the interface of the bullet with soil particles (Figure 3.3). Soil minerals are present within the fracture that passes through the slug and Pb-rich interlayer of the bullet. The tip of the fracture has little exposure to soil while, at the base of the fracture, soil grains are the predominant material. As a result, we identified three different areas within a single region of the sample that experienced differing degrees of exposure to soil and exhibited different degrees of weathering and alteration. Relative mole percentages of Pb and Sb found within Region 1 are presented in Table 3.2.

The Pb and Sb distribution in the area at the tip of the fracture is similar to that seen in the pristine bullet (Figure 3.3a). The Sb-rich hotspots in this region have WDS totals equal to 100% with contributions from only Sb and Pb, indicative of the metals being present in their elemental form. As shown in Figure 3.1, the Pb/Sb alloy used to make the core of bullets is not a homogenous mixture, but instead it appears as Sb inclusions in a matrix of metallic Pb. The axis of the fracture becomes progressively more soil rich until eventually, in areas of the sample further from the bullet, fragments of slug material are completely incased in soil material such as seen in Figure 3.3c. As the abundance of soil particles increases, there is a corresponding decrease in the relative abundance of Pb and Sb, as illustrated in the WDS elemental maps (Figure 3.3), suggesting that weathering occurs along the axis of the fracture.

The weathering crust and bullet to soil interface is primarily comprised of Pb, whereas Sb is present in segregated clusters (depicted in Figure 3.4). Back scatter electron imaging and chemical analyses by electron microprobe reveal the crust appears to act as a cement between the bullet fragments and surrounding soil particles as well as between individual soil particles.

Similar weathering crusts have previously been observed around bullets weathering in shooting range soils (Jorgensen and Willems, 1987; Lin et al., 1995; Hardison et al., 2004; Vantelon et al., 2005; Ackermann et al., 2009). The alteration crust in the current study is discontinuous; it does not entirely surround any single bullet fragment. The distance the alteration crust extends away from the bullet fragments varies between individual fragments.

In previous work studying two bullet samples, Vantelon et al. (2005) report an average crust thickness of 100 μm. The change in relative Pb intensity with distance from the bullet is shown in Figure 3.5. The Pb profile represents the average Pb intensity at every pixel from the bullet-soil interface to the edge of the mapped area. To obtain this profile, an area on the sample was chosen that had relatively linear features with respect to bullet to soil interface (shown in Figure 3.4) and the Pb intensity change at the bullet-soil interface was mathematically defined. The particular pixel fulfilling the mathematical definition of the bullet-soil interface was defined in each column of image intensity data and the x coordinate of that pixel was set to be at a distance equal to 0 micrometers. After identification of the 0 μm pixel in each column, the columns were adjusted to align the pixels representing x = 0 micrometers. Once the data was aligned, the Pb intensities in each pixel in every column of data were averaged. The Pb intensity decreases by ~60% over the first ~20μm beyond the bullet-soil interface. At a distance of 20-50 μm from the interface, the Pb intensity continues to decrease though at a slower rate, reaching 20% of the original Pb signal at a distance of 50 μm from the bullet. The Pb intensity remains relatively constant over the distance of 50-120 μm before beginning a steady decline to 3% of the original Pb intensity at 190 μm from the bullet-soil interface.

The concentration of Pb decreases with increasing distance from the bullet-soil interface (Figure 3.5). Analysis of the chemical composition of the alteration crust at different distances

from the bullet-soil interface did not reveal a systematic variation in Pb content of the crust with the distance. Thus, the decreasing Pb concentration with distance is due, instead, to a decrease in the abundance of the alteration crust with distance from the bullet (visible in Figure 3.4). There is a sharp decrease in Pb concentration over the first 20 μm away from the bullet-soil interface. Within this area, relatively unaltered but physically separated shards of the Pb-rich interlayer are concentrated. The shards are not found at slightly greater distances from the bullet-soil interface which likely accounts for the further decrease in Pb intensity. At approximately 50 um from the bullet-soil interface the Pb intensity is ~25% of the intensity in the Pb-rich interlayer. This level of Pb extends another ~70 μm (from 50 – 120 μm away from the bullet-soil interface). By a distance of 200 μm away from the bullet-soil interface, the abundance of the alteration crust has greatly decreased, reaching a Pb intensity only 3% of the signal from the Pb-rich interlayer. In a previous study where the Pb concentration was measured over a much longer transect, the profile revealed a strong decrease in Pb over a distance of a few hundred micrometers from the weathering crust (Vantelon et al., 2005). Distribution of Sb is discontinuous and appears to be random in the bullet alloy and cemented crust, which caused difficulty when trying to determine concentration as a function of distance from bullet. As mentioned previously, Sb concentrations present in the soil fraction were low indicating Sb might be considerably mobile in the soil system, which is consistent with previous studies on Sb mobility (Ilgen et al., 2014).

3.4.3.2 Pb-L_{III} XANES Analysis

Detailed micro-scale analysis of the Pb speciation in the weathering feature in Region 1 revealed the presence of oxidized Pb species most adjacent to the fracture, in addition to containing metallic parent material. Multiple energy mapping and PCA of Region 1 showed distinct distributions of Pb components (Figure 3.6) and representative spots (1-4) were further

analyzed by XANES methods, with results shown in Figure 3.7 with respective fit parameters for the model spectra generated by the LCF function detailed in Table 3.3. Cerussite (42%) with lesser amounts of litharge (32%) and hydrocerussite (28%) comprise spot 1, corresponding to the yellow principle component distribution (Figure 3.6b). Spot 2 best fit analysis corresponds to primarily metallic Pb (88%) with lesser amounts of cerussite (15%), represented by the red component distribution (Figure 3.6b). Spot 3 XANES spectra contains relatively equal contributions of litharge (52%) and cerussite (51%). Spot 4 best fit analysis corresponds to Pb(II) sorption product with Fe oxides present in soil, in addition to relatively equal contributions from litharge and hydrocerussite, as denoted by the green component distribution (Figure 3.6b). Lead speciation analysis of Region 1 suggests there are unique distributions correlated to both distance from alloyed parent material and distance from soil particles. Lead is distributed in low, relative concentrations closest to soil particles along the axis of the fracture in Region 1 (Figure 3.6a) in comparison to the higher concentrations of Pb found approximately 5-10 μm from the fracture. In addition to micro-scale speciation measurements, the weathering crust of approximately 15 bullets was scraped and consolidated into a powder sample and the bulk Pb speciation was analyzed, results shown in Figure 3.7, Table 3.3. The crust was comprised of predominantly cerussite (54%), with lesser, relatively equal contributions of litharge (26%) and hydrocerussite (23%).

3.4.3.3 Sb K-edge EXAFS Analysis

Antimony K-edge EXAFS analysis was carried out on four separate samples from the historic shooting range (Region 1, the consolidated weathering crust, a laboratory soil sample, and an unaltered bullet alloy) and revealed various Sb oxidation states. The absorption edge energies (Figure 3.8) range from 30,491 eV, corresponding to the unfired bullet alloy, to 30,495

eV, belonging to the consolidated weathering crust scraped from the outside of the bullet fragments. The Sb species in Region 1 exhibits intermediate edge energy at 30,492 eV. Similarly, the local, uncontaminated soil that was mixed with metallic Sb powder in the laboratory also has absorption energy of 30,492 eV. The normalized absorption for the new bullet is dampened due to self-absorption effects, as the cross-section sample was thick (approximately 1 mm) and comprised entirely of bullet core alloy. In addition, the two samples with intermediate edge energies (Sb soil and Region 1) also display a less pronounced normalized absorption line than the weathering crust sample and the Sb-O peaks at approximately 1.5 Å (not corrected for phase shift) in the EXAFS Fourier Transform plot are much larger for the weathering crust than for the Sb soil and Region1 sample.

Shell-by-shell fitting of the backscattering features was carried out to elucidate the local structure of the Sb species most prevalent in the samples. The respective fit parameters are shown in Table 3.4. The two samples with intermediate edge energies exhibited comparable backscattering features and were fit with an O with a coordination of 2.6 (Sb soil) and 3.1 (Region 1) at distance 1.96 and 1.97Å, consistent with trivalent Sb speciation. Based on assumptions concerning the structure of the two samples, the higher order shells were fit with Sb-Sb scattering paths, but iterations did not significantly improve the fit. Particularly for Sb hotspot Region 1, there likely is a heavy atom in a more distant shell based on the small backscattering feature at 2.8Å (uncorrected for phase shift) and an unfit oscillation feature in the k^3 weighted EXAFS spectra at approximately 7.2 $Å^{-1}$. However, the backscattering features are weak, indicating a relatively disordered system. Therefore, only the first shell fittings are presented for Sb soil and Region 1 (Table 3.4). The weathering crust was the most oxidized sample analyzed, bearing a more prominent white line than the other samples with an absorption

edge energy of 30,495 eV (Figure 3.8). The Sb-O path was best fit with a coordination number of 5.3 at a distance of 1.99 Å, indicative of an octahedral-coordinated pentavalent Sb species. The larger distance FT peaks were fit with an Fe atom at 3.15 Å and a coordination number of 3 (Table 3.4).

3.5 Discussion

3.5.1 Heterogeneous Distribution of Pb and Sb in a Pristine Bullet

The starting distribution of Pb and Sb in bullets discharged into a 15+ year old shooting berm at Fort Greeley, Delta, AK is not homogeneous (Figure 3.2). Chemically distinct regions of the bullet contain metallic Pb and Sb in varying quantities (Table 3.2). A relatively well-mixed Pb/Sb slug (87 norm wt% Pb, 13 norm wt% Sb) is surrounded by a discontinuous, higher Pb content interlayer (96 norm wt% Pb, 4 norm wt% Sb) and Sb occurs as discrete, ~2-5 μm diameter Sb-rich hotspots (Figure 3.1). Observing the heterogeneous distribution of Pb and Sb in bullets is not unique to this study, but supports previous findings by Ackermann et al. (2009).

The distinct nature of the heterogeneous distribution of Pb and Sb in a bullet contributes to the overall discontinuous oxidation of Pb and Sb, likely resulting in sporadic mobilization. The historic bullets from this shooting range were not highly fragmented. Instead, they remained relatively intact though deformed. This is attributed to the Fe casing present between the Cu-jacket and the core/slug. This steel casing surrounding the exposed Pb is not consistently present in munitions testing (Grund et al., 2010) and likely creates an additional barrier to fragmentation processes. The initial composition of bullets and the extent to which they are weathered are often

not reported in studies, but typically play a role in overall Pb exposure after impact. Commonly the bullets found in this study were bent, but the Cu-jacket and steel enclosures remained together with the slug, effectively lowering the surface area exposed to weathering processes. Relatively large, intact bullet fragments that have separated from the main bullet were found embedded between soil particles (as seen in Figure 3.2). These fragments were relatively unaltered and metallic parent materials remained the main component of these fragments. The Fe encapsulation protected the interior from excessive weathering.

3.5.2 Characterization of a Pb/Sb Alteration Crust

Back scatter electron imaging and chemical analyses by electron microprobe revealed the presence of a Pb-rich alteration crust around bullet fragments. The crust acts as a cement between the bullet fragments and surrounding soil particles as well as between individual soil particles (Figure 3.4). The existence of alteration crusts around bullets has been observed in shooting range soils (Jorgensen and Willems, 1987; Lin et al., 1995; Hardison et al., 2004; Vantelon et al., 2005; Ackermann et al., 2009). The alteration crust in the current study was discontinuous; it did not entirely surround any single bullet fragment. The distance the alteration crust extends away from the bullet fragments varies between individual fragments. In previous work studying two bullet samples, the average crust thickness was 100 μm (Vantelon et al., 2005).

Semi-quantitative EDS and quantitative WDS analyses revealed that the alteration crust is predominantly composed of O, Pb, Si and Al. Elements originating from the surrounding soil (Fe, Mg, Ca, Na), were not a major component of the crust; present at only low levels (~2 wt%). The abundance of oxygen in the crust relative to the primary bullet material suggests that the Pb

is likely oxidized. The presence of Si, Al, Fe, Mg, Ca, Na suggests a reaction between the oxidized Pb and soil to form a crust with components originating from both the bullets and the surrounding soil. Thus, a portion of the metallic Pb weathered and released from the primary bullet was re-precipitated in oxidized secondary phases. The combination of elements sourced from bullets and soil to form an alteration crust has been noted in previous work (Lin et al., 1995; Vantelon et al., 2005).

3.5.3 Speciation of Sb and Pb in the Alteration Crust and Soil

3.5.3.1 Speciation of Sb

The speciation of Sb in the alteration crust is dominated by an Sb-Fe sorption complex (Figure 3.8). Antimony is bound to O atoms at a distance of 1.99 Å with coordination number of 5.3 and Fe atoms in the second shell at a distance of 3.15 Å with a coordination number of 3. The lower (<6) coordination number for Sb-O (5.3) could potentially be due to self-absorption of the sample, e.g. Ackermann et al. (2009), where pentavalent Sb had a coordination number of 3.72 (R = 1.98 Å) and 3.1 (R = 1.97 Å). The Sb-Fe distance for the weathering crust sample (3.15 Å) is consistent with edge-sharing (~3.10 Å Scheinost et al., 2006; ~3.11-3.13 Å Ackermann et al., 2009). Both edge and corner-sharing between Sb and Fe were reported in Scheinost et al. (2006) and Ackermann et al. (2009) studies, but we could only fit an edge-sharing Fe scattering pattern. However, the coordination number best fit for this sample (3 ± 1) is higher than observed by these two studies for edge-sharing sorption complex, and with higher error. It is more closely associated with what has been observed for corner-sharing sorption complexes, but with a lower fitted atomic distance. A higher Sb-Fe coordination number has been attributed to the presence of tridentate Sb octahedral complexes or direct incorporation of Sb into the structure of Fe

oxides, e.g. 2.0-2.5 (Guo et al., 2014); 2.9-3.5 for Sb(V) in ferrihydrite (Mitsunobu et al., 2006). While this could likely explain the higher coordination number, we would expect a larger atomic distance between Sb and Fe in our sample if this were the case. The Sb-Fe atomic distance indicates an edge-sharing association, but the higher coordination number suggests a corner-sharing structure or co-precipitation species. Incorporating the error associated with the Fe coordination number measurement in addition to the Sb-Fe distance, it is more likely that the sorption complex between Sb and Fe is inner sphere.

The trivalent Sb weathering product in the fracture in Region 1 is likely a transient weathering product and not stable long-term unless in reducing conditions (Johnson et al., 2005; Ilgen et al., 2014). However, the occurrence has implications to the overall mobility and toxicity of Sb. Antimony (V) species will have enhanced mobility at circum-neutral pHs, whereas the mobility of Sb (III) species is independent of pH (Johnson et al., 2005) and trivalent Sb compounds have a ten times higher acute toxicity than pentavalent species (Krachler et al., 2001). Besides in the alteration crust and bullet fracture (Region 1), Sb was not detected in the soil either independently or associated with Fe. Rapid oxidation of Sb(III) to Sb(V) (e.g. Ilgen et al., 2014) in berm water could explain the low concentration of soil-bound Sb. Other potential sorbents for Sb were investigated including organic fractions and clay mineral surfaces, all of which were detected in the soil, but did not contribute significantly to the overall best fits for the x-ray absorption spectra.

3.5.3.2 Speciation of Pb

The speciation of Pb in the weathering crust was primarily cerussite, $PbCO_3$ (53-55%), with minor amounts of litharge, PbO (25-27%), and hydrocerussite, $Pb_3(CO_3)_2(OH)_2$ (22-24%).

The distribution of litharge dominated near the metallic Pb core, whereas cerussite accumulated in the outer crust in contact with soil. This finding is consistent with that of previous studies (Hardison et al., 2004; Vantelon et al., 2005). Lead was also found in association with Fe in the soil fraction, distal to the parent material. Surrounding the predominantly cerussite layer, was a species of Pb that was best fit with Pb(II) sorbed to Fe oxide model compound (Figure 3.6, Table 3.3). Iron (oxy)hydroxides are known to be an effective sink for Pb (Gustafsson et al., 2011) and has often been sourced as one of the major species limiting Pb mobility in soils (Manceau et al., 1996; Mozafar et al., 2002). The accumulation of Pb bound to Fe is important in determining the overall mobility of Pb as it accumulates at the bullet-soil interface. However, it accounts for only a small contribution to the overall distribution of Pb species, in comparison to cerussite in the regions studied in the historic shooting range samples (Figure 3.7).

3.5.4 Microscale Chemical Variations Influence Behavior During Weathering

The characterization of the alteration crust of a 15 year old shooting range indicates that bullet materials are highly susceptible to weathering. Solid phase chemical investigations reveal the heterogeneous distribution of Pb and Sb in the primary bullet materials, as well as the heterogeneous distribution of the alteration crust around bullet fragments and in the surrounding soil. A model of the microscale weathering process of the historic bullets is depicted in Figure 3.9. We hypothesize that the alloyed bullet material in direct contact with soil weathers first and most extensively. This process releases the bulk of Pb and Sb to solution. Antimony-rich hotspots found in the alloy initially oxidize to Sb(III) upon exposure. We hypothesize that the Sb(III) further oxidizes to Sb(V) and becomes incorporated (primarily sorbed) with Fe(III) found adjacent to the bullet. As a result, the Sb(V) sorption species with Fe(III) becomes part of the

weathering bullet crust. We were unable to characterize any Sb in the soil fraction of the historic samples, likely indicating Sb is more mobile than Pb in the system studied.

The activity of Pb in solution is primarily controlled by the partitioning between various species found in the weathering crust and throughout the soil fraction. Zero-valent Pb present in either the Pb alloy or the Pb-rich interlayer is oxidized to PbO or $PbCO_3$. We suspect PbO is the initial oxidation product due to its proximity to the crust/soil interface. It remains unclear whether $PbCO_3$ forms solely as a result of PbO alteration or also due to Pb^0 oxidation via reaction with porewaters. Cerussite and hydrocerrusite comprise the majority of the weathering crust surrounding the historic bullet and the dissolution of these secondary minerals in the alteration crust gives rise to mobile Pb species that can interact with soil particles (Figure 3.6). The majority of Pb associated with the soil fraction is Pb(II) sorbed species to Fe(III) oxides (Figure 3.7, Table 3.3) and $PbCO_3$ indicating that precipitation and sorption are primary mechanisms of Pb immobilization in the historic shooting range soil.

Portions of Pb and Sb released from the primary bullet material transform into oxidized phases composing the bulk of the alteration crust found in association with bullet fragments. The formation of secondary Sb/Pb-bearing phases act as a limit on the initial amount of Sb/Pb released to solution. However, they could also serve as a secondary source of Pb/Sb to solution as they dissolve under different conditions (Jorgensen and William, 1987; Lin et al., 1995) or over a weathering time scale that differs from that of the primary bullet material. Additionally, the alteration crust appears to cement together soil particles and as such may impact the microscale porosity and permeability thereby limiting or slowing further weathering.

3.6 Conclusion

Our results highlight the complexity of Pb and Sb speciation as a function of distance from the parent source and interaction with surrounding soil. There are limited studies on shooting range soils in Alaska and the majority are published by army-controlled organizations (Tardy et al., 2003), focusing more on applied aspects of bullet weathering like total concentrations instead of overall detailed speciation. As a result, there is a lack of technically-focused studies on the speciation of Pb and Sb and concentration as a function of distance from bullet in Alaska's military shooting ranges. Presently, this study provides a baseline of data for future monitoring in Alaska and offers many improvements on previous efforts.

Our findings show that the transport and ultimate fate of Pb and Sb in a historic shooting range in Alaska is largely controlled by oxidation, dissolution, sorption and precipitation reactions in addition to reactions with individual soil particles present. The fact that soil particles are cemented to the bullet alteration crust likely impacts the microscale porosity and permeability, thus affecting the weathering rate. Micro-scale characterization techniques established a correlation between Pb/Sb and Fe present in the soil, indicating the importance of naturally occurring Fe as a remediation sink for oxidized metal(loid)s. Lead was not found to be in association with Fe in the weathering crust, contrary to Sb. Instead, Pb was observed in associated with Fe in the soil fraction, highlighting potential differences between Sb and Pb speciation with respect to Fe in shooting range soil systems. In addition, analysis of transitory oxidation products revealed Sb(III) is found in shooting range soil samples that contain bullet material actively weathering. It is likely that the distinct nature of the heterogeneous distribution of Pb and Sb in a pristine, unfired bullet contributes to the overall discontinuous oxidation of Pb and Sb resulting in sporadic mobilization.

3.7 Acknowledgments

Funding for this project was from the Department of Defense, Strategic Environmental Research and Development Program (ER-1770). Cold Regions Test Center provided access to the Meadows Shooting Range on the Donnelly Training Area, Ft. Greely, Alaska. GSE-CARS at the Advanced Photon Source, Argonne National Laboratory in Chicago, Illinois and the Stanford Synchrotron Radiation Lightsource of Stanford Linear Accelerator Center in Menlo Park, California provided assistance with collection of x-ray absorption and fluorescence data. Numerous students and collaborators are acknowledged on this project for field and laboratory assistance. Ken Severin and Karen Spaleta from the Advanced Instrumentation Laboratory at the University of Alaska Fairbanks assisted in analyzing samples and fellow graduate students, Tiffany Gatesman and Erik Talvi provided data collection support.

3.8 References

Ackermann, S.; Gieré, R.; Newville, M.; Majzlan, J. Antimony sinks in the weathering crust of bullets from Swiss shooting ranges. *Sci. Total Environ.* **2009**. *407*, 1669-1682.

Adriano, D.C. Trace Elements in Terrestrial Environments: Biogeochemistry, Bioavailability, and Risks of Metals; Springer; New York, **2001**.

Agency for Toxic Substances and Disease Registry (ATSDR). Toxicological Profile for Antimony. U.S. Public Health Service, U.S. Department of Health and Human Services, Altanta, GA. **1992**.

Barker, A.J.; Douglas, T.A.; Jacobson, A.D.; McClelland, J.W.; Ilgen, A.G.; Khosh, M.S.; Lehn, G.O.; Trainor, T.P. Late season mobilization of trace metals in two small Alaskan arctic watersheds as a proxy for landscape scale permafrost active layer dynamics. *Chemical Geology*. **2014**. *381,* 180-193.

Basunia, S.; Landsberger, S. Contents and leachability of heavy metals (Pb, Cu, Sb, Zn, As) in soil at the Pantex firing range, Amarillo, Texas, *Air Waste Manage. Assoc*. **2001**. *51*, 1428-1435.

Cao, X.D.; Ma, L. Q.; Chen, M.; Hardison, D.W.; Harris, W.G. Weathering of lead bullets and their environmental effects at outdoor shooting ranges. *J. Environ. Qual.* **2003**. *32*, 526-534.

Chen, M.; Daroub, S.H.; Ma, L.Q.; Harris, W.G.; Cao, X.D. Characterization of lead in soils of a rifle/pistol shooting range in central Florida, USA. *Soil Sediment. Contam.* **2002**. *11*, 1-17.

Clausen, J.; Korte, N. The Distribution of Metals in Soils and Pore Water at Three U.S. Military Training Facilities. *Soil and Sediment Contamination: An International Journal*. **2009**. *18*, 5, 546-563.

Conesa, H.M.; Wieser, M.; Gasser, M.; Hockmann, K.; Evangelou, M.W.; Studer, B.; Schulin, R. Effects of three amendments on extractability and fractionation of Pb, Cu, Ni and Sb in two shooting range soils. *J. Hazard Mater.* **2010**. *181*, 1-3, 845-850.

Defense Ammunition Center (DAC), Munitions Items Disposition Action System (MIDAS). Detailed Structure for CTG 5.56 mm Ball M855. **2010**.

Eppinger, R.G.; Briggs, P.H.; Crock, J.G.; Meier, A.L.; Sutley, S.J.; Theodorakos, P.M. Environmental–geochemical study of the Slate Creek antimony deposit, Kantishna Hills, Denali National Park and Preserve, Alaska. Studies by the U.S. Geological Survey in Alaska. **2000**: *U.S Geological Survey Professional Paper, 1662*.

Filella, M.; Williams, P.; Belzile, N. Antimony in the environment: knowns and unknowns. *Environ. Chem.* **2009**, *6*, 95-105.

Grund, M.D.; Cornicelli, L.; Carlson, L.T.; Butler, E.A. Bullet fragmentation and lead deposition in white-tailed deer and domestic sheep. *Human-Wildlife Interactions*. **2010**. *4*, 2, 257-265.

Guo, X.; Wu, Z.; He, M.; Meng, X.; Jin, X.; Qiu, N.; Zhang, J. Adsorption of antimony onto iron oxyhydroxides: adsorption behavior and surface structure. *J. Hazard. Mater.* **2014**. *276*, 339-345.

Gustafsson, J.P.; Tiberg, C.; Edkymish, A.; Berggren, K. Modelling lead (II) sorption to ferrihydrite and soil organic matter. *Environmental Chemistry*. **2011**. *8*, 485-492.

Hardison Jr. D.W.; Ma, L.Q.; Luongo, T.; Harris, W.G. Lead contamination in shooting range soils from abrasion of lead bullets and subsequent weathering. *Science of the Total Environment*. **2004**. *328*, 175-183.

IARC. IARC Monograph 47. Lyon: International Agency for Research on Cancer; **1989**.

Ilgen, A.; Trainor, T. Sb(III) and Sb(V) sorption onto Al-rich phases: hydrous Al oxide and the clay minerals kaolinite KGa-1b and oxidized and reduced nontronite NAu-1. *Environ. Sci. Technol.* **2012**. *46*, 843-851.

Ilgen, A.G.; Majs, F.; Barker, A.J.; Douglas, T.A.; Trainor, T.P. Oxidation and mobilization of metallic antimony in aqueous systems with simulated groundwater. *Geochimica et Cosmochimica Acta*. **2014**. *132*, 16-30.

(ITRC) Interstate Technology and Regulatory Council Small Arms Firing Range Team. Characterization and Remediation of Soils at Closed Small Arms Firing Ranges. *Technical/Regulatory Guidelines*. **2003**.

Jansen, M. Die kristallstruktur von antimon(V)-oxid. *Acta Crystallographica B35,* **1979**. 539-542.

Johnson, C.; Moench, H.; Wersin, P.; Kugler, P.; Wenger, C. Solubility of antimony and other elements in samples taken from shooting ranges. *J. Environ. Qual.* **2005**. *34*, 248.

Jorgensen, S.S.; Willems, M. The fate of lead in soils-the transformation of lead pellets in shooting-range soils. *Ambio*. **1987**. *16*, 11-15.

Kelly, S.D.; Hesterberg, D.; Ravel, B. Analysis of Soils and Minerals Using X-ray Absorption Spectroscopy in *Methods of Soil Analysis. Part 5. Minerological Methods.* (pp. 387-465). **2008**. SSSA Book Series, no. 5.

Knechtenhofer, L.; Xifra, I.; Scheinost, A.C.; Flühler, H,; Kretzschmar, R. Fate of heavy metals in a strongly acidic shooting range-soil: Small-scale metal distribution and its relation to preferential water flow. *J. Plant Nutr. Soil Sci.* **2003**. *166*, 84-92.

Knox, A.S.; Seaman, J.; Adriano, D.C.; Pierzynski, G. Chemophytostabilization of metals in contaminated soils. In: Bioremediation of contaminated soils, ed. D. L: Wise, D. J. Trantolo, E. J. Cichon, H. I. Inyang, and U. Stottmeister.. Marcel Dekker, Inc., New York, **2000**, pp. 811-836.

Krachler, M.; Emons, H.; Zheng, J.; Speciation of antimony for the 21th century: promises and pitfalls. *Trends Anal. Chem.* **2001**. *20*, 79-90.

Laporte-Saumure, M.; Martel, R.; Mercier, G. Characterization and metal availability of copper, lead, antimony and zinc contamination at four Canadian small arms firing rangers. *Environmental Technology*. **2011**. *32*, 7, 767-781.

Lin, Z.; Comet, B.; Qvarfot, U.; Herbert, R. The Chemical and Mineralogical Behaviour of Pb in Shooting Range Soils from Central Sweden. *Environmental Pollution*, **1995**. *89*, 3, 303–9.

Manceau, A.; Boisset, M.C.; Sarret, G.; Hazemann, R.L.; Mench, M.; Cambier, P.; Prost, R. Direct determination of lead speciation in contaminated soils by EXAFS spectroscopy. *Environ. Sci. Technol*. **1996**, *30*, 1540-1552.

Mitsunobu, T.; Harada, T.; Takahashi, Y. Comparison of antimony behavior with that of arsenic under various soil redox conditions. *Environ. Sci. Technol.* **2006**. *40*, 7270-7276.

Mozafar, A.; Ruh, R.; Klingel, P.; Gamper, H.; Egli, S.; Frossard, E. Effect of heavy metal contaminated shooting range soils on mycorrhizal colonization of roots and metal uptake by leek. *Environ. Monit. Assess.* **2002**. *79*, 177-191.

Newville, M.; Livins, P.; Yacoby, Y.; Rehr, J.; Stern, E. Near-edge x-ray-absorption fine structure of Pb: a comparison of theory and experiment. *Phys. Rev. B Condens. Matter Mater. Phys.* **1993**. *47*, 14126-14131.

Newville, M. IFEFFIT: interactive XAFS analysis and FEFF fitting. *J. Synch. Radiat.* **2001**. *8*, 322-324.

Okkenhaug, G.; Amstätter, K.; Bue, H.L.; Cornelissen, G.; Breedveld, G.D.; Henriksen, T.; Mulder, J. Antimony (Sb) Contaminated Shooting Range Soil: Sb Mobility and Immobilization by Soil Amendments. *Environ. Sci. Technol.* **2013**. *47*, 6431-6439.

Onishi, H.; Sandell, E.B. Notes on the geochemistry of antimony. *Geochimica et Cosmochimica Acta*. **1955**. *8*, 4, 213-221.

Randich, E.; Duerfeldt, W.; McLendon, W.; Tobin, W. A metallurgical review of the interpretation of bullet lead compositional analysis. *Forensic Sci. Int.* **2002**. *127*, 174-191.

Ravel, B.; Newville, M. ATHENA, ARTEMIS, HEPHAESTUS: data analysis for X-ray absorption spectroscopy using IFEFFIT. *J. Synch. Radiat.* **2005**. *12*, 537-541.

Ritchie, V. J.; Ilgen, A.G.; Mueller, S.H.; Trainor, T.P.; Goldfarb, R.J. Mobility and chemical fate of antimony and arsenic in historic mining environments of the Kantishna Hills district, Denali National Park and Preserve, Alaska. *Chemical Geology*. **2013**. *335*, 172-188.

Rooney, C.P.; McLaren, R.G.; Cresswell, R.J. Distribution and phytoavailability of lead in a soil contaminated with lead shot. *Water, Air and Soil Pollution*. **1999**. *116*, 3, 535-548.

Sanderson, P.; Naidu, R.; Bolan, N. Effectiveness of chemical amendments for stabilization of lead and antimony in risk-based land management of soils of shooting ranges. *Environ. Sci. Pollut. Res.* **2015**. *22*, 8942-8956.

Scheetz, C.D.; Rimstidt, J.D. Dissolution, transport, and fate of lead on a shooting range in the Jefferson National Forest near Blacksburg, VA, USA. *Environmental Geology*. **2008**. *58*, 3, 655-665.

Scheinost, A.; Rossberg, A.; Vantelon, D.; Zifra, I.; Kretzschmar, R.; Leuz, A.; Funke, J.; Johnson, C. Quantitative antimony speciation in shooting range soils by EXAFS spectroscopy. *Geochim. Cosmochim. Acta*. **2006**. *70*, 3299-3312.

Singh, B.; Gräfe, M. Eds. *Developments in Soil Science-Volume 34*: *Synchrotron-based Techniques in Soils and Sediments*, 1st, ed.; Elsevier, Burlington, MA, **2010**.

Soil Survey Division Staff. Soil survey manual. United States Department of Agriculture. **1993**.

Tardy, B.A.; Bricka, R, M.; Larson, S.L. Chemical stabilization of Lead in Small Arms Firing Range Soils. *Environmental Quality and Technology Program*. **2003**. ERDC/EL TR-03-20.

Thanabalasingam P.; Pickering W. Specific sorption of antimony (III) by the hydrous oxides of Mn, Fe, and Al. *Water Air Soil Pollut.* **1990**. *49*, 175-185.

Tighe, M.; Lockwood, P.; Wilson, S. Adsorption of antimony (V) by floodplain soils, amorphous iron (III) hydroxide and humic acid. *J. Environ. Monit.* **2005**. *7*, 1177-1185.

U.S. Army Corps of Engineers Fort Worth District, Forth Worth, TX. Remedial Investigation/Feasibility Study for the U.S. Border Patrol Firing Range. U.S. Customs and Border Protection. **2014**. Contract Number: W9126G-06-D-0016. Task Order 0039.

US EPA Report EPA-902-B-01-001. Best management practices for lead at outdoor shooting ranges. **2005**.

US EPA, Water Related Fate of the 129 Priority Pollutants; USEPA: Washington, DC, **1979**; Vol.1.

Vantelon, D.; Lanzirotti, A.; Scheinost, A.C.; Kretzschmar, R. Spatial distribution and speciation of lead around corroding bullets in a shooting range soil studied by micro-x-ray fluorescence and absorption spectroscopy. *Environ. Sci. Technol.* **2005**. *39*, 4808-4815.

Whitten, A.; Dittrich, B.; Spackman, M.; Turner, P.; Brown, T. Charge density analysis of two polymorphs of antimony (III) oxide. *Dalton Trans.* **2004**. 1, 23-29.

WHO, *Antimony in Drinking Water;* Background Document for Development of WHO Guidelines for Drinking Water Quality; World Health Organization, **2003**.

Wyckoff, R.W.G. Crystal Structures 1. *Interscience Publishers*, **1963**, New York, New York.

Zabinsky, S.I.; Rehr, J.J.; Ankudinov, A.; Albers, R.C.; Eller, M.J. Multiple-scattering calculations of x-ray-absorption spectra. *Phys. Rev. B.***1995**. *52*, 2995.

Zotov, A.; Shikina, N.; Akinfiev, N. Thermodynamic properties of the Sb(III) hydroxide complex Sb(OH)3 (aq) at hydrothermal conditions. *Geochim. Cosmochim. Acta.* **2003.** *67*, 1821-1836.

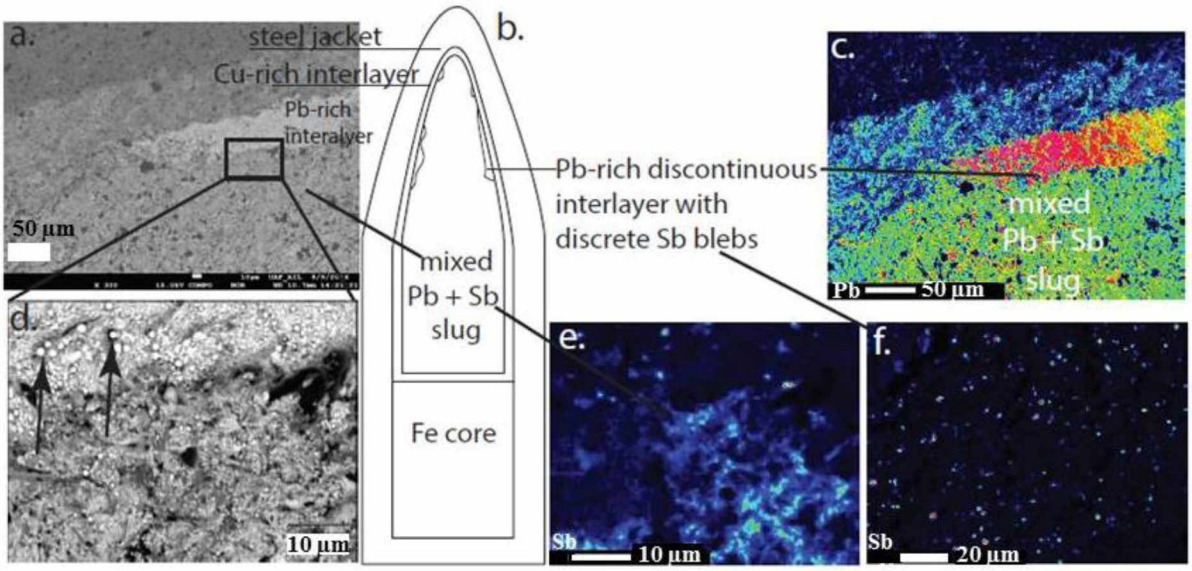

Figure 3.1 Characterization and composition of an unweathered bullet

Anatomy and composition of an unweathered 5.56 mm bullet. (a) Back scatter electron image showing chemically distinct zones. (b) Schematic depiction of bullet anatomy. (c) WDS elemental map showing heterogeneous distribution of Pb. (d) Metallic Pb spheres designated by arrows are the result of melting during analyses at high beam current (≥ 100nA). (e) WDS elemental map showing that Sb is relatively well-mixed within Pb in the slug but exists mainly as discrete hotspots (2-5 µm) within the (f) Pb-rich interlayer.

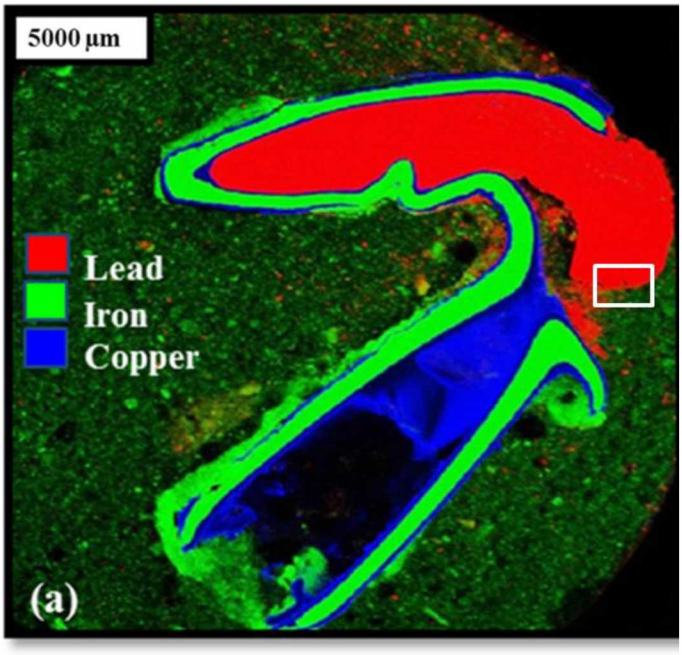

Figure 3.2 Pb, Fe and Cu distributions

(a) Tri-color plot showing x-ray fluorescence distributions of Pb (red), Fe (green) and Cu (blue) within the historic shooting range soil. Specific area of interest outlined as a white square and classified as Region 1 (b).

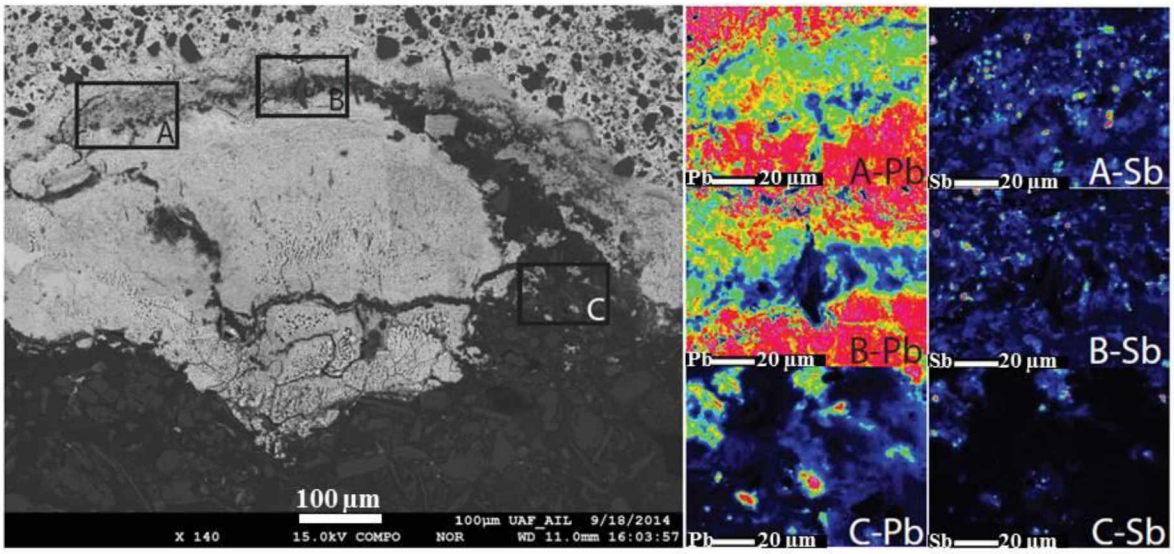

Figure 3.3 BSE image of Region 1

BSE image of Region 1 in a historic shooting range sample. The sample features a crack within the Pb-rich rim that propagates and is increasingly (left to right) filled by soil (dark particles). A,B,C represent different areas analyzed.

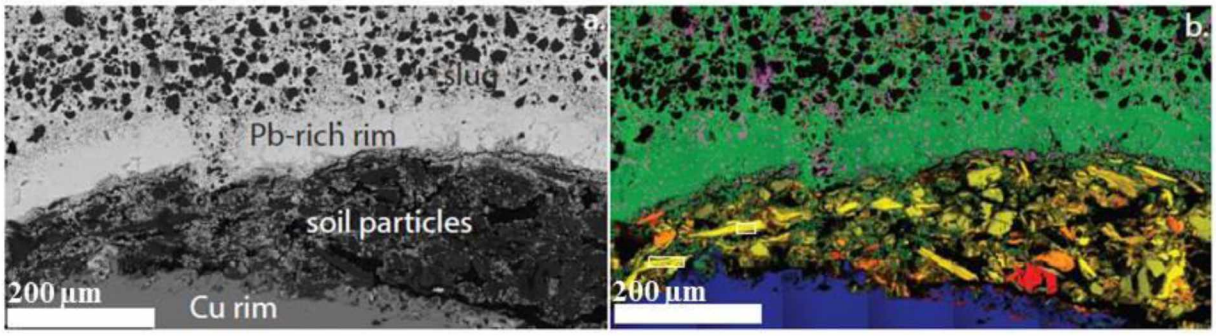

Figure 3.4 BSE image of Region 2

BSE image (a) showing soil particles embedded between the Cu rim and the Pb-rich interlayer of the bullet. (b) WDS map showing elemental distribution in the bullet and soil, Cu = blue, Pb = green, Al = yellow, Sb = magenta.

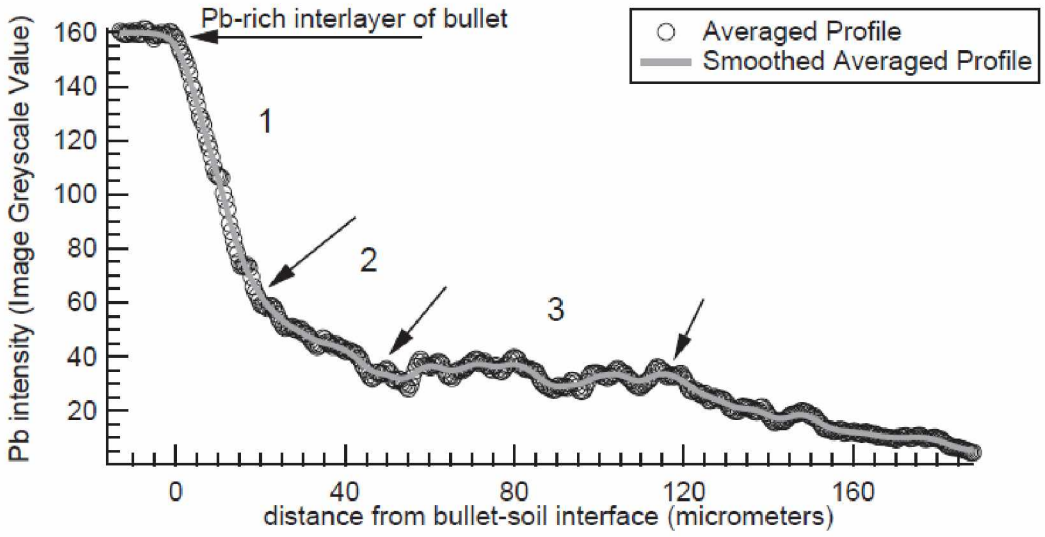

Figure 3.5 Pb intensity profile

Pb intensity profile in historic shooting range sample, calculated using image greyscale values from the Pb distribution WDS map.

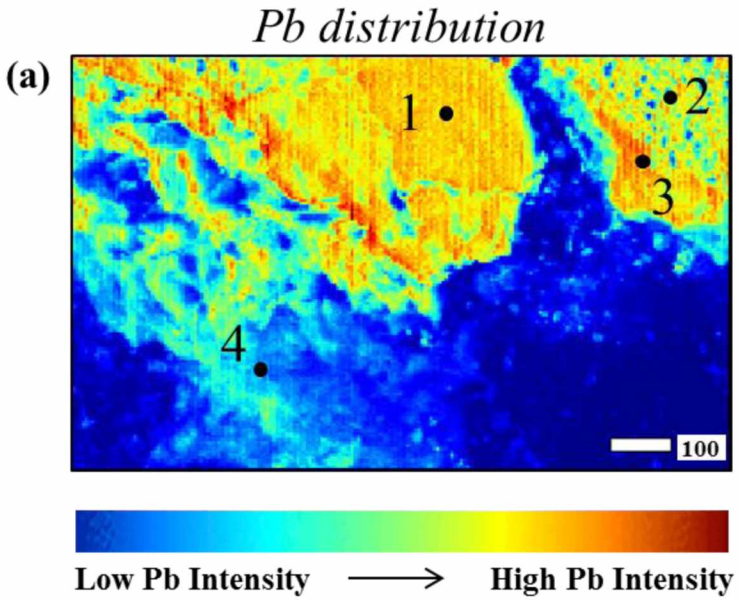

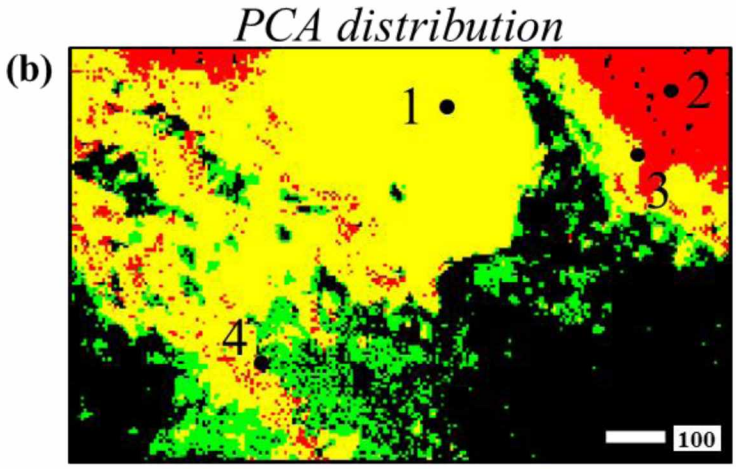

Figure 3.6 Pb distribution and component analysis

Region 1 (a) Pb distribution marked by differences in intensity (concentration) and corresponding (b) distributions of principle Pb components determined by PCA of multiple energy mapping. Spots 1-4 correspond to collected XANES. Scale bars are in units of microns.

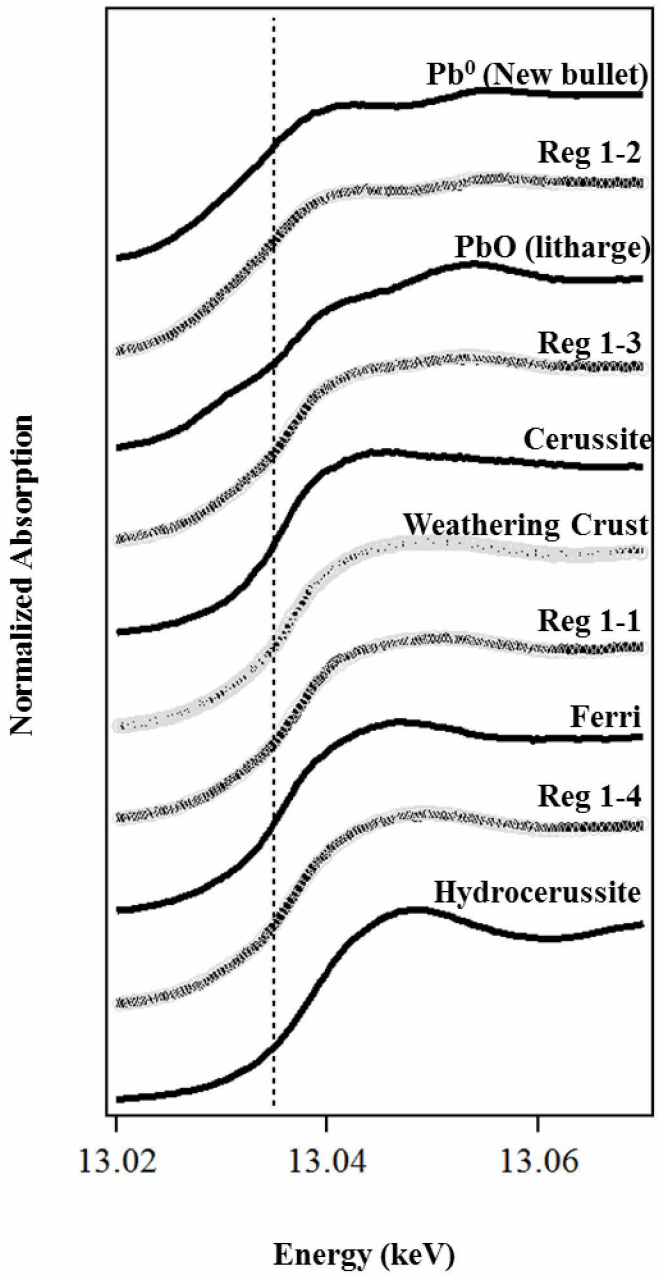

Figure 3.7 Normalized Pb-LIII μ-XANES

Normalized Pb-L_{III} μ-XANES spectra (solid lines) of Region 1 from the historic shooting range sample, spots 1-4 are denoted. Corresponding linear combination fits are shown in gray circle markers based on the reference spectra, which are shown as black solid lines.

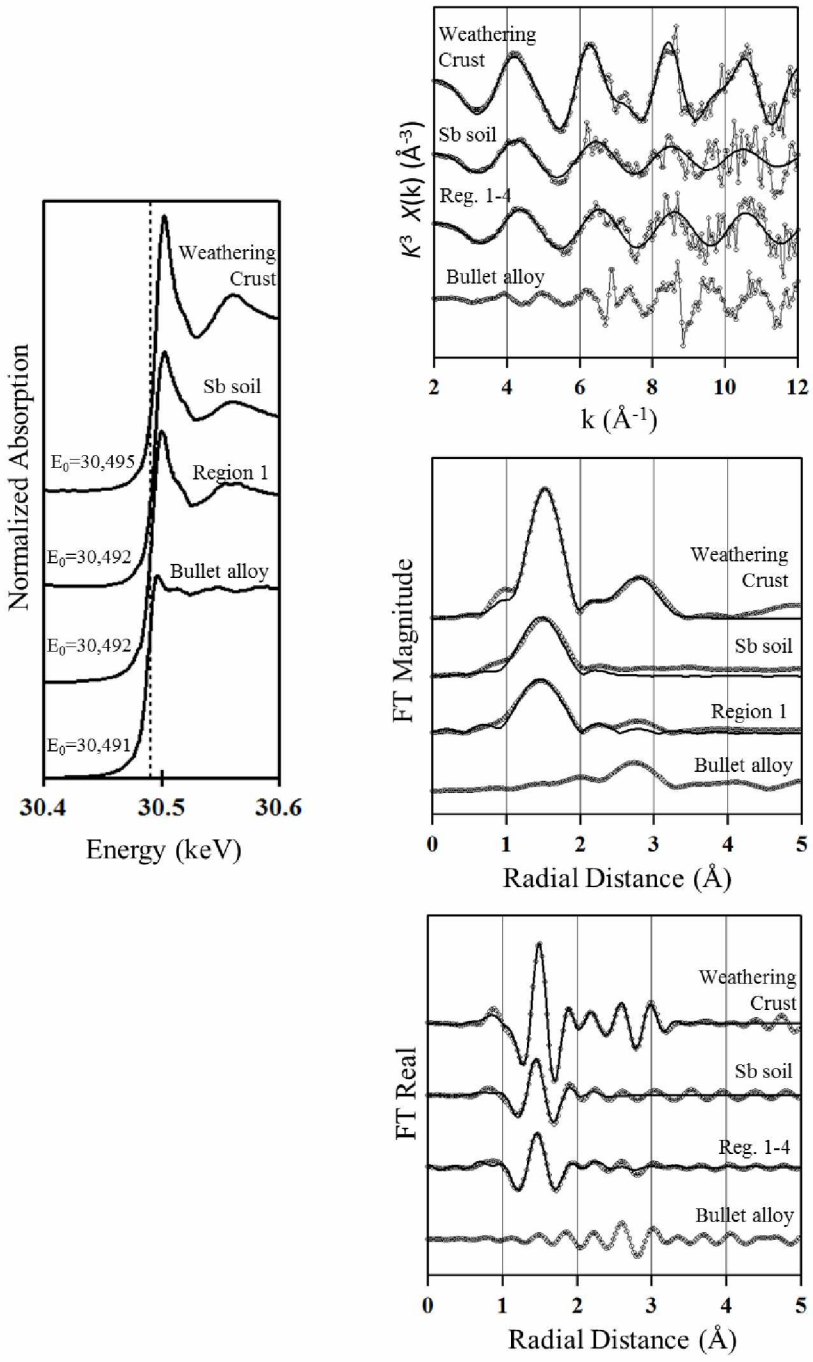

Figure 3.8 Sb K-edge EXAFS

Sb K-edge EXAFS spectra of samples collected from the historic shooting range (weathering crust and Region 1), a laboratory generated sample (Sb soil) and an unfired, new bullet. Empty gray circles correspond to experimental data and solid black lines represent best fit.

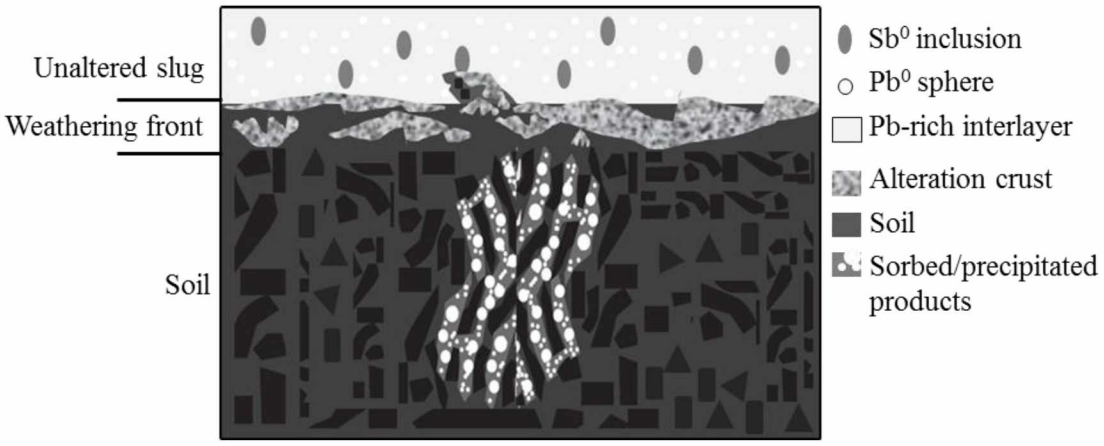

Figure 3.9 Simplified weathering process of weathering bullets

Depiction of morphological and chemical constraints on the weathering of historic bullets.

Table 3.1 Total metal concentrations in soil

Total metal concentrations for historic shooting range berm including lower limit of detection (LLD) for the analytical method.

	Amount	Unit	+/-	LLD
Al_2O_3	14.29	wt. %	0.01	7.35
CaO	1.86	wt. %	0.01	/
Fe_2O_3	5.49	wt. %	0.01	1.30
SiO_2	57.78	wt. %	0.02	14.53
As	17.37	mg/kg	1.81	10.06
Ba	789.19	mg/kg	3.21	/
Cr	122.10	mg/kg	1.21	2.98
Cu	32.99	mg/kg	0.53	1.28
Mn	578.01	mg/kg	2.94	5.47
Ni	31.41	mg/kg	0.51	1.30
Pb	77.91	mg/kg	0.79	2.47
Rb	82.59	mg/kg	0.24	0.79
Sb	8.43	mg/kg	1.50	5.91
Sn	7.74	mg/kg	1.04	3.43
Sr	206.25	mg/kg	0.30	0.54
Ti	9684.35	mg/kg	7.21	6.10
U	6.20	mg/kg	0.55	1.72
V	112.84	mg/kg	1.15	4.45
Zn	66.18	mg/kg	0.37	1.07
Zr	402.74	mg/kg	0.35	0.87

'/' indicates LLD not calculated

Table 3.2 Relative mole percentages of Pb and Sb

Relative mole percentages of Pb and Sb within chemically and morphologically distinct regions in a pristine 5.56 mm bullet and Region 1 of a spent bullet/soil thin section, analyzed by EMPA.

Sample/Region	Pb (mol %)*	Sb (mol %)*
Pristine Bullet		
Pb-rich rim**	96	4
Slug**	87	13
Pb sphere	100	0
Sb hotspot in Pb-rich rim	12	88
Sb hotspot in slug	60	40
Region 1		
Pb-rich rim**	93	7
Slug**	86	14
Pb sphere	100	0
Sb hotspot in Pb-rich rim	3	97
Sb hotspot in slug	4	96
Alteration crust matrix	100	0
Pb sphere in alteration crust	100	0

*Mol % was calculated from standardized, normalized EDS or WDS analyses

** Data was collected from large areas that include both Pb spheres and Sb-rich hotspots

Table 3.3 Fitting parameters for LCF of Region 1

Linear combination fitting results for Region 1 from the historic shooting range berm using reference spectra. Sum (%) refers to the actual sum of the partial contributions of reference spectra for the overall best fit. X^2 and reduced X^2 are derived from the fit refinement process. Pb(0) = Metallic Pb from a new bullet, PbO = Litharge, C = Cerussite, H = Hydrocerussite, 'Ferri' refers to Pb(II) sorption model compounds with Fe oxides.

Sample name	Pb(0)	PbO	C	H	Ferri*	sum (100%)	χ^2	red. χ^2
Reg 1-1		32 (1)	42 (1)	28 (1)		102	1.4E-02	1.0E-04
Reg 1-2	88 (1)		15 (1)			103	7.4E-03	5.5E-05
Reg 1-3		52 (1)	51 (1)			103	1.4E-02	1.0E-04
Reg 1-4		27 (1)		29 (1)	46 (1)	102	1.2E-02	9.0E-05
Weathering Crust		26 (1)	54 (1)	23 (1)		103	1.2E-02	9.1E-05

*Refers to Pb(II) sorption product with synthesized Fe(III) oxides
(#) Refers to linear combination fitting error

Table 3.4 Fitting parameters for EXAFS analysis

Fitting parameters and EXAFS results for historic shooting range samples. Fitting was done in R-space, k-weights of 1,2 and 3 were fitted simultaneously and the amplitude reduction factor (S_0) was set at 0.97.

Sample	E_0 (eV)	k-range	R-range (Å)	Shell	CN[d]	R (Å)[e]	σ^2 (Å^2)[f]	ΔE_0 (eV)[g]	R-factor[h]	Red χ^2 [i]	Ind. Pts.[j]
[a] Weathering Crust	30,495	3.0 -10.5	1.1 - 4	Sb-O	5.3(1)	1.99(2)	0.002(2)	11(2)	0.007	62.9	14
				Sb-Fe	3(1)	3.15(3)	0.006(8)				
[b] Sb soil	30,492	3.0 - 9.0	1 - 5	Sb-O	2.6(8)	1.96(3)	0.002(4)	10(4)	0.06	30.1	15
[c] Region 1-4	30,492	3.0 - 9.0	1 - 4.5	Sb-O	3.1(2)	1.97(3)	0.005(4)	7(3)	0.03	45.4	13

[a] Weathering crust surrounding approx. 15 bullets from the historic shooting range site, removed and consolidated

[b] Metallic Sb powder sorbed onto local, uncontaminated soil adjacent to the historic shooting range site

[c] Sb hotspot from Region 1-4 historic shooting range sample

[d] Coordination number

[e] Bond length

[f] Debye-Waller factor (mean-square amplitude reduction factor) including thermal and static disorder components

[g] Energy shift between the theoretical and measured spectrum

[h] $R\text{-factor} = \frac{\sum_i (\text{data}_i - \text{fit}_i)^2}{\sum_i \text{data}_i^2}$

[i] $\text{Red}\,\chi^2 = \frac{N_{idp}}{N_{pts}} \sum_i \left(\frac{\text{data}_i - \text{fit}_i}{\varepsilon_i} \right)^2 \Big/ N_{idp} - N_{var}$

[j] Independent points ($N_{pts} - N_{var}$)

Chapter 4 Attenuation of Pb and Sb in Shooting Range Soils by Fe Amendments [1]

4.1 Abstract

Lead (Pb) and antimony (Sb) contamination pose a major environmental concern at firing ranges used by the U.S. Department of Defense (DoD), threatening training land sustainability. Methods for the stabilization of metal contaminants to prevent migration off site are of particular interest. In the present study, two remediation treatments ($FeCl_2$ + $CaCO_3$ and nanoscale zero-valent iron (NZVI)) were applied to column studies constructed from the same materials used to construct field-scale berms in Chapter 2. The columns were constructed using four well-characterized soils (sand, sandy loam, loamy sand and silt loam) to study Pb and Sb behavior. The soil fraction and soil runoff were continuously monitored for three months before amendment addition and 10 months afterward using bulk and micro-scale techniques for both the liquid and solid phase. We found that Sb was more mobile than Pb in all soil systems and primarily present in the dissolved fraction, whereas Pb was associated with both soil organic matter (SOM) and Fe colloids. Dominant Pb solid phase species were determined to be Pb^0, PbO, $PbCO_3$ and Pb sorbed to Fe(III) oxides while Sb was present as fully oxidized Sb(V) in soil and soil solution. The nZVI addition had little effect on Pb and Sb immobilization in comparison to the control soil columns. The $FeCl_2$ and $CaCO_3$ amendment decreased Sb concentrations by >80% for all soil types and >96% reduction in the soil type end members. Lead was more mobilized due to an initial drop in pH, but additional soil treatments have the potential to be effective for system-wide immobilization with adequate additions of $CaCO_3$ buffer.

[1]Barker, A.J., Douglas, T.A., Spaleta, K.J., Trainor, T.P. Attenuation of Pb and Sb in shooting range soils by Fe amendments. Prepared for submission in Geochimica et Cosmochimica Acta.

4.2 Introduction

The remediation of Pb and Sb in shooting range soils has been the subject of recent studies due to the overwhelming amount of ammunition deposited on military training lands (Jardine et al., 2007; Conesa et al., 2010; Griggs et al., 2011; Moon et al., 2013a-c; Dorjee et al., 2014). The production of ammunition accounts for a large portion of the yearly Pb and Sb consumption with the U.S. Department of Defense (DoD) expending more than 2 million pounds of Pb annually (ITRC, 2003). Lead and Sb comprise the bulk of a bullet core. Antimony is added to Pb in bullets as a hardening agent and accounts for anywhere between 0.7 Sb wt.% (Randich et al., 2002) to 1.9 Sb wt.% (Laporte-Saumure et al., 2011) to 2-5 wt.% reported by Johnson, et al., 2005 with Pb reported at 93.1 wt.% of the bullet mass (Laporte-Saumure et al., 2011). A large portion of the ammunition produced end up in outdoor shooting ranges and small arms training areas (Basunia and Landsberger, 2001; Cao et al., 2003; Hardison et al., 2004; Johnson et al., 2005; Rooney et al., 2007; Ackermann et al., 2009; Strømseng et al., 2009; Martin et al., 2013). Concentrations of Pb in shooting range soils containing bullet fragments have been found to range from approximately 50,000 – 500,000 mg/kg with Sb concentrations ranging from approximately 1 – 17,500 mg/kg (Manninen and Tanskanen, 1993; Basunia and Landsberger, 2001; Knechtenhofer et al., 2003; Johnson et al., 2005; Dermatas et al., 2006; Spuller et al., 2007; Robinson et al., 2008; Sanderson et al., 2013). Since Pb and Sb are both toxic and Sb is a suspected carcinogen (US EPA, 1979; IARC, 1989; Rooney et al., 1999; WHO, 2003), there is a risk of contamination to groundwater, surface water, local plants and animals all of which culminate in the need to minimize adverse environmental impacts (US EPA, 1994; Mellor and McCartney, 1994; Rooney et al., 1999; Martin et al., 2013).

Understanding the speciation of both Pb and Sb contamination in the environment is critical for predicting the overall mobility in addition to evaluating the potential for off-site migration. Lead is typically found in the environment in one oxidation state, Pb(II), and the activity of Pb^{2+} in solution has been shown to be limited in shooting range soils by secondary minerals phases (i.e. $PbCO_3$; cerussite, $Pb_3(CO_3)_2(OH)_2$: hydrocerussite, PbO polymorphs; massicot and litharge, and $PbSO_4$;anglesite) that form as an alteration crust around deposited bullets (Chen et al., 2002; Cao et al., 2003; Hardison et al., 2004; Vantelon et al., 2005). These secondary mineral phases are in addition to any amorphous species that may form as a result of Pb^{2+} in solution having a strong affinity to soil organic matter, clays and iron (Fe) or manganese (Mn) oxides (Manceau et al., 1996; Mozafar et al., 2002; Bargar et al., 2004). Antimony primarily exists in the environment with an oxidation state of either +3 and/or +5 and, similar to Pb, has also been shown to have an affinity for natural sorbents present in soil, particularly, Fe, Mn and Al hydr(oxides), clay minerals, organic ligands and humic acids (Thanabalasingam and Pickering, 1999; Johnson et al., 2005; Tighe et al., 2005; Ilgen and Trainor, 2012; Ritchie et al., 2013).

Various environmental conditions will affect the overall speciation of both Pb and Sb in a particular system; therefore remediation techniques must have a specific strategy for targeting any or all of these potential species. In addition, remediation strategies designed for small arms ranges must be able to limit both Pb and Sb mobility, which is complicated due to Sb being an oxyanion and Pb a cation in soil systems. Many strategies have been studied to limit Pb mobility including additions of phosphate to form insoluble lead-phosphate compounds (Jardine et al., 2007), carbonate to buffer the pH and form less soluble lead-carbonate phases (Spuller et al., 2007; Griggs et al., 2011), and red mud, fly ash, oyster/mussel shells, cow bone and biochar to

reduce metal availability (Lee et al., 2009; Moon et al., 2013a-c; Ahmad et al., 2014). Overall, the soil additions limited Pb mobility, biochar was shown to also limit Sb mobility to some extent, but cow bone and mussel shell increased Sb mobility (Ahmad et al., 2014). Antimony may also be displaced from solids via competition with other anionic species such as phosphate or carbonate, thus increasing the mobility (Conesa et al., 2010). Therefore, it is essential to apply the appropriate amendment that immobilizes both Pb and Sb.

While Pb amendment strategies are the focus of numerous studies, a lesser number of have focused on limiting Sb mobility in shooting range soils and the majority have centered around natural attenuation via sorption complexes with Fe present in soil (Scheinost et al., 2006; Mitsunobu et al., 2010) and manual Fe soil additions (Spuller et al., 2007; Okkenhaug et al., 2016). Antimony concentrations in solution have been shown to be reduced with the addition of polyaluminum chloride, ferric chloride and freshly precipitated ferrihydrite (Bagby and West, 1995; Kang et al., 2003; Guo et al., 2009). In addition, iron oxyhydroxides have the ability to form surface complexes with both cationic and anionic species due to variable charged surface groups (Dzombak and Morel, 1990), giving them potential to work as an effective sorbent for both Pb and Sb (Belzile et al., 2001; Leuz et al., 2006; McComb et al., 2007).

In more recent studies, nano-scale zero valent iron (nZVI) has been shown to be effective at removing metals from groundwater and aqueous solutions, including antimony(III/V), lead(II) arsenic(III/V), chromium(III/VI), and uranium(VI) (Ponder et al., 2000; Kanel et al., 2005; 2006; Manning et al., 2007; Dorjee et al., 2014; Sheng et al., 2014). Nanoscale Fe particles are flexible for use as remediation solution because they are cost-effective, have a large surface area (Sun et al., 2006 showed synthesized nZVI particles with an average surface area of 14,500 m^2/kg) and high surface reactivity (Zhang, 2003). Dorjee et al. (2014) found that nZVI has a strong potential

to reduce Sb(V) to Sb(III) and the ability of nZVI to adsorb Sb is minimized in the presence of soil-derived humic acid. Kanel et al. (2005; 2006) showed that 25% of As(V) was reduced to As(III) by nZVI after 90 days and As(III)/As(V) adsorption kinetics were rapid (within minutes) and both species formed inner-sphere surface complexes with nZVI (in separate systems). Manning et al. (2007) saw reduction of Cr(VI) to Cr(III) along with the production of highly insoluble Cr species as a result of nZVI addition. Sun et al. (2006) showed nZVI has dual chemical properties of possessing a core of zero-valent Fe (~44%) acting as a reductant and a shell of mainly iron oxides (FeO, ~56%) acting as a sorbent.

In the present study, we employed two types of Fe amendments to separate, duplicate soil columns containing spent bullet shooting range soil. The amendments were composed of: (1) a slurry solution of nZVI and (2) an $FeCl_2$ solution with $CaCO_3$ to act as a pH buffer. Twelve acrylic soil columns were loaded with four types of characterized Alaskan soil (loamy soil, sandy soil, sandy loam and loamy sand) that were fired into with 5.56 mm bullets in a controlled firing event in central Alaska prior to loading the columns, results outlined in Chapter 2. Once the columns were loaded they were continuously reverse-flushed with an electrolyte solution to simulate 'wet' and 'dry' events typically seen throughout the summer in Alaskan conditions. The runoff was monitored for major and minor elemental species and the four types of soil were studied in triplicate for three months. This was part of a larger, ongoing study, which compares laboratory soil columns in a relatively controlled environment to paralleled field berms at a military shooting range site on Ft. Greely, Alaska in Delta, Junction, AK. Iron soil amendments were added to 8 of the soil columns (nZVI added to the 4 types of soil, $FeCl_2$ added to the 4 types and 4 columns remaining that were unamended used as controls) 4 months into the column study and allowed to react for 10 months with analogous raining and drying events as the

unamended columns. After completion of the runoff study, the soil from all columns was analyzed for bulk metal concentrations and a subset of the soil from each column was analyzed for Pb and Sb speciation using synchrotron x-ray absorption spectroscopy (XAS). The overall goals of this study were to investigate the speciation and mobility of Pb and Sb as a function of saturation time and soil type in recently contaminated soil and determine the overall effectiveness of two Fe amendments on limiting the mobility of both Pb and Sb in all of our respective systems.

4.3 Methods

4.3.1 Experiment Design and Setup

4.3.1.1 Soil

Soil material was contaminated from a controlled firing event in conjunction with a bullet deposition test carried out by Cold Regions Test Center (CRTC) on the Donnelly Training Area (DTA), Ft. Greely, Alaska. Cold Regions Test Center designed a bullet trap that guided fired rounds into plastic buckets (Home Depot) filled with 10 liters of the soil that would be utilized in the columns. Fifty bullets were fired into each type of soil using 0.22 caliber (5.56 mm) rounds. The buckets were frozen and stored in a cold room until the construction of the columns.

The frozen soil was allowed to thaw for 2 hours to ensure uniform consistency and transferred onto a plastic liner sheet (Home Depot) for mixing. The soil was thoroughly mixed by hand using nitrile gloves (VWR International, Radnor, PA) and then shaped into a cone in the center of the sheet. The cone was flattened and divided into four even quarters separate from

each other. Two opposite quarters were removed and mixed together and then the two remaining quarters. This process was repeated 10 times for each of the four types of soil.

4.3.1.2 Columns

Twelve acrylic columns purchased from Soil Measurement Systems, LLC (Tucson, Arizona) were packed with the 4 types of soil (silt loam, loamy sand, sandy loam and sand) in triplicate. The column setup scheme is presented in Table 4.1. Each column was packed with soil in centimeter increments using the bottom of a heavy weighted glass 250 mL beaker until 0.1 m was reached. Columns were saturated upwards (reverse-flow) from the base using 125 mL of electrolyte solution using a peristaltic pump and Tygon tubing (Saint-Gobain Performance Plastics, Courbevoie, France) at a flow rate of 2 mL/min. The electrolyte solution was modified and prepared according to the fluid chemistry in Bormann et al., 1989 and the fluid chemistry monitored for background metal concentrations of Pb and Sb. Reagent grade Na_2SO_4, KCl, $CaCl_2 \cdot 2H_20$, $MgCl_2 \cdot 6H_2O$, and NaCl (J.T. Baker, Center Valley, PA) in respective masses of 0.06, 0.01, 0.01, 0.02, 0.01 g were dissolved in 'DI water' (ultrapure water with a resistivity of 18.1 MΩ (Barnstead Nanopure, Thermo Scientific, Waltham, MA) and diluted for total concentrations of 0.22 and 0.26 mg/L for Na^+ and Cl^-, respectively (1:100 dilution). The pH was adjusted to 7 ± 1 with ultrapure HNO_3 (BDH Aristar Plus, Poole Dorset, UK).

Columns were allowed to sit for 1 hour fully saturated and then drained. That initial drainage sample was 'runoff' sample 1. The columns were repeatedly flushed and drained for the next 100 days for a total of 15 runoff sampling events. Each sampling event had various 'saturation' times and 'drying' durations to simulate raining and drying events. After the collection of runoff sample 15, two types of Fe amendments were introduced after runoff sample

15 to a subset of the columns (5-8 and 9-12) representing the duplicates of the 4 main soil types in columns 1-4. The saturation durations for the remainder of the runoff samples (16-30) were kept constant at 1 hour. Nano-scale zero-valent Fe (nZVI) was added to columns 5-8 and $FeCl_2/CaCO_3$ was added to columns 9-12. Both amendments were introduced to the column systems in reverse-flow in a slurry solution and allowed to fully saturate the soils. For columns 5-8: 1 g of nZVI was added to 125 mL of DI water and introduced. For columns 9-12: 1 g of Fe(II) in the form of $FeCl_2$ was added to 62.5 mL of DI water and introduced then immediately 0.75 g of $CaCO_3$ in 62.5 mL of DI water was introduced after the Fe(II). The columns with additions were allowed to sit and the column sampling restarted when the columns were fully dried after 22 days, giving the amendments sufficient time to saturate the soils and replicating the ideal amendment application in field conditions. The columns were then flushed and drained 1 hour later and that runoff sample was sample 16. The columns were saturated and drained repeatedly until the total runoff sample reached 30. In total, the columns reacted for 412 days with 30 runoff samples.

4.3.2 Sample Analysis

4.3.2.1 Solid Phase Characterization

Soil samples were collected of the 4 types of soil prior to the bullet deposition and upon completion of the experiment; the soils were allowed to dry for 24 hours, removed from the columns and spread onto separate plastic liners. Complete description of the identification of crystalline phases, total metal concentrations and Pb and Sb distribution in the column soil can be found in section 2.3.3.2.

4.3.2.2 Column Effluent

All runoff samples were collected from each column using acid-washed (rinsed with 25 mL of 2% HNO_3) HDPE trace-metal grade wide-mouth bottles. From that bottle, aliquots were dispersed for analysis. The procedure for determine element concentration in the runoff is outlined in section 1.3.3 and the pH and Sb speciation of each runoff sample was analyzed according to the procedure in section 2.3.3.1.

Raw runoff samples were collected in 15 mL amber centrifuge tubes (VWR International, Radnor, PA) and analyzed for size fraction analysis using a Postnova AF2000-FFF (Postnova Analytics, Landsberg, Germany) coupled to a UV-VIS diode array detector (UV-DAD; Shimadzu SPD-M20A). The setup was made metal free by using plastic PEEK fittings. The channel was equipped with a 500 μm spacer and a 300 Da nominal cut-off polyethersulfone (PES) membrane and the absorption wavelengths on the UV-DAD detector were set independently to 254 and 284 nm. The carrier solution was an 8 mM NaCl (J.T. Baker, Center Valley, PA) solution prepared with DI water and filtered to 0.45 μm using vacuum filtration. Sample aliquots of 0.5 mL were introduced into the sample loop using a glass syringe (Postnova Analytics) at 0.3 mL/min and injection time was typically 9 minutes. The method utilized a power decay flow consisting of 4 mL/min for 10 minutes then decayed to 0.1 mL/min within 25 minutes and stayed constant for 25 minutes. Detector flow was set at 0.3 mL/min. Bovine serum albumin (BSA) was used to calibrate the channel thickness. To investigate colloid-element associations, the FFF was also coupled in-line to an ICP-MS (instrument described previously in section 1.3.3). The outflow from the UV-DAD detector was introduced to the ICP-MS along with a 50 ppb Indium standard (2% HNO_3) and a blank (DI water) was analyzed after every sample. Elements measured include Pb, Sb, Fe, Ni, Cu for the sandy loam and Pb, Sb, Fe, Ca, K,

Na, Mg, Mn and Zn. Raw counts were divided by the internal standard and normalized to 1 for each sample.

4.4 Results

4.4.1 Pristine Soil Characterization

Pristine samples of the four soil types (silt loam, sand, loamy sand and sandy loam) before the controlled firing event were analyzed for soil texture, bulk elements, background concentrations and mineral phases. Tabulated results can be found in section 2.4.1.

4.4.2 Total Elements in Runoff

Analysis of the column runoff highlights unique solution behavior for both Pb and Sb in relation to soil type. Antimony concentrations were the highest in the sand column effluent (sand 'a'), and lowest in the silt loam and loamy sand draining columns (silt loam 'b' and loamy sand 'a, b, c'). Results are shown in Figure 4.1 and depicted using box plot diagrams for each triplicate column as a function of soil type. Statistically significant differences between columns are indicated using lettered levels. In general, the results from the soil column analysis showed similar behavior between triplicates columns (levels connected by the same letter are not significantly different at $p < 0.05$), except for the sand column 'a', which contained the highest concentrations, overall. The solution behavior of Pb in relation to soil type is different than the behavior observed for Sb. Lead concentrations were highest in the effluent draining from silt loam column 'a' and lowest in the effluent draining from sand column 'b' (Figure 4.2). Despite differences between silt loam 'a' and sand 'b' end members, distributions of Pb for the mixed

soil effluent and the other end member columns were not statistically different at $p < 0.05$ (Figure 4.2). Lead distributions of the column effluent showed no difference between the triplicate analyses within the same soil type. The column runoff analysis highlighted major differences between Pb and Sb mobility. Antimony concentrations are higher than Pb in the column runoff. Particularly for sand and the sand mixed soils, the concentration of Sb is an order of magnitude higher than Pb in some samples, demonstrating the tendency of Sb to become mobilized in shooting range systems more so than Pb, despite Pb comprising ~90% of the bullet mass. The higher content sand soil promotes the retention of Pb, whereas the higher content silt loam and loamy sand soil promotes the retention of Sb.

The addition of the two Fe amendments to the soil columns caused varying responses to Pb and Sb retention versus mobilization. Antimony was immobilized in systems implementing the $FeCl_2/CaCO_3$ amendment (Figure 4.3). Concentrations of Sb for the soil types in the sample prior to the Fe addition were approximately 200 µg/L for the silt loam draining systems and 1000 µg/L for the sand draining system and both systems saw an instantaneous decrease in concentrations (Figure 4.3). Figure 4.3 shows Sb concentrations as a function of sample for the end member soil types only (mixed soils exhibited similar behavior as their respective end members). The addition of the nZVI had moderate effect on immobilizing Sb, particularly in the silt loam runoff, but had little effect in the sand soil runoff (Figure 4.3). The general decrease in Sb concentrations in the unamended systems could be attributable to the lower saturation times for this phase of the experiment, where the saturation was kept constant at 1 hour per sampling event, which in the previous 15 samples, saturation time varied. It could also be due to natural fluctuations in the soil solution as a result of the dissolution of small bullet fragments.

Concentrations of Pb were initially mobilized upon the addition of $FeCl_2/CaCO_3$ amendment. The rise in concentration is consistent with an observed drop in pH caused by not adding adequate amounts of $CaCO_3$ in excess to buffer the pH drop caused by the hydrolysis of Fe(II) when added to water. Once the pH began to rise and stabilize, concentrations of Pb were reduced for the remainder of the sampling with the exception of Pb in the loam systems after sample 20 (Figure 4.4). The addition of the nZVI amendment also mobilized Pb initially in the silt loam draining columns, but not the sand columns. However, Pb concentrations in the sand columns remained similar to the Pb concentrations in the control columns (Figure 4.4). Overall, the Pb concentrations were lowest in the control columns, except for the silt loam draining soils with the nZVI addition after sample 21.

4.4.3 Colloidal Fraction in Column Runoff

Size fraction analysis was performed on a mixed column runoff sample in order to minimally investigate the presence of colloids as any elemental association with colloids would indicate colloid-facilitated mobility. The FFF fractogram of UV signal of the mixed soil runoff is shown in Figure 4.5a with the corresponding element counts that are all normalized to 1 shown in Figure 4.5c. The void peak (0-100 seconds) is indicative of all particles passing through the 300 Da membrane and is co-eluted with Cu, Fe and Sb. In addition to the void peak, there are increases in UV detector signal approximately 200, 600 and 1200 seconds in the UV spectra (Figure 4.5a). The shoulder peak at 200 seconds (visually expanded in Figure 4.5f) correlates with peaks of Ni and Pb counts and is mostly likely indicative of SOM particles that are absorbent of UV light, particularly 254 nm wavelength (humic/fulvic acids). The increase in UV detector signal at this range of an elution time is often attributed to organic particles that absorb UV light present in the sample (Regelink et al., 2013). Further methods need to be carried out to

characterize the exact colloidal species in relation to standards and in order to differentiate between humic and fulvic acids based on molecular weight size standards. The peak at 600 seconds is correlated with primarily Fe and Pb and is indicative of an inorganic Fe colloid. The counts of Fe versus Pb are shown in 5e, which indicates that Fe concentrations are greater than Pb when the signal is not normalized. The peak from 1200-3000 seconds is broad and poorly separated indicative of a wide range of colloidal sizes and there is likely conglomeration of particles. This broad peak when coupled to the ICP-MS shows increases in Ni, Cu and Fe concentrations. Antimony and Pb do not seem to be co-eluted with this peak. The sandy loam column runoff contained 4 characteristic peaks: (1) void peak co-eluting with Sb, Fe and Cu (2) SOM particles co-eluting with Pb and Ni (3) colloids correlated with Pb signal and (4) colloids correlated with Ni, Cu and Fe signal. The SOM particle separation is difficult to detect on the FFF fractogram, but clear increases with Pb and Ni counts were detected in the ICP-MS normalized signal.

Size fraction analysis was also performed on a silt loam draining runoff sample from the Fe(II) amended column (Column 9). One of the major differences upon the addition of Fe(II) amendment was the increase in the void peak, indicating higher amount of dissolved species. There is evidence of Pb, Zn, Sb, Mg, K, Fe, Ca and Al in the dissolved fraction. The FFF fractogram of UV signal of the loam soil upon the addition of Fe(II) amendment is shown in Figure 4.5b with the corresponding element counts that are all normalized to 1 shown in Figure 4.5d. A greater number of elements were analyzed after the addition of Fe, but there is evidence that Pb, Zn, Sb, Mn, Mg, K, Fe, Ca and to a lesser extent Al are all transported by SOM particles. Small increases in element count (normalized) can be seen in Figure 4.5d in relation to the increase in UV detector signal seen in Figure 4.5b. Further methods need to be carried out to

characterize the exact colloidal species in relation to standards and in order to differentiate between humic and fulvic acids based on molecular weight size standards. There is also an increase in Pb counts at approximately 800 seconds, similar to what was detected for the sandy loam soil (Figure 4.5c), corresponding with an increase in UV signal that was difficult to distinguish due to the large void peak, but is depicted in Figure 4.5g. The increase in Pb concentrations in relation to the location of the peak in the UV detector signal is most likely Fe colloids similar to the particle separation in the sandy loam soil runoff. Counts of Fe when not normalized are shown in Figure 4.5h and are indicative of a small increase in Fe around the same time as Pb. The addition of the Fe(II) amendment changed the particle size distribution of the system by increasing the dissolved species in the soil runoff.

4.4.4 Speciation

4.4.4.1 Pb Speciation

The predominant Pb species present in the column soil fraction were most similar to Pb, PbO, $PbCO_3$ and Pb sorbed to the surface of Fe(III) oxides. The speciation of Pb was investigated using micro-focused Pb-L_{III} XANES on polished thin sections collected from the columns after the flushing experiment. Linear combination fitting for Pb XANES spectra determination was carried out using a set of standards and model compounds, shown in Figure 4.6 with corresponding fit parameters shown in Table 4.2. Overall, approximately 30 samples were analyzed and the samples with the best fits are presented (Figure 4.6) with consideration to represent the species distribution accurately among all samples analyzed. We were able to describe the sample XANES using various contributions of metallic Pb from the bullet alloy,

lead oxide (litharge), lead carbonate (cerussite) and laboratory-prepared Pb(II) sorbed to synthetic Fe(III) oxides.

While XANES does not yield direct information about the local structure and nearest neighbors of the absorbing Pb, the XRF maps displaying elemental associations show a widespread correlation between Pb and Fe (XRF maps shown in Appendix A-2). With respect to soil type, there was little distinction between the two end members, sand and loam, except for the greater presence of $PbCO_3$ in sand (Table 4.2). The sand soil contained the highest concentrations of $PbCO_3$ in comparison to the loam. One sample draining the silt loam soil contained detectable cerussite, but the amount used towards the LC fits is 10%. While XANES linear combination fitting has been shown to be approximately ±10% error (Foster et al., 1998), the inclusion of cerussite is still worth mentioning as the component contribution borders on 10% and likely plays a role in the weathering of bullets. Hydrocerussite did not significantly contribute to the overall best fits. With respect to Fe amendments, we saw little distinction in the near edge absorption spectra for Pb in the unamended, nZVI and $FeCl_2/CaCO_3$ columns, indicating Pb and Fe associations are present within all soil types, regardless of amendment.

4.4.4.2 Sb Speciation

The speciation of mobile Sb species was investigated for runoff sample 1 and 2, results shown in Appendix B, Figure 4.13. Standards of 100 µg/L Sb(III) and Sb(V) are shown in dotted lines with the samples shown in solid lines. Analysis of the sand and sandy loam runoff samples were fully oxidized from Sb(0) to Sb(V) within 1 hour and Sb(III) was never detected. Antimony oxidation is slower in the loam-containing columns, but still on the order of hours. There is detectable Sb(III) in the loam and loamy sand runoff of one of the triplicate set of columns and is

slightly above the detection limit of the analytical method for the LC-ICP-MS. Concentrations are estimated between 1-5 μg/L, in comparison to ~500 μg/L Sb(V) in the corresponding sample. The rapid oxidation of Sb is expected to be fast as observed in Ilgen et al., 2014 for similar samples.

Antimony L_{III}-edge absorption energies for the column samples were consistent with Sb(V) coordination. Sample energies ranged from 4139.3 eV to 4143.0 eV, while absorption energies for Sb(V) standards analyzed ranged from 4140.9 to 4143.6 eV. X-ray fluorescence maps, absorption edge energies and XANES spectra for the standards and samples are shown in Appendix B, Figure 4.14 through Figure 4.15 and Appendix B, Table 4.4. Metallic Sb edge energy is 4132.0 eV and Sb(III) standards range from 4133.1 to 4133.4 eV. The detection of Sb(V) in the column soil fraction is consistent with liquid speciation data. Sample spectra was not fit using LCF due to the majority of the spectra obtained was generally noisy due to the low overall concentrations and diffuse distribution of Sb in the samples.

Antimony distribution in the XRF maps show correlations may exist with other elements in the soil, particularly Fe, but Sb L_{III}-edge signal is weak making precise characterization difficult in our systems. The Sb, Ca and Fe distributions for a silt loam column sample are shown in Figure 4.7a along with a micro XRF map of the smaller area (b). Antimony is distributed in small accumulation spots diffuse throughout the soil fraction. Calcium fluorescence is shown because studying Sb L_{III}-edge in soil samples can be difficult due to abundance of Ca typically found in natural soil samples. The Sb L_{III}-edge is at 4132 eV, whereas the Ca K-edge is at 4038.5 eV. This difference in less than 100 eV leads to some overlap in the fluorescence channel data. Filtering and masking techniques within the program MicroToolKit (Webb, 2005) were implemented in an effort to separate Sb and Ca fluorescence overlap culminating in the color

differentiation between Sb, Ca and Fe in the tri-color plots (Figure 4.7), but the overlap is significant and elemental associations could not be successfully characterized.

4.5 Discussion

4.5.1 Trends Between Saturation Time and pH with Pb and Sb Mobilization

Concentrations of Pb increased with increasing saturation time for the majority of the soil types, except for the 100% sand systems where Pb concentrations decreased at approximately 120 hours. Lead concentrations as a function of saturation time are shown in Figure 4.8. Lead concentrations are grouped by soil type and in order of increasing % of sand content. For the remainder of the soil types (silt loam, loamy sand and sandy loam), Pb concentrations continue to increase as a function of increasing saturation time, indicating Pb in soil solution is likely not saturated even after 120 hours. The decreasing concentration of Pb in the sand soil after 120 hours of saturation time is likely a result of saturation of Pb in solution and subsequent precipitation and/or sorption processes occurring between 80 and 120 hours of saturation. Cerussite and Pb sorbed were the most common species found in the sand soil column samples. In addition, the sand soil has a larger fraction of carbonates than any of the other soils (0.75% for sand versus 0.00% determined by Midwest Laboratories, Inc. Omaha NE), possibly explaining why Pb saturation only occurs in the sand soils after 120 hours. Elzahabi and Yong (2001) showed that the presence of carbonates in the soil increased the retention of heavy metals and also enhanced the buffering capacity of the soil. This could explain the decrease in Pb concentrations in primarily the sand soil after 120 hours saturation time. There are initial increases and decreases in Pb concentrations before the 80 hour mark in all soil types, which are

likely not explained by carbonate availability. Contaminated soils have been shown to have high solubility initially, due to the small fragments and small particle sizes derived from deposition (Rieuwerts et al., 1998). This could explain the initial increase of Pb dissolution in the column runoff samples regardless of saturation time. However, it is likely that once the soils release the initial outflux of Pb to solution, concentrations will decrease as precipitation and sorption reactions occur. For the four soil types, these reactions take place faster in the sand soil than the silt loam-containing soils and Pb becomes saturated quicker.

Antimony enters solution and becomes saturated in soil solution to a greater extent than Pb (Figure 4.9). For the most part, Sb concentrations increase with increasing saturation time and decrease after approximately 120 hours. In two out of the three triplicate measurements of the sand soil (Figure 4.9a, b), Sb concentrations did not decrease substantially after 120 hours saturation time in comparison to the remaining sand system. It appears that Sb concentrations decrease at 80 hours saturation time and then Sb is released into solution to a greater extent between 80 and approximately 120 hours saturation time. It is likely that Sb is released in pulses to the soil solution considering the Pb alloyed core is comprised of pockets of Sb instead of being uniformly dispersed (see Chapter 3, Section 3.5.1). For the remainder of the triplicate soil column runoff measurements, Sb concentrations decline after 120 hours saturation time. The decrease in Sb concentration as a function of saturation time suggests Sb is saturation in soil solution, however little Sb in the solid phase was detected by XANES analysis, potentially signifying that Sb accumulation in the soil fraction requires time. In a waterlogging pot experiment, Wan et al. (2013) observed decreases in Sb concentration in soil solution as a function of saturation time due to reduction of Sb(V) to Sb(III). However, the timeframe of this experiment was on the order of months of waterlogging in comparison to a maximum of 120

hours in this study. The first measurement in Wan et al. (2013) after the initial baseline measurement was 6 days, where total Sb decreased in the systems containing plants, indicative of Sb(III) uptake primarily by the roots. In the system containing no plants, the total Sb concentrations only decreased by 5 µg/L and are well within error bars. While this study measured only the first 2 column runoff samples (until the complete oxidation of Sb(III) to Sb(V) was measured), it is unlikely that the formation of Sb(III) occurred in the column systems as a result of saturation considering Sb(III) was first observed in Wan et al. (2013) after 5 weeks of soil waterlogged conditions. Comparing Sb behavior as a function of soil type, concentrations increase initially in the order sand > sandy loam > loamy sand > silt loam, indicating Sb enters into soil solution faster and to a greater extent depending on the % of sand in the soil. For the sandy loam soil, there are two major spikes in Sb concentration that occur at low saturation times (Figure 4.9b and c). This is most likely due to the initial high solubility of species in contaminated soil due to the small fragments and small particle sizes derived from deposition (Rieuwerts et al., 1998).

Upon the addition of the Fe(II) amendment, the solution pH dropped to 3.15 (silt loam) to 4.25 (sand). Lead and Sb concentrations behaved dissimilar when comparing the concentration as a function of pH in the Fe(II) amended columns. The log of the Pb and Sb concentrations are plotted as a function of pH of the column runoff in Figure 4.10. In general, Pb concentrations were negatively associated with pH, whereas Sb was positively associated. The decrease in pH caused by the hydrolysis of Fe in solution and lack of adequate carbonate buffer led to an increase in Pb concentration, which was not observed for Sb. This is supported by other studies that observed Sb mobility increasing with increasing pH (except for very acidic environments; pH <2 and environments with high phosphate fraction) (Johnson et al., 2005; Okkenhaug et al.,

2016) and Pb mobility increasing with decreasing pH, similar to other metal cations in solution (Elzahabi and Yong, 2001; Cao et al., 2003; Rooney et al., 2007). For circumneutral pH ranges (6.5-8), the Pb concentrations are relatively stable and begin to increase below pH 6.5, indicative of Pb mobility at this pH regime. The availability of surface sites for sorption reactions from the addition of Fe(II) to the columns immobilized Sb regardless of a decrease in pH. For the most part the Sb concentrations are below detection limit (<0.1 µg/L), but in the silt loam soil corresponding to pH of 3.15, Sb concentrations peak at approximately 1 µg/L. This potentially indicates low pH may play a role in the mobilization of Sb, but this data point also corresponds to the sample immediately following the addition of the Fe(II) amendments, therefore it is also likely that the small peak in the log concentration is a result of the Fe addition requiring more than an hour time to be effective.

4.5.2 Dissolution of Sb Versus Colloidal Transport of Pb

The mobility of Pb in the mixed (sandy loam) column runoff is facilitated by colloidal transport, primarily SOM particles that absorb UV wavelengths at 254 nm and inorganic Fe colloids present in the soil solution. This is consistent with other studies that found Pb associated with colloidal sized particles (Denaix et al., 2001; Cao et al., 2003; Yin et al., 2010; Plathe et al., 2013; Ogawa et al., 2014). In these studies, Pb was found to be associated with biocolloids (Denaix et al., 2001), Ti oxides (Plathe et al., 2013), humic acids (Tang and Weisbrod, 2009), Fe/Mn oxides (Ogawa et al., 2014) and present in the dissolved form (Yin et al., 2010). A portion of the studies only determined if Pb was associated with 'colloid' sized particles in general and did not investigate the composition of the particles directly (Cao et al., 2003; Yin et al., 2010). This study found minimal Pb present in the dissolved fraction, which is consistent with one study that found 'Pb is only mobile when associated with colloids' (Tang and Weisbrod, 2009).

Instead, there were associations of Pb primarily with Fe colloids and SOM particles, to a lesser extent. Further methods need to be carried out to characterize the exact colloidal species in relation to standards and in order to differentiate between humic and fulvic acids based on molecular weight size standards.

Antimony in the column runoff (without Fe amendments added) is present primarily in the dissolved fraction (<300 Da), which is consistent with other studies that found Sb preferentially dissolved (Klitzke et al., 2012) and was more mobile than Pb (Ogawa et al., 2014). The study done by Ogawa et al. (2014) observed that Sb was transported further than Pb in shooting ranges and is 'transported easily through water migration' as an oxyanion, whereas Pb is transported by colloids. An overall depiction of the primary Pb and Sb soil solution fractions are shown in Figure 4.11. The sandy loam column runoff contains 4 characteristic soil solution fractions: (1) void peak co-eluting with Sb, Fe and Cu (2) SOM particles co-eluting with Pb and Ni (3) colloids correlated with Pb signal and (4) colloids correlated with Ni, Cu and Fe signal (Figure 4.5). Further methods need to be carried out to characterize the exact colloidal species in relation to standards and in order to differentiate between humic and fulvic acids based on molecular weight size standards.

While this study did not measure Al, Si or major ions (Ca, K, Mg, Na) in the total element counts for the sandy loam runoff sample, there could be contributions from these elements in the larger colloidal sized fraction indicative of clay mineral colloids. Regelink et al. (2013) found small contributions of Fe to colloidal size fractions can indicate Fe that is structurally incorporated into clay minerals and the study also suggested that an increase in the number of particle sizes (broad peaks and conglomeration) was indicative of clay mineral nanoparticles in soil solution, which is consistent with the shape of the peak for the largest size

fraction in Figure 4.5. This size fraction was associated with Fe, in addition to Ni and Cu. Both the colloidal facilitated transport of Pb and primarily dissolved fraction of Sb present in the mixed soil solution have implications on shooting range remediation overall. This study minimally investigated the separation of the colloidal fractions after the Fe amendments were added and the addition affected the overall fractionation of the colloidal particles present in that there was a greater dissolved fraction. We also found Sb correlations to SOM in the silt loam after the Fe addition, but not in the sandy loam before the Fe addition. While Sb is present primarily in the dissolved fraction, there could be some association to SOM that were not fully characterized in this study.

4.5.3 Unique Distributions of Pb Corrosion Products

The observation of unique Pb distributions across the soil types within the column samples significantly furthers the understanding of Pb speciation in relation to bullet weathering. Representative depictions of each type of distribution are shown in Figure 4.12. The XRF maps are plots of the relative fluorescence Pb signals with brightness correlating with signal intensity (high counts). The first characteristic Pb distribution can be characterized by small (~1-5 μm), discrete, intense Pb hotspots present scattered throughout the soil fraction. Each Pb hotspot typically contains various contributions from secondary weathering phases of PbO and/or cerussite. This study hypothesizes the small particle size and solitary distribution of the unique Pb^0 hotspots causes it to weather rapidly, initially oxidizing to PbO and $PbCO_3$. These metallic Pb deposits likely weather relatively quickly upon fragmentation, due to the small size (increased surfaces) and isolated nature of the metallic Pb deposits. We detected no hydrocerrusite in any of the column systems.

Surrounding the Pb hotspots (Figure 4.12a) is a more diffuse distribution of Pb, further outlined in Figure 4.12b. This distribution was common throughout all samples and is characteristic of a Pb sorption corrosion product, typically best fit with Pb sorbed to Fe(III) oxides. The majority of these diffuse Pb distributions contain no Pb^0 and are entirely comprised of oxidize Pb species (PbO, cerussite and Pb sorbed to Fe fraction) in varying percentages. This Pb distribution represents the traveling Pb species that was mobilized at one point, transported away from the parent source and subsequently precipitated as PbO and/or cerussite or adsorbed to the surface of Fe particles present in the soil fraction (or Fe amendment). This type of unique Pb distribution likely has major implications for long-term systems as the more Pb that is leached from parent bullet material; the greater the potential transport distance will be for Pb to be immobilized by surface sorption reactions.

The unique distribution outlined in Figure 4.12c was observed in the majority of samples containing fragments of Fe bullet core. The thin line of Pb on the surface of the Fe bullet core is likely there as a product of the fragmentation process and has since created a 'weathering crust' on the surface. This distribution has weathered since exposure and often contains secondary mineral phase, PbO and cerussite, as well as Pb sorption products distal to the crust. For the most part, these Pb distributions are likely a remnant of the fragmentation process and were observed in a variety of samples. When a select bullet impacts soil the Fe core can break away from the Pb-alloyed slug at the weak interface resulting from the casting process. As a result, some of the Pb^0 remains intact and adjacent to the Fe core. We hypothesize the sudden exposure of this Pb^0 creates a weathering front where there is a clear separation between zero-valent Pb and Pb(II). The best fit for the Pb species adjacent to the Pb^0 is comprised of PbO, cerussite and Pb sorbed to Fe.

The fourth type of Pb distribution distinguishable from visual and spectral comparison of the columns is Pb encrusted on the surface of mineral grains present in the soil fraction (Figure 4.12d). This LCF for this type of Pb distribution predominantly features of sorbed Pb and in particular, Pb sorbed to the fine fraction of the silt-loam soil type. The model compound 'Pb sorbed to fine fraction' was used in addition to Pb sorbed to Fe(III)oxides in order to embody an umbrella 'Pb sorption' term, which may include Pb sorbed to Fe, clay particles, humics, organics and/or other surfaces present in soil. While the LCF for this type of Pb distribution are quality fits to the collected data, the summations are the lowest and highest out of all of the spectra collected (ranging from 88.6-104.3%), indicating there is potentially a missing contribution from the fitted spectra. The encrustation and immobilization of Pb via mineral grains or surface coatings on mineral grains acting as a sink has been observed previously (Freedman et al., 1994; Coston et al., 1995; Fuller et al., 1996) and has potentially important implications for future shooting range remediation scenarios.

4.5.4 Efficiency of Fe Amendments

Overall, each Fe amendment affected the soil and solution chemistry in different ways by either creating environments with greater ability to retain metals or promoting mobilization. To quantify the effects of the additions, percent reductions of Pb and Sb in the soil columns are tabulated in Table 4.3. Reductions were calculated based on the value of Pb and Sb in runoff sample 15 in comparison to runoff sample 30 after the addition. Concentrations of Sb and Pb (for the loam and sandy loam columns) were reduced in the control berms, likely a result of the quick 1 hour flushes the saturation profile in comparison to previous saturation times in the experiment. Concentrations of Pb in the loamy sand increased, which could solely be due to

natural fluctuations in Pb concentrations as a function of time as the Pb values in the end of the sampling period are well within the natural fluctuations observed in samples 1-15.

The nZVI addition proved to be minimally successful overall at immobilizing both Pb and Sb within all soil types. We hypothesize that the expected decrease in solution potential (Frohne et al., 2011) along with the slow overall oxidation kinetics of Fe^0_{nano} – Fe(II) – Fe(III) hindered the overall effectiveness of this amendment. Sun et al., 2006 observed only ~56% formation of FeO from nZVI after 3 weeks and solution. In addition, the presence of soil organic matter (humic acid particles) could hinder the ability for nZVI to be an effective sorbent for Sb as found by Dorjee et al. (2014). For these reasons, we hypothesize that the nZVI amendment may have greater potential over longer periods of reaction time.

The $FeCl_2$ and $CaCO_3$ amendment was remarkable at immobilizing Sb, particularly upon fresh addition. Overall, there was >80% reduction of Sb in the runoff for all soil types and a >96% reduction in the soil type end members. After ~40 days of reaction time, Sb concentrations began to steadily increase above detectable levels (for 3 out of the 4 soil types), suggesting that multiple additions may be necessary for continued Sb immobilization. Multiple additions may prove problematic for Pb immobilization, however, due to the potential pH drop that can occur without an efficient buffering partner. Pb concentrations dramatically decreased after the first initial pH-induced mass mobilization and we expect would continue to decrease. Additional soil treatments have potential to be effective for system-wide immobilization of Pb and Sb with adequate addition of $CaCO_3$ buffer so the pH remains stable, overall.

4.6 Conclusion

The goals of this study were to investigate the speciation and mobility of Pb and Sb as a function of time and soil properties in shooting range soils and determine the overall effectiveness of two Fe amendments on limiting the mobility of both Pb and Sb in all of our respective systems. Soil type (silt loam and sand end members) played a role in the mobilization versus retention of Pb and Sb, naturally. Antimony was more mobile than Pb in all soil systems and primarily present in the dissolved fraction, whereas Pb was associated with both SOM and Fe colloids. Antimony was found to be more mobile in sand than silt loam, whereas Pb was found to be more mobile in the silt loam soil than sand, highlighting potentially differing solution behavior. Lead and Sb were both found to be positively correlated to saturation time, highlighting the potential of element mobilization as a result of water-logging soils. However, Sb entered solution and became saturated in soil solution to a greater extent than Pb, whereas Pb concentrations, for the most part, continued to increase as a function of saturation time. Antimony was found to be positively associated with pH, whereas Pb was found to be negatively associated with pH, which contributed to the mobilization of Pb as a result of the Fe(II) amendment addition. Overall, the results from the column runoff samples provided an informative sample set for understanding the overall mobility of Pb and Sb with respect to soil type and soil conditions.

Lead in the bullet crust and soil fraction was found to be comprised of primarily cerussite, litharge and Pb sorbed to Fe(III) oxides in this study. Unique distributions of these species were represented as discrete Pb^0 hotspots with crusts of PbO and $PbCO_3$, diffuse Pb dispersed throughout the soil primarily comprised of Pb sorbed fraction, oxidized Pb present as a rim along the surface of the Fe bullet core and Pb sorbed to the surface of mineral grains. These

species are sinks for Pb and also acted as a control on the overall mobility of Pb in solution. The speciation of Sb was found to be fully oxidized Sb(V) present in the soil and soil solution. While there may have been Sb associations with Fe, this study did not detect any strong correlations as observed with Pb.

Overall, the Fe amendments proved to be moderately successful treatments for the immobilization of Pb and Sb from shooting range soil solution. The nZVI addition was moderately successful at immobilizing both Pb and Sb within all soil types, but was more capable of decreasing runoff concentrations of Sb than Pb. The $FeCl_2$ and $CaCO_3$ amendment was remarkable at immobilizing Sb, particularly upon fresh addition. Overall, there was >80% reduction of Sb in the runoff for all soil types and a >96% reduction in the soil type end members. Although Pb was initially mobilized upon the addition due to a initial drop in pH, additional soil treatments have the potential to be effective for system-wide immobilization of Pb and Sb with adequate addition of $CaCO_3$ buffer so the pH remains stable.

4.7 Acknowledgments

Funding for this project was from the Department of Defense, Strategic Environmental Research and Development Program (ER-1770). Cold Regions Test Center built the bullet trap, provided 600 5.56 mm bullets and provided access to the Donnelly Training Area, Ft. Greely, Alaska where the firing event occurred. The Stanford Synchrotron Radiation Lightsource of Stanford Linear Accelerator Center in Menlo Park, California provided assistance with collection of x-ray absorption and fluorescence data. The project received continual support from Dr. Sam Webb, Dr. Benjamin Kocar, Dr. Courtney Roach and Cynthia Patty of SSRL throughout the

beamtime allocations. Numerous students and collaborators are acknowledged on this project for field and laboratory assistance. Dr. Maciej Śliwiński, Karen Spaleta and Dr. Ken Severin from the Advanced Instrumentation Laboratory at the University of Alaska Fairbanks assisted in analyzing samples. Graduate students, Tiffany Gatesman and Erik Talvi, assisted with data collection at SSRL. Dr. James Ranville (Colorado School of Mines) and Dr. Soheyl Tadjiki (PostNova Analytics) assisted in FFF setup and training and Megan Roberts and Karen Spaleta assisted with method development for FFF analysis.

4.8 References

Ackermann S., Gieré R., Newville M. and Majzlan J. (2009) Antimony sinks in the weathering crust of bullets from Swiss shooting ranges. *Sci. Total Environ.* **407**, 1669-1682.

Ahmad M., Lee S.S., Lim J.E., Lee S.E., Cho J.S., Moon D.H., Hashimoto Y. and Ok Y.S. (2014) Speciation and phytoavailability of lead and antimony in a small arms range soil amended with mussel shell, cow bone and biochar: EXAFS spectroscopy and chemical extractions. *Chemosphere* **95**, 433-441.

Bagby E.L. and West C.M. (1995) Treatment of an anionic metal by adsorption on iron oxides. In *Emerging Technologies in Hazardous Waste Management V,* Tedder, D.W.; Pohland, F.G., Eds.; American Chemical Society: Washington, DC, **607**, 64-73.

Bargar J.R., Trainor T.P., Fitts J.P., Chambers S.A. and Brown G.E. Jr. (2004) In-situ grazing incidence EXAFS study of Pb(II) chemisorption on hematite (0001) and (1-102) surfaces. *Langmuir* **20**, 1667-1673.

Basunia S. and Landsberger, S. (2001) Contents and leachability of heavy metals (Pb, Cu, Sb, Zn, As) in soil at the Pantex firing range, Amarillo, Texas, *Air Waste Manage. Assoc.* **51**, 1428-1435.

Belzile N., Chen Y.W. and Wang Z. (2001) Oxidation of antimony (III) by amorphous iron and manganese oxyhydroxides. *Chemical Geology* **174**, 379-387.

Bormann B.T., Tarrange R.F., McClellan M.H. and Savage T. (1989) Chemistry of Rainwater and Cloud Water at Remote Sites in Alaska and Oregon. *Journal of Environmental Quality* **18**, 2.

Cao X.D., Ma L. Q., Chen M., Hardison D.W. and Harris, W.G. (2003) Weathering of lead bullets and their environmental effects at outdoor shooting ranges. *J. Environ. Qual.* **32**, 526-534.

Chen M., Daroub S.H., Ma L.Q., Harris W.G. and Cao X.D. (2002) Characterization of lead in soils of a rifle/pistol shooting range in central Florida, USA. *Soil Sediment. Contam.* **11**, 1-17.

Conesa H.M., Wieser M., Gasser M., Hockmann K., Evangelou M.W.H., Studer B. and Schulin R. (2010) Effects of three amendments on extractability and fractionation of Pb, Cu, Ni and Sb in two shooting range soils. *Journal of Hazardous Materials* **181**, 845-850.

Coston J.A., Fuller C.C. and Davis J.A. (1995) Pb2+ and Zn2+ adsorption by a natural aluminum- and iron-bearing surface coating on aquifer sand. *Geochimica et Cosmochimica Acta* **59**, 17, 3535-3547.

Denaix L., Semlali R.M. and Douay F. (2001) Dissolved and colloidal transport of Cd, Pb, and Zn in a silt loam soil affected by atmospheric industrial deposition. *Environmental Pollution* **113**, 29-38.

Dermatas D., Cao X., Tsaneva V., Shen G. and Grubb D.G. (2006) Fate and behavior of metal(loid) contaminants in an organic matter-rich shooting range soil: Implications for remediation. *Water, Air, & Soil Pollution: Focus* **6**, 1, 143-155.

Dorjee P., Amarasiriwardena D. and Xing B. (2014) Antimony adsorption by zero-valent iron nanoparticles (nZVI): Ion chromatography-inductively coupled plasma mass spectrometry (IC-ICP-MS) study. *Microchemical Journal* **116**, 15-23.

Dzombak D.A. and Morel F. M. M. (1990) Surface Complexation Modeling, Hydrous Ferric Oxide; John Wiley & Sons: New York.

Elzahabi M. and Yong R.N. (2001) pH Influence on sorption characteristics of heavy metal in the vadose zone. *Engineering Geology* **60**, 61-68.

Foster A.L., Brown G.E., Tingle T.N. and Parks G.A. (1998) Quantitative arsenic speciation in mine tailings using X-ray absorption spectroscopy. *Am. Mineral.* **83**, 5-6, 553-568.

Freedman Y.E., Magaritz M., Long G.L. and Ronen D. (1994) Interaction of metals with mineral surfaces in a natural groundwater environment. *Chemical Geology* **116**, 111-121.

Frohne T., Rinklebe J., Diaz-Bone R.A. and Laing G.D. (2011) Controlled variation of redox conditions in a floodplain soil: Impact on metal mobilization and biomethylation of arsenic and antimony. *Geoderma* **160**, 3-4, 414-424.

Fuller C.C., Davis J.A., Coston J.A. and Dixon E. (1996) Characterization of metal adsorption variability in a sand and gravel aquifer, Cape Cod, Massachusetts, U.S.A. *Journal of Contaminant Hydrology* **22**, 165-187.

Griggs C.S., Martin A.W., Larson S.L., O'Connor G., Fabian G., Zynda G. and Mackie D. (2011) The effect of phosphate application on the mobility of antimony in firing range soils. *Science of the Total Environment* **409**, 12, 2397-2403.

Guo X., Wu Z. and He M. (2009) Removal of antimony(V) and antimony(III) from drinking water by coagulation-flocculation-sedimentation (CFS). *Water Research* **43**, 4327-4335.

Hardison Jr. D.W., Ma L.Q., Luongo T. and Harris W.G. (2004) Lead contamination in shooting range soils from abrasion of lead bullets and subsequent weathering. *Science of the Total Environment* **328**, 175-183.

IARC. (1989) IARC Monograph 47. Lyon: International Agency for Research on Cancer.

Ilgen A. and Trainor T. (2012) Sb(III) and Sb(V) sorption onto Al-rich phases: hydrous Al oxide and the clay minerals kaolinite KGa-1b and oxidized and reduced nontronite NAu-1. *Environ. Sci. Technol.* **46**, 843-851.

Ilgen A.G., Majs F., Barker A.J., Douglas T.A. and Trainor T.P. (2014) Oxidation and mobilization of metallic antimony in aqueous systems with simulated groundwater. *Geochimica et Cosmochimica Acta* **132**, 16-30.

(ITRC) Interstate Technology and Regulatory Council Small Arms Firing Range Team. (2003) Characterization and Remediation of Soils at Closed Small Arms Firing Ranges. *Technical/Regulatory Guidelines*.

Jardine P.M., Parker J.C., Stewart M.A., Barnett M.O. and Fendorf S.E. (2007) Decreasing Toxic Metal Bioavailability with Novel Soil Amendment Strategies. SERDP ER-1350 Final Report.

Johnson C., Moench H., Wersin P., Kugler P. and Wenger, C. (2005) Solubility of antimony and other elements in samples taken from shooting ranges. *J. Environ. Qual.* **34**, 248.

Kanel S.R., Manning B., Charlet L. and Choi, H. (2005) Removal of Arsenic(III) from Groundwater by Nanoscale Zero-Valent Iron. *Environ. Sci. Technol.* **39**, 1291-1298.

Kanel S.R., Greneche J.M. and Choi H. (2006) Arsenic(V) Removal from Groundwater Using Nano Scale Zero-Valent Iron as a Colloidal Reactive Barrier Material. *Environ. Sci. Technol.* **40**, 2045-2050.

Kang M., Kamei T. and Magara Y. (2003) Comparing polyaluminum chloride and ferric chloride for antimony removal. *Water Res.* **37**, 17, 4171-4179.

Klitzke S., Lang F., Kirby J., Lombi E. and Hamon R. (2012) Lead, antimony and arsenic in dissolved and colloidal fractions from an amended shooting-range soil as characterized by multi-stage tangential ultrafiltration and centrifugation. *Environ. Chem*, **9**, 462-473.

Knechtenhofer L., Xifra I., Scheinost A.C., Flühler H. and Kretzschmar R. (2003) Fate of heavy metals in a strongly acidic shooting range-soil: Small-scale metal distribution and its relation to preferential water flow. *J. Plant Nutr. Soil Sci.* **166**, 84-92.

Laporte-Saumure M., Martel R. and Mercier G. (2011) Characterization and metal availability of copper, lead, antimony and zinc contamination at four Canadian small arms firing rangers. *Environmental Technology* **32**, 7, 767-781.

Lee S.H., Lee J.S., Choi Y.J. and Kim J.G. (2009) In situ stabilization of cadmium-, lead-, and zinc-contaminated soil using various amendments. *Chemosphere* **77**, 1069-1075.

Leuz A.K., Hug S.J., Wehrli B. and Johnson C.A. (2006) Iron-Mediated Oxidation of Antimony(III) by Oxygen and Hydrogen Peroxide Compared to Arsenic(III) Oxidation. *Environ. Sci. Technol.* **40**, 8, 2565-2571.

Manceau A., Boisset M.C., Sarret G., Hazemann R.L., Mench M., Cambier P. and Prost R. (1996) Direct determination of lead speciation in contaminated soils by EXAFS spectroscopy. *Environ. Sci. Technol.* **30**, 1540-1552.

Manninen S. and Tanskanen N. (1993) Transfer of lead from shotgun pellets to humus and three plan species in a Finnish shooting range. *Arch. Environ. Contam. Tosicol.* **24**, 410-414.

Manning B.A., Kiser J.R., Kwon H. and Kanel S.R. (2007) Spectroscopic Investigation of Cr(III)- and Cr(VI)-Treated Nanoscale Zerovalent Iron. *Environ. Sci. Technol.* **41**, 586-592.

Martin A.W., Lee L.S. and Schwab P. (2013) Antimony migration trends from a small arms firing range compared to lead, copper, and zinc. *Science of the Total Environment* **463-464**, 222-228.

McComb K.A., Craw D. and McQuillan A.J. (2007) ATR-IR Spectroscopic Study of Antimonate Adsorption to Iron Oxide. *Langmuir* **23**, 24, 12125-12130.

Mellor A. and McCartney C. (1994) The effects of lead shot deposition on soils and crops at a clay pigeon shooting site in northern England. *Soil Use Manage.* **10**, 124-129.

Mitsunobu S., Takahashi Y., Terada Y. and Sakata M. (2010) Antimony (V) Incorporation into Synthetic Ferrihydrite, Goethite, and Natural Iron Oxyhydroxides. *Environ. Sci. Technol.* **44**, 10, 3712-3718.

Moon D.H., Cheong K.H., Khim J., Wazne M., Hyun S., Park J.H., Chang Y.Y. and Ok Y.S. (2013a) Stabilization of Pb2+ and Cu2+ contaminated firing range soil using calcined oyster shells and waste cow bones. *Chemosphere* **91**, 1349-1354.

Moon D.H., Park J.W., Cheong K.H., Hyun S., Koutsospyros A., Park J.H. and Ok Y.S. (2013b) Stabilization of lead and copper contaminated firing range soil using calcined oyster shells and fly ash. *Environ. Cheochem. Health.* **35**, 705-714.

Moon D.H., Park J.W., Chang Y.Y., Ok Y.S., Lee S.S., Ahmad M., Koutsospyros A., Park J.H. and Baek K. (2013c) Immobilization of lead in contaminated firing range soil using biochar. *Environ. Sci. Pollut. Res.* **13**, 1964-1967.

Mozafar A., Ruh R., Klingel P., Gamper H., Egli S. and Frossard E. (2002) Effect of heavy metal contaminated shooting range soils on mycorrhizal colonization of roots and metal uptake by leek. *Environ. Monit. Assess.* **79**, 177-191.

Okkenhaug G. Gebhardt K.A.G., Amstaetter K., Bue H.L., Herzel H., Mariussen E., Almås A.R., Cornelissen G., Breedveld G.D., Rasmussen G. and Mulder J. (2016) Antimony (Sb) and lead (Pb) in contaminated shooting range soils: Sb and Pb mobility and immobilization by iron based sorbents, a field study. *Journal of Hazardous Materials* **307**, 336-343.

Ogawa S., Katoh M., Sato T. (2014) Microscopic range of immobilization between heavy metals and amendment in soil through water migration. *Int. J. of Geomat.* **6**, 2, 870-877.

Plathe K.L., Kammer F.v.d., Hassellöv M., Moore J.N., Mitsuhiro M., Hofmann T. and Hochella M.F. (2013) The role of nanominerals and mineral nanoparticles in the transport of toxic trace metals: Field-flow fractionation and analytical TEM analyses after nanoparticle isolation and density separation. *Geochim. Cosmochim. Acta* **102**, 213-225.

Ponder S.M., Darab J.G. and Mallouk T.E. (2000) Remediation of Cr(VI) and Pb(II) Aqueous Solutions Using Supported, Nanoscale Zero-valent Iron. *Environ. Sci. Technol.* **34**, 2564-2569.

Randich E., Duerfeldt W., McLendon W. and Tobin W. (2002) A metallurgical review of the interpretation of bullet lead compositional analysis. *Forensic Sci. Int.* **127**, 174-191.

Regelink I.C., Weng L., Koopmans G.F., and van Riemsdijk W.H. (2013) Asymmetric flow field-flow fractionation as a new approach to analyse iron-(hydr)oxide nanoparticles in soil extracts. *Geoderma* **202-203**, 134-141.

Rieuwerts J.S., Thornton I., Farago M.E. and Ashmore M.R. (1998) Factors influencing metal bioavailability in soils: preliminary investigations for the development of a critical loads approach for metals. *Chemical Speciation & Bioavailability* **10**, 2, 61-75.

Ritchie V.J., Ilgen A.G., Mueller S.H., Trainor T.P. and Goldfarb R.J. (2013) Mobility and chemical fate of antimony and arsenic in historic mining environments of the Kantishna Hills district, Denali National Park and Preserve, Alaska. *Chemical Geology* **335**, 172-188.

Robinson B.H., Bischofberger S., Stoll A., Schroer D., Furrer G., Roulier S., Gruenwald A., Attinger W. and Schulin R. (2008) Plant uptake of trace elements on a Swiss military shooting range: Uptake pathways and land management implications. *Environmental Pollution* **153**, 668-676.

Rooney C.P, McLaren R.G. and Cresswell R.J. (1999) Distribution and phytoavailability of lead in a soil contaminated with lead shot. *Water, Air and Soil Pollution* **116**, 3, 535-548.

Rooney C.P., McLaren R.G., Condron L.M. (2007) Control of lead solubility in soil contaminated with lead shot: Effect of soil pH. *Environmental Pollution* **149**, 149-157.

Sanderson P., Naidu R. and Bolan N. (2013) Effectiveness of chemical amendments for stabilization of lead and antimony in risk-based land management of soils of shooting ranges. *Environ. Sci. Pollut. Res.* **22**, 8942-8956.

Scheinost A., Rossberg A., Vantelon D., Zifra I., Kretzschmar R., Leuz A., Funke J. and Johnson C. (2006) Quantitative antimony speciation in shooting range soils by EXAFS spectroscopy. *Geochim. Cosmochim. Acta* **70**, 3299-3312.

Sheng G., Shao X., Li Y., Li J., Dong J., Cheng W., Gao X. and Huang Y. (2014) Enhanced Removal of Uranium (VI) by Nanoscale Zerovalent Iron Supported on Na-Bentonite and an Investigation of Mechanism. *J. Phys. Chem. A.* **118**, 2952-2958.

Spuller C., Weigand H. and Marb C. (2007) Trace metal stabilisation in a shooting range soil: Mobility and phytotoxicity. *Journal of Hazardous Materials Stabilisation/Solidification Treatment and Remediation: Advances in S/S for Waste and Contaminated Land.* **141**, 378-387.

Strømseng A.E., Ljones M., Bakka L. and Mariussen E. (2009) Episodic discharge of lead copper and antimony from a Norwegian small arm shooting range. *J. Environ. Monit.* **11**, 6, 1259-1267.

Sun Y.P., Li X.Q., Cao J., Zhang W.X. and Wang H.P. (2006) Characterization of zero-valent iron nanoparticles. *Advances in Colloid and Interface Science* **120**, 47-56.

Tang X.Y. and Weisbrod N. (2009) Colloid-facilitated transport of lead in natural discrete fractures. *Environmental Pollution* **157**, 2266-2274.

Thanabalasingam P. and Pickering W. (1999) Specific sorption of antimony (III) by the hydrous oxides of Mn, Fe, and Al. *Water Air Soil Pollut.* **49**, 175-185.

Tighe M., Lockwood P. and Wilson S. (2005) Adsorption of antimony (V) by floodplain soils, amorphous iron (III) hydroxide and humic acid. *J. Environ. Monit.* **7**, 1177-1185.

US EPA. (1979) Water Related Fate of the 129 Priority Pollutants. USEPA, Washington, DC, Vol.1.

US EPA. (1994) Proceeding under Section 7003 of the Solid Waste Disposal Act. Westchester County Sportsmen's Center. Administrative Order of Consent. Docket no. II RCRA-94-7003-0204. USEPA, Washington, DC.

Vantelon D., Lanzirotti A., Scheinost A.C. and Kretzschmar R. (2005) Spatial distribution and speciation of lead around corroding bullets in a shooting range soil studied by micro-x-ray fluorescence and absorption spectroscopy. *Environ. Sci. Technol.* **39**, 4808-4815.

Wan X., Tandy S., Hockmann K. and Schulin R. (2013) Changes in Sb speciation with waterlogging of shooting range soils and impacts on plant uptake. *Environmental Pollution* **172**, 53-60.

Webb S.M. (2005) SIXPack: a graphical user interface for XAS analysis using IFEFFIT. *Phys. Scr.* **T115**, 1011-1014.

WHO. (2003) Antimony in Drinking Water; *Background Document for Development of WHO Guidelines for Drinking Water Quality*, World Health Organization.

Yin X., Gao B., Ma L.Q., Saha U.K., Sun H. and Wang G. (2010) Colloid-facilitated Pb transport in two shooting-range soils in Florida. *Journal of Hazardous Materials* **177**, 1-3, 620-625.

Zhang W. (2003) Nanoscale iron particles for environmental remediation: An overview. *Journal of Nanoparticle Research* **5**, 323-332.

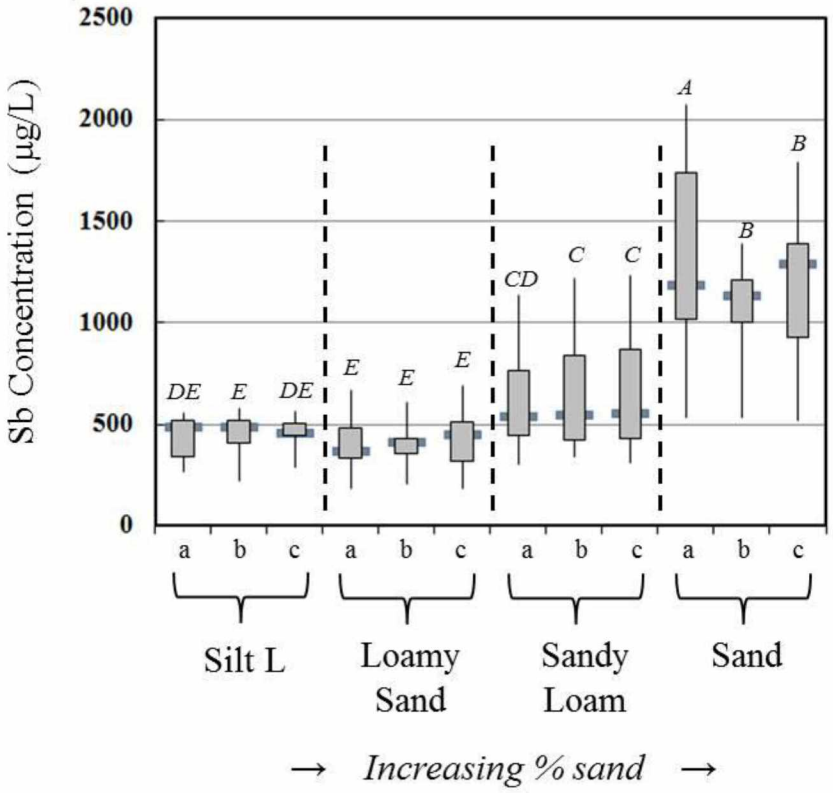

Figure 4.1 Box plot of Sb concentrations

Box plot of Sb concentrations in runoff leachate for each of the soil types in all the columns prior to the Fe additions. Concentrations of Sb in each soil type leachate were measured in triplicate indicated by 'a, b, c' on the plot. Plot is arranged in order of increasing % of sand. Dark gray lines indicate median values during the runoff experiment (prior to the Fe additions) and the gray boxes depict the lower (25^{th} percentile) and upper (75^{th} percentile) quartiles. A, B, C, D, E indicates levels that are statistically different between data sets using one-way ANOVA with bivariate analysis and Student's t-test to compare means, p-value <0.05. Levels connected by the same letter were determined to not be significantly different at $p < 0.05$.

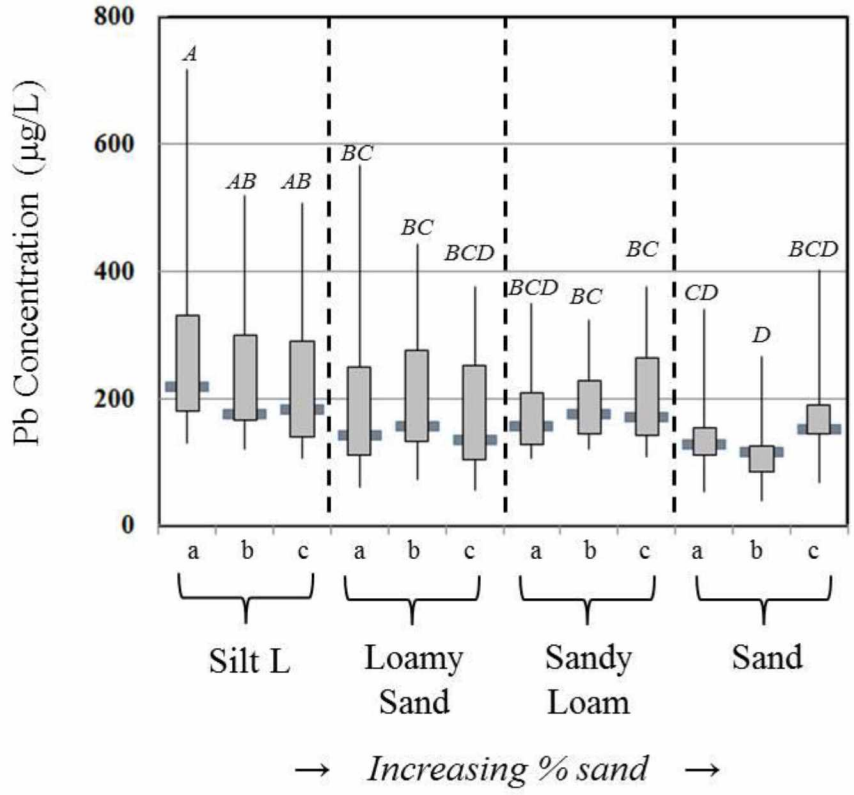

Figure 4.2 Box plot of Pb concentrations

Box plot of Pb concentrations in runoff leachate for each of the soil types in all the columns prior to the Fe additions. Concentrations of Sb in each soil type leachate were measured in triplicate indicated by 'a, b, c' on the plot. Plot is arranged in order of increasing % of sand. Dark gray lines indicate median values during the runoff experiment (prior to the Fe additions) and the gray boxes depict the lower (25th percentile) and upper (75th percentile) quartiles. A, B, C, D indicates levels that are statistically different between data sets using one-way ANOVA with bivariate analysis and Student's t-test to compare means, p-value <0.05. Levels connected by the same letter were determined to not be significantly different at $p < 0.05$.

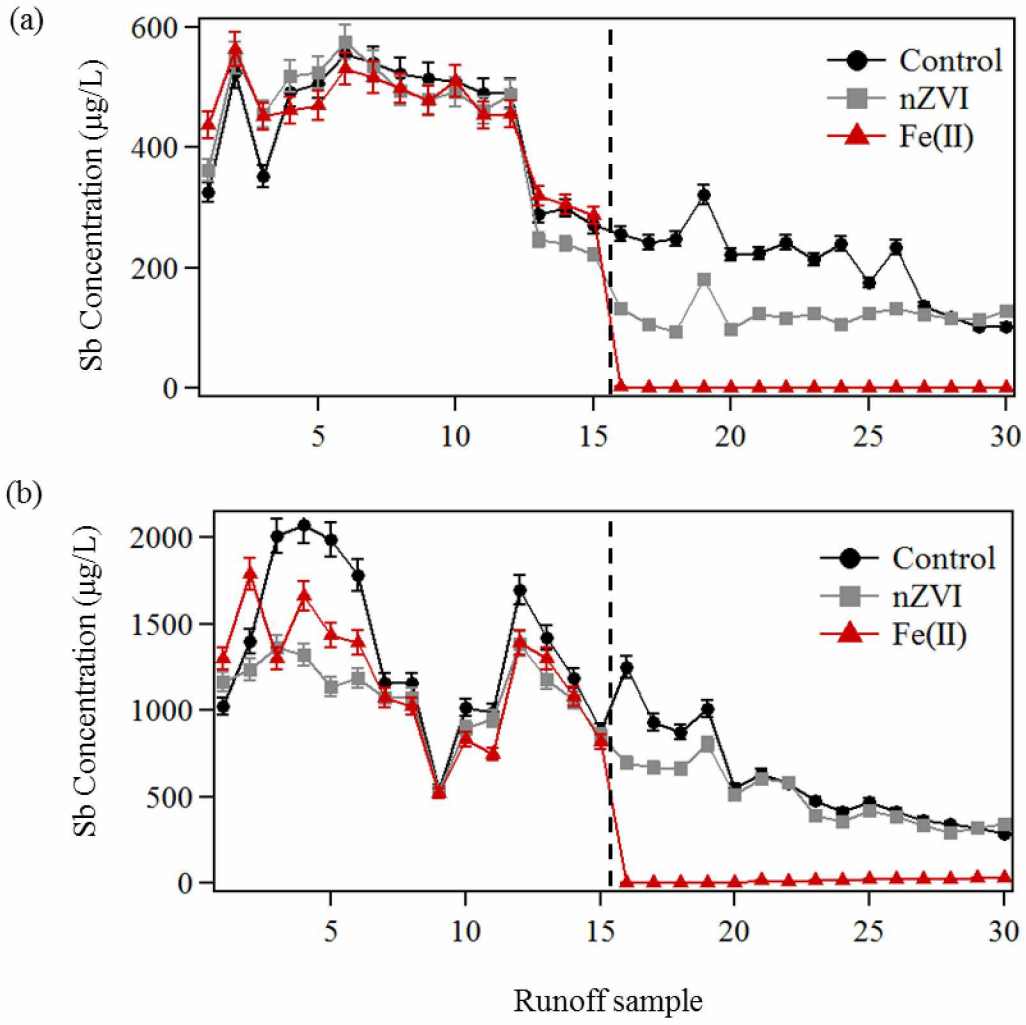

Figure 4.3 Sb concentrations in runoff with Fe additions

Antimony concentrations in runoff leachate for the (a) silt loam column set and the (b) sand column set (soil type end members). The amendments were added after runoff sample 15 and were (1) no amendment in the controls, (2) nZVI and (3) $FeCl_2$ + $CaCO_3$. Black dotted line indicates when the amendments were added.

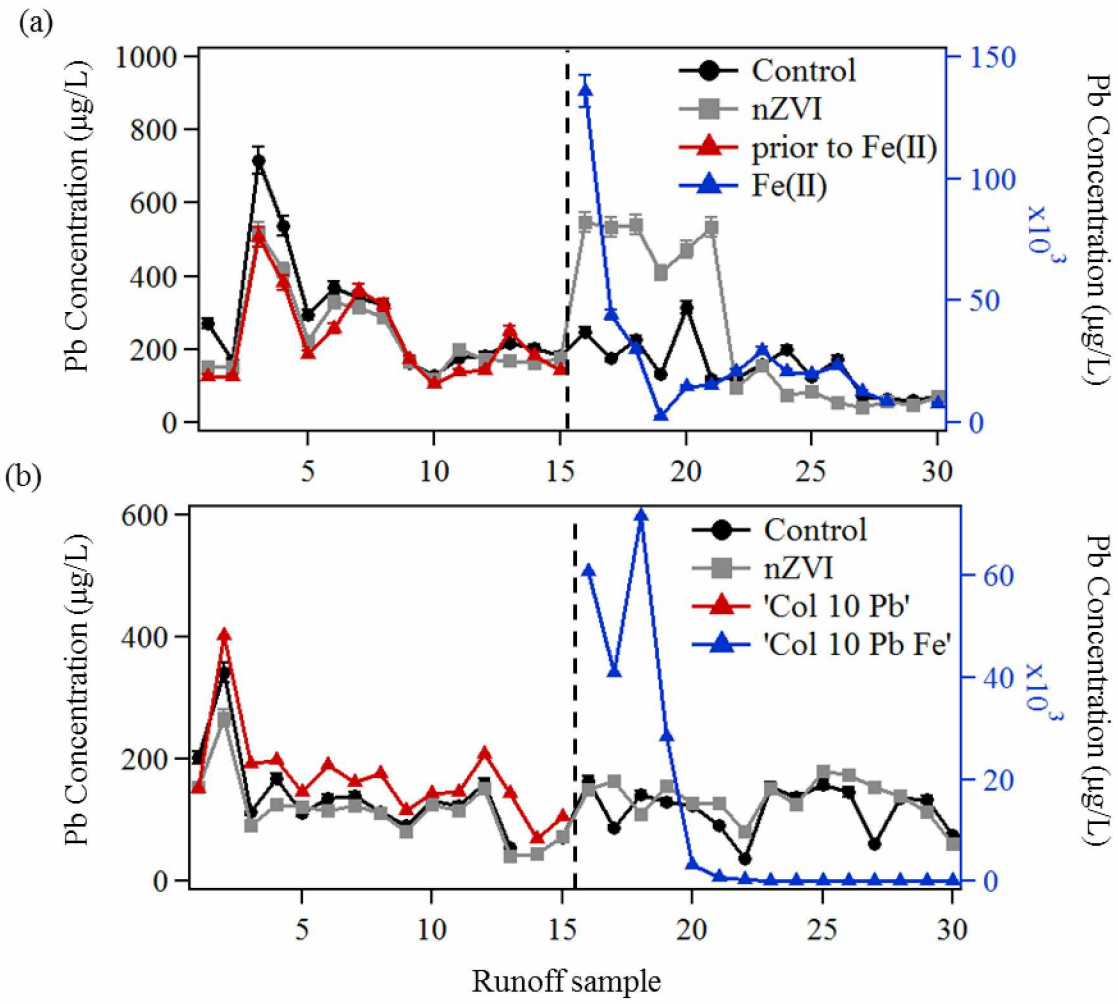

Figure 4.4 Pb concentrations in runoff with Fe additions

Lead concentrations in runoff leachate for the (a) silt loam column set and the (b) sand column set (soil type end members). The amendments were added after runoff sample 15 and were (1) no amendment in the controls, (2) nZVI and (3) $FeCl_2$ + $CaCO_3$ (plotted on the right axis for scale). Black dotted line indicates when the amendments were added.

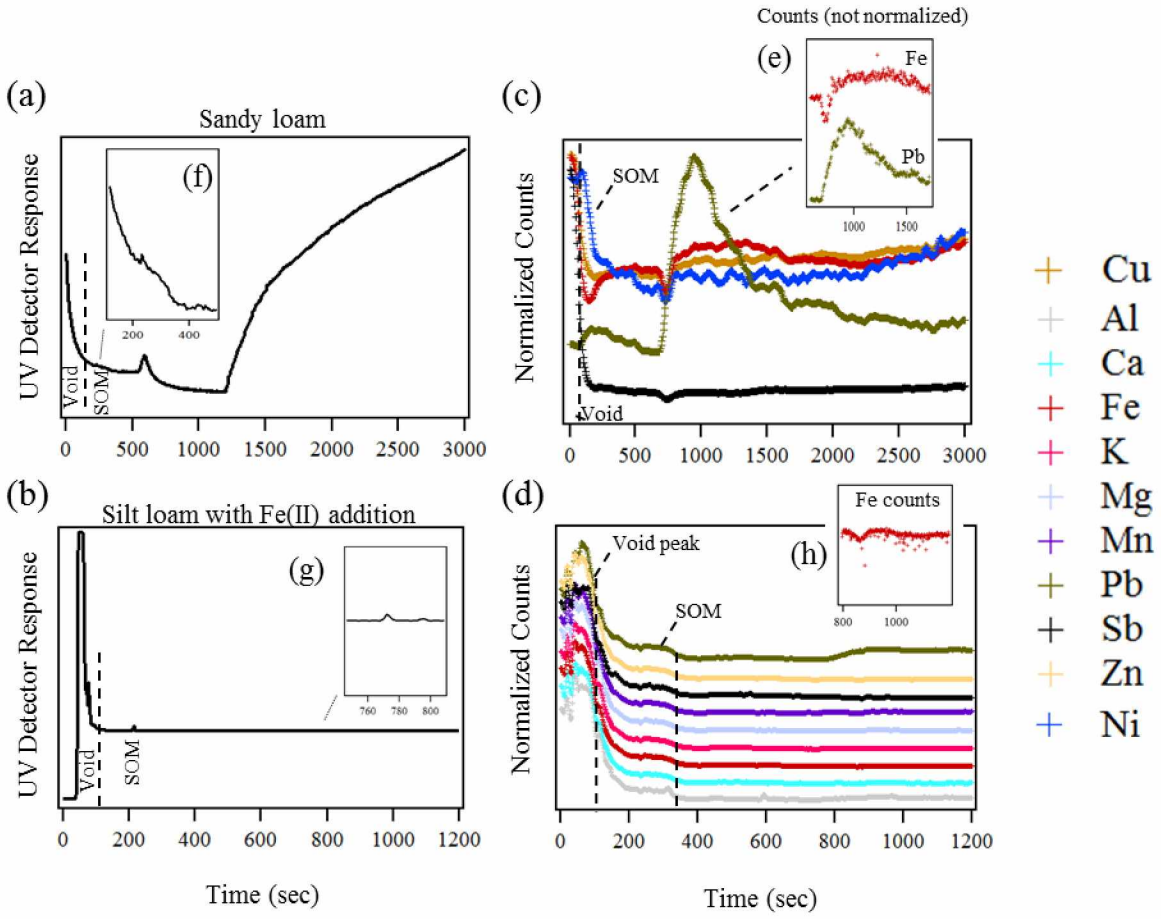

Figure 4.5 Colloid particle separation

FFF-ICP-MS results of the sandy loam mixed soil column runoff experiment and the silt loam soil after the addition of the Fe(II) amendment. (a, b) correspond to FFF fractogram of time versus UV detector response (a; 254 nm and b; 284 nm) and (c, d) refers to in-line coupling to ICP-MS detector counts. There is approximately a 100 second delay between FFF and ICP-MS signal. The ICP-MS data has been normalized to 1 and stacked. The UV detector signal has been visually increased in (f) for the sandy loam and (g) for the silt loam with Fe(II) addition. The ICP-MS counts (not normalized) were visually increased in (e) for the sandy loam and (h) for the silt loam with Fe(II) addition.

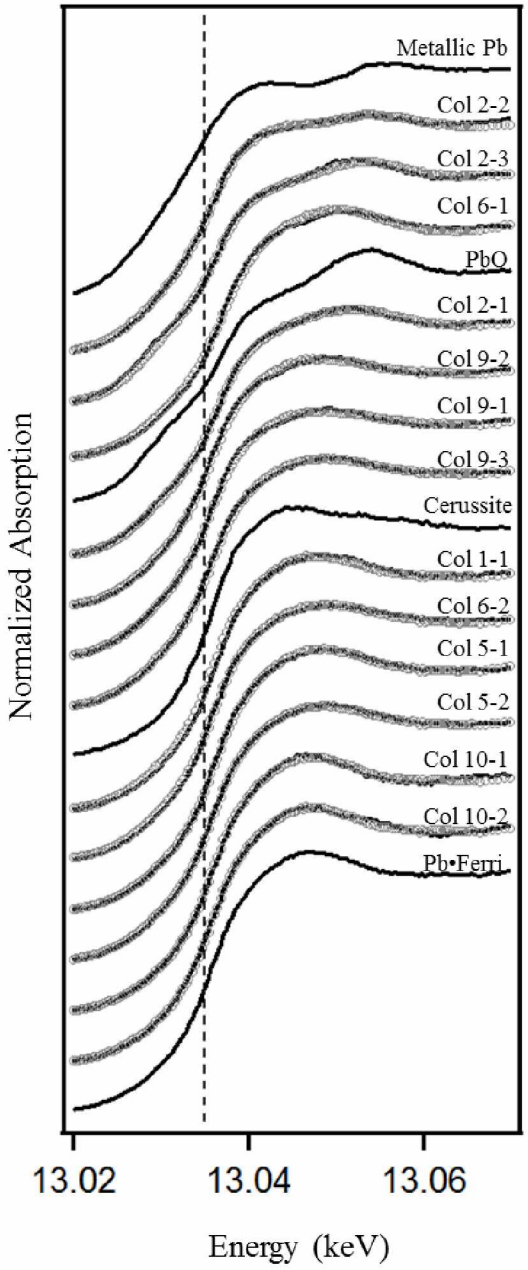

Figure 4.6 Normalized Pb-LIII µ-XANES

Normalized Pb-L_{III} μ-XANES spectra of end member column samples and corresponding linear combination fits (black lines correspond to samples with attached gray circles representing the LCF fits. Black dotted line represents the absorption edge of Pb L_{III}-edge.

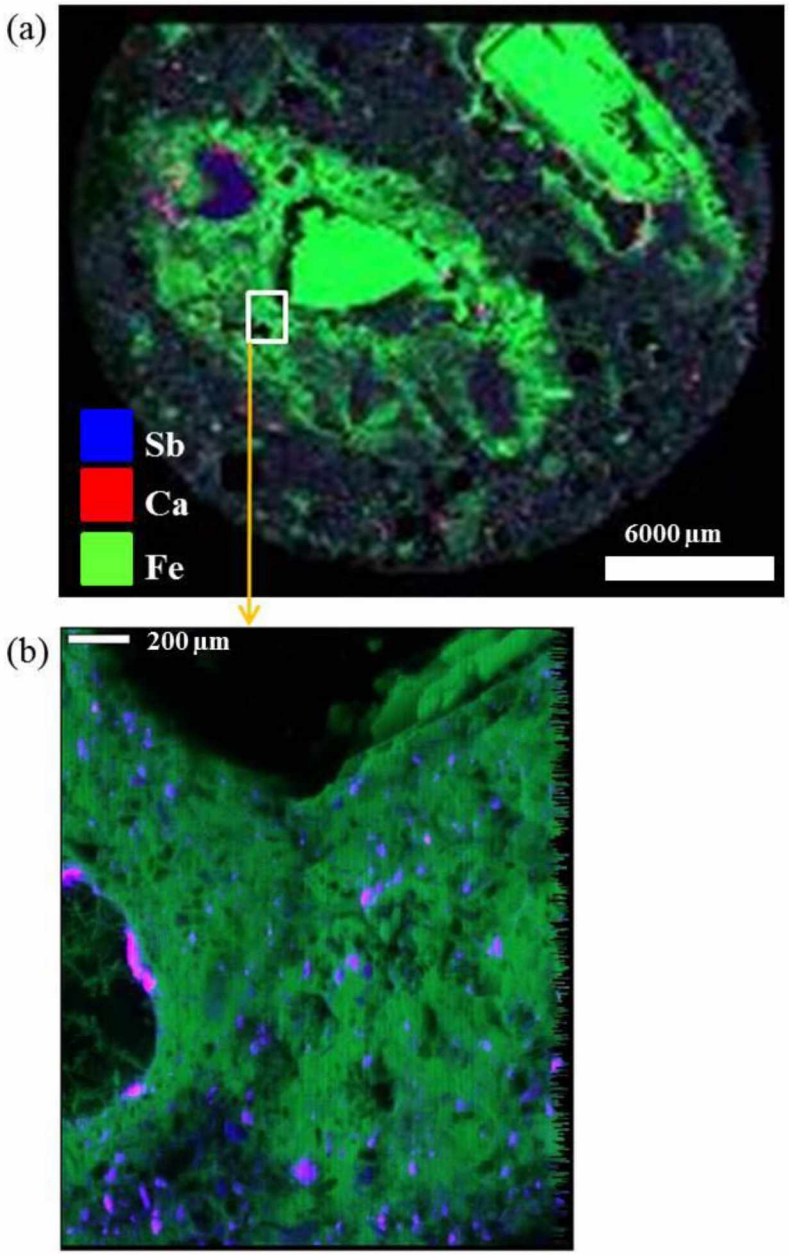

Figure 4.7 Sb distribution in soil

XRF maps showing the distribution of Sb (blue), Ca (red) and Fe (green) in the silt loam soil (a) macro-scale ~1x1mm soil plug thin section the remaining maps are sample subsets of various hotspots for microanalysis.

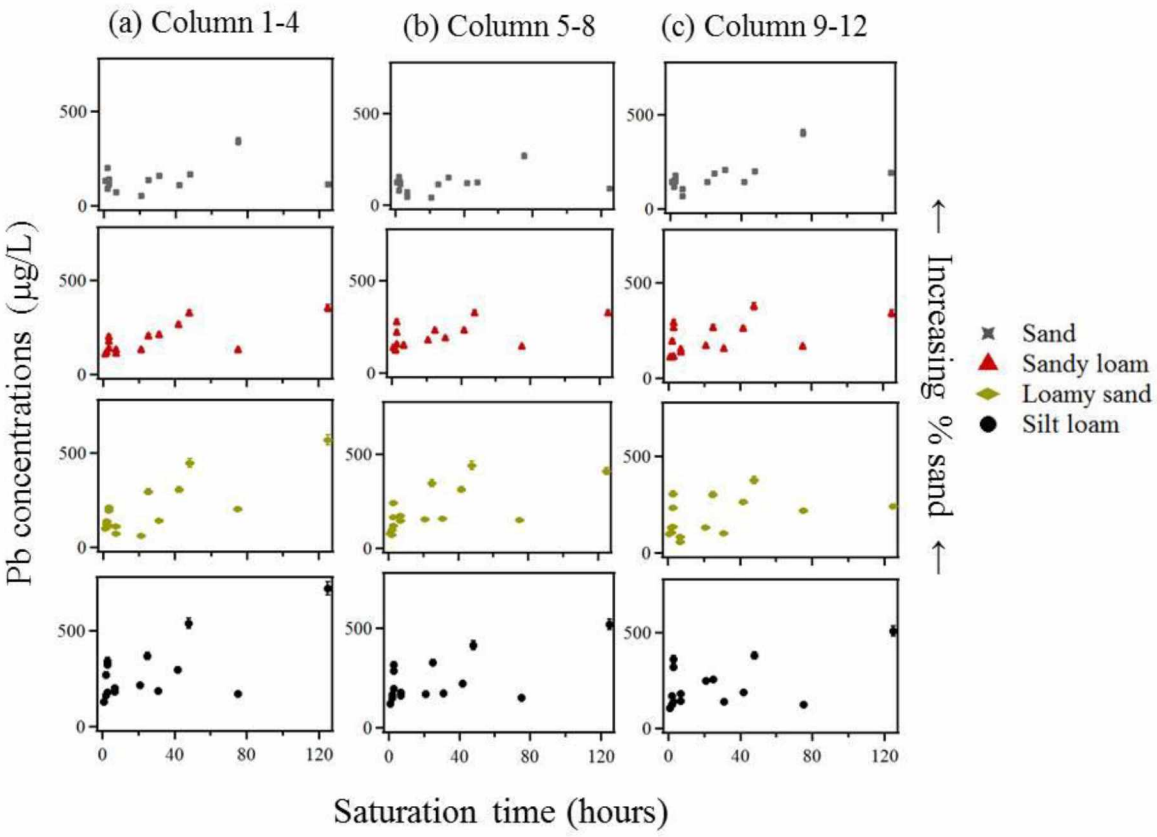

Figure 4.8 Effects of saturation time on Pb concentrations

Effects of saturation time on Pb concentrations (µg/L) as a function of soil type and column set (a, Columns 1-4; b, columns 5-8; and c, columns 9-12) in triplicate in the column runoff experiment. Pb concentrations are grouped by soil type and in order of increasing % of sand content.

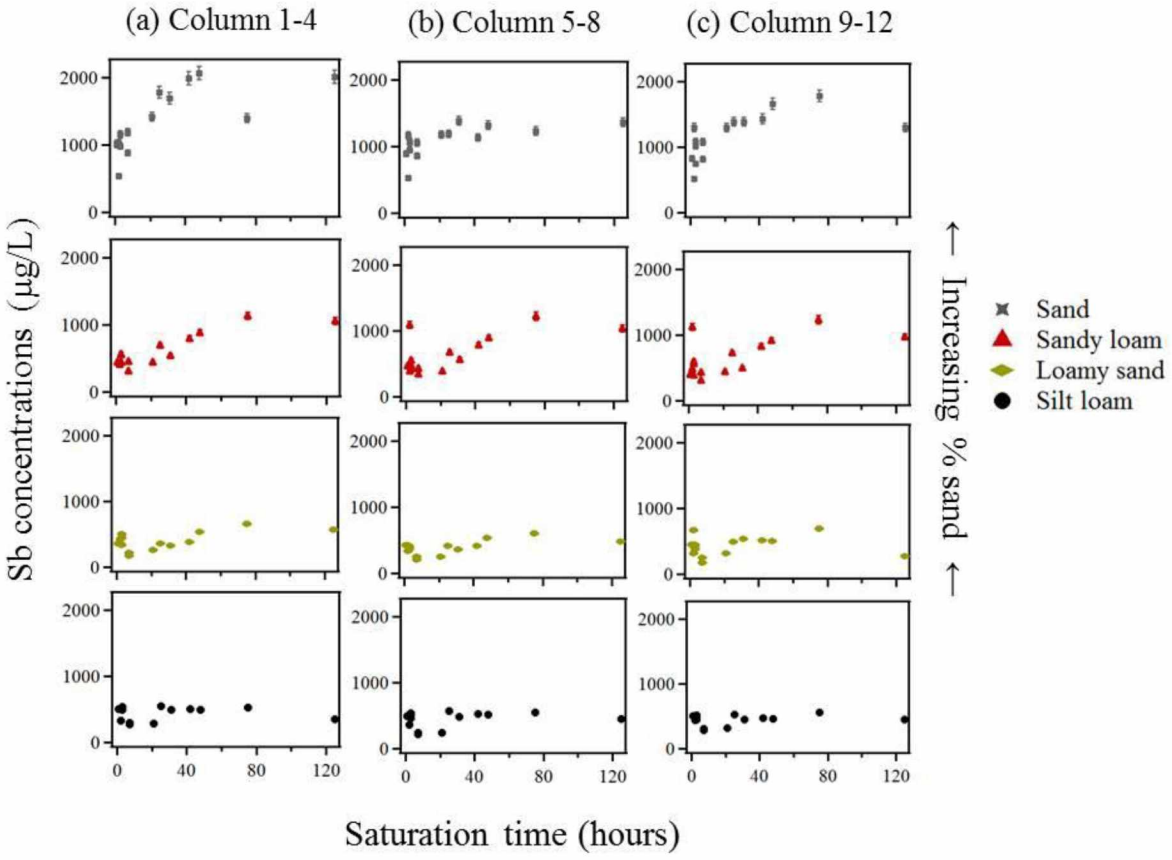

Figure 4.9 Effects of saturation time on Sb concentrations

Effects of saturation time on Sb concentrations (µg/L) as a function of soil type and column set (a, Columns 1-4; b, columns 5-8; and c, columns 9-12) in triplicate in the column runoff experiment. Sb concentrations are grouped by soil type and in order of increasing % of sand content.

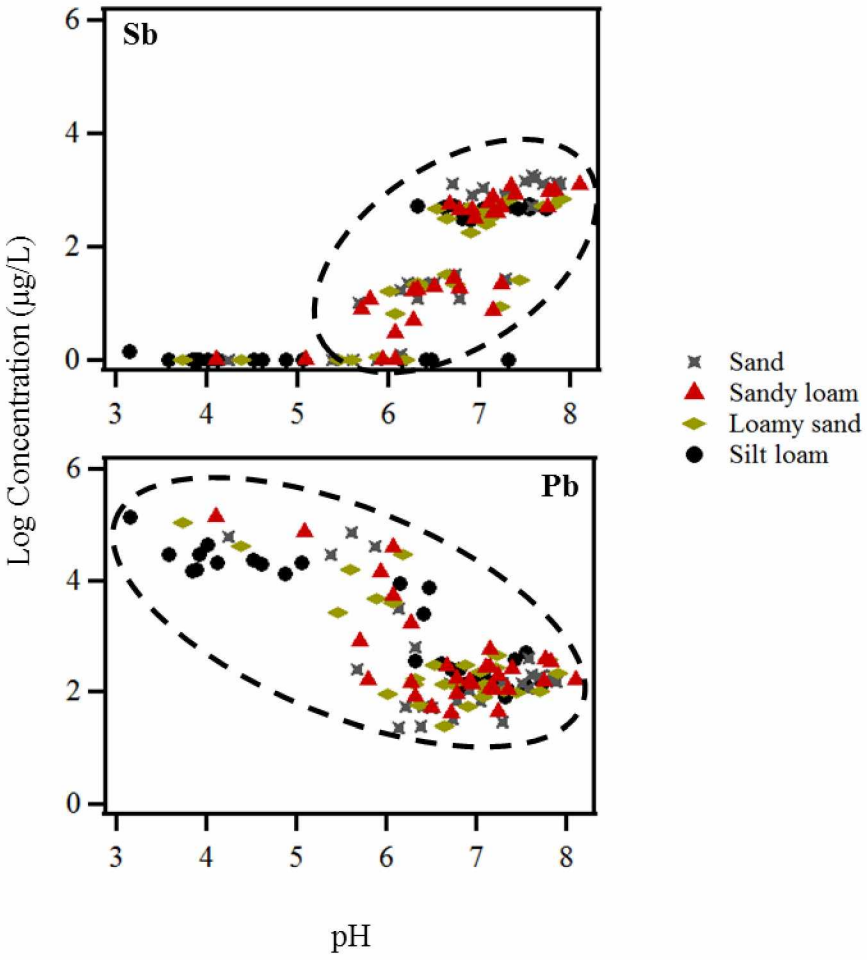

Figure 4.10 Pb and Sb in relation to pH

Trends between log Pb and Sb concentrations (µg/L) and pH as a function of soil type in the Fe(II) amended columns that experienced a drop in pH due to the hydrolysis of Fe in solution and lack of carbonate buffer.

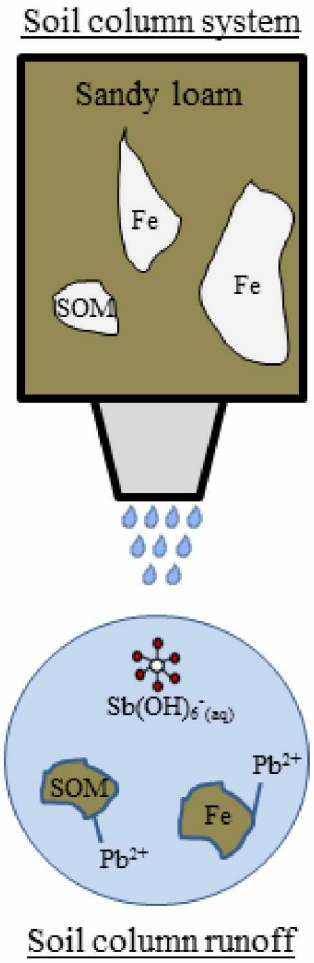

Figure 4.11 Schematic of colloidal transport

Overall schematic of colloidal transport of Pb and Sb in the column soil and runoff. The column soil depicts the identify of the primary colloids (humic acid particles and Fe colloids) associated with the sandy loam (mixed soil) system studied. This is for contaminated shooting range systems (sandy loam) and the Fe amendment addition was not included.

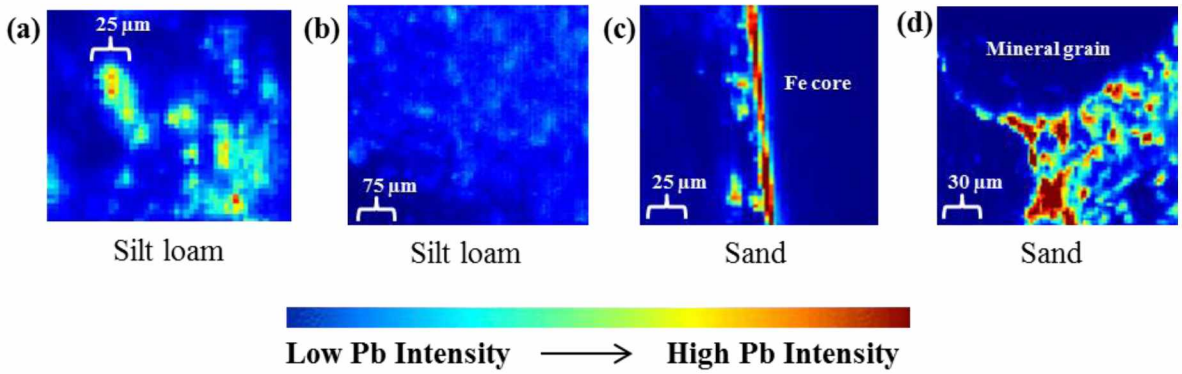

Figure 4.12 Unique distributions of Pb

Unique distributions of Pb in representative columns samples, XRF maps show relative Pb intensities. The distribution in (a) shows discrete Pb^0 hotspots with varying amounts of oxidized products (b) represents diffuse Pb dispersed throughout the soil (c) is characterized by a thin rim of oxidized Pb running along the surface of the Fe bullet core (d) illustrates the occurrence of Pb sorbed to the surface of mineral grains.

Table 4.1 Column setup scheme

Column	Soil Type	Amendment
1	Silt loam	none
2	Sand	none
3	Loamy sand	none
4	Sandy Loam	none
5	Silt loam	nZVI
6	Sand	nZVI
7	Loamy sand	nZVI
8	Sandy Loam	nZVI
9	Silt loam	$FeCl_2 + CaCO_3$
10	Sand	$FeCl_2 + CaCO_3$
11	Loamy sand	$FeCl_2 + CaCO_3$
12	Sandy Loam	$FeCl_2 + CaCO_3$

Table 4.2 LCF results for Pb-LIII XANES

Linear combination fitting results for column experiment end member soil types using reference spectra. Sum (%) refers to the actual sum of the partial contributions of reference spectra for the overall best fit. χ^2 and reduced χ^2 are derived from the fit refinement process. Pb(0) = Metallic bullet alloy; L = Litharge (PbO); C = Cerussite; Ferri = Pb(II) sorbed to Fe(III) oxides; error associated with fit in parenthesis.

Sample	Soil type	Addition	Spot	Pb(0)	L	C	Ferri	Sum	χ^2	red. χ^2
Col 1	Loam	none	1		10 (2)		85 (2)	95.4	2.3E-02	1.7E-04
Col 2	Sand	none	1		49 (1)		47 (1)	96.5	3.4E-03	2.5E-05
Col 2	Sand	none	2	29 (1)	23 (1)	48 (1)		99.5	8.8E-03	6.5E-05
Col 2	Sand	none	3	19 (1)	50 (2)		28 (1)	96.6	1.2E-02	9.4E-05
Col 5	Loam	nZVI	1		14 (1)	10 (1)	75 (1)	99.2	4.3E-03	3.2E-05
Col 5	Loam	nZVI	2		20 (1)		77 (1)	97.1	3.3E-03	2.5E-05
Col 6	Sand	nZVI	1		31 (1)	29 (1)	37 (2)	96.2	1.7E-02	1.3E-04
Col 6	Sand	nZVI	2		23 (1)	8 (5)	67 (4)	98.3	1.1E-02	8.2E-05
Col 9	Loam	Fe(II)	1	22 (1)	8 (1)		67 (1)	96.8	8.2E-03	6.2E-05
Col 9	Loam	Fe(II)	2	19 (1)	8 (1)		70 (1)	96.9	9.6E-03	7.1E-05
Col 9	Loam	Fe(II)	3	12 (1)	15 (1)		69 (1)	97.0	4.6E-03	3.4E-05
Col 10	Sand	Fe(II)	1			<5 (5)	94 (5)	94.3	1.2E-02	9.2E-05
Col 10	Sand	Fe(II)	2			<5 (4)	93 (4)	94.4	9.4E-03	7.0E-05

Table 4.3 Percent reductions of Pb and Sb

Percent reductions of Pb and Sb in the soil columns as a result of the Fe amendments. Reductions were calculated based on the value of Pb and Sb in porevolume sample 15 in comparison to porevolume sample 30 after the addition.

			% Reduction	
Column	Soil type	Addition	Pb	Sb
1	Loam	None	62	62
2	Sand	None	-6	60
3	Loamy sand	None	-99	8
4	Sandy loam	None	4	14
5	Loam	nZVI	59	43
6	Sand	nZVI	16	51
7	Loamy sand	nZVI	80	36
8	Sandy loam	nZVI	-11	27
9	Loam	$FeCl_2 + CaCO_3$	-6152	100
10	Sand	$FeCl_2 + CaCO_3$	69	96
11	Loamy sand	$FeCl_2 + CaCO_3$	-313	83
12	Sandy loam	$FeCl_2 + CaCO_3$	43	91

4.9 Appendix B

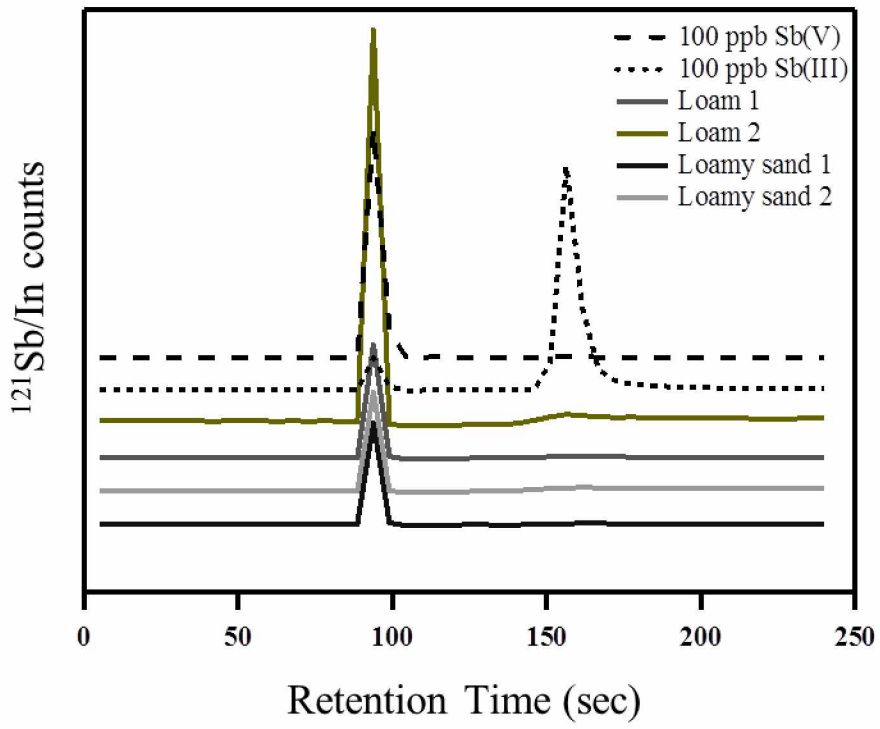

Figure 4.13 Sb aqueous speciation.

Antimony aqueous speciation in porevolume sample 1 and 2 from silt loam and loamy sand columns.

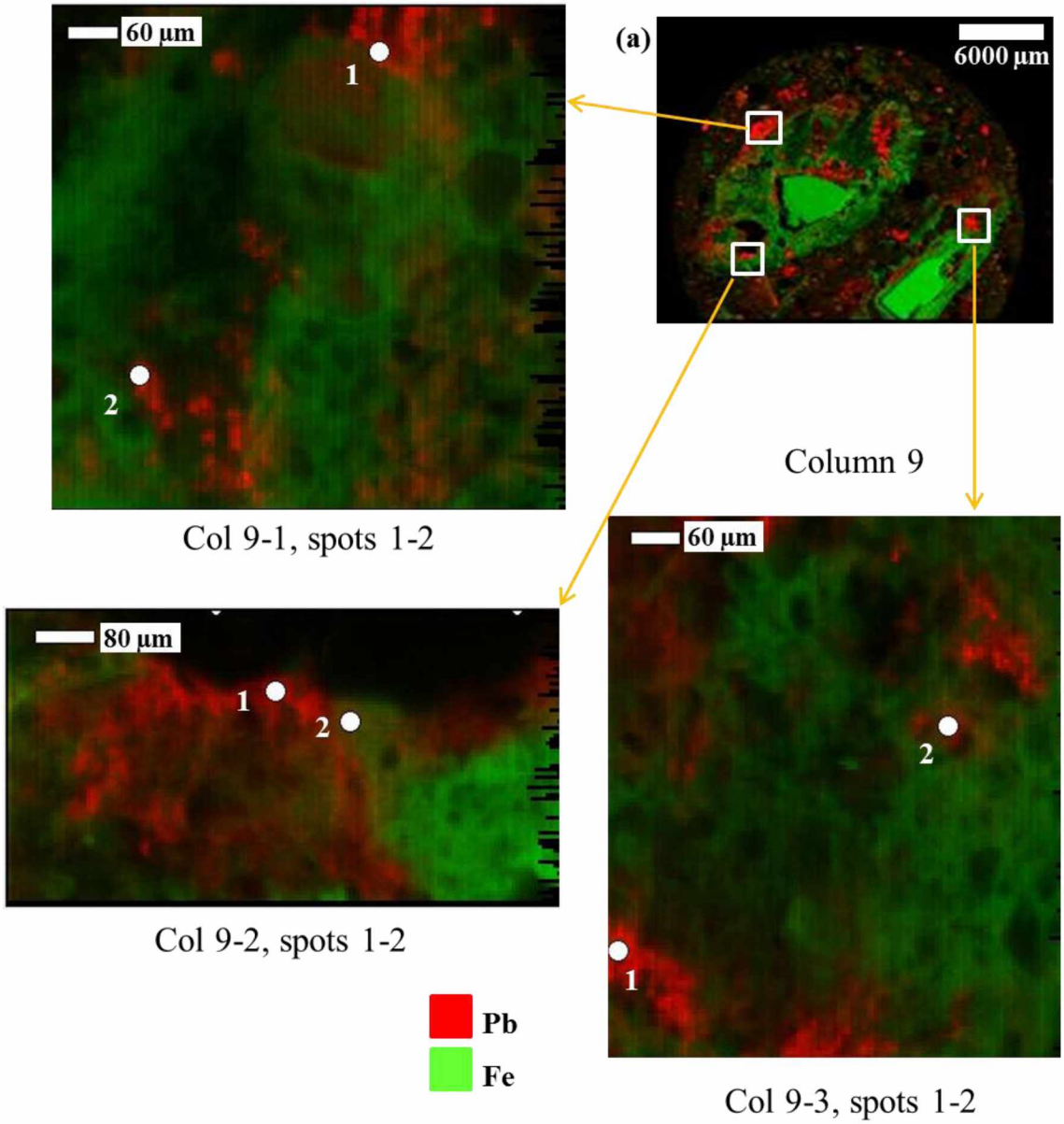

Figure 4.14 Pb and Fe distributions

XRF map showing Pb (red) and Fe (green) distribution in column 9 (loam soil $FeCl_2/CaCO_3$ amendment) (a) macro-scale ~1x1mm soil plug thin section the remaining maps are sample subsets of various hotspots for microanalysis.

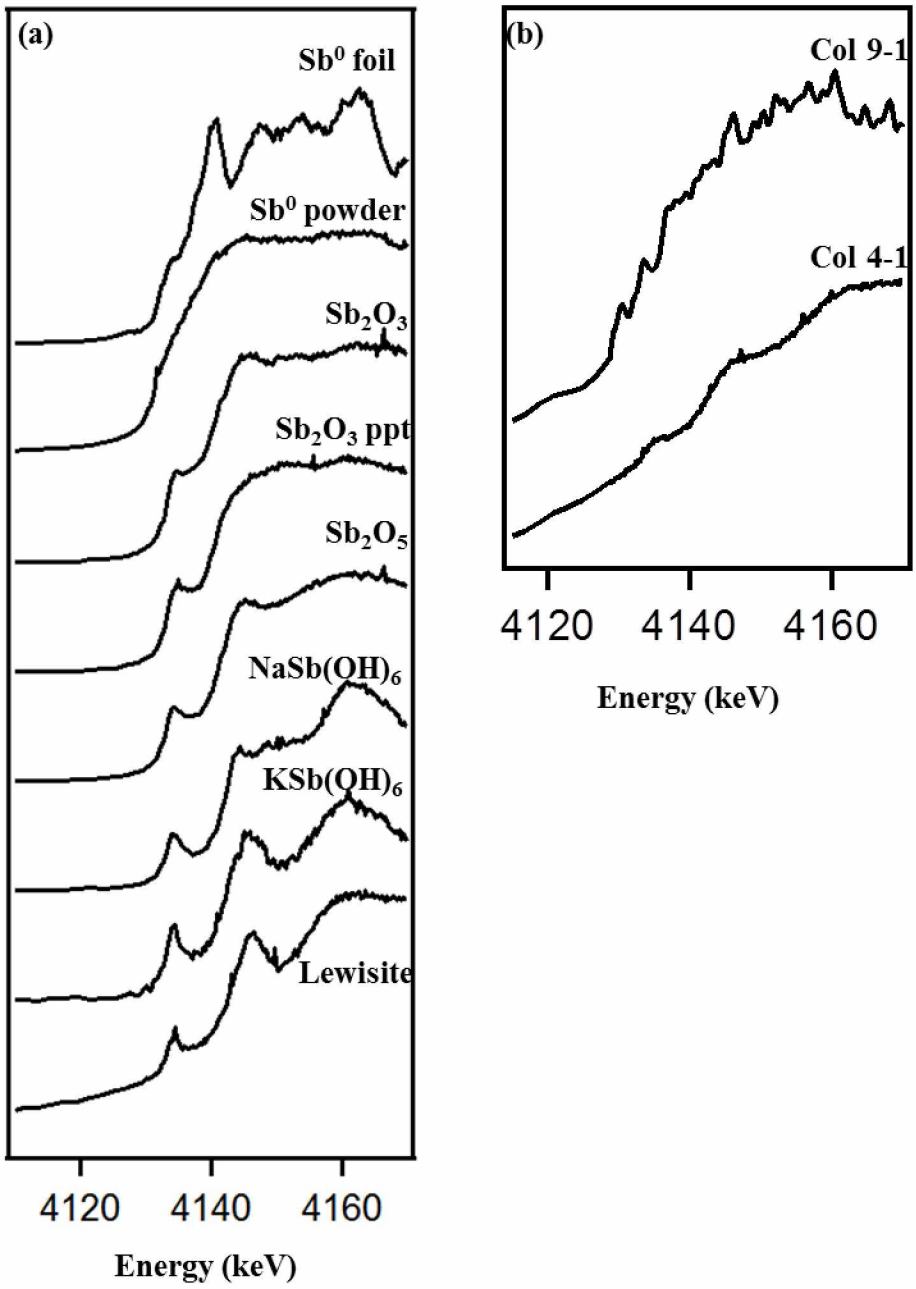

Figure 4.15 Sb solid speciation

Normalized Sb-L_{III} μ-XANES spectra of **(a)** standards and model compounds used for visual comparison with **(b)** column samples.

Table 4.4 Sb-LIII edge energies with standards

Absorption edge energies for Sb standards, model compounds and column samples.

Column	Amendment	Soil type	Spot	E_0
4	none	Sandy loam	1	4143.0
9	Fe(II)	Silt loam	1	4139.2
		Standards		
			Sb^0 powder	4131.6
			Sb^0 foil	4132.0
			Sb_2O_3 ppt	4133.1
			Sb_2O_3	4133.4
			$KSb(OH)_6$	4140.9
			Lewisite	4143.1
			Sb_2O_5	4143.1
			$NaSb(OH)_6$	4143.6

Conclusion

Overall, the results from this body of work contribute significantly to multiple scientific fields in the area of chemical speciation analysis, geochemical weathering and analytical chemistry. In the first field study (Chapter 1), the findings showed that metal transport and mobility as a result of pristine mineral weathering is complex and likely controlled by a variety of factors, particularly metal speciation. The transport and behavior of trace metals strongly depends on local soil conditions, especially the redox environment. The study offers many improvements on previous efforts and provides a baseline of data for future monitoring in Arctic Alaska. Our results capture the seasonality of trace metals in two Arctic watersheds from spring snowmelt until early winter, a season that is widely overlooked. Our findings highlight a correlation between the top-down freezing processes that occurs in Arctic soils to metal fluctuations in local surface waters. In addition, our results highlight the complexity of metal transport as a function of seasonality in the presence of permafrost, culminating in the need for longer summer sampling seasons in the Arctic.

The overall setup and design of the second study (Chapters 2-4) allowed initial transformation pathways and corrosion products of elemental Pb and Sb to be observed in newly constructed shooting range berms. The initial products formed have often been overlooked in previous studies due to a focus on older, heavily used shooting range samples. Liquid speciation analysis confirms the presence of $Sb(III)_{(aq)}$ in the berm runoff of the high content silt loam mixed soil, indicating Sb(III) is likely the initial oxidation product formed from the weathering of Sb^0 in the alloy, which was supported by bulk speciation analysis coupled with micro-scale methods that showed Sb(V) in octahedral coordination with 5 O and 3 Fe atoms are the predominant species present in the weathering crust. However, trivalent Sb bound to 3 O atoms

is likely the initial oxidation species as detected in the weathering bullet alloy and laboratory oxidation samples with metallic Sb. Solid-phase analysis of the newly constructed shooting range soils show Sb(V) dominance in the soil fraction and zero-valent Sb in the bullet alloy. Distribution of Pb in the samples and speciation analysis showed metallic Pb, cerussite, hydrocerussite and litharge comprise the bulk of the Pb concentration in the weathering crust, but Pb(II) sorbed to Fe(III) oxides are present in the soil fraction distal to the source material. Understanding the overall distribution of Pb and Sb speciation is necessary when designing overall remediation strategies, as the solid phase distribution likely control the activity of species in solution.

One of the most interesting results of the second project was the finding that Sb concentrations were higher than Pb in all the soil types in both the field and column studies indicating Sb is more mobile than Pb, despite the fact that Sb is present ~2 orders of magnitude less in bullets than Pb. The highest concentrations of Sb were found in the sand soil runoff and the highest concentrations of Pb were found in the mixed soil runoffs. The 100% silt loam soil runoff often contained lower concentrations of both species, highlighting the overall natural effectiveness silt loam soil has on metal(loid) retention. Lead and Sb were both found to be positively correlated to saturation time, highlighting the potential of element mobilization as a result of water-logging soils. However, Sb entered solution to a greater extent than Pb, whereas Pb concentrations, for the most part, continued to slowly increase as a function of saturation time. Antimony aqueous concentrations were found to be positively correlated with pH, whereas Pb aqueous concentrations were found to be negatively correlated with pH, which contributed to the mobilization of Pb as a result of the Fe(II) amendment addition. The mobility of Pb in the mixed (sandy loam) column runoff is facilitated by colloidal transport, whereas Sb (without Fe

amendments added) is present primarily in the dissolved fraction (<300 Da). Information from this study will be useful to understanding the overall mobility and speciation of Pb and Sb with respect to soil properties and reaction time in shooting range soils.

Of the two remediation amendments added (nZVI and $FeCl_2$+$CaCO_3$), the $FeCl_2$ and $CaCO_3$ amendment remarkably immobilized Sb, particularly upon fresh addition. Overall, there was >80% reduction of Sb in the runoff for all soil types and a >96% reduction in the soil type end members. Additional soil treatments have potential to be effective for system-wide immobilization of Pb and Sb with adequate addition of $CaCO_3$ buffer so the pH remains stable.

This study establishes an overall procedure for designing shooting ranges and implementing remediation strategies in parallel that is cost effective, easy to implement and effective at immobilizing both Pb and Sb. The design takes into account natural hillsides versus man-made berms that are often used to construct shooting ranges. One key difference in this study and other shooting range remediation studies is the addition of the amendment to only the runoff instead of the bullet pocket/soil to minimize mobilization of one element over the other since Pb and Sb behave differently in soil. Instead, the berms are constructed of 100% silt loam type soil, which this study showed was effective at naturally retaining Pb and Sb and minimizing local migration.

References

Barker A.J., Douglas T.A., Jacobson A.D., McClelland J.W., Ilgen A.G., Khosh M.S., Lehn G.O. and Trainor T.P. (2014) Late season mobilization of trace metals in two small Alaskan arctic watersheds as a proxy for landscape scale permafrost active layer dynamics. *Chemical Geology* **381**, 180-193.

Bird W.A. and Grossman E. (2011) Chemical Aftermath: Contamination and Cleanup Following the Tohoku Earthquake and Tsunami. *Environ. Health Perspect.* **119**, 7, a290-a301.

Bradl H. (2002) Heavy Metals in the Environment: Origin, Interaction and Remediation Volume 6. London, Academic Press.

Brusseau M.L. (1989) Modeling the transport of solutes influenced by multiprocess nonequilibrium. *Water Resour. Res.* **9**, 1971–1988.

Bullen T.D. (2012) Stable isotopes of transition and post-transition metals as tracers in environmental studies. In Handbook of Environmental Isotope Geochemistry, Chapter 10; Baskaran, M., Ed.; Springer: Heidelberg, pp 177−203.

Cai L., Tong M., Wang X. and Kim H. (2014) Influence of Clay Particles on the Transport and Retention of Titanium Dioxide Nanoparticles in Quartz Sand. *Environ. Sci. Technol.* **48**, 13, 7323-7332.

Cantwell M.G. and Burgess R.M. (2001) Metal-colloid partitioning in artificial interstitial waters of marine sediments: influences of salinity, pH, and colloidal organic carbon concentration. *Environ. Toxicol. Chem.* **20**, 11, 2420-2470.

Clemens S. and Ma J.F. (2016) Toxic Heavy Metal and Metalloid Accumulation in Crop Plants and Foods. *Annual Review of Plant Biology* **67**, 489-512.

Dinis M. and Fiúza A. (2006) Modeling the transport and fate of contaminants in the environment: soil, water and air in L. Simeonov and E. Chirila (Eds.), *Chemicals as Intentional and Accidental Global Environmental Threats*, (pp. 469-476). New York, Springer Publishing.

Dunnivant F.M. and Anders E. (2006) A Basic Introduction to Pollutant Fate and Transport (1st ed.). New Jersey: John Wiley & Sons.

Filella M., Williams P.A. and Belzile N. (2009) Antimony in the environment: knowns and unknowns. *Environ. Chem.*, **6**, 95-105.

Gunawardana C., Egodowatta P. and Goonetilleke A. (2015) Adsorption and mobility of metals in build-up on road surfaces. *Chemosphere* **119**, 1391-1398.

He Z.L., Yang X.E. and Stoffella, P.J. (2005) Trace elements in agroecosystems and impacts on the environment. *J. Trace Elem. Med. Biol.* **19**, 2–3, 125–140.

Hemond H.F. and Fechner E.J. (2014) Chemical Fate and Transport in the Environment (3rd ed.). California: Academic Press.

Hill S.J. (1997) Speciation of trace metals in the environment. *Chemical Society Reviews* **26**, 291-298.

Horowitz A.J. (1985) A Primer on Trace Metal-Sediment Chemistry. *United States Geological Survey Water-Supply Paper 2277.*

Horowitz A.J. and Elrick K.A. (1987) The relation of stream sediment surface area, grain size and composition to trace element chemistry. *Applied Geochemistry* **2**, 4, 437-451.

Houben D., Evrard L. and Sonnet P. (2013) Mobility, bioavailability and pH-dependent leaching of cadmium, zinc and lead in a contaminated soil amended with biochar. *Chemosphere* **92**, 11, 1450-1457.

Ilgen A. and Trainor T. (2012) Sb(III) and Sb(V) sorption onto Al-rich phases: hydrous Al oxide and the clay minerals kaolinite KGa-1b and oxidized and reduced nontronite NAu-1. *Environ. Sci. Technol.* **46**, 843-851.

Ilgen A.G., Majs F., Barker A.J., Douglas T.A. and Trainor T.P. (2014) Oxidation and mobilization of metallic antimony in aqueous systems with simulated groundwater. *Geochimica et Cosmochimica Acta* **132**, 16-30.

Jin L., Ravella R., Ketchum B., Bierman P.R., Heaney P., White T. and Brantley S.L. (2010) Mineral weathering and elemental transport during hillslope evolution at the Susquehanna/Shale Hills Critical Zone Observatory. *Geochim. Cosmochim. Acta* **74**, 3669-3691.

Johnson C., Moench H., Wersin P., Kugler P. and Wenger C. (2005) Solubility of antimony and other elements in samples taken from shooting ranges. *J. Environ. Qual.* **34**, 248.

Kabata-Pendias A. (2010) Trace Elements in Soils and Plants. (4^{th} Ed.) Boca Raton, Florida. Taylor & Francis.

Kaplan D.I., Bertsch P.M., Adriano D.C. (1995) Facilitated Transport of Contaminant Metals through an Acidified Aquifer. *Ground Water* **33**, 5.

Knechtenhofer L., Xifra I., Scheinost A.C., Flühler H. and Kretzschmar R. (2003) Fate of heavy metals in a strongly acidic shooting range-soil: Small-scale metal distribution and its relation to preferential water flow. *J. Plant Nutr. Soil Sci.* **166**, 84-92.

Knox A.S., Seaman J., Adriano D.C. and Pierzynski G. (2000) Chemophytostabilization of metals in contaminated soils. In: Bioremediation of contaminated soils, ed. D. L: Wise, D. J. Trantolo, E. J. Cichon, H. I. Inyang, and U. Stottmeister.. Marcel Dekker, Inc., New York, pp. 811-836.

Kossoff D., Hudson-Edwards K.A., Dubbin W.E. and Alfredsson M. (2012) Major and trace metal mobility during weathering of mine tailings: Implications for floodplain soils. *Applied Geochemistry* **27**, 3, 562-576.

Loretta Y.L. and Li F. (2001) Heavy Metal Sorption and Hydraulic Conductivity Studies Using Three Types of Bentonite Admixes. *J. Environ. Eng.* **10**, 420-429.

Lyman W.J. (1995) Transport and Transformation Processes in G.M. Rand (Ed.), *Fundamentals of Aquatic Toxicology: Effects, Environmental Fate and Risk Assessment,* 2nd Ed., (pp. 449-492). New York, Taylor & Francis.

Majedi S.M., Lee H.K. and Kelly B. (2013) Role of water temperature in the fate and transport of zinc oxide nanoparticles in aquatic environment. *J. Phys, Conf Ser.* **429**, 1. 2039.

Pachana K., Wattanakornsiri A. and Nanuam J. (2010) Heavy Metal Transport and Fate in the Environmental Compartments. *NU Science Journal* **7**, 1, 1-11.

Ritchie V.J., Ilgen A.G., Mueller S.H., Trainor T.P. and Goldfarb R.J. (2013) Mobility and chemical fate of antimony and arsenic in historic mining environments of the Kantishna Hills district, Denali National Park and Preserve, Alaska. *Chemical Geology* **335**, 172-188.

Rodriguez L., Ruiz E., Azvarate J.A. and Rincon J. (2008) Heavy metal distribution and chemical speciation in tailings and soils around a Pb-Zn mine in Spain. *Journal of Environmental Management* **90**, 1106-1116.

Scheinost A., Rossberg A., Vantelon D., Zifra I., Kretzschmar R., Leuz A., Funke J. and Johnson C. (2006) Quantitative antimony speciation in shooting range soils by EXAFS spectroscopy. *Geochim. Cosmochim. Acta* **70**, 3299-3312.

Seuntjens P., Mallants D., Šimůnek J., Patyn J. and Jacques D. (2002) Sensitivity analysis of physical and chemical properties affecting field-scale cadmium transport in a heterogeneous soil profile. *J. Hydrol.* **264**, 185-200.

Shiller A.M., Duan S., Erp P. and Bianchi T.S. (2006) Photo-oxidation of dissolved organic matter in river water and its effect on trace element speciation. *Limnol. Oceanogr.* **51**, 4, 1716-1728.

Singh B. and Gräfe M. (2010) Eds. *Developments in Soil Science-Volume 34*: *Synchrotron-based Techniques in Soils and Sediments*, 1st, ed.; Elsevier, Burlington, MA.

Sklodowski P., Maciejewska A. and Kwiatkowska J. (2006) The effect of organic matter from brown coal on bioavailability of heavy metals in contaminated soils. *Soil and Water Pollution Monitoring* **3**, 23, 299-307.

Walker C.H., Hopkin S.P., Sibly R.M. and Peakall D.B. (2006) Principles of ecotoxicology (3rd. ed.). New York: Taylor & Francis.

Wiederhold J.G. (2015) Metal Stable Isotope Signatures as Tracers in Environmental Geochemistry. *Environ. Sci. Technol.*, **49**, 5, 2606-2624.

Wilson S.C., Lockwood P.V., Ashley P.M. and Tighe M. (2010) The chemistry and behaviour of antimony in the soil environment with comparisons to arsenic: A critical review. *Environmental Pollution* **158**, 1169-1181.

Wuana R.A. and Okieimen F.E. (2011) Heavy Metals in Contaminated Soils: A Review of Sources, Chemistry, Risks and Best Available Strategies for Remediation. *ISRN Ecology* **2011**, 20 p.

Yin H., Tan N., Liu C., Wang J., Liang X., Qu M., Feng X., Qiu G., Tan W. and Liu F. (2016) The associations of heavy metals with crystalline iron oxides in the polluted soils around the mining areas of Guangdong Province, China. *Chemosphere* **161**, 181-189.

Zhang H. and Shan B. (2008) Historical records of heavy metal accumulation in sediments and the relationship with agricultural intensification in the Yangtze-Huaihe region, China. *Sci. Total. Environ.* **399**, 1-3, 113-120.